SPECTROSCOPIC STUDIES OF LIGNIN BIODEGRADATION

by

Gianfranco Gilardi

A Thesis submitted to The University of London for the degree of Doctor in Philosophy, and to Imperial College of Science, Technology and Medicine for the Diploma of Imperial College.

1991

Laboratory of Analytical Biotechnology
Centre for Biotechnology
Imperial College of Science, Technology and Medicine
London SW7 2AZ

ABSTRACT

This thesis describes the application of spectroscopic techniques, mainly nuclear magnetic resonance (N.M.R.), to the study of the biodegradation of lignin.

A key enzyme involved in lignin degradation is ligninase, a peroxidase secreted during secondary metabolism by the white rot fungus *Phanerochaete chrysosporium*. Several studies indicate that the production of ligninase is accompanied by the extracellular production of 3,4-dimethoxybenzyl alcohol (veratryl alcohol), a secondary metabolite that has been shown to enhance the degradation of lignin.
This thesis reports the use of proton N.M.R. to study the oxidation of veratryl alcohol by ligninase. A decrease in spin-spin and spin-lattice relaxation times of veratryl alcohol during its oxidation by ligninase is explained by the generation of radical intermediates. A substantial increase of the linewidths of the substrate is indicative of a fast exchange of the radical's unpaired electron between the paramagnetic and the diamagnetic molecules of veratryl alcohol. This finding supports the view that radical intermediates of veratryl alcohol are freely diffusing mediators, transferring oxidizing equivalents from the ligninase active site to the large, insoluble and hydrophobic lignin.
Carbon-13 and proton N.M.R. spectroscopy were also used to characterize a sample of organosolv spruce lignin. These techniques, combined with infra-red (FT/IR) spectroscopy, provided information on chemical groups that contribute the structure of lignin. Furthermore, two-dimensional proton N.M.R. studies revealed a potential structural content in this lignin sample. This was found to be compatible with N.M.R. spectral simulations and a preliminary molecular model is proposed. The presence of a specific structural content in lignin may be expected to shed light on the mechanism of its biodegradation by the fungal enzyme systems.
The determination of lignin molecular size by Langmuir-Blodgett trough, combined with light scattering techniques, molecular weight measurements, and scanning electron microscopy revealed that an aggregation process occurs between lignin molecular units. This finding may be of relevance when *in vitro* experiments with lignin and purified enzymes are carried out: the physical nature of lignin may affect the enzymatic action.
Studies of lignin biodegradation were also carried out on solid samples of wood inoculated with white rot and brown rot fungi. Solid state N.M.R. techniques were applied to study the biodegradation process occurring on these solid samples of wood. Wide-line solid state N.M.R. was used to measure the proton relaxation times of both the water in wood and wood components, in relation to the biodegradative process. As the degradation occurs, wood components and associated water develop differences in molecular mobility; these differences were detected by an increase in proton relaxation times. This method provides a potential non-destructive test to detect the degradative state of wood prior further detailed analysis.
High resolution cross polarization / magic angle spinning solid state N.M.R. (CP/MAS N.M.R.) was applied to characterize the same wood samples and to investigate their molecular modifications after fungal attack. This method provided a distinct analysis of the cellulose and lignin resonances, allowing quantitative considerations: white-rot fungi were found to extensively degrade the lignin component.

ACKNOWLEDGEMENTS

Firstly, I would like to thank Dr. Tony Cass for supervising me on this project, for not only providing me with the research facilities, but also for our many discussions and his useful comments throughout the research.
I also thank Dr. Pat Harvey and Prof. John Palmer for their contributions in developing this project, for our useful discussions and for giving me access to the facilities in the Plant Biochemistry group in Imperial College. Many thanks also to Dr. Paul McCormack for supplying the wood samples for solid state N.M.R.

I also thank Montedison S.p.A. (Italy) for financial support, Dr. Luigi Abis and Dr. Isa Camurati for the access to the solid state N.M.R. facilities in Istituto Guido Donegani in Novara (Enichem S.p.A., Italy).

Many thanks to all my friends and colleagues who helped me during these years in one way or another. In particular I thank Jyoti Lakhanpal and Alan Barrett for their friendship and for proof reading of this thesis.

I would like also to remember Prof. Maria Buffa for her advice and friendship during my University studies, and Prof. Carlo Giunta and Prof. Anna Lombard for teaching me Biochemistry.

Finally, I will always be grateful to my parents for all their help, support and motivation through the years of my education.

TABLE OF CONTENTS

Title I
Abstract III
Acknowledgements IV
List of Figures IX
List of Tables XV

Chapter 1 Introduction 3

1.1. Cell Wall: Structure, Composition and Biotechnological Importance 3
1.1.1. Cellulose 3
1.1.2. Hemicelluloses 7
1.1.3. Lignin 7
1.1.4. Biotechnological Importance of the Cell Wall 12
1.2. Lignin Biodegradation 14
1.2.1. Microbiology 15
1.2.1.1. Bacteria 15
1.2.1.2. Soft-rot Fungi 16
1.2.1.3. Brown-rot Fungi 16
1.2.1.4. White-rot Fungi 17
1.2.2. Lignin Degrading Enzymes 19
1.2.2.1. Ligninase 20
1.2.2.2. Other Lignin Degrading Enzymes 27
1.2.3. Chemistry of Lignin Biodegradation 31
1.3. Purpose of the Project 34

Chapter 2 Nuclear Magnetic Resonance Spectroscopy 37

2.1. N. M. R. Relaxation Times 39
2.1.1. Spin-lattice Relaxation 41
2.1.2. Spin-spin Relaxation 43
2.2. N. M. R. Multipulse Experiments 44
2.2.1. Inversion-recovery 44
2.2.2. Spin-echo 45
2.2.3. Solvent Suppression by Presaturation 46
2.2.4. Distortionless Enhancement by Polarization Transfer 46
2.3. Two-Dimensional N.M.R. 47

2.3.1. J-resolved Spectroscopy 47
2.3.2. Correlated Spectroscopy 48
2.4. Solid State N.M.R. 53
2.4.1. Wide-line Proton N.M.R. 54
2.4.2. Wide-line Deuterium N.M.R. 58
2.4.3. Line-narrowing Techniques: Cross Polarization and Magic Angle Spinning 60
2.4.4. Pulse Sequences in CP/MAS Experiments: Non-Quaternary Carbon Suppression and Total Sidebands Suppression 64

Chapter 3 Materials and Methods 67

3.1. Radical Intermediates in Veratryl Alcohol Oxidation by Ligninase 67
3.1.1. Proton N.M.R. Experiments and Linewidth Measurements 67
3.1.2. Inversion-recovery Experiment 68
3.2. One and Two-dimensional N.M.R. Experiments on Lignin 68
3.2.1. Carbon-13 N.M.R. Experiments 69
3.2.2. Proton N.M.R. Experiments 69
3.2.3. Homonuclear Decoupling Experiment 70
3.2.4. Hahn Spin-echo Experiment 71
3.2.5. Proton N.M.R. Spectra Simulation 71
3.3. Associative and Colloidal Behaviour of Lignin 72
3.3.1. Molecular Weight Determination of Lignin by HPLC Gel-filtration 72
3.3.2. Langmuir Blodgett Trough Experiments 72
3.3.3. Light Scattering Experiments 73
3.3.4. Spin-lattice Proton N.M.R. Relaxation Time of Lignin 74
3.3.5. Effect of pH on Lignin Association: HPLC and SEM Experiments 74
3.4. Wide-line Solid State N.M.R. of Wood 75
3.4.1. Wide-line Proton N.M.R. Experiments 75
3.4.2. Wood Moisture Content Determination by Proton N.M.R. 76
3.4.3. N.M.R. Relaxation Times Measurements 76
3.4.4. Variable Moisture Content Experiments 77
3.4.5. Variable Temperature Experiments 78
3.4.6. Wide-line Deuterium N.M.R. 78
3.4.7. Preparation of Samples for Degradation Experiments 78
3.5. CP/MAS N.M.R. and FT/IR Spectroscopy on Sound and Decayed Wood Cell Walls 79
3.5.1. CP/MAS N.M.R. Spectroscopy Experiments 80
3.5.2. FT/IR Spectroscopy Experiments 81

Chapter 4 Radical Intermediates in Veratryl Alcohol Oxidation by Ligninase 83

4.1. Dependence of Ligninase Activity on pH in Deuterated Medium 84
4.2. ^{1}H-N.M.R. Spectra Following the Veratryl Alcohol Oxidation by Ligninase 85
4.2.1. Effects on the Resonance Linewidths of Veratryl Alcohol 85
4.2.2. Effect on Longitudinal Relaxation Time of Veratryl Alcohol 89
4.3. Effect of the Presence of Radical Cation Intermediates on the ^{1}H-N.M.R. Spectrum of 1,4-dimethoxybenzene 91

Chapter 5 One and Two-dimensional N.M.R. Studies of Lignin 95

5.1. Carbon-13 N.M.R. of Lignin 96
5.1.1. BB-Decoupled and DEPT Carbon-13 N.M.R. Experiments 97
5.1.2. FT/IR Experiments 102
5.2. Proton N.M.R. of Lignin 104
5.2.1. One and Two-dimensional N.M.R. Experiments 104
5.2.2. Homonuclear Decoupling Experiment 115
5.2.3. Hahn Spin-Echo Experiment 117
5.2.4. Electron Spin Resonance Experiment 118
5.2.5. Lignin Spectra Simulation 119
5.3. Lignin: Potential Structural Content 122

Chapter 6 Associative and Colloidal Behaviour of Lignin 129

6.1. Lignin Molecular Weight Determination 130
6.2. Langmuir-Blodgett Trough Experiment: Determination of the Lignin Average Molecular Area 133
6.3. Light Scattering Experiments of Lignin Solutions 136
6.4. Influence of Lignin on Proton N.M.R. Relaxation Times of the Solvent ... 141
6.5. Effect of pH on Lignin Molecular Weight: HPLC Gel-filtration and Scanning Electron Microscopy Experiments 142

Chapter 7 Wide-line Solid State N.M.R. of Sound and Decayed Wood 149

7.1. Wide-line Proton N.M.R. of Wood 150
7.1.1. Moisture Content Determination 150

7.1.2. Proton N.M.R. Relaxation Time Measurements 153
7.1.2.1. T_1 measurements 153
7.1.2.2. T_2 measurements 155
7.1.3. Moisture Content Effects on N.M.R. Relaxation Times of Wood 158
7.2. Wide-line Deuterium N.M.R. of Deuterated Water in Wood: Temperature and Moisture Effects on the Linewidth 162
7.3. Proton Relaxation Times Measurements on Decayed Wood 166

Chapter 8 CP/MAS Solid State N.M.R. and FT/IR Spectroscopy of Wood Cell Wall Biodegradation 171

8.1. CP/MAS Carbon-13 N.M.R. Spectroscopy 171
8.1.1. Optimal Contact Time Determination 172
8.1.2. CP/MAS N.M.R. Spectra of Cellulose, Lignin and Whole Cell Wall 173
8.1.3. CP/MAS Spectra of Pine and Beech Woods 176
8.1.4. CP/MAS Spectra of Degraded Cell Walls 180
8.2. FT/IR Spectroscopy on Cell Wall Degradation 186

Conclusions and Future Perspectives 193

Bibliography 199

LIST OF FIGURES

Figure	**1.1.**	Cell wall multilayers structure	3
Figure	**1.2.**	Cellulose linear structure of repeating cellobiose units	4
Figure	**1.3.**	Parallel arrangement of cellulose chains to form microfibrils	4
Figure	**1.4.**	Model for cellulose enzymatic degradation by cellulases	6
Figure	**1.5.**	Pathways in biosynthesis of lignin precursors from carbon dioxide	9
Figure	**1.6.**	Schematic representation of lignin biosynthesis by action of cell wall peroxidases	10
Figure	**1.7.**	Qualitative depiction of an average conifer lignin structure	11
Figure	**1.8.**	Major oxidation products from various lignins	12
Figure	**1.9.**	Catalytic cycle for ligninase	21
Figure	**1.10.**	Two sequential one-electron oxidations of 1,4-dimethoxybenzene by ligninase	22
Figure	**1.11.**	Biosynthesis of veratryl alcohol from phenylalanine	23
Figure	**1.12.**	Veratryl alcohol oxidation by ligninase	24
Figure	**1.13.**	Products from the oxidation of veratryl alcohol in the presence and in the absence of oxygen	25
Figure	**1.14.**	Catalytic cycle for Mn-peroxidase	28
Figure	**1.15.**	Hypothesis for the ligninolytic system of *P. Chrysosporium*	31
Figure	**1.16.**	Some of the products from the oxidation of β-O-4 methoxylated lignin model compounds	33
Figure	**1.17.**	Two possible pathways for fungal aromatic ring cleavage on non-phenolic and phenolic lignin model compounds	33
Figure	**2.1.**	Energy levels and transitions of a nucleus with I = 1/2	38
Figure	**2.2.**	Aromatic ring current effect on the local magnetic field	39
Figure	**2.3.**	Effect of a radiofrequency pulse B_1 on the bulk magnetization vector	40
Figure	**2.4.**	Motion of two nuclei A and X within a molecule	42
Figure	**2.5.**	Pulse sequence for J-resolved proton N.M.R. experiment	48
Figure	**2.6.**	Pulse sequence for homonuclear and heteronuclear COSY experiments	49
Figure	**2.7.**	Pulse sequence for NOESY experiment	50
Figure	**2.8.**	Proton N.M.R. absorption curve of a two spin system in the solid state	55
Figure	**2.9.**	General behaviour of relaxation times as function of temperature	56

Figure 2.10. Energy levels scheme of a spin 1 nucleus, resulting from Zeeman interaction with the magnetic field and with the quadrupole moment of the nucleus 58
Figure 2.11. Powder pattern resulting from the sum of contributions of the random orientations of a spin 1 nucleus with respect to the magnetic field in a polycrystalline sample 59
Figure 2.12. Thermal contact between carbon-13 and proton spin reservoirs achieved by cross polarization technique 62
Figure 2.13. Cross polarization pulse sequence 62
Figure 2.14. Carbon signal intensity variations in function of the contact time 63
Figure 2.15. Non-protonated carbon selection pulse sequence 64

Figure 3.1. Pulse sequence for inverse-gated decoupling technique ... 71
Figure 3.2. Fluorescence spectrum of organosolv spruce lignin 73
Figure 3.3. Schematic representation of a light scattering apparatus ... 74

Figure 4.1. Ligninase activity as function of pH in deuterated and non deuterated phosphate buffer 85
Figure 4.2. ^{1}H-N.M.R. spectra following the oxidation of veratryl alcohol by ligninase at pH 2.75 86
Figure 4.3. ^{1}H-N.M.R. spectra following the oxidation of veratryl alcohol in the presence of ligninase and hydrogen peroxide; the reaction is quenched after 2 min 87
Figure 4.4. Width at half height of the veratryl alcohol methoxyl resonances 88
Figure 4.5. ^{1}H-N.M.R. spectra showing the decreasing longitudinal relaxation time T_1 of aromatic and methoxyl resonances of veratryl alcohol during oxidation by ligninase 90
Figure 4.6. ^{1}H-N.M.R. spectra following the oxidation of 1,4-dimethoxybenzene by ligninase in presence of hydrogen peroxide 92
Figure 4.7. Hypothetical mechanism of lignin degradation with veratryl alcohol as mediator 93

Figure 5.1. Carbon-13 N.M.R. spectra of organosolv spruce lignin in dimethylsulfoxide-d_6 99
Figure 5.2. Lignin substructures found by carbon-13 N.M.R. 101
Figure 5.3. FT-IR spectra of organosolv spruce lignin 103
Figure 5.4. ^{1}H-N.M.R. spectrum of organosolv spruce lignin in

deuterated dioxane/water (5:1) 105
Figure 5.5. J-resolved ^{1}H-N.M.R. spectrum of the same lignin sample as in figure 5.4. 108
Figure 5.6. ^{1}H-N.M.R. COSY spectrum of the same lignin sample as in figure 5.4. 109
Figure 5.7. ^{1}H-N.M.R. COSY spectra of the aromatic region of 4-hydroxycinnamic acid, 4-hydroxy-3-methoxycinnamic acid, 3,5-dimethoxy-4-hydroxycinnamic acid and organosolv spruce lignin in deuterated tetrahydrofuran 111
Figure 5.8. Spruce lignin substructures 114
Figure 5.9. Proton homonuclear decoupling experiment on aromatic region of organosolv spruce lignin 116
Figure 5.10. Hahn spin-echo ^{1}H-N.M.R. experiment on organosolv spruce lignin in deuterated dioxane-water (5:1) 117
Figure 5.11. First derivative of the E.S.R. absorption spectrum of organosolv spruce lignin in tetrahydrofuran 118
Figure 5.12. Computer simulated and experimental ^{1}H-N.M.R. spectra of lignin model compounds 120
Figure 5.13. Computer simulated ^{1}H-N.M.R. spectra of p-hydroxycinnamic and p-hydroxy-3-methoxycinnamic acids lignin model compound units, at increasing linewidths and compared to the experimental spectrum of lignin 121
Figure 5.14. Picture showing as chemically equivalent doublets in different environments would give rise to sets of COSY 2D ^{1}H-N.M.R. cross peaks 123
Figure 5.15. Structural formula of the lignin fragment considered for molecular modelling 124
Figure 5.16. Open and folded structure of β-O-4 lignin fragment 125
Figure 5.17. Structural formula and geometrically optimized structure of lignin model compound 126
Figure 5.18. Structural formula of 3.4-divanillyltetrahydrofuran and pinoresinol and their relative crystal structures 126

Figure 6.1. MW calibration curve of Zorbax PSM 60S HPLC column with Polystyrene standards in DMF 131
Figure 6.2. HPLC gel-filtration elution profile of organosolv spruce lignin in DMF (Zorbax PSM 60S column) 132
Figure 6.3. Surface pressure versus area per molecule isotherm obtained on the Langmuir-Blodgett trough for a organosolv spruce lignin monolayer on water surface 135

Figure 6.4. Schematic arrangement on water-air interface of a molecular monolayer of a lignin fragment (a) and of tri-p-cresyl phosphate (b) 135
Figure 6.5. Intensity of light scattered by organosolv spruce lignin solutions at 625 nm, as a function of lignin concentration.... 138
Figure 6.6. Exponential decay pattern of the time-correlated function in a dynamic light scattering experiment on a organosolv lignin sample in dioxane water (5:1) 139
Figure 6.7. Schematic representation of possible interactions between two lignin molecular fragments in a lignin aggregate 140
Figure 6.8. HPLC gel-filtration elution profiles of organosolv spruce lignin in DMF pretreated at different pHs 142
Figure 6.9. Results from molecular weight analysis of organosolv lignin exposed at different pHs 143
Figure 6.10. SEM micrographs of organosolv spruce lignin exposed to various pHs 145

Figure 7.1. Wide-line proton N.M.R. spectra of a beech wood sample before (a) and after (b) drying under vacuum 150
Figure 7.2. Free Induction Decay (F.I.D.) of proton N.M.R. signal of a beech sample 152
Figure 7.3. Plot of moisture content values determined by oven dry weight method, against water content values determined from F.I.D. intensities 152
Figure 7.4. Plot of T_1 data from an inversion recovery experiment on a beech sample 154
Figure 7.5. T_2 plot of beech sample obtained sampling the first part of the F.I.D. from a spin-echo experiment 156
Figure 7.6. Plot of T_2 obtained from a CPMG experiment on a beech sample 157
Figure 7.7. T_1 values as function of different moisture contents of a beech sample 158
Figure 7.8. T_2 values as function of different moisture contents of a beech sample 159
Figure 7.9. Multilayer model of water in wood 160
Figure 7.10. Intensities of T_2 components as a function of different moisture contents 161
Figure 7.11. Theoretical and experimental T_2 intensities of free water components at different moisture contents 161
Figure 7.12. Wide-line deuterium (a) and proton (b) N.M.R. spectra of a

beech sample, acquired in parallel during drying 163
Figure 7.13. Linewidth at half height variations of broad (a) and sharp (b) deuterium peaks during drying time intervals 164
Figure 7.14. Linewidth at half height variations of sharp and broad peaks of deuterium as function of temperature 165
Figure 7.15. T_1 increase as function of biodegradation for Scots pine and beech woods 168
Figure 7.16. T_{2s} component increase as function of decay by fungi on pine and beech moist samples 169

Figure 8.1. Plot of free induction decay (F.I.D.) intensities versus variable contact times 173
Figure 8.2. CP/MAS carbon-13 spectra of (a) cellulose, (b) spruce lignin, (c) addition of (a+b), and (d) whole cell walls from pine wood 174
Figure 8.3. CP/MAS-TOSS carbon-13 spectrum of pine wood 176
Figure 8.4. CP/MAS carbon-13 spectra of (a) pine and (b) beech woods 177
Figure 8.5. CP/MAS TOSS-NQS carbon-13 spectrum of pine wood ... 179
Figure 8.6. CP/MAS carbon-13 N.M.R. spectra of pine woods: (a) sound control, (b) subjected to brown-rot decay by *Coniophora puteana*, (c) subjected to white-rot decay by *Coriolus versicolor* 181
Figure 8.7. CP/MAS carbon-13 N.M.R. spectra of beech woods: (a) sound control, (b) subjected to brown-rot decay by *Coniophora puteana*, (c) subjected to white-rot decay by*Coriolus versicolor* 182
Figure 8.8. CP/MAS carbon-13 difference spectra 183
Figure 8.9. Dry-weight percent lignin content evaluated from integration of CP/MAS carbon-13 spectra of pine and beech samples before and after brown rot or white rot attack 185
Figure 8.10. FT/IR diffuse reflection spectra of pine (red trace) and beech (violet trace) woods 187
Figure 8.11. FT/IR diffuse reflection spectra of pine woods: sound control (violet trace); after brown rot attack (red trace); after white rot attack (blue trace) 189
Figure 8.12. FT/IR diffuse reflection spectra of beech woods: sound control (blue trace); after brown rot attack (violet trace); after white rot attack (red trace) 190
Figure 9.1. Schematic model for mechanism of lignin degradation ... 196

LIST OF TABLES

Table	**5.1.**	Organosolv spruce lignin carbon-13 chemical shifts assignments	100
Table	**5.2.**	Lignin IR absorption band assignments	102
Table	**5.3.**	Chemical shift assignments of ^{1}H-N.M.R. signals of organosolv spruce lignin	106
Table	**5.4.**	Chemical shift assignments of ^{1}H-N.M.R. signals of 4-hydroxycinnamic acid, 4-hydroxy-3-methoxycinnamic acid and 3,5-dimethoxy-4-hydroxycinnamic acid	112
Table	**5.5.**	Resonances chemical shifts from 2D ^{1}H-N.M.R. signals of organosolv spruce lignin	113
Table	**6.1.**	HPLC gel-filtration of polystyrene MW standards in DMF (Zorbax PSM 60S column, flow 1 ml/min)	130
Table	**6.2.**	Organosolv spruce lignin HPLC gel-filtration fractions	132
Table	**6.3.**	Viscosity values of soluble lignins, xylan and cellulose of MW 50000	139
Table	**6.4.**	T_1 relaxation times of dioxane-water 5:1 with and without lignin and at different temperatures	141
Table	**7.1.**	T_1 values of wood samples	154
Table	**7.2.**	T_2 relaxation times calculated by analysis of the peak linewidths (T_2^*), and by Gaussian fitting on F.I.D. echo intensities (T_2)	156
Table	**7.3.**	T_2 relaxation times obtained from CPMG experiments	157
Table	**7.4.**	T_2 relaxation times from a beech sample at different moisture contents	160
Table	**7.5.**	Variation of quadrupole constant C of deuterium at different deuterated water contents in a beech sample during drying time intervals	164
Table	**7.6.**	Relaxation time values of wood samples before and after fungal decay	167
Table	**8.1.**	Assignments of carbon-13 chemical shifts of CP/MAS N.M.R. spectra of wood	178
Table	**8.2.**	Percentage composition of pine and beech woods	180
Table	**8.3.**	Assignments of FT/IR bands of wood spectra	188

To my Mother

and *in memoriam* of my Father

Chapter 1

INTRODUCTION

1.1. Cell Wall: Structure, Composition and Biotechnological Importance

The cell wall is a robust protective structure external to and in contact with the plasma membrane, surrounding the plant cell. This structure is particularly developed in conducting tissue of woody plants, where cells died in maturity leaving their external organization to form tracheids and fibres. It is composed of three major biopolymers: cellulose (47%), hemicelluloses (33%) and lignin (20%), arranged to form a multilayered structure with different composition, as shown in figure 1.1.

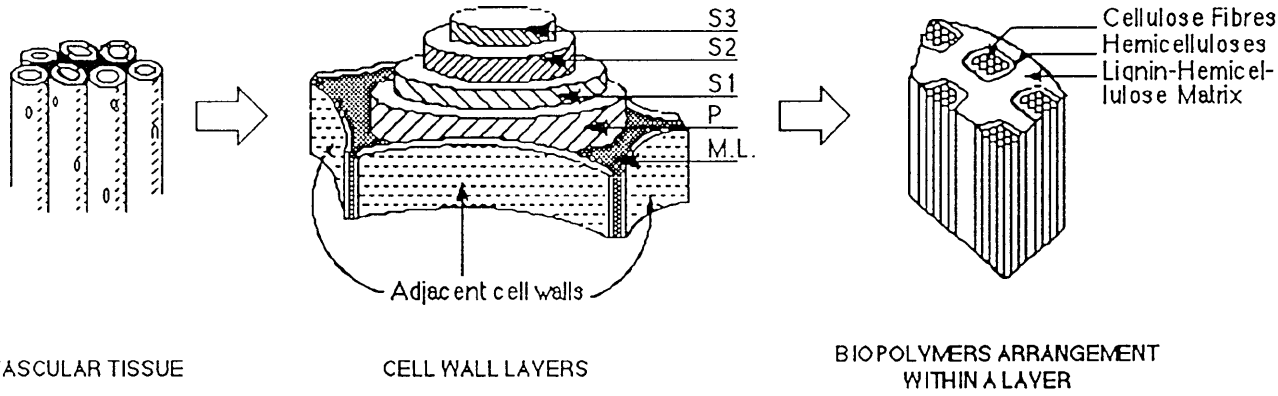

Figure 1.1. Cell wall multilayers structure: S = secondary wall (S1 first layer, S2 second layer, S3 third layer); P = primary wall; M.L. = middle lamella (structure between adjacent cell walls).

This assembly of biopolymers confers properties of high tensile strength and durability to wood, but at the same time is susceptible to biological decay of biotechnological interest.

1.1.1. Cellulose

Cellulose is the major polysaccharide in woody and fibrous plants (about 47% by weight), and is the most abundant polymer in the biosphere. It is a linear polymer of

D-glucose connected by ß(1-4) glycosidic bonds, with cellobiose as repeat unit (figure 1.2.).

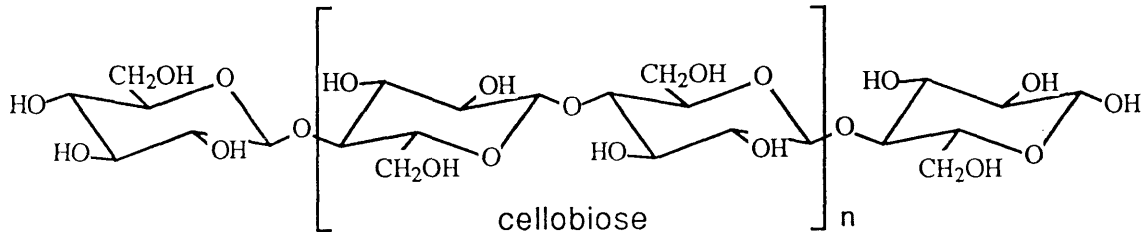

Figure 1.2. Cellulose linear structure of repeating cellobiose units.

The cellulose molecule is a linear chain of about 10000 anhydroglucose units, where each glucose residues in cellulose is flipped by 180° with respect to its neighbour, leading to a fully extended chain which can form ribbons in a side by side association with other chains through a network of intra and intermolecular hydrogen bonds as shown in figure 1.3. (Mathews and van Holde, 1990).

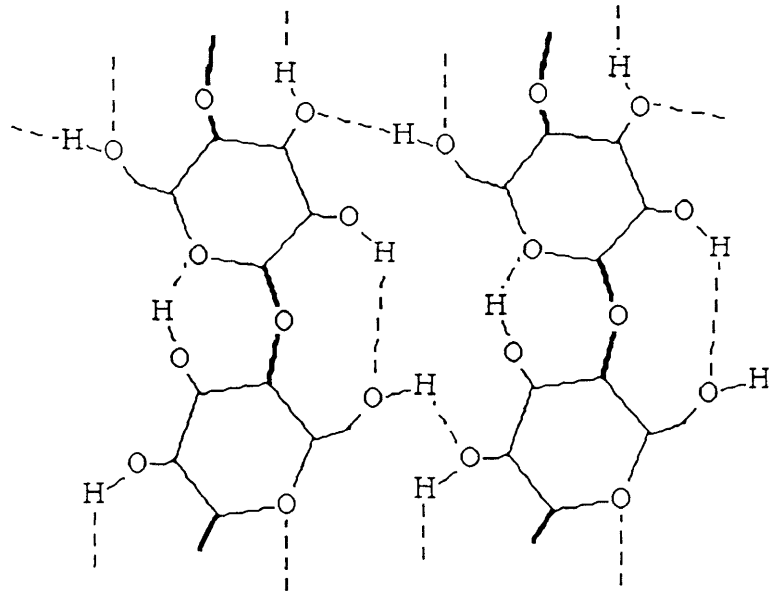

Figure 1.3. Parallel arrangement of cellulose chains to form microfibrils. Cellulose has a planar structure caused by β(1-4) linkages between glucose units (bold lines); the chains are linked together by a network of hydrogen bonds (dashed lines).

Chains of cellulose associate to form microfibrils of 35 Å diameter, which in turn link to form cellulose fibrils conferring great mechanical strength but limited extensibility to the cell wall (Chanzy, 1985). Fibril regions with strong interchain forces are known as crystalline regions, they are usually interspersed with para-crystalline or amorphous regions.

The resistance of cellulose to hydrolysis is caused by both the nature of ß(1-4) bonds and the crystalline state, preventing enzyme access to the inner microfibrils; however ß(1-4) linkages can be hydrolysed by cellulases, enzymes produced only by certain bacteria and fungi (Ljungdahl, 1989; Wood, 1989).

The biodegradation of cellulose is not the major focus of this thesis, but a brief mention is made, as the solid state N.M.R. studies presented in chapter 7 and 8 have been concerned with the degradation of both polysaccharidic and lignin components of whole cell walls.

Cellulases are enzyme systems comprising three main components: endoglucanase, exoglucanase (cellobiohydrolase) and ß-glucosidase (cellobiase). Bacterial cellulases are mainly cell-bound and have received little research attention until recently. Fungi tend to produce extracellular cellulase, and those from *Trichoderma reesii*, *Trichoderma viride*, *Trichoderma koningii*, *Fusarium solanii* and *Phanerochaete chrysosporium* are the most well characterized (Wood, 1985; Eveleigh, 1987). Literature data suggest that cellulase components cooperate in the polysaccharide degradation, and not all cellulases are able to hydrolyse both the amorphous and the crystalline cellulose forms.

The endoglucanases tend to attack cellulose at multiple internal sites in amorphous zones, producing water soluble oligosaccharides. They cannot hydrolyse crystalline cellulose or cellobiose, and are inhibited to some extent by cellobiose and glucose. These enzymes alone are able to hydrolyse soluble amorphous carboxymethylcellulose (CM-cellulose).

The exoglucanases (cellobiohydrolase) are able to split off cellobiose units from non-reducing end of cellulose. These enzymes are a major constituent of cellulose complex from microorganisms able to degrade crystalline cellulose, although when alone, they are essentially unable to to hydrolyse crystalline cellulose. Exoglucanases are unable to hydrolyse CM-cellulose and are strongly inhibited by both cellobiose and glucose.

Several other enzymes are involved in the hydrolysis of cellobiose, decreasing its concentration and overcoming any cellobiose inhibition of endoglucanases and exoglucanases. ß-glucosidase (cellobiase) hydrolyses cellobiose and soluble oligosaccharides to glucose, but cannot attack cellulose, it is inhibited by glucose.

Cellobiose oxidase, oxidises the C-1 hydroxyl at the reducing end of cellobiose in a coupled reaction involving reduction of dioxygen to superoxide (Ayers et al., 1978; Morpeth, 1985). This enzyme has a molecular weight of 74-93 kD, it contains cytochrome b_3 and flavin as a prosthetic groups, which is held by non-covalent interactions to the single peptide chain.

Cellobiose quinone oxido-reductase is an enzyme similar to cellobiose oxidase, and oxidises cellobiose to cellobiolactone (Westermark, 1974a; Westermark,

1974b). This enzyme has a molecular weight of 60 kD and contains flavin like cellobiose oxidase but has no haem.

A synergistic effect occurs for mixture of exoglucanases and endoglucanases. These enzymes cooperate to cause extensive degradation of ordered cellulose, showing a maximum efficiency when ß-glucosidase is also present, not because this enzyme takes part in the solubilization process, but because it removes the inhibiting effects of cellobiose (Wood and McCrae, 1979). It is relevant to note that multiple forms of each the enzymes outlined above have now been identified, varying in isoelectric point, size, carbohydrate content and composition, amino acid composition and frequently substrate specificity as well.

A simple model of cellulases action has been proposed by Wood in 1985, and is reported in figure 1.4. According to this model, the endoglucanases are thought to initiate the attack on cellulose at multiple internal sites in amorphous zones; then the exoglucanases attack the newly generated non-reducing termini, sequentially cleaving off cellobiose residues from the glucan chain. ß-glucosidases cleave cellobiose and soluble oligomers to glucose, relieving the inhibitory effects of cellobiose on the former two enzymes.

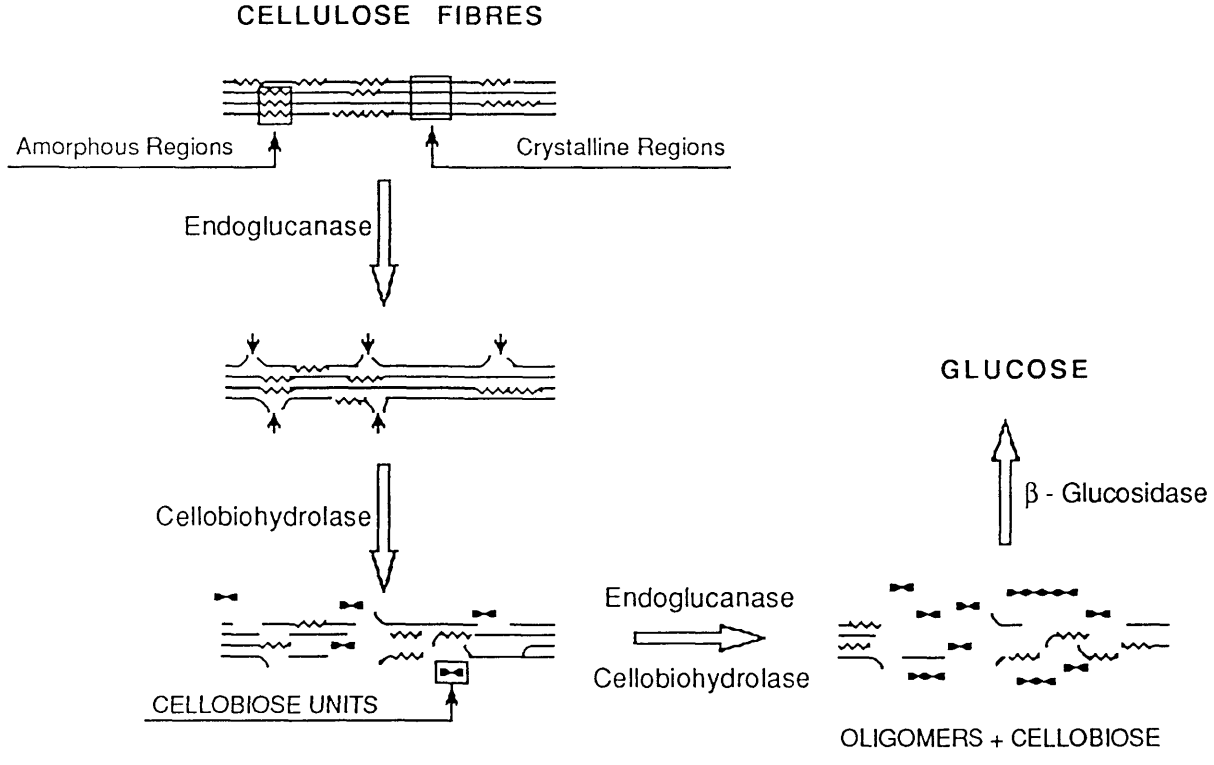

Figure 1.4. Model for cellulose enzymatic degradation by cellulases (Wood, 1985).

1.1.2. Hemicelluloses

Hemicelluloses are a heterogeneous group of branched amorphous polysaccharides that represent 20-40% by weight of the total cell wall. They are closely associated with cellulose cementing the microfibrils together, as well as being covalently bound to lignin to give a lignocarbohydrate complex.
Hemicelluloses are heteroglycans containing a variety of pentoses (xylose and arabinose), hexoses (glucose, galactose and mannose) and uronic acids, with degree of polymerization varying between 100 and 200 monosaccharide units. Depending on the origin, they have different types of sugar residues, with short appendages linked to the main backbone chain. There are four predominant types of hemicelluloses recognised: xylans, D-mannans, galactans and D-arabinans.
As the other cell wall biopolymer, hemicelluloses are susceptible to biodegradation: the enzymes involved in their degradation are classified according to the type of substrate hydrolysed. The enzymes degrading xylans might include (1-4)-ß-xylananses, ß-D-xylosidases, α-L-arabinosidases and α-D-glucuronidases, whereas enzymes degrading mannans include (1-4)-ß-D-mannanase, ß-D-mannosidase, ß-D-glucosidase and α-D-galactosidase (Puls and Poutanen, 1989; Zimmermann, 1989).
L-arabinases are usually secreted extracellularly and can be divided in exoarabinases and endoarabinases. The latter are the most studied and are able to degrade L-arabinan completely to L-arabinose, attacking the substrate from the non-reducing end by a multichain mechanism. D-galactanases are hydrolytic enzymes capable of degrading D-galactans and L-arabino-D-galactans. Other enzymes involved in hemicelluloses degradation are D-mannanases, degrading (1-4)-ß-D-mannopyranosyl linkages of D-mannans and D-galacto-D-mannans, (1-3)-ß-D-xylanases, constitutive enzymes secreted extracellularly, and (1-4)-ß-D-xylanases.

1.1.3. Lignin

Lignin represents 20% by weight of the cell wall biopolymers; it is abundant in woody tissues of vascular plants, and it is the second most abundant organic material, next to cellulose, in nature (Crawford 1981). From the chemical point of view, lignin is a polyaromatic macromolecule, composed of phenylpropane units linked by many stable carbon-carbon and ether bonds (Sakakibara, 1980). It is closely associated to the cellulose fibres, and it has been shown to be chemically bonded to hemicelluloses. Lignin is the last cell wall component to be laid down

and occurs when the cell wall surface growth has ceased as this process represents the ultimate stage prior cell degeneration and necrosis. It has been shown that the initial deposition of lignin takes place in the primary wall (P in figure 1.1.) at the cell corners. Lignification then extends to the intercellular spaces (middle lamella, M.L.), and also into the secondary wall (S) where lignin is deposited around the cellulose microfibrils.

Lignin has a major function in maintaining the cohesion of cell walls in the plant structure and because of its hydrophobic nature, it is responsible for the impermeability of the vascular tissues, and the resulting compartmentation facilitates the conducting functions of these tissues and protects the plant against microbial attack. Lignin is regarded as a heterogeneous biopolymer, synthesized by plants from carbon dioxide by way of shikimic acid (Higuchi et al., 1977). Shikimate is converted to L-phenylalanine, which precedes the three lignin precursors: p-coumaryl alcohol, coniferyl alcohol, and sinapyl alcohol (figure 1.5.). The cinnamyl alcohol is polymerized enzymatically by peroxidases, which occurs *via* random free radical coupling of the three alcohols. The lignification process occurs to a site removed from the cell membrane through which the monomers pass; the transport mechanism of monomers from the cytoplasm to the polymerization site in the cell wall, can be explained with the involvement of vesicles derived from the Golgi apparatus and the endoplasmic reticulum. Lignin precursors are transported as glycosidic derivatives in these vesicles, and are regenerated in the cell wall by action of a specific β-glucosidase (in Lewis and Yamamoto, 1990). At present virtually nothing is known about the enzymology of lignin formation; in general is only known that indeed this process is not casual but carefully orchestrated by the growing plant. For example it appears that a precise selection of monolignols is controlled by the cytoplasm at different developmental stages: it has been reported that different monomers are incorporated into the lignin framework of various subcellular locations at different stages of development. For example p-coumaryl alcohol (figure 1.5.) is preferentially deposited in the cell corners during initial stages of lignin deposition (in Lewis and Yamamoto, 1990). This temporal and spatial distribution differences may have profound effects on lignin structure in diverse subcellular locations.

The lignin polymerization is initiated by specific cell wall peroxidases that catalyse the one-electron oxidation of lignin precursors, producing phenoxy-radicals that can exist in several mesomeric forms. Coupling reactions occur between almost all of them, leading to different interunit C-C and C-O-C linkages for each alcohol, as shown in figure 1.6. The molar ratio of the different monomers, depends on the nature of the plant species, plant tree and within tissue of the same plant (Chen, 1989).

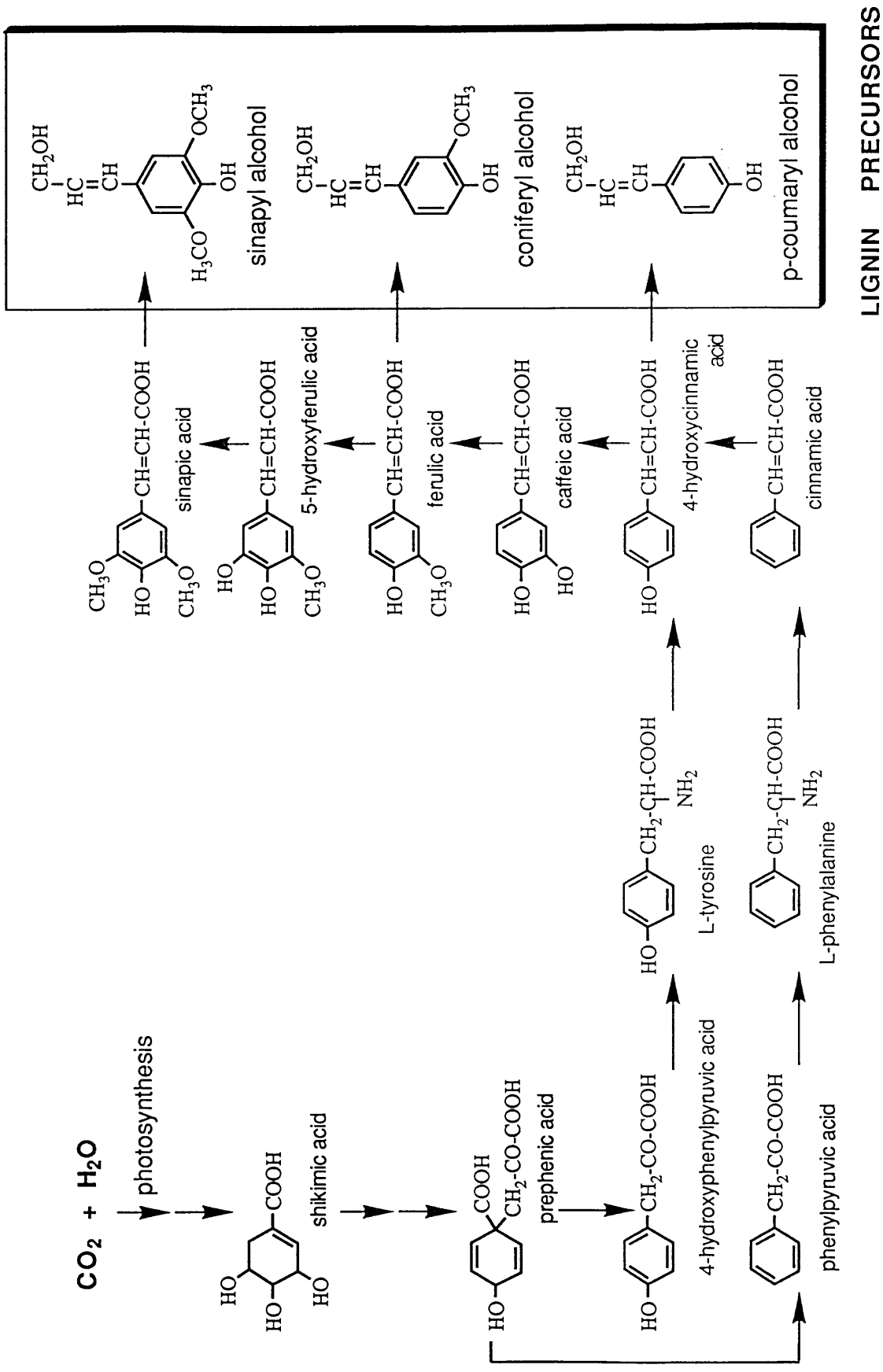

Figure 1.5. Pathways in biosynthesis of lignin precursors from carbon dioxide (adapted from Higuchi et al., 1977).

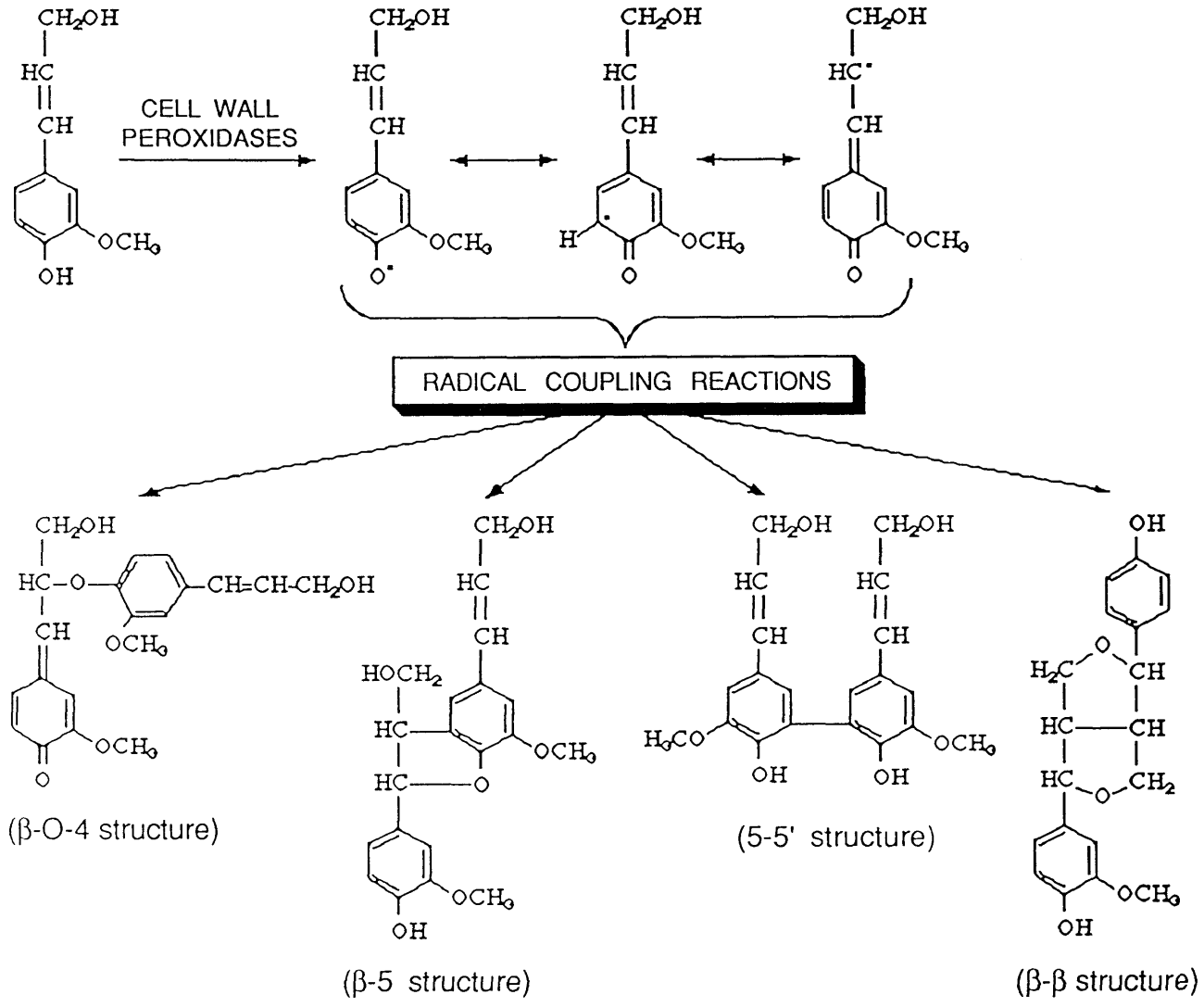

Figure 1.6. Schematic representation of lignin biosynthesis by action of cell wall peroxidases.

The structural analysis of lignin presents a fundamental problem: lignin can not be isolated in its native "unaltered state". Therefore structural representation of lignin such as that reported in figure 1.7., relies on the analysis of soluble lignin-derived preparations, that involved physical (solvent extraction), chemical (acidic hydrolysis) or biological (enzymatic) treatments. Some lignin preparations use strong chemical treatments (72% sulphuric acid for Kraft lignins), that can be expected to cause considerable chemical alterations. Few lignin isolation procedures such as those yielding to Bjorkman or Organosolv lignins, have been reported to be less severe. Bjorkman lignins, known as milled wood lignin, are

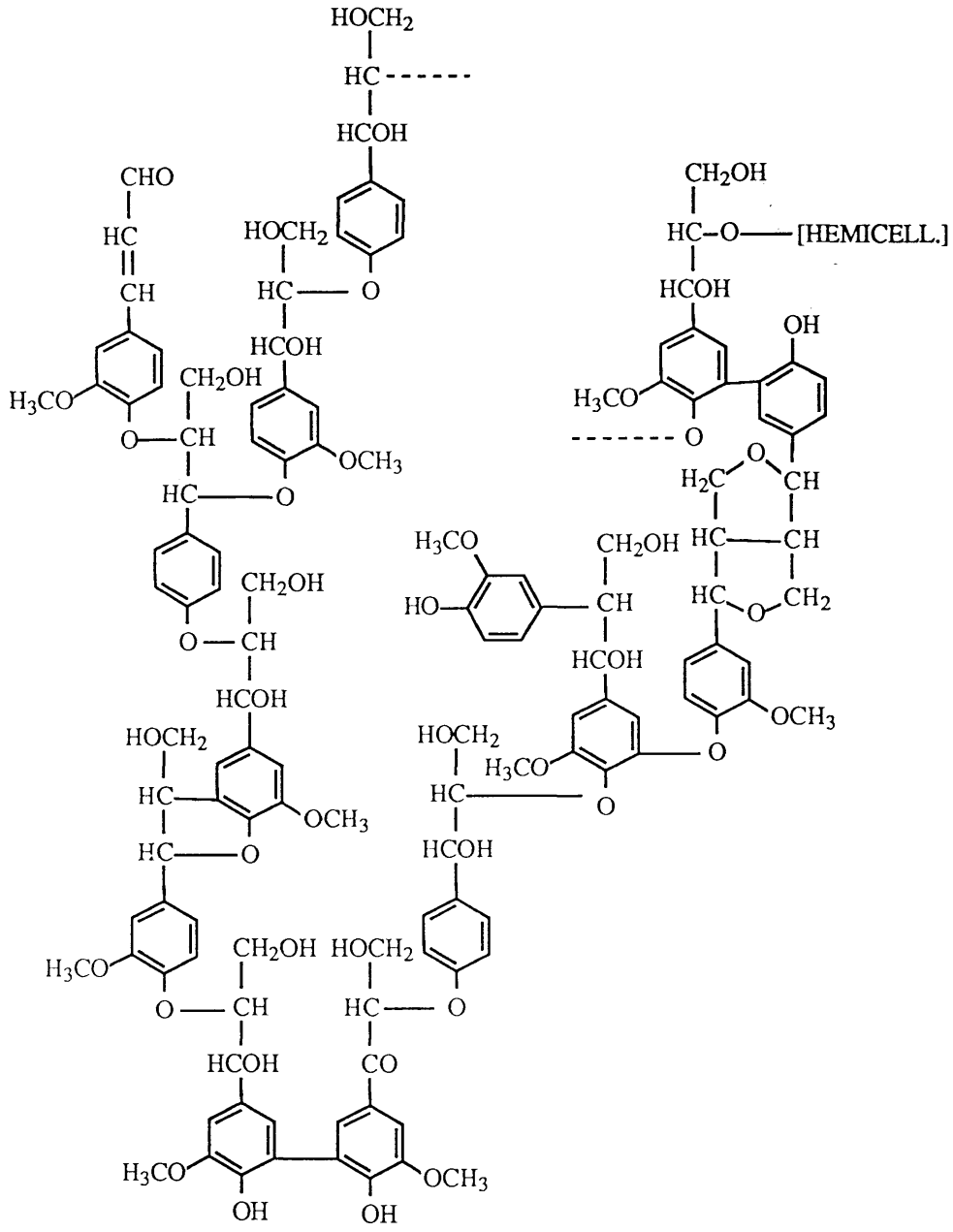

Figure 1.7. Qualitative depiction of an average conifer lignin structure (modified from Adler, 1977).

isolated from aqueous p-dioxane extract of finely milled wood, which has been first extracted with organic solvents to remove extraneous components. Organosolv lignins are extracted by mixture of organic solvent (aqueous ethanol and aqueous dioxane) at elevated temperatures (135-165°C), (Crawford, 1981). Once isolated, the elucidation on the lignin monomer and interunit linkages composition, is routinely carried out by various degradation processes. These consist on oxidations (alkaline nitrobenzene or permanganate oxidation) or hydrolysis (acidolysis or thioacidolysis) reactions, and the nature of their products allow a classification of lignins (Higuchi, 1977; Chen, 1989):

i. Guaiacyl lignins, also called softwood lignins, mainly contain 4-hydroxy-3-methoxy aromatic rings and are typical of gymnosperms. Vanillin is their major oxidation product (figure 1.8.).

ii. Guaiacyl-syringyl lignins, also called hardwood lignins, contain 4-hydroxy-3-methoxy and 3,5-dimethoxy-4-hydroxy aromatic rings and are typical of angiosperms. Their oxidation products are vanillin and syringaldehyde.

iii. Guaiacyl-syringyl-p-hydroxyphenyl lignins, contain 4-hydroxy, 4-hydroxy-3-methoxy and 3,5-dimethoxy-4-hydroxy aromatic rings and are typical of grasses. Their oxidation leads to 4-hydroxybenzaldehyde, vanillin and syringaldehyde.

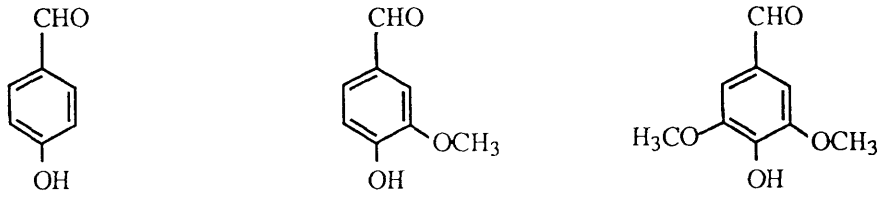

p-HYDROXYBENZALDEHYDE VANILLIN SYRINGALDEHYDE

Figure 1.8. Major oxidation products from various lignins.

The re-examination of lignin in the light of more recent analytical tools may offer new information on the lignin structure. An example is offered by the Nuclear Magnetic Resonance (N.M.R.) spectroscopy; this non-destructive technique can provide information on the cell wall at the molecular level. Results obtained from this approach are reported in the chapter 5 of this thesis.

1.1.4. Biotechnological Importance of the Cell Wall

Cell wall components are the most abundant organic materials in the biosphere: cellulose being the first and lignin the second.

Vegetal cells accumulate these polymers by trapping the sun's radiant energy with the process of oxygenogenic photosynthesis, converting carbon dioxide and water into organic molecules, mainly biomass.

However, the carbon and oxygen that had been temporarily sequestered in biomass, can be mineralized again to the level of simple inorganic substrates. This can happen because cellulose, hemicelluloses and lignin are biodegradable. The biodegradation process is often slow, especially for lignin, and it is probable that decomposition of lignins is the rate-limiting step in the biospheric carbon-oxygen cycle. This rate-controlling step is mediated by the catabolic activities of specific microorganisms (Crawford, 1981).

Biotechnology implies the technical utilization of biological processes that can lead to materials of interest to industry, by using organisms, enzymes or other type of biologically active molecules. In this view, the degradation of lignocellulosic materials is without doubt an interesting possibility for biotechnology.
Although there have been many attempts to develop industrial processes for the conversion of waste lignocellulosics to useful products, limited success has been achieved, as the bioconversion is limited by the intimate association of plant polysaccharides with lignin. This association acts as barrier to the removal and utilization of valuable polymer carbohydrates.
The importance of lignin as a barrier to microbial degradation of plant tissues is exemplified in the observation that lignification is an important mechanism of disease resistance in plants.
However, there is a great potential for the use of microorganisms to biologically transform plant materials and agricultural residues into industrially valuable products. Potential substrates for microbial conversions include agricultural wastes and surplus products, urban solid wastes, pulpmill wastes from the paper industry and peat. Desirable goals for microbial bioconversion of lignocellulosics include bioconversion of industrial lignins to chemicals such as polyphenols, binders, adhesives, organic acids, methane, glucose, alcohols and perhaps petrochemical substitutes (Farrell, 1987; Parisi and Parisi, 1989).
A considerable benefit from biomass conversion lies in its potential to supply motor fuels, perhaps in the future enough to offset shrinking world reserves of petroleum, and to avoid environmental damage from burning petrol in pistol engines. The attraction offered by biomass lies also in its renewable nature, availability and quantity, and an increase in its utilization would decrease the dependence from non renewable imported oil (Wayman and Parekh, 1990).

Between the wood components, certainly cellulose is the most exploited by industry. Industrial use of cellulose is focussed mainly on paper industry, but also manufactures for conversion to film (i.e. cellulose acetate, cellulose nitrate) or fibres (i.e. cotton, viscose rayon) or other regenerated derivatives. An alternative use of cellulose is a treatment with enzymes as cellulases and ß-glucosidase to hydrolyse the polysaccharide to glucose; glucose so formed may be fermented to ethanol.
Enzyme treatment of hemicelluloses could lead to xylose, which can be further hydrogenated to xylitol. Xylitol is a non-cariogenic and insulin-independent sweetener, widely used in chewing gum. Xylose can also be dehydrate to furfural, furan or tetrahydrofuran for the uses of chemical industry (Parisi and Parisi, 1989).
The pulping industry produces enormous amount of lignin wastes, the major part of which are burned as fuel within the industrial plant itself. This is because this

byproduct is regarded as a complicated mixture of partially degraded and partially condensed aromatic complexes. However, a better understanding of lignin structure, biochemical pathways and mechanism of degradation by certain microorganisms, can notably change this view.
Lignin may be a potential versatile source of aromatic compounds which can be of interest of the chemical industry. For example, an important lignin derivative is vanillin, a widely used flavouring agent, and also raw material for production of L-dopa, a pharmaceutical used for treatment of Parkinson's disease. Another potential application is to use lignin as source of feedstock for biobased plastics.

A better cognition of wood chemistry and the biochemistry involved in its microbial degradation, would support many biotechnological applications in the future. An example is given by the pulp and paper industry: the spent liquor from conventional bleaching of chemical pulps when released into receiving waters, represents the most important environmental problem caused by this kind of industry. These waste waters contain acutely toxic aromatic chlorinated compounds, which are unstable and can evolve in more persistent and toxic chlorinated veratroles or dioxins (Eriksson, 1989). Understanding the enzymatic mechanisms involved in lignin degradation could facilitate a biotechnological approach to this problem. New biotechnical processes for bleaching wood pulps (Farrell, 1987), or the use of ligninolytic system to develop efficient waste water purification treatments (Eriksson, 1989) can offer a solution.

1.2. Lignin Biodegradation

The previous paragraph examined the structure, organization and biotechnological relevance of the plant cell wall. It has been considered as the photosynthetic production of the cell wall is balanced in nature by the degradative activity of different wood degrader organisms. It seems that the cell wall structural components, cellulose, hemicelluloses and lignin are designed not to be easily degraded, and furthermore even when the individual polysaccharides can actually be degraded fairly easily by particular enzymes or microorganisms, their complex combination in wood presents much more difficult problems. In particular, in surrounding the individual cellulose fibres, the lignin component effectively protects them against microbial attack. However, some microorganism are able to degrade this aromatic polymer. The study of the lignin biodegradation is the concern of this thesis and the present knowledge on the microorganisms and enzyme involved in the process are examined in this section.

1.2.1. Microbiology

In the past years a variety of saprophytic microorganisms, ranging from Bacteria, *Fungi Imperfecti* and *Actinomycetes*, were thought to be capable of lignin degradation under aerobic or anaerobic conditions. The apparent inability of microorganisms to use lignin as sole carbon/energy source for growth, precludes the isolation of lignin degraders by standard enrichment procedures and the use of growth on lignin as criterion for degradative ability.
In the light of more recent data, only aerobes and mainly wood decomposing members of *Basidiomycetes*, are found to metabolize lignin efficiently (Crawford, 1981). Members of other taxa can only degrade lignin partially.
Microorganisms that are able to degrade lignin, are essentially the same ones that can degrade intact wood, due to the protective function of lignin on cellulose and hemicelluloses from enzymatic attack. Even though a wide range of bacteria and fungi degrade isolated cellulose and hemicelluloses, only those with ligninolytic capability gain access to these polymers in intact wood. Experiments conducted on carbon-14 labelled lignins under anaerobic conditions revealed no degradation process in absence of oxygen. On the other hand, anaerobic metabolism of isolated cellulose, hemicelluloses and finely ground wood is well known. The lack of lignin degradation in absence of molecular oxygen may be related to the molecular size of the polymer. Thus, low molecular weight aromatics (less than 300 daltons) related to lignin are metabolized anaerobically, whereas high molecular weight ones (more than 850 daltons) are not. This result suggests that the initial fragmentation of the lignin polymer apparently requires oxygen.

1.2.1.1. Bacteria

Numerous bacteria have been reported in early papers to decompose lignin, but weaknesses in experimental methods may have led to erroneous or questionable conclusions (Kirk, 1971).
Some Bacteria, including strains of *Nocardia* and *Streptomyces* are known to mediate a certain amount of lignin degradation, but their true ability in this regard is not clear. *Nocardia* can degrade synthetic lignin (a dehydrogenation polymer, known as DHP), but does not efficiently attack the natural polymer associated with an organised cell wall (Crawford D.L. and Crawford R.L., 1980 and 1984). These organisms can cause slow and partial degradation of isolated lignin; studies conducted with carbon-14 lignin specifically labelled on the side chain, aromatic ring and methoxyl groups, showed that all three structural components are converted to ^{14}C-enriched carbon dioxide to various extent (Trojanowski et al., 1977).

It seems that grass lignin and lignin in phloem tissues may be more susceptible to bacterial degradation than are lignins in xylem tissues of woody plants. It is important to note that is not clear whether bacteria degrade lignin in the absence of an alternative energy source.
In summary, the ability to decompose lignin shown by bacteria is very slow and much less extensive than that shown by fungi; therefore they play a secondary role in lignin biodegradation.

1.2.1.2. Soft-rot Fungi

Soft-rot fungi attack wood under conditions of high humidity, causing softening of surfaces of the woody tissues, accompanied by weight loss. Various soft-rots of wood are caused by members of *Fungi Imperfecti* and *Ascomycetes*. . These decays involve lignin degradation, although many soft-rotters studied showed to attack preferentially the polysaccharides (Buswell and Odier, 1987). Lower fungi, *Phycomycetes* are known to degrade wood. Very little attention has been spent on these microorganisms, whose enzymology is still not clear.

1.2.1.3. Brown-rot Fungi

The major wood decays are caused by *Basidiomycetes*. Depending on the appearance of the rotted substrate, *Basidiomycetes* can be divided as white-rot and brown-rot fungi .
Brown-rot fungi are usually defined as those wood-rotting fungi that decompose and remove mainly carbohydrates, leaving a residue of modified lignin that is typically dark-brown and almost equal in weight to the lignin in the original wood (Kirk, 1971). Evidences indicate that brown-rot fungi degrade cellulose and hemicelluloses in intact wood; their oxidative action can penetrate the woody matrix (Kirk and Shimada, 1985). Because lignin apparently presents no real barrier to the brown-rot fungi, they seem to be an exception to the generalization that only lignin degraders can attack intact wood. The brown lignin residue left in brown-rotted wood is often called "enzymatically liberated lignin", and it has been found to be chemically modified as compared to lignin of sound wood (Kirk and Shimada, 1985), with a lower methoxyl content and a higher phenolic hydroxyl and carboxyl groups content (Kirk and Adler, 1970; Kirk, 1975a). The process is largely oxidative: demethylation of phenolic or non-phenolic units is the major degradative reaction. Studies conducted on spruce wood, showed that the lignin methoxyl content was decreased to 35% after brown-rot attack, with a concomitant increase in phenolic hydroxyl groups. Also the number of α-carbonyl and carboxyl groups were increased, reflecting the oxidative nature of the degradative attack (Buswell and Odier, 1987). These fungi appear initially to decay lignin in a manner similar to

white-rot fungi with demethylations, hydroxylations, but studies using carbon-14 labelled lignin showed that brown-rot fungi have limited ability to degrade side chain and aromatic ring moieties in lignin (Kirk et al., 1975b).
Therefore, when compared to white-rot fungi, brown-rot appear less capable to complete lignin breakdown. This suggests that their ligninolytic system lacks of certain components present in white-rot; little attempt has been made to optimize conditions for lignin biodegradation by brown-rot fungi.

1.2.1.4. White-rot Fungi

White-rot *Basidiomycetes* are probably the most efficient lignin degraders, and are considered to the main agents of lignin decomposition in nature. They are able to extensively decompose all the important structural components of the cell wall to the stage of carbon dioxide and water. These fungi characteristically produce extracellular enzymes involved in the process of lignin degradation and deplete the lignin and carbohydrate components of wood at about the same proportional rates (Crawford, 1981). Amongst these fungi *Phanerochaete chrysosporium* (*Sporotrichum pulverulentum*) is the most widely studied and the best lignin degrader found so far. Extensive studies conducted on optimized culture conditions for lignin biodegradation (Kirk and Farrell, 1987a), have shown that lignin degrading enzymes of *P. chrysosporium* are produced only during secondary metabolism. The composition of the growth medium employed, can influence the results of investigations of wood component degradation patterns and the production and activity of the ligninolytic system; the presence of readily utilizable growth substrate other than lignin, presence of oxygen, nitrogen, medium pH and culture agitation have marked effects on lignin degradation rates (Kirk and Farrell, 1987a). Considerable influence is also showed by the presence of carbohydrates in the growth medium, cellulose or glucose being obligate co-substrates. Lignin degradation *in vivo* always occurs simultaneously with degradation of at least one of the cell wall polysaccharides. It appears that lignin in its natural condition is not a readily utilizable carbon/energy source. For unknown reasons, the net energy gain from lignin may be insufficient to support growth, or lignin degradation occurs too slowly to sustain some minimal essential metabolic rate and the process is transiently interrupted if more carbohydrates are added in the cultural media (Buswell and Odier, 1987). The necessity of minimal levels of cellulose or glucose as co-substrate, might serve to provide sufficient energy to support the synthesis of lignin degrading enzymes the production of hydrogen peroxide associated with some of these enzymes' activities, and possibly to support the potential effectors of the ligninolytic system, for example veratryl alcohol.

Increased oxygen levels in fungal culture have been shown to considerably enhance lignin degradation. No degradation has been detected in anaerobic conditions; absence of anaerobic mineralisation of lignin is probably the basis for the formation of coal and peat deposits in the biosphere (Kirk and Farrell, 1987a). The stimulative effect of molecular oxygen on lignin biodegradation is complex and probably involve the interaction of several factors. Oxygen could enhance the hydrogen peroxide production required by the peroxidases of the ligninolytic systems. High oxygen concentrations have also been reported to enhance *de novo* synthesis of the secondary metabolite veratryl alcohol in cultures of *P. chrysosporium* (Shimada et al., 1987). This metabolite in turn is known to increase the titer of ligninase, a peroxidase that is part of the ligninolytic system of the same fungus.

Nitrogen level also have influence: limitation of nitrogen sources triggers the onset of secondary metabolism, with subsequent formation and activity of the lignin degrading system. The production of the ligninolytic system is repressed by addition of L-glutamate, glutamine and histidine (Kirk and Farrell, 1987a). The pH of the culture medium strongly influences lignin degradation by *P. chrysosporium* . Activity was only observed between pH 3.5 and 5.5, with an optimum at pH 4.5, which probably reflects the average optimum for several degradation steps, as for example ligninase maximum activity is shown at pH 2.75. The effect of agitation is still not clear. Early studies reported a suppression on ligninolytic activity by culture agitation; this was explained by the formation of fungal pellets, in which the oxygen concentration may be too low for biosynthesis and activity of ligninolytic enzymes (Faison and Kirk 1985). However, more recently lignin oxidation in agitated cultures have been detected in several laboratories (Buswell and Odier, 1987).

Induction experiments show that the rate of degradation is considerably enhanced when higher concentrations of lignin are used (Ulmer et al., 1984; Faison et al., 1986). The stimulation effect is not apparent until 24 hours after the addition of lignin; it is probable that lignin breakdown products are the potential inducers.

Also veratryl alcohol (3,4-dimethoxybenzyl alcohol), a secondary metabolite, was found to be able to induce the biosynthesis of lignin degrading enzymes (Leisola et al., 1984; Faison et al., 1986). This molecule seems to play a relevant role in the lignin biodegradation process, as will be extensively discussed later.

White-rotted lignins contains more oxygen, more carbonyl groups and more carboxyl groups than sound lignins. The decrease of methoxyl groups (25%) is not significantly accompanied by increase in phenolic groups. Oxidative process occurs by demethylation, hydroxylation of aromatic rings to produce diphenolic structures, oxygenolytic cleavage of polyhydroxylated aromatic nuclei, yielding

aliphatic products that can be further degraded by hydrolytic and aldolytic reactions (Kirk and Shimada, 1985). These reactions are catalysed by extracellular or cell surface-bound enzyme systems. Data support the view that only a small part of lignin is attacked at any one time; the lignin that is attacked is degraded and utilized before decay proceeds to the rest of the lignin molecule (Crawford, 1981). It was observed that certain white-rot fungi attack the aromatic rings of lignin faster than the side-chains. Cleavage of lignin's aromatic rings occurred while they were still bound in the polymer. This leads to a loss of aromaticity and retention of high molecular weight. Decayed lignin was found to be enriched in condensed ring structures (biphenyl moieties and aryl-alkyl, carbon-carbon bonded structures), that are known to be more resistant to fungal attack than are other lignin linkages.

1.2.2. Lignin Degrading Enzymes

Lignin is a peculiar biopolymer because unlike other natural polymers, such as polysaccharides, proteins and nucleic acids, it does not have a readily hydrolysable bond recurring at periodic intervals, along a linear backbone. The heterogeneity of its structure has implications for the mechanism of biodegradation, excluding the involvement of enzymes with limited substrate specificity.

Early lack of success on the identification of extracellular lignin-degrading enzymes, led various authors to suggest that the enzymes involved in lignin breakdown were not interacting directly with the polymer itself. According to these hypotheses, these enzymes would generate diffusable activated oxygen species, such as hydrogen peroxide, superoxide radical anion, hydroxyl radical, and singlet oxygen, which interact independently with the lignin causing the oxidation processes (in Buswell and Odier, 1987).

However, recent studies demonstrated as these species can not be responsible of the extensive oxidation process of lignin, and although the mechanism of lignin biodegradation is still largely matter of speculation, the isolation in 1983 of the first lignin degrading enzyme from *P. chrysosporium*, ligninase, threw some light on the subject (Tien and Kirk, 1983; Glenn et al., 1983). A manganese-dependent peroxidase was also isolated in 1984, from the ligninolytic culture of the same white-rot fungus (Kuwahara et al., 1984; Glenn and Gold, 1985). These enzymes have since been purified from culture filtrates of several other white-rot fungi, as *Coriolus versicolor* and *Phlebia radiata* (Dodson et al., 1987; Niku-Paavola, 1987).

In general, lignin degrading enzymes are extracellular, and can be obtained from fungal cultures when secondary metabolism is triggered by environmental stress,

such as scarce readily utilizable source of carbon (i.e. glucose), nitrogen limitation and oxygen abundance.

1.2.2.1. Ligninase

Ligninase (LiP) is a haem containing peroxidase, requiring hydrogen peroxide for its catalytic function. It is a glycoprotein containing about 13% carbohydrate (Tien and Kirk, 1984), with a molecular mass between 38 and 42 kD. The carbohydrate components consist of neutral sugars, mannose, xylose, glucose, galactose and glucosamine (Kirk, 1987b), and resemble the extracellular polysaccharides which are synthesized by the fungi at the onset of ligninolysis (Leisola et al., 1982).

LiP purified from *P. chrysosporium* is a mixture of 15 isoenzymes (Tien and Kirk, 1983; Glenn et al., 1983) with isoelectric points varying between 3.2 and 4.9. They have different kinetic properties towards various substrates suggesting different substrate affinities or active site accessibilities; however, all LiP isoenzymes are able to oxidize veratryl alcohol to veratraldehyde in the presence of hydrogen peroxide. This reaction is the basis for a U.V. assay for the determination of LiP activity, measured by detecting the increase in absorbance at 310 nm associated with the product of veratryl alcohol oxidation, i.e. veratraldehyde.

The catalytic site of LiP contains one iron protoporphyrin IX prosthetic group per molecule. Although early studies described LiP as a peculiar oxygenase (Glenn et al., 1983; Gold et al., 1984; Tien and Kirk, 1984; Renganathan et al., 1985), subsequent more accurate studies, confirmed that this enzyme is indeed a peroxidase (Kuila et al., 1985; Renganathan and Gold, 1986), as earlier suggested by Harvey and coworkers (1985). These authors reported no oxygen consumption in the oxidation of veratryl alcohol by LiP in presence of hydrogen peroxide.

Resonance Raman spectra showed that the local LiP haem environment is very similar to those of other peroxidases. The haem iron in the native protein is in the high spin ferric state, with histidine coordinate as fifth ligand at 25°C, and with a vacant coordination position available to bind peroxide or other ligand. However, the high spin hexacoordinate state dominates at below 2°C, with water as the sixth ligand (Kuila et al., 1985; Andersson et al., 1987). A catalytic cycle for ligninase has been proposed, and is shown in figure 1.9.

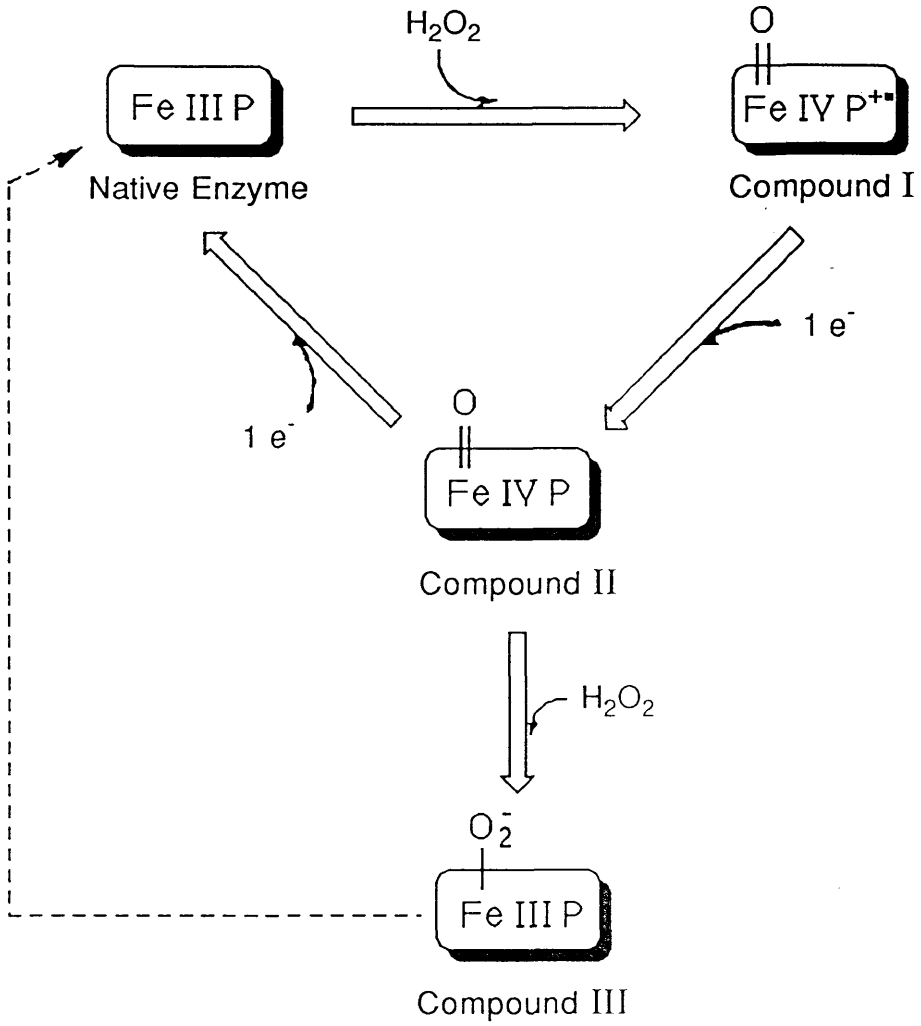

Figure 1.9. Catalytic cycle for ligninase.

With the addition of one molar equivalent of hydrogen peroxyde, the native ferric enzyme is activated to compound I, the electron deficient intermediate. Spectral characteristics of ligninase resemble to those of horseradish peroxidase (HRP) compound I, suggesting the presence of a Fe(IV)=O porphyrin radical cation. Compound I is then reduced in the presence of electron donors, by two consecutive one electron steps *via* compound II Fe(IV)=O, back to the native ferric enzyme. In the presence of an excess of hydrogen peroxide, LiP is inactivated to compound III. This last oxidation intermediate, known as oxyperoxidase, is a sluggish electron acceptor inhibiting the peroxidase reaction. Compound II and compound III have been spectrally characterised and found to be analogous to the equivalent oxidised intermediate of HRP (Renganathan et al.,1985; Renganathan and Gold, 1986).

Radical Intermediates in Ligninase Catalysis

Ligninase has been shown to oxidize with low specificity various non-phenolic methoxylated compounds.

Kersten and coworkers in 1985 reported ESR spectra of aryl cation radicals generated during LiP catalysis of 1,4-dimethoxybenzene, 1,2,3,4,-tetramethoxybenzene and 1,2,4,5,-tetramethoxybenzene, in presence of hydrogen peroxide. Major products from 1,4-dimethoxybenzene oxidation are methanol and benzoquinone; this is in agreement with studies conducted on ligninolytic fungal culture, which have reported methanol generation from lignin.

The demethoxylation mechanism is thought to involve an one-electron oxidation of the substrate, and subsequent addition of water to the radical cation, followed by methoxyl elimination as methanol (figure 1.10.).

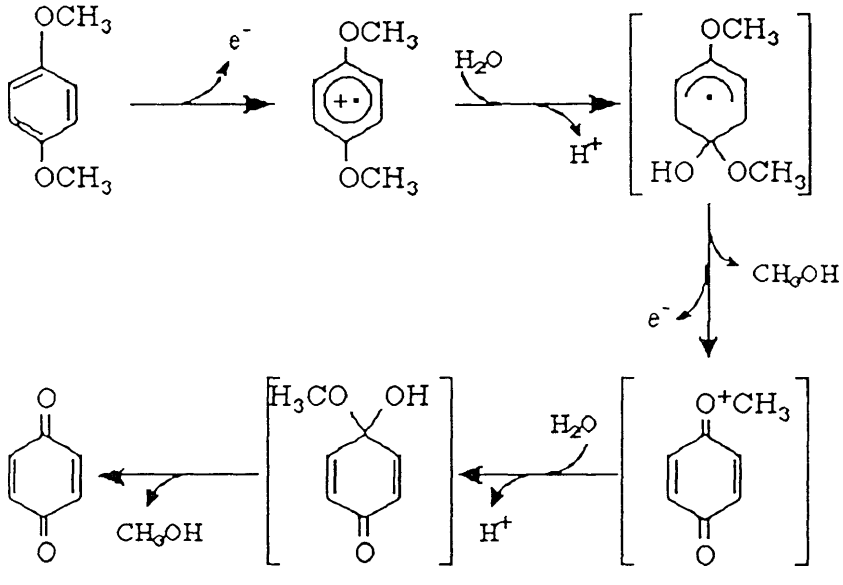

Figure 1.10. Two sequential one-electron oxidations of 1,4-dimethoxybenzene by ligninase, with addition of water and loss of methanol (adapted from Kersten et al., 1985).

Several aromatic pollutants and related compounds, such as polycyclic aromatic hydrocarbons and dibenzodioxins, have also been reported to be oxidized through radical cations by LiP (Haemmerli et al., 1986a; Hammel et al., 1986). The radical cations generated with one-electron oxidation by LiP from these substrates will breakdown by addition of water or oxygen. These observations are consistent with the mechanism proposed by Harvey and coworkers (1985), which suggest that the LiP catalyzed oxidation reactions are mediated *via* single electron transfer.

The two-step one-electron oxidations correspond to the compound I /compound II and compound II /native enzyme redox couples, whose existance have been confirmed by Resonance Raman spectroscopy (Renganathan and Gold, 1986; Andersson et al., 1987)

The production of radical cations during enzyme catalysis, is an important phenomenon, as radicals exhibit several properties with relevant implications in lignin biodegradation (Palmer et al., 1987). Firstly, radicals can act as one electron oxidants (Camaioni and Franz,1984), that are able to oxidize an appropriate donor and become reduced themselves to the ground state. Secondly, radicals can undergo side-chain reactions, the products of which depends on the nature of the radical cation. This accounts, for example, for the Cα-Cβ bond cleavage observed in lignin and model compounds, described later in this thesis. Furthermore, radical cations can add water, for example converting methoxybenzenes to quinones, as shown above.

All the reactions exhibited by radical cations, can adequately account for the variety of oxidation products observed in lignin degradation. This suggest that radicals play a major role in this process.

Veratryl Alcohol

Veratryl alcohol (VA) is a secondary metabolite synthesized *de novo* from phenylalanine in ligninolytic culture of *Phanerochaete chrysosporium* , during secondary metabolism (figure 1.11.). Its biosynthesis is enhanced by elevated oxygen concentrations (in Buswell and Odier, 1987).

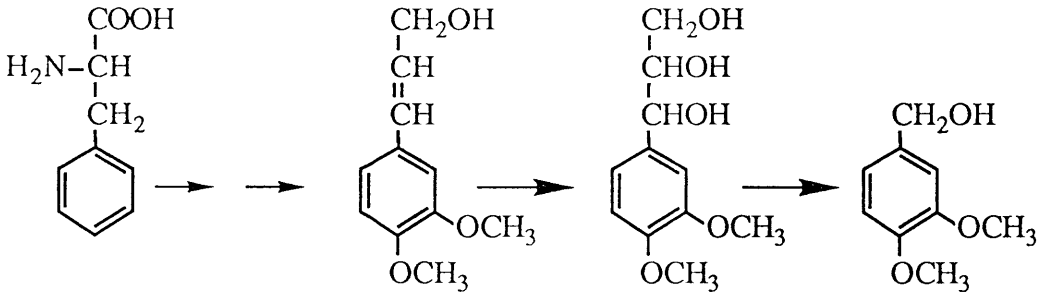

Figure 1.11. Biosynthesis of veratryl alcohol from phenylalanine (adapted from Buswell and Odier, 1987).

It has been confirmed that VA effects a marked increase in the titer of LiP in fungal culture filtrates, and it is oxidized itself to veratraldehyde by LiP in presence of hydrogen peroxide. This reaction is the basis for the LiP activity assay, which involves the measurement of the veratraldehyde formed during enzymatic activity by detecting the increased absorbance at 310 nm (figure 1.12.).

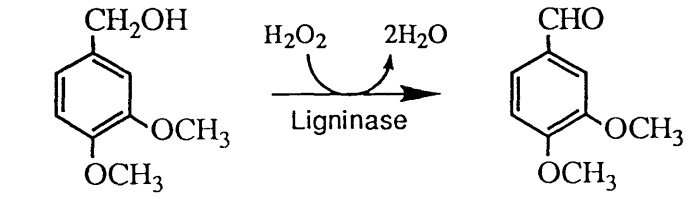

Veratryl Alcohol

Veratraldehyde
(A_{max} 310 nm)

Figure 1.12. Veratryl alcohol oxidation by ligninase.

Kinetic studies on VA oxidation by LiP, have confirmed a stoichiometry of one mole of hydrogen peroxide consumed per mole of aldehyde formed. The enzyme operates through a ping-pong mechanism; hydrogen peroxide exhibits a K_M of 29 μM, VA a K_M of 72 μM at pH 3.5 (Tien et al., 1986). Furthermore, excess concentrations of hydrogen peroxide inhibit the enzyme activity through formation of compound III. VA has been shown to protect LiP against hydrogen peroxide inactivation to compound III, by acting both as substrate which reduced LiP compound II back to the native enzyme, and by stimulating the conversion of compound III to the native enzyme (Harvey et al., 1989a; Wariishi and Gold, 1989). Harvey and coworkers proposed that VA radical cations would remain in proximity to compound II, increasing its oxidation capacity, and therefore enhancing the rate of oxidation of compound II to the native state (Harvey et al., 1989a).

An alternative model has been developed to explain the stimulative effect of VA. This model proposes a special role of VA to convert compound III back to the native enzyme, without its oxidation to veratraldehyde (Valli et al., 1990), and negates the participation of VA radical cations as charge transfer units. This last conclusion is however in contradiction with many previous reports (Wariishi and Gold, 1989; Harvey et al., 1989a; Harvey et al., 1989b; G. Gilardi et al., 1990), and will be discussed later in this thesis.

More recent studies reported the formation of products other than veratraldehyde during VA oxidation, both in *Phanerochaete chrysosporium* ligninolytic cultures (Leisola et al., 1985), and in incubation experiments with purified LiP (Shimada et al., 1987; Leisola et al., 1988; Tuor et al., 1990).

In fact, VA can undergo several oxidation pathways, including aromatic ring cleavage with oxygen addition from water or dioxygen, specifically in position C3 and C4 (Shimada et al., 1987). Leisola and coworkers (Tuor et al., 1990) have shown that a mixture of veratraldehyde, quinones and lactones can be obtained as products in aerobic oxidation (figure 1.13.); the presence of some of these products involves VA aromatic ring cleavage by LiP.

Reaction products were found to vary in function of pH: ring cleavage products were more abundant at low pH, and their concentrations decrease considerably at higher pHs. Under all conditions, the major oxidation product of oxidation was veratraldehyde, representing 75% of the total products at pH 3.0, and virtually 100% at pH 5.0 (Tuor et al., 1990).

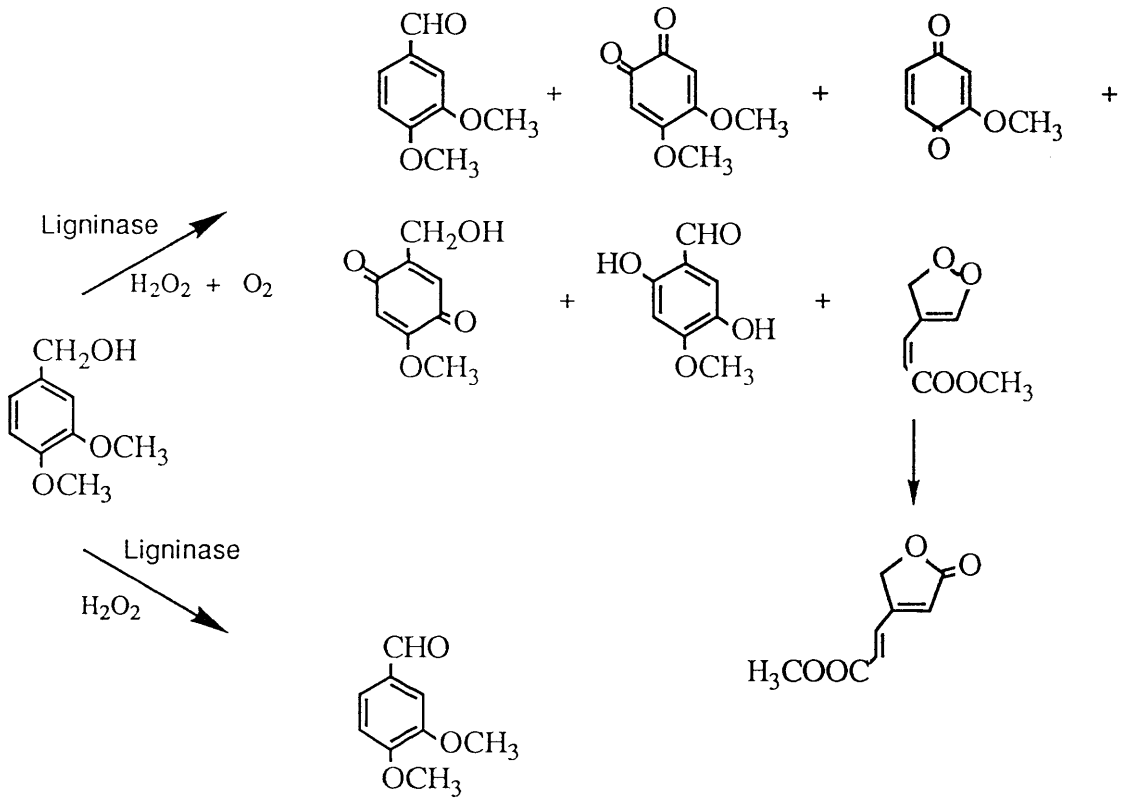

Figure 1.13. Products from the oxidation of veratryl alcohol in the presence and in the absence of oxygen (adapted from Tuor et al., 1990).

These data are in agreement with oxygen measurements conducted by Palmer and coworkers (1987) during aerobic oxidation of VA by LiP. These authors concluded that oxygen is a reactant, and it probably leads to other products than veratraldehyde. In this view, oxygen active species when reacting with radical cations from VA, whose existance was postulated by Harvey and coworkers (1986), are responsible for ring opening reactions. Therefore, ring opening reactions only occur in aerobic conditions. In support of this hypothesis, Leisola and coworkers (1988) reported that veratraldehyde is in fact the only product when the reaction is conducted under anaerobic conditions.

Many observations on the characteristics of VA, such as occurrence in ligninolytic culture and high affinity for LiP (Tien et al., 1986), induction stimulative effect on LiP biosynthesis (Faison et al., 1986), protection role on ligninase against inactivation

by hydrogen peroxide (Tonon and Odier, 1988) provide a sound background from which to consider a major involvement of this metabolite in lignin biodegradation. Harvey et al. in 1986 proposed that VA can act as mediator for transferring oxidising equivalent from the enzyme to the lignin network. The lack of success in detection of VA radical cations by ESR techniques (Tien el al., 1986), delayed development of this views.

Ligninase Role in Lignin Degradation

The hydrogen peroxide oxidized states of LiP have been shown to be more oxidizing that the analogous states of classical peroxidases; Hammel and coworkers (1986) reported that LiP is able to oxidize a series of polycyclic aromatic compounds with ionization potentials inferior or equal to 7.55 eV. From oxidation studies, it emerges that the important factor to determine whether a substrate will be oxidised or not by the enzyme is overall the redox potential.

Electron-donating substituents on aryl units, such as methoxyl groups, tend to lower the oxidation potential of the substrate, activating aromatic structures towards oxidation. By contrast, aryl structures with ring electron-withdrawing substituents (fluoro, chloro, bromo and nitro groups) or with electron-withdrawing Cα-carbonyl groups (Kirk et al., 1986) tend to raise the oxidation potential and lower the tendency of aromatic structure to be oxidised. Furthermore, reactivity appears to be influenced by resonance stabilization of the ensuing radical cation. For example, p-dimethoxybenzene has been found to be a better substrate for LiP oxidation than o-dimethoxybenzene (Kersten et al., 1985). However, the process is complicated by the presence of two redox couples involved in the peroxidase cycle, compound I / compound II and compound II / ferric enzyme, that behave differently. The rate of conversion of compound II to the ferric enzyme is slower, probably due to steric reasons.

Aromatic ring cleavage by LiP has been observed to occur on lignin model compounds. ß-aryl ether dimers have been reported to undergo ring-opening reactions, leading to several products (Miki et al., 1988). The multiplicity of products has been ascribed to a process initiated by one-electron oxidation of the substrate by LiP compound I, to form an aryl cation radical. This aryl cation radical; undergoes a variety of non-enzymatic reactions, including nucleophilic substitutions by water or intramolecular hydroxyls or coupling with molecular oxygen, leading to unstable peroxy-radical cleavages, yielding the ring cleaved products. The nature of the products is greatly influenced by the substituents on the aromatic ring of the substrate, and by the stability of the reaction intermediates (Miki et al., 1988).

Aromatic ring cleavage is only part of the various range of oxidation reactions that LiP has shown to be able to catalyse. Other reactions carried out by LiP include

side-chain cleavage (Hammel et al., 1985), demethoxylation (Kersten et al., 1985), intramolecular addition and rearrangements (Kirk et al., 1986). Side-chain cleavage on model dimer compounds, has been reported to occur between Cα and Cβ, leading to multiple products. Electron spin resonance experiments showed that Ca-Cß cleavage yields to α-hydroxybenzyl radicals as intermediate products. Non-enzymatic reactions lead to multiple products; furthermore some of the products of side-chain cleavage are themselves substrate for the enzyme (Hammel et al., 1985).

Cα-Cβ cleavage in dimeric β-O-4 aryl ether and β-1 diarylpropane lignin model compounds assume a certain relevance considering that these kind of bonds represent more than 50% of the linkages types in lignin. The capacity of LiP to cleave such bonds can account for extensive lignin depolymerization potential of this enzyme.

Many of the oxidation products obtained from the incubation of lignin model compounds with LiP, have been previously detected in ligninolytic cultures of *Phanerochaete chrysosporium*. The involvement of this enzyme in lignin breakdown has also been proved by Leisola and coworkers in 1988. These authors showed that the addition of this enzyme in washed *Phanerochaete chrysosporium* mycelial pellets, enhances considerably the release of ^{14}C-enriched carbon dioxide from ^{14}C-enriched lignin present in the media. On the other hand the addition of horseradish peroxidase to the same culture and under the same conditions, did not have any effect on lignin degradation (Leisola et al., 1988).

1.2.2.2. Other Lignin Degrading Enzymes

Mn-Peroxidase

Mn-peroxidase is an extracellular enzyme which has been identified in fungal culture of *P. chrysosporium* (Kuwahara et al., 1984; Glenn and Gold, 1985) and is able to catalyse the Mn(II)-dependent oxidation of a variety of phenols and dyes. It is a haem glycoprotein with a molecular mass of about 45-47 kD, containing about 17% neutral carbohydrate (Gold et al., 1987) and manifesting six isoenzymes.

This enzyme presents one haem per enzyme molecule; electronic absorption, electron spin resonance and Resonance Raman studies has shown as the haem is a high spin iron protoporphyrin IX complex, with the haem hexacoordinate, histidine being the fifth ligand while the sixth is available for hydrogen peroxide (Glenn and Gold, 1985; Mino et al., 1988; Wariishi et al., 1988). A catalytic cycle for Mn-peroxidase has been proposed (Gold et al., 1987; Wariishi et al., 1988) and is reported in figure 1.14.

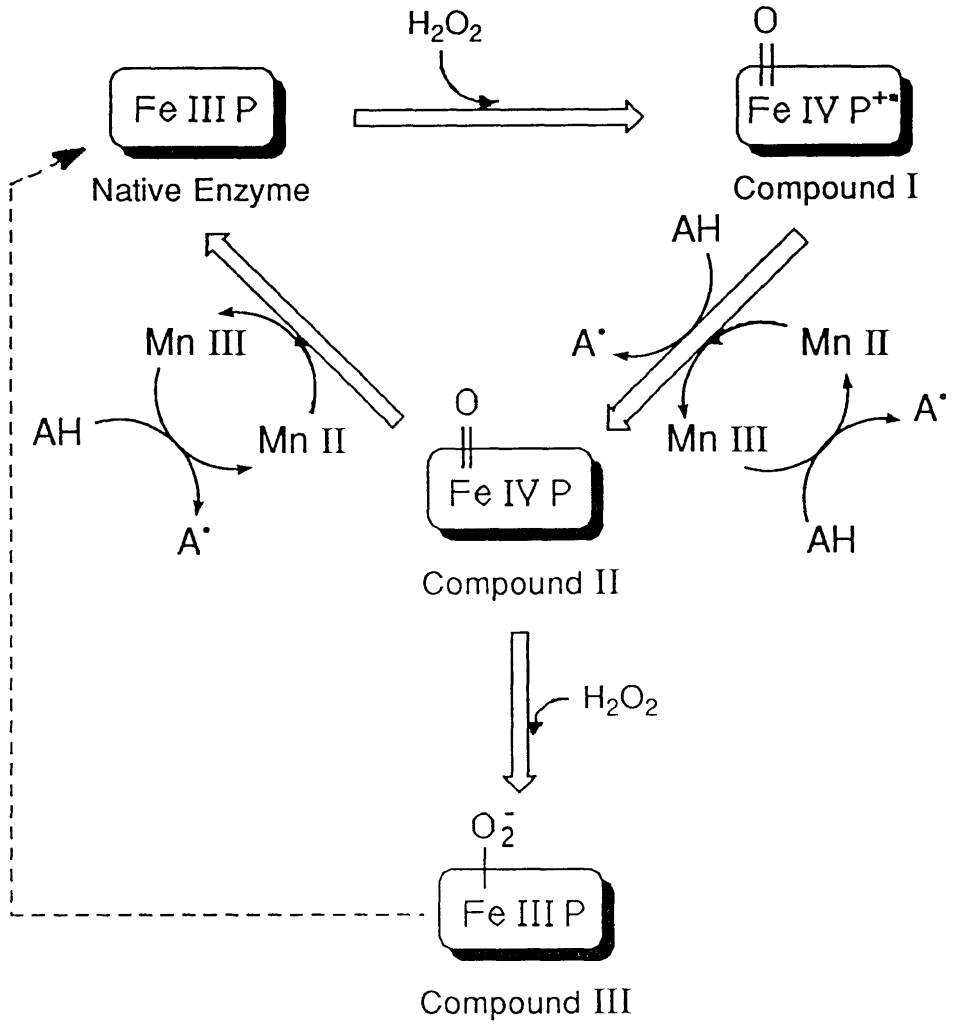

Figure 1.14. Catalytic cycle for Mn-peroxidase.

The oxidation of the native enzyme by one molecule of hydrogen peroxide per molecule of enzyme, gives Mn-peroxidase compound I, whose spectral properties, like those of ligninase, suggest a $FeIV(O)P^{+\bullet}$ configuration (Gold et al., 1987). In presence of Mn(II), the iron centre cycles back, *via* intermediate compound II, to the Fe(III) form of the native enzyme (Paszczynski et al., 1985). The Mn(III) generated can in turn oxidize phenols and be reduced back to give Mn(II) again. The Mn(II)/Mn(III) redox couple thus act as a mediator for the Mn-peroxidase catalyzed oxidations. Whereas compound I can be reduced by Mn(II) or other one electron donors (such as phenols), compound II can only be reduced by Mn(II) to the native enzyme. Thus Mn(II) is necessary to maintain the catalytic cycle of Mn-peroxidase; in its absence compound II reacts with hydrogen peroxide to yield inactive intermediate compound III (Gold et al., 1987).

Furthermore, Mn-peroxidase activity is stimulated by the presence of α-hydroxy acids, as lactate, gluconate, pyrophosphate and tartrate (Kuwara et al., 1984; Glenn and Gold, 1985). This effect has been explained involving the formation of Mn(III) complexes with α-hydroxy acids, the stability of which depends on the nature of the

ligand. These complexes are now capable of oxidising a wide range of organic substrates such as phenols, glycols, ketols, carboxylic acids as well as glutathione (Cui and Dolphin, 1990).

Mn-peroxidase can oxidise phenolic compounds through the Mn(II) / Mn(III) couple (Pasczcynski et al., 1986), and can also oxidize some non-phenolic compounds. Mechanisms for Cα-Cβ cleavage of β-O-4 substructures with free phenolic groups, alkyl phenyl cleavage, thiol-mediated oxidation of non-phenolic lignin model compounds, oxidation of benzyl alcohols in presence of thiols have been reported (Gold et al., 1990). This enzyme in absence of hydrogen peroxide it behaves as an oxidase (Pasczcynski et al., 1986), oxidizing NADPH, glutathione and dithiothreitol to give hydrogen peroxide; this is similar to horseradish peroxidase, and it suggests that Mn-peroxidase might work as hydrogen peroxide generating system for the lignin degrading enzymes of *P. chrysosporium* (Pasczcynski et al., 1986; Bono et al., 1987).

Laccase

Laccase is a copper containing oxidase widely distributed in Basidiomycetes, but not present in *P. chrysosporium*. It is abundant in ligninolytic white-rot fungi, but absent in brown-rot fungi.

Laccase is present in at least 12 isoenzymes, with isoelectric points varying between 3.07 and 6.8 (Jonsson et al., 1986). Its molecular mass varies from 50 to 100 kD depending on the amount of carbohydrate present, generally between 10-45 %. Most laccases have 4 copper ions per molecule. This enzyme catalyses the reduction of dioxygen to water by oxidising substrates in a mechanism which involves four steps of single electron transfer from substrate to enzyme. Although like ligninase it exhibits low specificity toward the substrates, it is not capable of oxidation of methoxylated aromatics. Therefore its role in lignin breakdown is only through its ability to oxidise phenolic containing aromatic moieties.

Because of its non-specificity and its reaction characteristics, laccase may have a role in detoxifying phenolic intermediates of lignin breakdown, as well in preparing lignin substructures for depolymerization by ligninase, which is known to be inhibited by phenols (Harvey and Palmer, 1990).

Hydrogen Peroxide Producing Enzymes

The presence of hydrogen peroxide producing enzymes is required to support peroxidases activity in the extracellular environment. Glucose-1-oxidase and glucose-2-oxidase were first thought to be part of the hydrogen peroxide generating system (Eriksson et al., 1989). Further studies confirmed that both these enzymes are intracellular, and also it has not been demonstrated that the action of these

intracellular hydrogen peroxide producing oxidases actually results in extracellular hydrogen peroxide. Therefore they are unlikely able to substain hydrogen peroxide levels required by peroxidase activities (Kersten and Kirk, 1987a).
Recently the discovery of glyoxal oxidase has been reported: this is a hydrogen peroxide producing enzyme from ligninolytic cultures of *P. chrysosporium* . This enzyme appears in the culture medium at the same time as both its substrates, glyoxal and methylglyoxal, and ligninase, during fungal secondary metabolism. It is an extracellular glycoprotein, with molecular weight of 68 kD; it is monomeric and it presents two isoenzymes with isoelectric points of 4.7 and 4.9 (Kersten et al., 1990). The enzyme is capable of oxidizing several simple aldehydes such as methylglyoxal, glycolaldehyde, acetaldehyde, formaldehyde, glyoxal and dihydroxyacetone. This broad substrate specificity may allow versatility of the organism when grown on complex lignocellulosic material.
It is interesting to note that proposed products of ligninolysis such as glycoaldehyde, are also substrate for glyoxal oxydase. The turnover number measured by kinetic studies on glyoxal oxidase, is considerably higher than those observed for ligninase with veratryl alcohol (Kersten et al., 1990); this suggests that glyoxal oxidase activity in culture may match that of peroxidases, despite the relatively low levels of this enzyme in cultures.
Mn-peroxidase has also been suggested to play a role in hydrogen peroxide production. As earlier mentioned, this enzyme primarily oxidises Mn(II) to Mn(III), but can also produce hydrogen peroxide oxidizing glutathione, dithiothreitol, dihydroxymaleic acid, NADH or NADPH (Glenn and Gold, 1985; Paszczynski et al., 1985). However, the role of the hydrogen peroxide generation by this system remains uncertain.

Figure 1.15. shows a schematic picture on how various extracellular enzymes and components of the ligninolytic system of *P. chrysosporium* can cooperate. According to this scheme, ligninase oxidizes various non-phenolic aromatic nuclei by one electron to give cation radical intermediates which decay spontaneously (Kirk and Farrell, 1987a). Veratryl alcohol is also secreted by the fungus and may serve as oxidation mediator and may also protect lignin peroxidase from inactivation. Mn-peroxidase oxidises Mn(II) to Mn(III) which in turn may serve as oxidant of certain phenolic aromatics. Glyoxal oxidase appears to provide hydrogen peroxide required by the peroxidases.

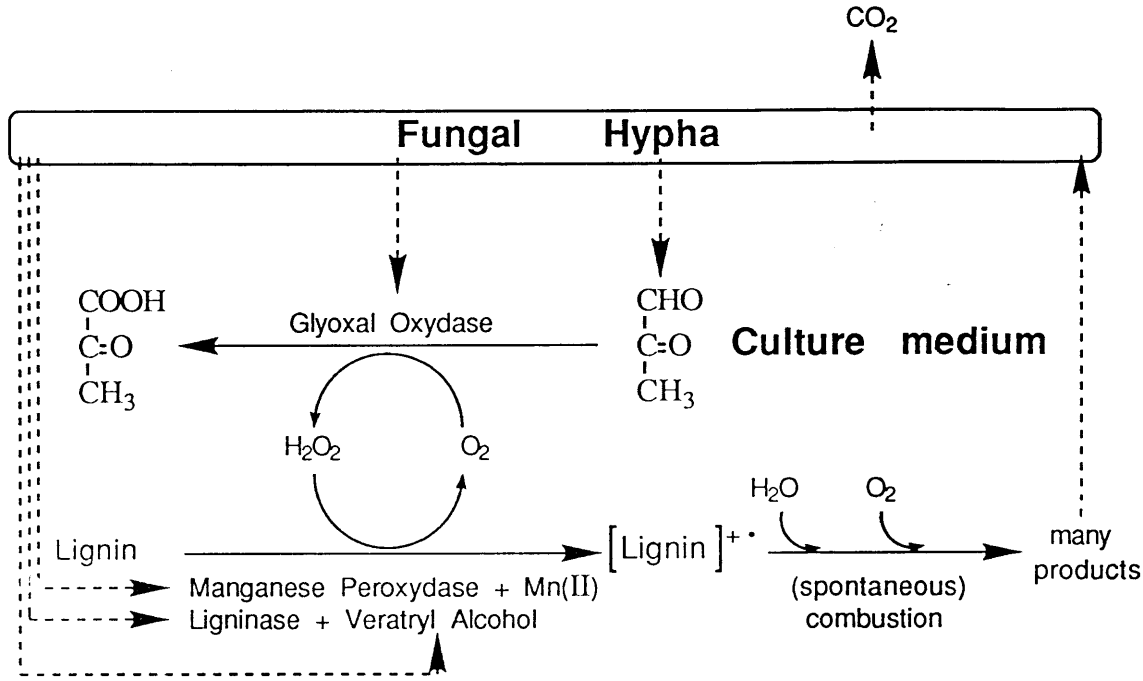

Figure 1.15. Hypothesis for the ligninolytic system of *P. Chrysosporium.*

1.2.3. Chemistry of Lignin Biodegradation

Biodegradation of the cell wall proceeds by invasion of the wood cell lumens by the fungal hyphae, which penetrates from one cell wall to another through bore holes or pits. The attack progresses from the cell lumen to the middle lamella, with gradual thinning of the cell wall.

Changes in lignin caused by fungal degradation at any given time during decay are limited to only a small portion of the total lignin, as the bulk of the lignin remain structurally unchanged (Chen and Chang, 1985). The progressive depolymerization lead to a release of a wide array of low molecular weight fragments. *P. chrysosporium* has been proved to exhibit the highest reported rate of lignin degradation: with a 15% protein in the mycelium, this rate is about 200 mg lignin per gram of mycelium per day (Kirk and Farrell, 1987a).

Soluble portions of decayed lignin can be separated by extraction with organic solvents and characterized, providing valuable information on type of reactions and pathways involved in fungal degradation of lignin.

Although structural identification and characterization of low molecular weight compounds is relatively easy, there are some limitations related to the method leading to several uncertainties. In fact, it is difficult to determine whether an identified compound is a fungal degradation product or a fungal metabolite, whether it is a primary degradation product or a secondary degradation product, whether a major identified product is a true product or an accumulated structure that

the fungus is not capable of assimilating, and whether there major degradation products not identified because of rapid assimilation by the fungus after their formation.

Lignin model compounds representing a portion of a structure known to occur in lignin, have been extensively used in biodegradation studies. It still remains uncertain whether the ligninolytic system can degrade lignin model compounds in the same way it degrades lignin.

However, the combination of these two approaches provides a good basis for deducting reaction pathways and molecular mechanisms involved in the degradation of lignin by *P. chrysosporium* (Chen and Chang, 1985; Higuchi, 1985).

During its biodegradation, lignin undergoes many oxidative reactions, such as cleavage and oxidations of the side chain, hydroxylation, dimethoxylation and cleavage of the aromatic ring. Side chain reactions involves Cα-Cβ and Cβ-Cγ bonds cleavage. Identification of benzoic acid, benzyl alcohol and benzaldehyde derivatives from biodegradation products, clearly demonstrates that Cα-Cβ cleavage is the major degradative reaction pathway (Chen and Chang, 1985). Oxidation of α-hydroxyl group to α-carbonyl group is another reaction often observed on partially degraded lignin. It is interesting to note that when Cα is oxidized, Cα-Cβ cleavage is no longer observed, and instead Cβ-Cγ cleavage occurs. Figure 1.16. reports reactions and products observed on β-O-4 lignin model substructures.

Aromatic ring dimethoxylation is a consequence of attack by water at C3 and it could be responsible for the formation of methanol from lignin and related low molecular weight aromatics by *P. chrysosporium* .

Aromatic ring cleavage can occur in two separate pathways. For aromatic rings with a free phenolic hydroxyl group, the cleavage occurs between C3 and C4 after demethylation on C4 (figure 1.16.). For aromatic rings with an etherified phenolic hydroxyl group, the cleavage occurs between C2 and C3 after demethylation on C3 and hydroxylation on C2 (figure 1.17.). The initial ring cleavage product is muconic acid.

The majority of the reactions observed on non-phenolic model compounds in intact cultures of *P. chrysosporium* can be attributed to ligninase (Kirk and Farrell, 1987a).

Although is proved that ligninase can degrade lignin model compounds and lignin, leading to extensive depolymerization in fungal subcultures, experiments conducted *in vitro* showed a more complex behaviour. While a partial depolymerization of methylated lignin was observed by some authors (Tien and Kirk, 1983), others found a re-polymerization on several types of untreated lignins (Haemmerli et al., 1986b).

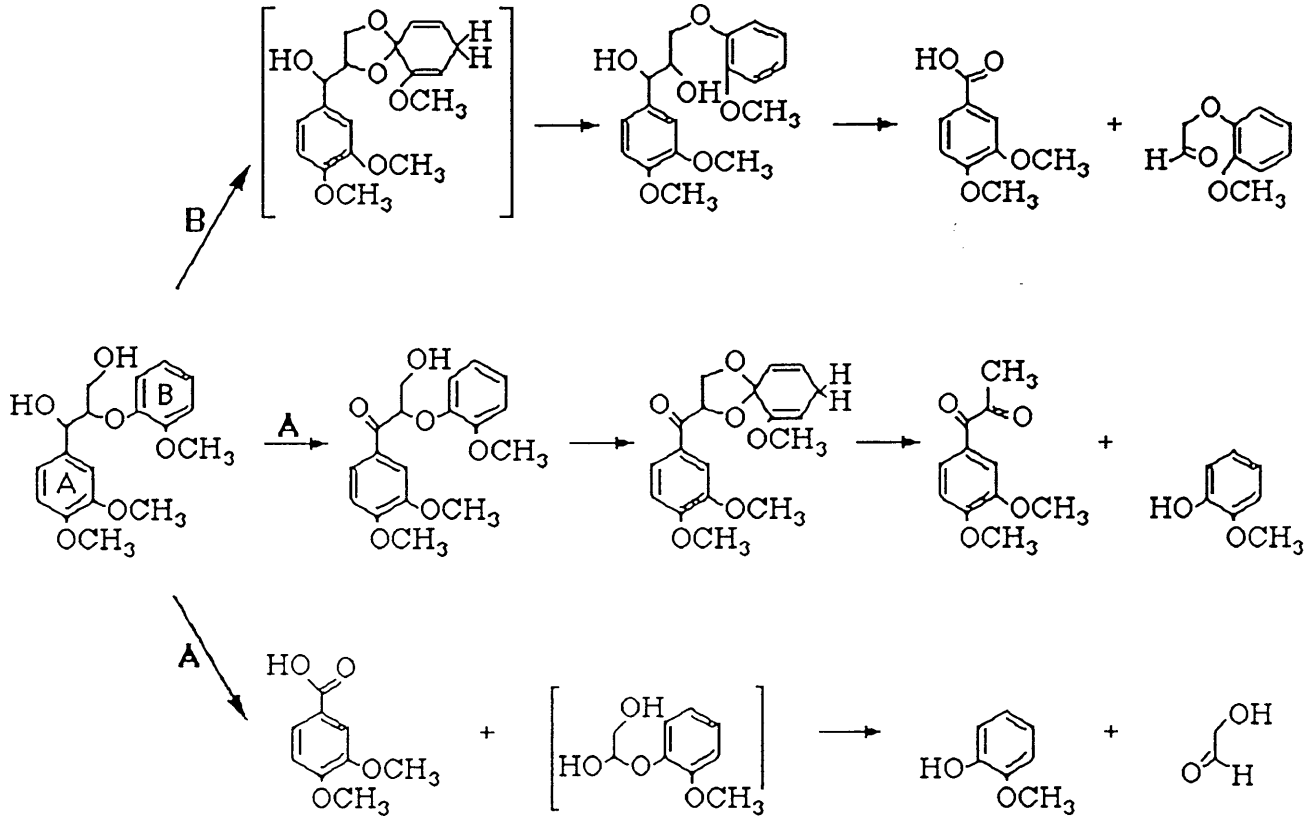

Figure 1.16. Some of the products from the oxidation of β-O-4 methoxylated lignin model compounds. The labels A and B indicate the oxidation on the two aromatic rings (modified from Kirk and Farrell,1987a).

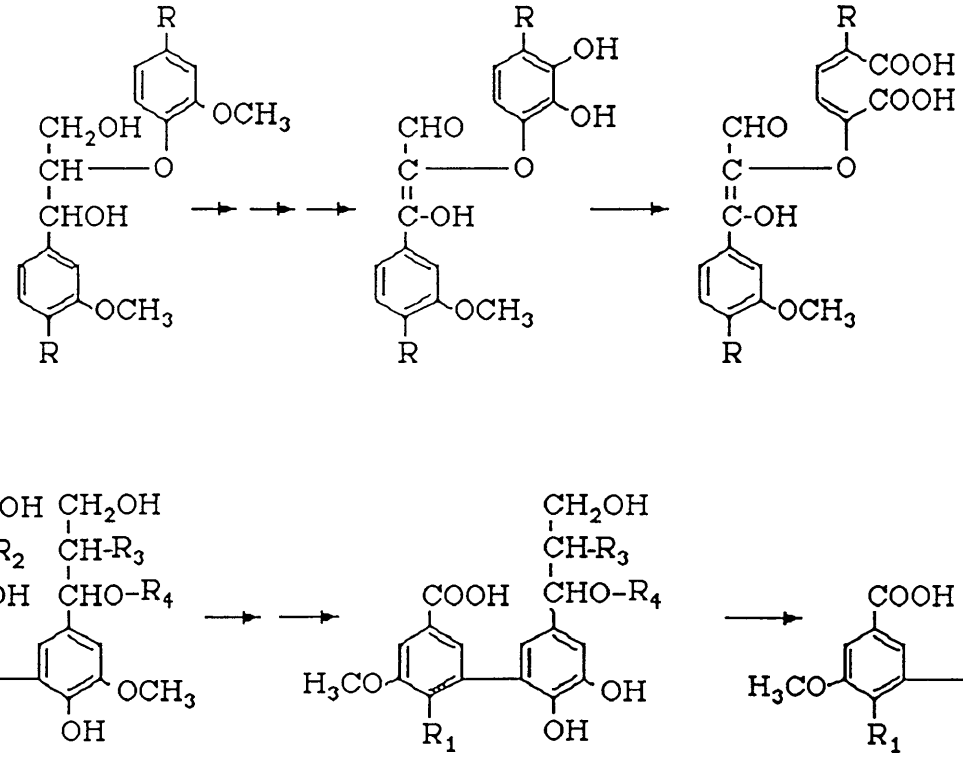

Figure 1.17. Two possible pathways for fungal aromatic ring cleavage on non-phenolic and phenolic lignin model compounds (from Chen and Chang, 1985).

Therefore, addition of ligninase to ligninolytic *P. chrysosporium* cultures enhance their lignin degrading capacity (Leisola et al., 1988), purified ligninase catalyses further polymerization of milled wood lignin (Haemmerli et al., 1986b). This apparent contradiction may be explained taking into account the inhibition effect showed by phenolic compound on ligninase (Harvey et al., 1990). Phenolic compounds are preferentially oxidised over methoxylated aromatic compounds, but this leads to enzyme inactivation. Phenolic moieties present in lignin molecule are responsible for further polymerization catalysed by ligninase (Harvey et al., 1990). In this view, successful depolymerization observed "in vitro" on methylated lignin is explained by the blockage of phenolic groups by previous methylation, preventing enzyme inhibition.
However, more recently Hammel and Moen (1991) reported the fragmentation of synthetic hardwood lignin by crude ligninase from *Phanerochaete chrysosporium*, in the presence of hydrogen peroxide and veratryl alcohol.
The capacity showed by ligninolytic system to operate depolymerization in fungal culture even in presence of phenolic groups, may explained by a cooperation between different enzymes. Mn-peroxidase ability to attack phenolics, may prevent ligninase inhibition, being then able to conduct extensive lignin degradation.

1.3. Purpose of the Project

The plant cell wall components, cellulose, hemicelluloses and lignin are the most abundant organic material in nature and a major agricultural waste. A biotechnological approach to understanding and optimizing the conditions under which these biopolymers are degraded by microorganisms can be of economic importance.
Major focus in this research is lignin, the cell wall component whose structure and mechanism of degradation is less well understood compared to cellulose and hemicelluloses. Lignin physically protects the polysaccharides fibres in the cell wall from microbial attack, limiting the rate of degradation of the whole cell wall. The study of the microorganisms, mainly fungi, and the enzymes involved in the lignin breakdown is of paramount importance for future development in this area of research. The complexity of the lignin polymer, its intimate association with the cell wall polysaccharides, the difficulties in lignin solubilization, the questions still open on the lignin structure in the cell wall, are all challenging problems yet to be solved. The diverse enzymes involved in the biodegradation of this polymer and the questions on their mechanism of action on the heterogeneous insoluble lignin network are an attractive and open field of research.

The intrinsic nature of these problems presents considerable analytical difficulties, and the achievements in the research may be limited by the potentials of the analytical techniques applied to their study. A promising modern analytical approach is the nuclear magnetic resonance (N.M.R.) spectroscopy: the availability of high field N.M.R. superconducting magnets has increased the signal dispersion and the sensitivity of this technique.

This project is to investigate various aspects of lignin biodegradation in the light of new analytical techniques.

N.M.R. spectroscopy can be used both for studying molecular structure and for following the dynamics of chemical reactions. The frequency and hyperfine structure of peaks in the spectrum of a molecule can be interpreted in terms of its structure whilst the resonance's linewidth can provide information on dynamic processes. Recently the advent of two dimensional N.M.R. methods has considerably increased the power of this technique, improving the resolution available and allowing the experimentalist to select for specific structural and dynamic features (Derome, 1987). In addition, solid state N.M.R. techniques allow the study of solid samples, providing information on both dynamic processes through relaxation time measurements (wide-line N.M.R.) and molecular structure through high resolution technique (cross polarization - magic angle spinning).

The application of these analytical probes to different aspects of the lignin biodegradation problems is the concern of this thesis. Solution N.M.R. offers good means of investigation of the dynamics and mechanism of ligninase catalysis. This can provide information on a potential mechanism for the catalytic attack of ligninase on lignin. One and two-dimensional N.M.R. applications on soluble samples of lignin permit the study of the lignin network from a chemical and structural point of view, revealing information that may not be available to other spectroscopic techniques. Finally, solid state N.M.R. offers the possibility of non-invasively studying lignocellulose in the native cell wall; the molecular modifications caused by fungal attack can be followed *in situ* by the spectral features. Other analytical techniques can also be applied to various aspects of these problems to complement the N.M.R. information.

Chapter 2

NUCLEAR MAGNETIC RESONANCE SPECTROSCOPY

Nuclear magnetic resonance (N.M.R.) is the major spectroscopic technique used in this thesis to investigate the biodegradation of lignin. In this chapter I describe an overview of the methods and the pulse sequences applied in these studies both in solution and in the solid state.

The N.M.R. phenomena rely on the property exhibited by certain nuclei: the nuclear spin. This can be visualized as a spinning motion of the nucleus around its axis. Associated with the nuclear spin is a magnetic property: if an external magnetic field is applied, such nuclei will align in respect to it. According to the quantum mechanic formalism, nuclei have a quantum number, the nuclear spin I, which for those nuclei exhibiting the N.M.R. phenomena is different from zero. Associated to the nuclear spin I, is the nuclear magnetic moment μ, that is directly proportional to the magnetogyric ratio γ, which is a constant characteristic for each nucleus:

$$\mu = \gamma I h / 2\pi$$

where h is the Planck constant.

When an external magnetic field is applied, the selection rules for N.M.R. transitions dictate that the nucleus can take (2I + 1) possible orientations, which are given by the magnetic quantum number m_I. All the N.M.R. experiments reported in this thesis are concerned with either proton or carbon-13 nuclei. These nuclei have nuclear spin I of 1/2 and therefore two orientations are possible in respect to the applied magnetic field. The energy difference between the two state is proportional to the magnetogyric ratio of the nucleus and to the magnitude of the applied field B_0:

$$\Delta E = \gamma h B_0 / 2\pi$$

Transition of nuclear spins between energy states are allowed by absorption of discrete energy quanta with frequency ω_0, which matches the difference in energy ΔE between levels:

$$\Delta E = h \omega_0$$
$$\omega_0 = \gamma B_0 / 2\pi$$

where ω_0 is the Larmor frequency, that is the energy at which nuclei precess around the direction of the field B_0. Associated this frequency is the energy

capable of inducing nuclear spin transitions, which is the basis of the N.M.R. phenomena. These transitions are stimulated in the N.M.R. experiment by applying a suitable oscillating magnetic field B_1 in the xy plane perpendicular to the static magnetic field B_0 (z axis).

The populations of the nuclear energy states are determined by the Boltzmann distribution (figure 2.1.). The number of nuclei present in the two energy states, with parallel and antiparallel orientation in respect to the applied field, depends on the field and the temperature:

$$n_{-1/2} / n_{+1/2} = \exp(-\Delta E / kT)$$
$$n_{-1/2} / n_{+1/2} = \exp(-\gamma h B_0 / 2\pi kT)$$

where $n_{+1/2}$ are the spins parallel to B_0, $n_{-1/2}$ are the spins antiparallel to B_0, k is the Boltzmann constant and T is the temperature. It can be calculated that the excess population of spins in the lower state is *circa* 1 in 10^5. This is due to the small energy difference between the states relative to thermal energies, and is responsible for the inherently low sensitivity of N.M.R. compared with infrared and ultraviolet spectroscopy. Higher sensitivity can be achieved by increasing the applied magnetic field, within the allowed limits of superconducting magnet technology.

However, as the coefficient of absorption is a constant for any nucleus, the N.M.R. signal intensity is a constant for any nucleus, and hence the N.M.R. signal from a transition is directly proportional to the number of nuclei producing it.

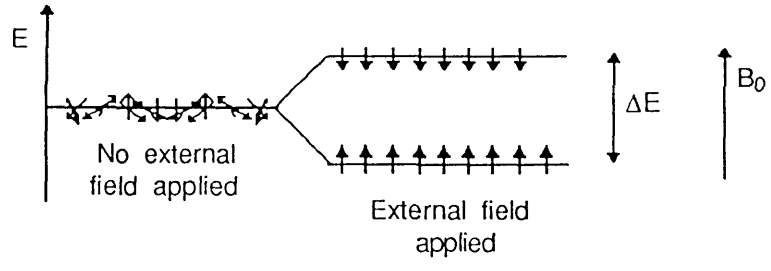

Figure 2.1. Energy levels and transitions of a nucleus with I = 1/2 in a magnetic field B_0.

The applied magnetic field B_0 induces electronic currents in atoms and molecules, which in turn produce locally a further small field $B_0\sigma$. Therefore the effective field B_{eff} experienced by nuclei will differ within the sample, depending on the electronic surrounding:

$$B_{eff} = B_0 (1 - \sigma)$$

It follows that the exact resonance frequency of a particular nucleus also will depend on the local environment:

$$\omega_0 = \frac{\gamma}{2\pi} B_0 (1 - \sigma)$$

where σ is a dimensionless constant, known as shielding constant with values between 10^{-6} and 10^{-3}. Its magnitude depends upon electronic environment of the nucleus, therefore nuclei in different chemical environments give signals at different frequencies. The separation from a chosen reference frequency is the chemical shift.

An example of the influence of the electronic environment on the resonance frequency is given by the ring current effect. In aromatic systems, the delocalized π electrons give rise to a ring current when the applied magnetic field has a component perpendicular to the plane of the ring. This current generates a secondary field whose direction and magnitude at a given nucleus, depends highly upon the orientation of the nucleus relative to the plane of the ring: a nucleus in the plane of the ring experiences an enhanced field, whereas a nucleus above or below the ring experiences a reduced field (figure 2.2.).

The chemical shift is of fundamental importance as it is the basis of chemical characterization of molecules by nuclear magnetic resonance spectroscopy.

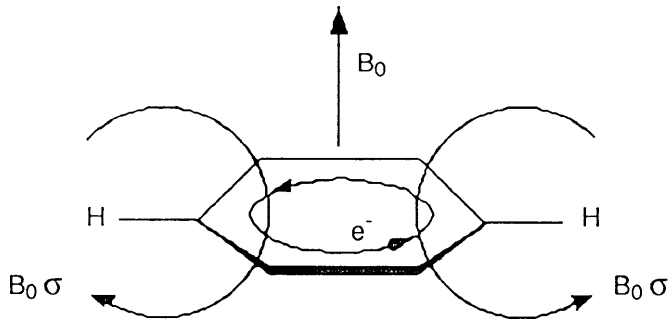

Figure 2.2. Aromatic ring current effect on the local magnetic field.

2.1. N. M. R. Relaxation Times

Chemical structure is not the only information available from N.M.R. experiments. In fact N.M.R. provides also data about molecular motions, chemical exchange and the presence of radicals, through the analysis of variations in N.M.R. relaxation times.

When a sample containing nuclei of nuclear spin 1/2 is placed in a permanent magnetic field B_0, the nuclei will precess around the direction of the field at their Larmor frequency ω_0. Since there is a slight Boltzmann excess of nuclei aligned with the magnetic field, these will give rise to a resultant magnetisation vector M_0 in the same direction of B_0. In a Cartesian axes system xyz, if B_0 is aligned along the z axis, then M_0 will precess around the z axis at ω_0 frequency. However, if the reference axes system xy are rotating at the same frequency ω_0, then in a new Cartesian axes system x'y'z, the magnetization M_0 will appear stationary and coincident with the magnetic field axis z (figure 2.3.).

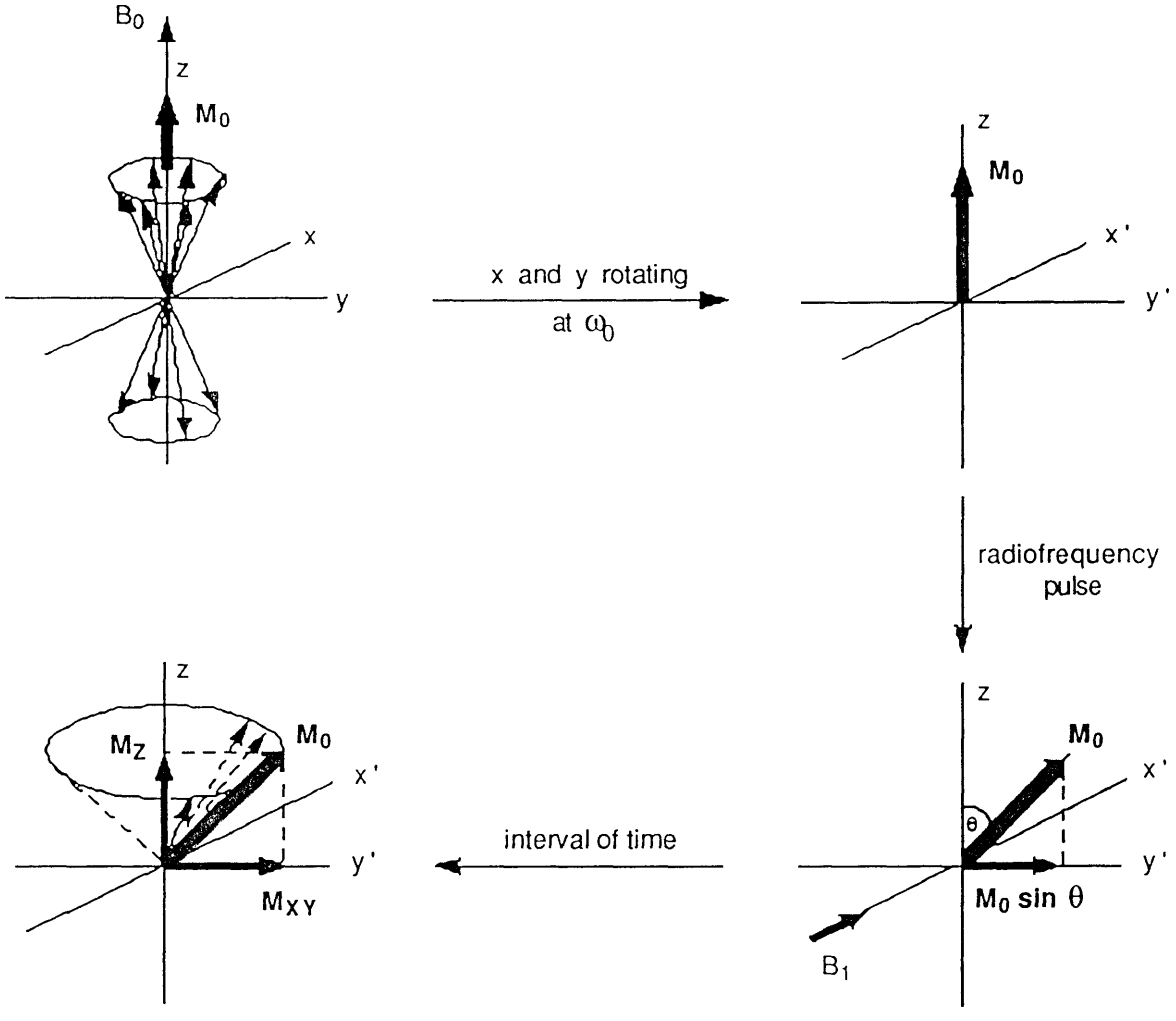

Figure 2.3. Effect of a radiofrequency pulse B_1 on the bulk magnetization vector M_0 of nuclear spins (I = 1/2) rotating rotating at Larmor frequency ω_0 in a magnetic field B_0. Relaxation mechanism.

The effect of a radiofrequency radiation at the resonant frequency ω_0 applied along the x' axis, will be to rotate the magnetization M_0 about the x' axis, and towards the y' axis. The effect of such radiofrequency pulse is equivalent to apply a transient

magnetic field B_1 along the x' axis. Immediately after the pulse, the components of M_0 along the three axes are:

$$M_{x'} = 0$$
$$M_{x'y'} = M_0 \sin\theta$$
$$M_z = M_0 \cos\theta$$

where θ is the rotation angle. Once such pulse has been removed, the perturbed spin system will relax back towards the original equilibrium condition. This is achieved by two separate means: the spin-lattice and the spin-spin relaxation processes.

2.1.1. Spin-lattice Relaxation

Spin-lattice relaxation is the return of the M_z component to its equilibrium value M_0. This relaxation is characterized by a time constant T_1, the spin-lattice or longitudinal relaxation time, and is described by the equation:

$$\frac{d M_z}{d t} = \frac{1}{T_1} (M_0 - M_z)$$

The processes responsible for relaxation involve exchange of energy between the nuclear spins and their molecular framework or surroundings, the lattice. This is a complex phenomenon, to which a number of mechanisms can contribute. Each of these mechanism combine to produce an overall spin-lattice relaxation time T_1, as described in the following equation:

$$1/T_1 = 1/T_{1D} + 1/T_{1SR} + 1/T_{1CS} + 1/T_{1SC} + 1/T_{1Q} + 1/T_{1P}$$

where the contributions arise from T_{1D} the dipole-dipole interaction, T_{1SR} the spin rotation interaction, T_{1CS} the chemical shift anisotropy, T_{1SC} the scalar coupling, T_{1Q} the quadrupolar interaction and T_{1P} paramagnetic interactions.

The dipole-dipole relaxation assumes importance when the nucleus undergoing relaxation is interacting through bonds or space with a second nucleus possessing a magnetic spin. When the molecule is tumbling in solution, this second nucleus can produce fluctuating magnetic fields in the lattice, with component close to the Larmor frequency of the former nucleus, causing efficient relaxation. The magnetic field H_D produced by the nucleus A of spin 1/2 is given by:

$$H_D = \frac{h \gamma_A}{4 \pi} \frac{(3 \cos^2\theta - 1)}{r^3_{AX}}$$

The parameters of this formula are illustrated in figure 2.4. . Because the molecule is tumbling in solution, the relative orientations of A and X change randomly, the angle θ and hence the field H_D also fluctuates, causing relaxation, and bringing the nuclear spin system into thermal equilibrium with the lattice.

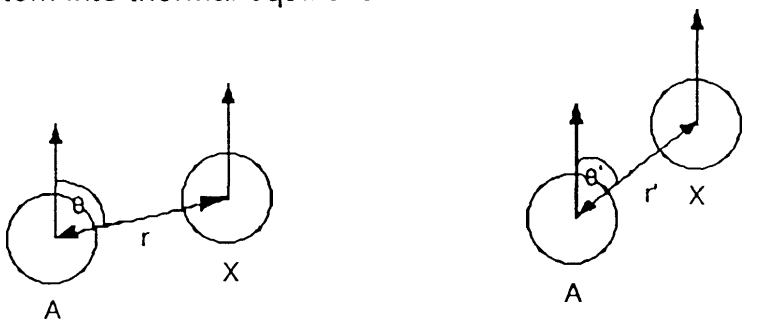

Figure 2.4 Motion of two nuclei A and X within a molecule, generating fluctuations in the angle θ and internuclear distance r.

The contribution of T_{1D} is found to decrease the overall T_1, and its effect is normally found to decrease with increasing the temperature. T_{1D} has considerable importance in solid state N.M.R., as discussed later.

The spin-rotation relaxation is the result of segmental motions of small highly symmetrical groups, such as short side-chains or methyl groups. This leads to a decrease in the effectiveness of dipolar relaxation mechanism, and to an increase of the overall relaxation time. Unlike the dipolar relaxation, the spin-rotation generally increases with increasing the temperature.

Scalar coupling and chemical shift anisotropy have generally been found not to play an important role in relaxing organic molecules in solution. However, they are important contributions in solid state N.M.R., and will be discussed later.

Quadrupolar relaxation is important for nuclei with spin > 1/2, such as deuterium (I = 1/2). Such nuclei posses a quadrupole moment, which gives rise to an electric field gradient at the nucleus, providing a highly efficient relaxation mechanism.

The paramagnetic component is present for molecules containing unpaired electrons. The electric field associated with the unpaired electron generates local magnetic field, producing a very efficient relaxation by a dipolar mechanism; this is because the magnetic moment of the electron is *circa* 2000 times that of the proton.

The distribution of frequencies associated with the random fluctuating magnetic field is expressed as the spectral density function $J_{(\omega)}$:

$$J_{(\omega)} = \tau_c / (1 + \omega^2\tau_c^2)$$

where τ_c is the correlation time, which expresses the time scale of molecular motions (in solution 10^{-12} to 10^{-8} seconds).

The relaxation rate $1/T_1$ is therefore dependent upon the magnitude of the fluctuating fields and upon the spectral density function at the resonance frequency ω_0:

$$\frac{1}{T_1} \propto H_D^2 \frac{\tau_c}{1 + \omega_0^2 \tau_c^2}$$

2.1.2. Spin-spin Relaxation

Spin-spin relaxation phenomena occur on the basis of a spread of the frequencies inherent in the N.M.R. experiment, due for example to exchange of magnetization between nuclei. This will cause a loss in coherence in the precessing nuclei, they will precess at slightly different frequencies, spreading on the x'y' plane and randomly eliminating a net magnetization. The larger the frequency spread, the faster the M_{xy} component will decay to zero. The relaxation time T_2 is directly related to an inherent broadening of the resonance linewidth:

$$1/T_2 = \pi \Delta\nu_{1/2}$$

where $\Delta\nu_{1/2}$ is the linewidth at half height of a given resonance signal.
The nuclear spins have a finite lifetime in a given energy state, as result of spin-lattice relaxation processes, therefore there is an uncertainty in the resonance frequency, given by:

$$\Delta\nu_0 \approx 1/T_1$$

This causes an inherent lifetime broadening of the resonances. It follows that all processes that contribute to T_1 also affect T_2, therefore:

$$T_1 \geq T_2$$

The relatively fast motions of molecules in solution, tend to average the components of the field produced by A and X (figure 2.4.). These motions tend to average the nuclear interactions, so each nucleus experiences the same time-averaged field; this process become more complete as the speed of the motions increases, and therefore resonances linewidths decrease as the motion increases. For nuclei in solution the resonance linewidths are proportional to the fluctuating fields and to the correlation times τ_c, characteristic for their motions:

$$1/T_2 \propto H_D^2 \tau_c$$

It can be noted that for $1/T_2$: $J_{(\omega)} = \tau_c$ when $\omega \approx 0$

whereas for $1/T_1$: $J_{(\omega)} = \tau_c$ when $\omega \approx \omega_0$

This implies that components of motions at low frequencies contribute to T_2 but not to T_1. Because $T_1 \geq T_2$, T_1 is sensitive to motions at high frequencies ($\sim 10^7\ s^{-1}$), close to the resonant frequency ω_0 , whereas T_2 is sensitive to both motions at high and low frequencies ($\sim 10^4\ s^{-1}$).

2.2. N. M. R. Multipulse Experiments

N.M.R. multipulse techniques are multi-steps experiments, in which the nuclear spins are subject to more than one specific excitation pulse followed by variable delays.
In general, a multipulse experiment is considered as a three step process. The first step is the "preparation" period, during which nuclear spins are prepared, allowing them to align with the applied magnetic field for the radiofrequency pulses which are to follow. The second step is the "evolution" period, which is the time in which the spin system is allowed to evolve, followed by the "detection" step during which the N.M.R. signal is acquired.
The one-dimensional multipulse techniques used for experiments in solution that are reported in this thesis are: the Inversion-recovery, the Spin-echo, the Solvent Presaturation and the Distortionless Enhancement by Polarization Transfer (DEPT); their basis is discussed in the following sections.

2.2.1. Inversion-recovery

The inversion-recovery pulse sequence is a widely used method for determining spin-lattice relaxation times T_1.
This pulse sequence consists of a 180° pulse (π) which inverts the magnetization along the -z axis, followed by a delay (τ) during which the magnetization undergoes to a partial relaxation. A final 90° pulse ($\pi/2$) is applied to transfer the magnetization from the z axis to the xy plane where can be detected by the receiver coils. This pulse sequence can be written as:

$$\pi - \tau - \pi/2 - \text{collect}$$

It is possible to map the recovery of the magnetization along the z axis , by using variable delays τ. This dependence of M_z on τ is described by the equation:

$$M_z = M^0_z [1 - 2 \exp(-\tau/T_1)]$$

where M_z is the component of M along the z axis, and M^0_z is its equilibrium value. This equation describe the exponential recovery of the magnetization and it allows the calculation of T_1.

2.2.2. Spin-echo

A quick estimation of the spin-spin relaxation time can be obtained by the analysis of the lineshape of the resonances, as their half height linewidth is proportional to T_2. However, such estimation is purely indicative, as it is strongly affected by magnetic field inhomogeneity, and for this reason is written as T_2^*:

$$T_2^* = 1 / \pi \Delta\nu_{1/2}$$

The spin-echo method of Carr-Purcell-Meiboom-Gill (CPMG) has been developed to eliminate magnetic field inhomogeneities and to calculate a more precise value of T_2. The CPMG pulse sequence consists of a $\pi/2$ pulse which rotates the magnetization along the x' axis. Once in the x'y' plane, the nuclear spins begin to fan out and lose phase coherence, both due to spin-spin relaxation and magnetic field inhomogeneity. After a delay τ, a π pulse along the y' axis will invert the magnetization vectors that will refocus after another delay τ, generating an echo signal in the receiver. A sequence of π pulses applied at regular intervals τ, will continue to invert the dephased nuclei, giving rise to a series of echoes at times 2τ, 4τ, 6τ until the spin vectors are relaxed by effect of T_2.
This pulse sequence can be written as:

$$\pi/2 - (\tau - \pi - \tau)_n - \text{echo}$$

The process is described by the equation:

$$M_z = M_0 \exp(-\sqrt{\tau / T_2})$$

This equation describes the exponential decay of the magnetization measured as intensity at each echo, allowing an accurate determination of T_2.

2.2.3. Solvent Suppression by Presaturation

The presence of a large solvent peak is often a problem, because it causes overloading of the spectrometer's analogue to digital converter, and also because the large solvent peak obscures part of the spectrum. The technique most commonly used to eliminate the solvent signal is the presaturation method. This consists of selectively irradiating the solvent peak for a period long enough to equalize the spin populations of the two energy states. The solvent spin system is saturated, and as consequence, there will be no net absorption following a non-selective excitation of the whole spectrum. The N.M.R. absorption signal of the solvent will no longer be observed.

2.2.4. Distortionless Enhancement by Polarization Transfer (DEPT)

The DEPT pulse sequence is designed for improving sensitivity and resolution of mainly carbon-13 spectra. This technique is based on the polarization transfer phenomena, which consist in increasing the sensitivity of a rare nucleus such as carbon-13, by transferring magnetization to it from the coupled protons. Protons exhibit a strong magnetic moment and a high natural abundance. Polarization transfer is very similar to cross polarization used in solid state N.M.R. which will be illustrated later in this thesis. The difference lies both in the pulse method used and in the nature of the coupling interaction involved, that is the strong dipolar coupling in solids and the weaker scalar couplings in liquids and solutions. This technique involves the use of 180° pulses applied to specific transitions giving rise to changes in the population of other coupled heteronuclei (population transfer). As consequence, the resonance signals show a change in their intensity, and the maximum possible intensity's variation follow the ratio of the magnetogyric constants that for carbon-13 and proton is approximately 4. Therefore the effect of irradiating for example one line of a proton doublet that is coupled to a carbon-13 nucleus, is to vary the intensities and phases of the carbon signals. The effect in the carbon-13 resonances os sampled by a non-selective 90° pulse.
In general, this technique consists in the irradiation of both carbon-13 and proton nuclei, detecting carbon-13 signals. The DEPT pulse sequence can be written as:

Proton Excitation:	$\pi/2_x$ - Δ - π_x - Δ - θ_y - Δ -			decoupling
Carbon Excitation:		$\pi/2_x$	π_x	collect

Variation of the length of the last proton pulse yields to different intensities for CH,CH_2 and CH_3 fragments. For a fixed delay $\Delta = 0.5 / J_{(CH)}$, an editing of carbon signals can be achieved as follow:

$\theta = \pi/4$ gives CH,CH_2 and CH_3 signals all positive
$\theta = \pi/2$ gives CH signals only
$\theta = 3\pi/4$ gives CH and CH_3 signals positive and CH_2 negative

The choice of different proton pulse angles allow to select different carbons, editing subspectra with increased resolution. This technique has been proved to be very useful for very crowded spectra, as those of lignin. In this case can be applied for both increasing resolution, and confirming assignments.

2.3. Two-Dimensional N.M.R.

Two-dimensional N.M.R. (2D-N.M.R.) spectroscopy is a multipulse technique, in which series of free induction decays (F.I.D.) are acquired after various evolution periods. The collection of data forms a 2D array, in which the signal a is function of both the time of acquisition (t_1) and the evolution period (t_2) over which it has been allowed to evolve. The 2D array of data $A(t_1t_2)$ containing all the information about the spin system over the acquisition and evolution times, is then Fourier transformed twice: once in respect to t_2 and then in respect to t_1. This leads to the corresponding frequency matrix $A(f_1f_2)$, which forms the conventional 2D-N.M.R. spectrum. These spectra are usually represented as contour plot on a plane of the three dimensional peaks at a chosen height.
In general, a 2D-N.M.R. experiment may be performed for any system, provided that some of its properties vary with a systematic variation of the evolution period.
There are two distinct types of 2D experiments: "J-resolved" and "correlated spectroscopy" (Kessler et al., 1988).

2.3.1. J-resolved Spectroscopy

J-resolved spectroscopy is characterized by two frequency axes, one (F_1) containing scalar coupling information, and the other (F_2) containing the chemical shifts. In this thesis only proton homonuclear J-resolved experiments are reported, therefore the attention will be only focussed on this system.
The pulse sequence of a homonuclear J-resolved experiment is the Spin-echo reported in figure 2.5.

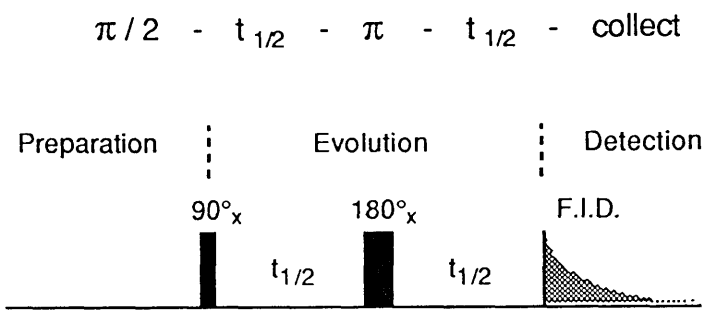

Figure 2.5. Pulse sequence for J-resolved proton N.M.R. experiment.

The evolution of the spin system is initiated by a $90°_x$ pulse. During the variable delays $t_{1/2}$, the spin system is allowed to evolve according to the chemical shift and coupling components. A $180°_x$ pulse reflects the spin components about the x'-axis, refocussing the magnetizations vectors fanned out because of magnetic field inhomogeneity, but not the components whose spin states have been also changed by the pulse. The size of $t_{1/2}$ determines the intensity of the signal collected.
2D J-resolved spectra obtained directly from Fourier transformations present one domain (F_1) containing coupling information alone, and another domain (F_2) containing both chemical shift and coupling constants: coupled multiplets lie on a line which is inclined 45° to the $F_1(F_2)$ axes. This allow a computer operation called "tilting", which tilts the data matrix about a 45° axis, yielding to spectra which contain chemical shifts only along F_2 , to give a "proton decoupled" proton spectrum, and coupling constants along F_1 .

2.3.2. Correlated Spectroscopy

In correlated spectroscopy, both frequency axes contains chemical shift information, and are connected *via* selected coupling processes.
Spin- spin coupling are revealed in Correlated Spectroscopy (COSY). The basis of this experiment is the process of coherence transfer in which magnetization is transferred between coupled spins; this can be applied to both homonuclear and heteronuclear spin systems.
The pulse sequence of a homonuclear COSY experiment is reported in figure 2.6a. The homonuclear COSY experiment consists of two 90° pulses separated by a time period t_1 . The effect of the initial $90°_x$ pulse is to flip the bulk magnetization into the x'y' plane. During the delay t_1 , the magnetization vectors fan out on the x'y' plane. The second 90° pulse, called "mixing pulse", mixes the components of the transverse magnetization, causing coherence transfer between the coupled signals. For spin system AX, this second pulse has no effect when J(AX) is zero. In the 2D

matrix this leads to two peaks with coordinate (δ_A , δ_A) and (δ_X , δ_X) : these are two "diagonal peaks", which form the feature of the conventional 1D spectrum along the diagonal of the COSY spectrum. However, when J(AX) is not zero, that is the two nuclei A and X are coupled, the mixing pulse will transfer coupling information between the spins. In this case, the 2D spectrum consists of the diagonal peaks (δ_A , δ_A) and (δ_X, δ_X) and also of the "off-diagonal" or "cross-peaks" with coordinate (δ_A , δ_X) and (δ_X, δ_A) . The presence of cross-peaks indicates that A is indeed coupled to X .

As in the proton homonuclear COSY where the ^1H-^1H spin-spin couplings provide the means for the transfer of magnetization, in the heteronuclear case one-bond ^1H-^{13}C couplings show directly which protons are attached to which carbon atoms. The heteronuclear COSY pulse sequence is reported in figure 2.6b.

a) $\pi/2_x$ - t_1 - $\pi/2_x$ - collect

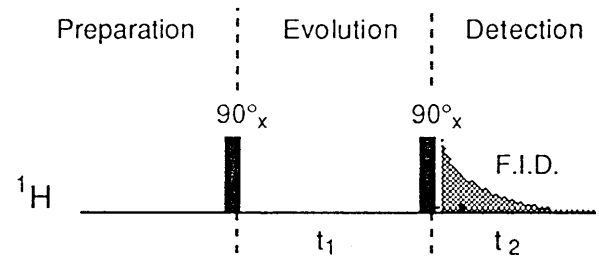

b) ^1H : $\pi/2_x$ - $t_{1/2}$ - $t_{1/2}$ - Δ_1 - $\pi/2_y$ - decoupling

^{13}C: π_x - $\pi/2_x$ - Δ_2 - collect

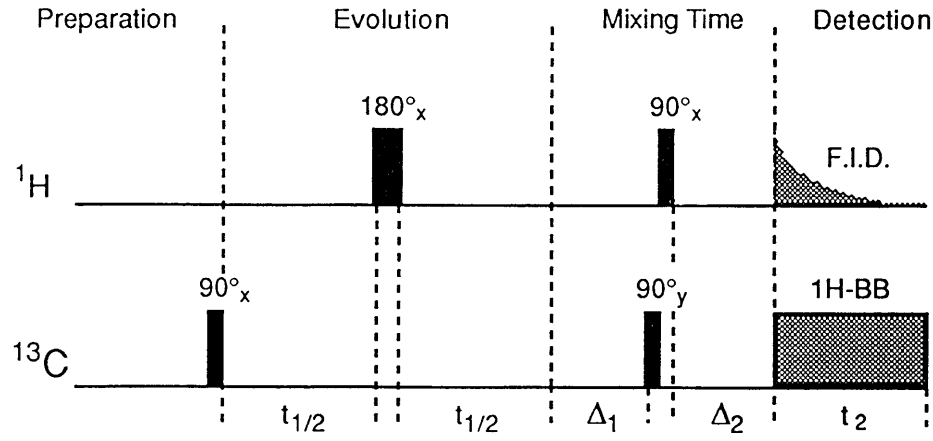

Figure 2.6. Pulse sequence for homonuclear (a) and heteronuclear (b) COSY experiments.

The initial $90°_x$ pulse on proton nuclei, rotates the spin vectors into the x'y' plane, which are left to evolve during $t_{1/2}$. At this point a time delay Δ_1 equal to half J_{CH} will cause the proton components to be 180° out of phase with each other, and a $90°_y$ pulse on proton will rotate these spin vectors into the ± z axis. This polarization of the proton magnetization along the ± z direction, leads to a simultaneous polarization of the carbon magnetization which is transferred into the x'y' plane by a $90°_x$ pulse at the resonance frequency of the carbon nuclei. Carbon-13 spins will fan out during a further time interval Δ_2 and are refocussed to give a singlet when broad band proton decoupling is applied during signal detection.

In the final heteronuclear COSY spectrum, the F_2 and F_1 axes contain respectively the proton and carbon-13 chemical shifts. Cross-peaks indicate which protons are bound to which carbon atoms.

Another type of correlated spectroscopy revealing the dipolar coupling connections is the Nuclear Overhauser Enhancement Spectroscopy (NOESY). The NOESY experiment is in fact based on the Nuclear Overhauser Effect (NOE), the phenomenon responsible for signal intensity variations caused by irradiation on dipolar coupled nuclei.

When a decoupling field is applied selectively on a resonance X of an AX spin system, an enhancement may be observed in the signal intensity of the coupled resonance A. In the NOE experiment, a strong pulse is applied at the resonance frequency of the nucleus X, and then switched off. The spin population of X returns to equilibrium *via* dipolar interactions with neighbouring nuclei, for example A, B, C. If the resonance frequency of A is irradiated in a similar manner, the same result is achieved, as A relaxes through X which in turn may relax through B and C. The time required for the NOE to build up yields information about correlation times and distances between the nuclei concerned.

The NOESY pulse sequence consists of three 90° pulses, as reported in figure 2.7.

$$\pi/2_x \; - \; t_1 \; - \; \pi/2_x \; - \; \Delta \; - \; \pi/2_x \; - \; \text{collect}$$

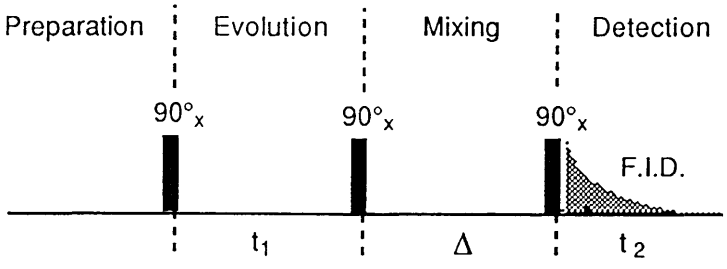

Figure 2.7. Pulse sequence for NOESY experiments.

The time delay Δ which follows the second 90° pulse is called "mixing time", and has a key importance as it allows the NOE to build up. The third $90°_x$ allows the detection of the signal. The length of the mixing time depends on the property of the molecule being investigated: small molecules require long delays (1-5 s), while large molecules require short delays (50-200 ms).

NOESY spectra are interpreted in the same way as COSY spectra; in this case the presence of cross-peaks indicates nuclei close in space. The NOE peak intensity is proportional to the cross-relaxation rate σ_{NOE} of the spin system, which is given by the expression:

$$\sigma_{NOE} = \frac{1}{10} \frac{\gamma^4 h^2 \tau_c}{4\pi^2 r^6} \left[\frac{6}{1 + 4\omega_0^2 \tau_c^2} - 1 \right]$$

where

γ is the gyromagnetic ratio of the nucleus being studied

h is the Planck's constant

τ_C is the correlation time, which is proportional to the molecular size, the solvent viscosity, and inversely proportional to the temperature

r is the internuclear distance

ω_0 is the Larmor frequency

The value of σ_{NOE} determines the efficiency of a magnetization transfer due to dipolar relaxation, and its sign determines the appearance of peaks in the spectrum. It is interesting to distinguish the following situations:

1) when the term $[6 / (1 + 4 \omega_0\tau_c^2) > 1]$, the σ_{NOE} is positive, leading to negative cross-peaks in the spectrum; this is characteristic of small molecules

2) when the term $[6 / (1 + 4 \omega_0\tau_c^2) < 1]$, the σ_{NOE} is negative, leading to positive cross-peaks in the spectrum, this is characteristic of large molecules in viscous solvents

3) when the term $[6 / (1 + 4 \omega_0\tau_c^2) \approx 1]$, the $\sigma_{NOE} \approx 1$ and no or very small cross-peaks will be observed; this case is characteristic of medium size molecules. In this case the interpretation of NOESY spectra is very difficult, because the absence of cross-peaks can be interpreted as due to both no cross relaxation between two nuclei, or the interaction is only too small to be measured.

For medium size molecules the ROESY experiment (ROE spectroscopy) can be performed. This technique is based on the ROE phenomenon, that is the NOE caused by relaxation in the rotating frame $T_{1\rho}$; the mixing step in the ROESY experiment is done in a spin-lock period. In contrast to NOE, the ROE is always positive as can be seen from the cross relaxation rate σ_{ROE} :

$$\sigma_{ROE} = \frac{1}{10} \frac{\gamma^4 h^2 \tau_c}{4\pi^2 r^6} \left[\frac{3}{1 + \omega_0^2 \tau_c^2} + 2 \right]$$

This always yields negative cross-peaks.

Although ROESY and NOESY experiments are quite different in operation, they are very similar with respect to the information which can be extracted. The magnitude of the cross peak integrals is directly determined by the value of the cross relaxation rate. Therefore, the relative intensities of the cross-peaks within a ROESY or a NOESY spectrum provide important structural information. For a given sample at a given experimental conditions, the cross relaxation is proportional to the spatial distance of two spins within the molecule (Kessler et al., 1988):

$$I_{ROESY} \propto \sigma_{ROE} \propto 1 / r^6 \qquad \text{and} \qquad I_{NOESY} \propto \sigma_{NOE} \propto 1 / r^6$$

If only one intermolecular distance within the molecule under investigation is known, it is possible to calculate all other distances from the integrals of the cross-peaks. This calculation is identical in both experiments:

$$I_{ref} / I_{ij} = r_{ij}^6 / r_{ref}^6$$
$$r_{ij} = r_{ref} (I_{ref} / I_{ij})^{1/6}$$

where I_{ref} and r_{ref} are integral and distance for a known cross-peak of a known internuclear distance. I_{ij} and r_{ij} are integral and distance of any pair of nuclei within the same molecule.

The spatial information obtained from the analysis of these spectra is over very short distances, as NOE and ROE only extend to about 4.5 Å. Within these short distances, NOE and ROE can provide very accurate information. Being proportional to r^{-6}, the difference in intensity of an NOE or ROE between two pairs of protons separated by 2.8 and 2.6 Å will come to a factor of 1.5, which is within the accuracy limits attainable. Typically cross-peaks are classified as strong, medium or weak, corresponding to distances of below 2.5 Å, below 3.0 Å, and below 4.0 Å respectively.

2.4. Solid State N.M.R.

The main interactions which may occur with a nucleus with a magnetic moment, can be described by a general Hamiltonian H:

$$H = H_Z + H_D + H_{CS} + H_{SC} + H_Q$$

where:

H_Z describes the Zeeman interaction with the magnetic field

H_D describes the direct dipole-dipole interactions with other nuclei

H_{CS} describes the magnetic shielding by the surrounding electrons giving chemical shifts

H_{SC} describes the spin-spin couplings to other nuclei

H_Q describes the quadrupolar interactions which is present for nuclei with spin > 1/2

In a particular solid state system, one or two of the terms will usually dominate the Hamiltonian, and hence determine the characteristics of the spectrum (Voelkel, 1988).

The Zeeman contribution H_Z originates from the interaction between the magnetic moment of the nucleus and the applied field, over a range of 10^6 - 10^9 Hz, and is responsible of the N.M.R. phenomenon. The interaction is linear with the applied magnetic field; larger separations of spin energy levels occur at higher fields with a corresponding increase in the spin population difference, and increase in N.M.R. sensitivity.

The dipolar contribution H_D arises from the direct dipole-dipole interactions between nuclei, and occurs over a range of 0 - 10^5 Hz. It depends on the magnitude of the magnetic moments of the nuclei involved, is independent from the applied field B_0 and falls off very rapidly with the internuclear distance ($1/ r^3$). This interaction is the most important for spin 1/2 nuclei with large magnetic moments like the proton.

The chemicals shift interaction H_{CS} is due to the shielding effect of the fields produced by the surrounding electrons on the nucleus. It is linear with the applied field and will be proportionately larger and more important at higher magnetic field strengths. The chemical shift broadening is therefore field dependent, occurs over a range of 0 - 10^5 Hz, and is very sensitive to the geometry and identity of the other atoms surrounding a particular nucleus.

The spin-spin coupling interaction H_{SC} occurs between a pair of coupled spins, is field independent and usually smaller than the other contributions under consideration (0 - 10^4 Hz).

The quadrupolar contribution H_Q occurs only when $I > 1/2$, and arises from the interaction of the nuclear quadrupole moment with the non-spherically symmetrical

field gradient around the nucleus. It is field independent, and its magnitude (0 - 10^9) is such that when present it often completely dominates the spectrum.
For all these phenomena the parameters involved, such as spin systems and applied field, are vector quantities, possessing both a magnitude and a directional character. The interaction between them must be therefore described by a 3 x 3 matrix. The critical difference between solution and solid state N.M.R. is that in the former case, the fast and isotropic motions of the molecules give an averaging of many of the interactions. In some cases a discrete average value is the result from these motions, as for chemical shifts and scalar spin-spin couplings. In other cases, the average value obtained is zero and the effect is not observed at all in the spectrum, as for dipolar and quadrupolar components. N.M.R. spectra of solids are more complex and contain an orientation dependence, yielding potentially more information than solution spectra. Because of the larger magnitude of the interactions in the solid state, N.M.R. spectra of solids are very broad absorptions, and are referred as wide-line N.M.R. spectra.
However, line-narrowing techniques have been developed to improve the resolution and extract chemical shift and scalar coupling information as in conventional N.M.R. spectra in solution. One of these techniques is the Cross-Polarization Magic Angle Spinning (CP/MAS). Both wide-line and CP/MAS N.M.R. have been used in the investigations of wood decay by fungi in this thesis, and will be illustrated in more details in the following pages.

2.4.1. Wide-line Proton N.M.R.

Wide-line proton N.M.R. spectra in the solid state are broad featureless absorption lines ($\Delta\nu$ typically 10 to 100 kHz). The major contribution to these proton spectra is from the dipolar interactions between the abundant nuclear spins. Therefore the Hamiltonian describing the interactions can be approximated to:

$$H = H_Z + H_D$$

This is because in the case of proton, the terms H_{CS} and H_{SC} are usually too small to be detected and H_Q is zero. The spectrum produced by a pair of nuclei with spin 1/2 (AX) consists of two lines whose positions is defined by:

$$H = H' \pm \frac{3}{4} \frac{\gamma h}{2\pi} \frac{(3\cos^2\theta - 1)}{r^3_{AX}}$$

where H' is the resonance position that would result from the Zeeman component alone, and θ is the angle between the internuclear vector r_{AX} and the static magnetic field B_0. The two lines present in the spectrum are due to the pair of nuclei, there being no chemical shift resolution. The angular dependence shown in the above equation, yields to different separation distances between the two lines, depending on the orientation of the molecules in the solid lattice in respect of B_0.

Pake in 1948 conducted the earliest study on the orientation dependence of the dipolar interaction in the water of crystallisation of calcium sulphate. In polycrystalline materials, Pake showed that an averaging process occur for the above equation for all possible orientations, yielding to the spectrum shown in dotted lines in figure 2.8., which is the so-called "Pake doublet".

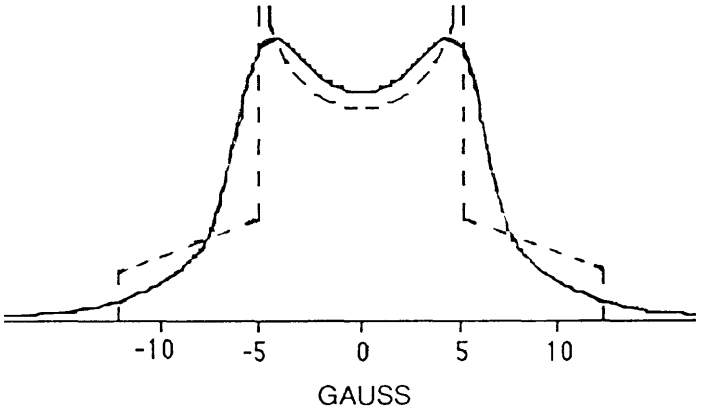

Figure 2.8. Proton N.M.R. absorption curve of a two spin system. The dotted curve gives the absorption for an isolated system, the full curve shows the effect of neighbouring nuclei on the isolated system (adapted from Fyfe, 1983).

The feature illustrated in figure 2.8., is characteristic of the distribution function of an isolated two spin system; a broadening due to dipolar interactions with other nuclei in the lattice must be taken into account. This leads to the spectrum shown in the full curve of figure 2.8. .

Although at first sight the broad features of these spectra seem to be quite uninformative, the analysis of experimental variables as linewidth, second moment $(\Delta H)^2$ and relaxation times can provide unique valuable information about molecular motions present in the sample under consideration. Linewidth and second moment are parameters strictly intercorrelated, the latter being the mean square deviation of the linewidth of the curve calculated from the analysis of the lineshape. The equation which defines ΔH^2 contains an angular term θ which is the angle between the field direction B_0 and the internuclear vector, and a distance term r which is the internuclear distance. These two terms make ΔH^2 very strongly distance dependent, and the spectra very sensitive to the occurrence of molecular

motions. The presence of the latter has the effect of partially averaging the dipolar interactions, leading to a narrowing of the linewidths and a decrease of the second moment. If the motions are very fast then the dipolar contributions are averaged to zero and it may be possible to observe other interactions such as chemical shifts and scalar couplings, provided they are large enough. Also these interactions will experience an averaging effect to the limit of their isotropic values, as in solution.
This exceptional situation is typical of systems in non-viscous solutions and can be described by the total Hamiltonian:

$$H = H_Z + H_{CS} + H_{SC}$$

Other parameters sensitive to molecular motions are the relaxation times. The strength of the dipolar interactions within a system in the solid state, results in all of the nuclei having a single common set of relaxation times, generally referred as "spin temperature".
Bloembergen, Purcell and Pound in 1948, and subsequently Redfield in 1965, developed a theory according to which, assuming a dipolar mechanism for the relaxation process, and a single molecular reorientation characterized by a temperature dependent correlation time τ_c, the T_1 is given by:

$$\frac{1}{T_1} = C\left[\frac{\tau_c}{1 + \omega_0^2 \tau_c^2} + \frac{4\tau_c}{1 + 4\omega_0^2 \tau_c^2}\right]$$

where τ_c is the correlation time for the motion, ω_0 the Larmor precession frequency, C a constant which contains the proton second moment parameter. Assuming that the correlation time obeys an Arrhenius type of temperature dependence, the temperature dependence of T_1 is described in figure 2.9.

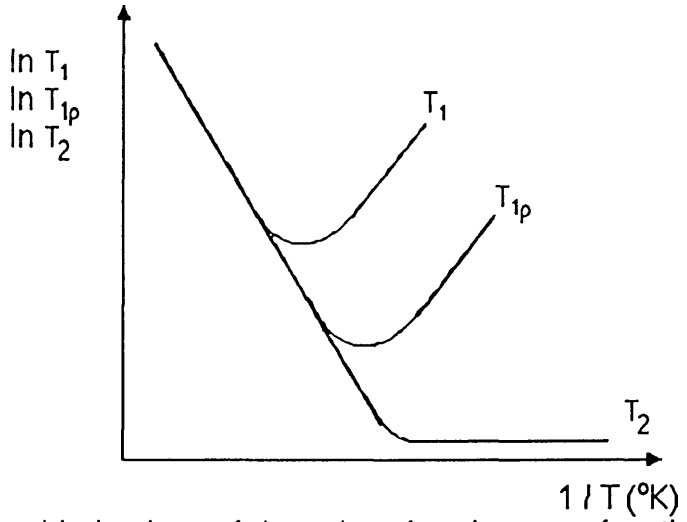

Figure 2.9. General behaviour of the relaxation times as function of temperature.

The variation of log T_1 with 1/T is a V shaped curve with a minimum at $\omega_0\tau_c = 0.62$. The curve is dependent on the spectrometer frequency, as lower frequency spectrometers shift the minimum to lower temperatures. Activation energies E_a may be extracted from both the high and low temperature limiting slopes of the curves, which have gradients $(- E_a / R)$ and $(+ E_a / R)$ respectively.
Since T_2 is proportional to the linewidth, changes in linewidth and second moment due to molecular motions are reflected in T_2 values. The equation which describes T_2 is:

$$\frac{1}{T_2} = \frac{1}{2} C \left[3\tau_c + \frac{5\tau_c}{1 + \omega_0^2 \tau_c^2} + \frac{2\tau_c}{1 + 4\omega_0^2 \tau_c^2} \right]$$

and its temperature dependence is also shown in figure 2.9. .
Another useful relaxation time parameter is the spin lattice relaxation time in the rotating frame, $T_{1\rho}$. This is the time constant for the decay of the magnetization along the on-resonance radio frequency field (B_1) in the rotating frame. The experimental technique used to observe $T_{1\rho}$ is spin-locking, which consists of an on-resonance $90°_x$ pulse that flips the magnetization along the y' axis, followed by a $90°_y$ pulse. This second pulse is called "spin-locking" as it acts as a static field B_1, locking the magnetization along the y' axis. It is applied for a time τ, during which there will be some decay of the y' magnetization, which is detected immediately after the spin-locking pulse has been removed. The τ_c dependence of $T_{1\rho}$ is given by:

$$\frac{1}{T_{1\rho}} = C \left[\frac{5}{2} \frac{\tau_c}{1 + \omega_0^2 \tau_c^2} + \frac{\tau_c}{1 + 4\omega_0^2 \tau_c^2} + \frac{3}{2} \frac{\tau_c}{1 + \omega_1^2 \tau_c^2} \right]$$

where ω_0 is the precession frequency along B_0 and ω_1 that along B_1 . The temperature dependence of $T_{1\rho}$ is illustrated in figure 2.9. .
The different behaviour of the relaxation times in respect to the temperature allows to make some important considerations. The minimum in the T_1 curve occurs at higher temperature than that of $T_{1\rho}$, whose minimum in turn occurs at temperatures much closer to the linewidth changes. Therefore the relaxation times are sensitive to processes with different activation energies: T_1 is sensitive to high frequency motions, T_2 to low frequency motions and $T_{1\rho}$ to intermediate processes. It follows that nuclear relaxation time measurements of wide-line proton spectra provide a direct and very sensitive probe of dynamic processes in solids. However, because a single set of relaxation time exists for all of the nuclei in the sample and there is

no discrimination based on chemical shifts, it is difficult from N.M.R. data alone to unambiguously decide which motions of which groups are occurring.

2.4.2. Wide-line Deuterium N.M.R.

Deuterium is a quadrupolar nucleus, having spin quantum number 1. Therefore solid state N.M.R. spectra of this nucleus are usually dominated by the nuclear quadrupolar interaction H_Q. The quadrupolar term arises from the interaction of the nuclear charge with the non-spherically symmetric electric field gradient. The total Hamiltonian can be written as:

$$H = H_Z + H_Q$$

This is because the anisotropic chemical shift and the scalar coupling terms can be neglected in first approximation, whereas the dipolar interaction is larger and may affect the final spectrum as linebroadening. H_Q is the result of a vectorial interaction, and as such has a three dimensional nature. When the Zeeman interaction is much larger than that of the the quadrupolar component, the energy level diagram from the combined interactions for I = 1 is depicted in figure 2.10. .

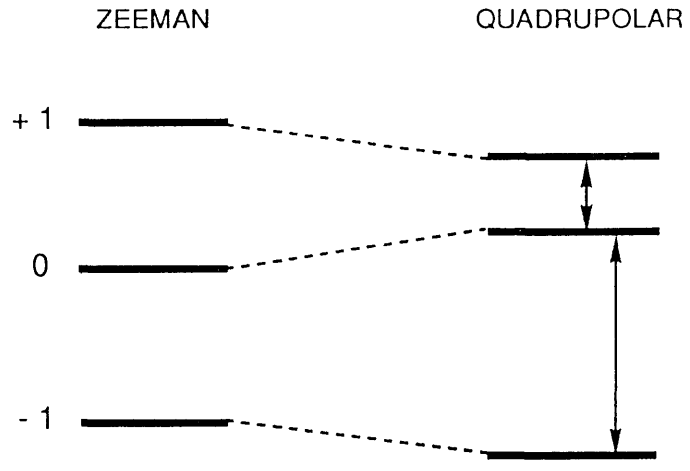

Figure 2.10. Energy levels scheme of a spin 1 nucleus, resulting from Zeeman interaction with the magnetic field and with the quadrupole moment of the nucleus.

The allowed transitions are (m = - 1)⇔(m = 0) and (m = 0)⇔(m = +1) , therefore the spectrum for the nuclear spin interacting with an axially symmetric field gradient consists of a doublet with a peak separation given by:

$$\Delta\nu = \frac{3}{4} C \quad (3\cos^2\theta - 1)$$

where $\Delta\nu$ is the separation in frequency units, θ is the angle between the principal component of the electric field gradient tensor and the magnetic field, C is the quadrupole coupling constant. It follows that the spectrum of a single deuteron in a crystalline material is a doublet whose peak separation reflects the angle of its orientation in the magnetic field. Thus, single crystal deuterium N.M.R. spectra provide a very direct way of probing orientation and electron distributions about hydrogen atoms and their dynamic structures.
However, for polycrystalline materials an averaging process occurs for all possible orientations of every single deuteron, yielding a spectrum with a feature called "powder pattern" shown in figure 2.11.

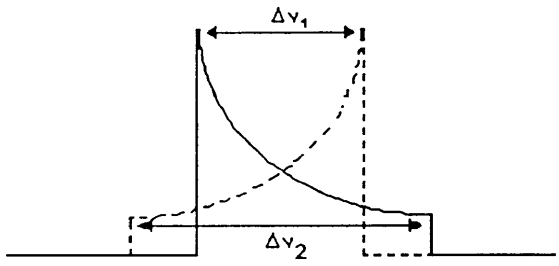

Figure 2.11. "Powder pattern" resulting from the sum of contributions of the random orientations of a spin 1 nucleus with respect to the magnetic field in a polycrystalline sample.

The steps at the wings of the spectrum correspond to $\theta = 0°$, and the central pair of peaks to $\theta = 90°$ and the mid point to the orientation with $\theta = 54°44'$, where the two peaks from the quadrupolar splitting coalesce and the interaction effect vanishes. The separation of the two doublets is given by:

$$\Delta\nu_1 = \frac{3}{4} C$$

$$\Delta\nu_2 = \frac{3}{2} C$$

where $\Delta\nu_1$ and $\Delta\nu_2$ are shown in figure 2.11., and C is the quadrupole coupling constant.
Because the spectra of quadrupolar nuclei are extremely broad, it is experimentally difficult to avoid distortions, given the high power pulses needed to excite the complete frequency range. This problem has been circumvent with the development of the "quadrupolar spin-echo" technique implemented by Bloom and coworkers in 1976. This pulse sequence is related to the spin-echo used to measure T_2 in solution N.M.R., and has the effect of refocussing the spin vectors to produce and echo in the F.I.D. . The loss of critical data points from the beginning

of the F.I.D. caused by the receiver dead-time and pulse breakthrough is avoided in the echo, which is well removed in time from the excitation pulse.

2.4.3. Line-narrowing Techniques: Cross Polarization and Magic Angle Spinning (CP/MAS)

In the case of protons in a solid sample the dipole-dipole interaction is dominant. Its expression contains two terms: the first describes the spatial relationship of the spins with respect to each other and the field (spatial term), the second the orientation of the spins between themselves (spin term). The spin system can be manipulated so that either the spatial or the spin terms are reduced to zero, so that the total dipolar interaction is averaged to zero.
The spatial term can be averaged to zero by the technique of Magic Angle Spinning (MAS), and the spin term by high power decoupling. However, in the homonuclear case of protons this is very difficult to achieve, due to homonuclear decoupling and short chemical shift range problems. These difficulties are eliminated if the nucleus being observed is "dilute" in the spin system considered, i.e. it is a nucleus of spin 1/2 widely distributed in the molecule, but with a small natural isotopic abundance, such as carbon-13.
The effect of the spin dilution can be seen by comparing the different contributions to the interactions of proton and carbon-13 nuclei:

proton : $H = H_{Zeeman} + H_{H\text{-}H\ dipolar}$

carbon: $H = H_{Zeeman} + H_{H\text{-}C\ dipolar} + H_{C\text{-}C\ dipolar} + H_{Shift\ anisotropy}$

It can be noted that while for proton the dipolar interaction dominates, more contributions play role in the carbon-13 spectra. However, in this latter case several important simplification can be applied: the ^{1}H-^{13}C dipolar interaction may be removed by powerful heteronuclear decoupling, and the ^{13}C-^{13}C dipolar interactions are negligible because the low abundance of this isotope (1%) makes very unlikely that two carbon-13 nuclei are close enough to give homonuclear interaction of any importance, given also its $1/r^3$ distance dependence. Thus, all dipolar interactions are eliminated, leaving the chemical shift as dominant line-broadening cause.
In solution the chemical shift of a nucleus is characteristic of the nuclear environment of the nucleus, that is of the magnetic shielding due to the surrounding electrons. In the solid state the chemical shift is characteristic of the magnetic environment of the nucleus in a particular orientation of the molecule with respect to the magnetic field. In this case it contains more information regarding structure and

bonding than the solution isotropic average value. Ideally, in a single crystal where a limited number of orientations will occur, a series of sharp peaks will be observed for each carbon functional groups, one signal for for each magnetically distinct environment in the lattice. In the case of polycrystals, there will be a random distribution of each group over all possible orientations, giving a broad line from the superimposition of the very large number of sharp lines. When the sample is free of random motions, all these lines will tend to the averaged isotropic chemical shift, typical of solution N.M.R.
The contribution of the anisotropy to the chemical shift can be written as:

$$\Delta\sigma \propto (3\cos^2\theta - 1) / r^3$$

This equation shows that any shielding anisotropy falls to zero when the term $(3\cos^2\theta - 1)$ falls to zero, that is when $\theta = 54°44'$; this is the so-called magic angle. Chemical shift anisotropy can therefore be eliminated by spinning the rotor containing the sample exactly at the magic angle, with a spinning rate comparable to the linewidths (in the order of kHz): this is the Magic Angle Spinning (MAS) technique. The resonance linewidths obtainable by a combination of MAS and high power decoupling are comparable to those in solution N.M.R. .
The advantages obtained by using the diluted nucleus, carbon-13, are counteracted by the low sensitivity and extremely long relaxation times. In 1972 Pines and coworkers developed a technique to overcome these problems: the Cross Polarization (CP) pulse sequence. The crux of the experiment is the enhancement of the magnetization of the rare carbon-13 spins from that of the abundant proton spins, due to thermal contact between the two spin reservoirs. This can not be achieved in the laboratory frame, where the two nuclei experience the same applied field B_0, leading to different precession frequencies with different associated energies. The energy gap prevents transfer of polarization between the carbon-13 and proton reservoirs; this situation can be described as follows:

$$\omega_C = \gamma_C B_0 \quad \text{and} \quad \omega_H = \gamma_H B_0$$
$$\text{because} \quad \gamma_H \approx 4\,\gamma_C \quad \text{then} \quad \omega_H \approx 4\,\omega_C \quad \text{and} \quad \Delta E_H \approx 4\,\Delta E_C$$

However, in the rotating frame energy exchange is possible: the proton magnetizations can be spin locked along the y' axis, where it will experience the radiofrequency field B_1. The magnitudes of the two spin-locking fields B_{1H} and B_{1C} are chosen so that the "Hartmann-Hahn condition" is established. This condition is described in the following equation:

$$\gamma_H B_{1H} = \gamma_C B_{1C} \quad \text{and} \quad \Delta E_H = \Delta E_C$$

Since γ_H / γ_C is 4/1, the locking field B_{1C} must be four times B_{1H} to transfer spin-temperature between the two spin reservoirs during the time t, the "contact time". During this interval of time polarization is being transferred between the proton and the carbon-13 spin reservoirs, as depicted in figure 2.12.

Carbon-13 spins will adopt the more favourable spin distribution of the proton system, giving a maximum magnetization enhancement equal to the ratio of the magnetogyric ratios. The intensity of the carbon spectrum will effectively depend on the relaxation of the proton spin system in the rotating frame, that is $T_{1\rho}$. This involves that the recycle time for complete relaxation and efficient spectral accumulation is 5 times $T_{1\rho}$, and is in general much shorter than for a conventional carbon-13 experiment, yielding better carbon sensitivity.

The pulse sequence for cross polarization (CP) experiments is depicted in figure 2.13.

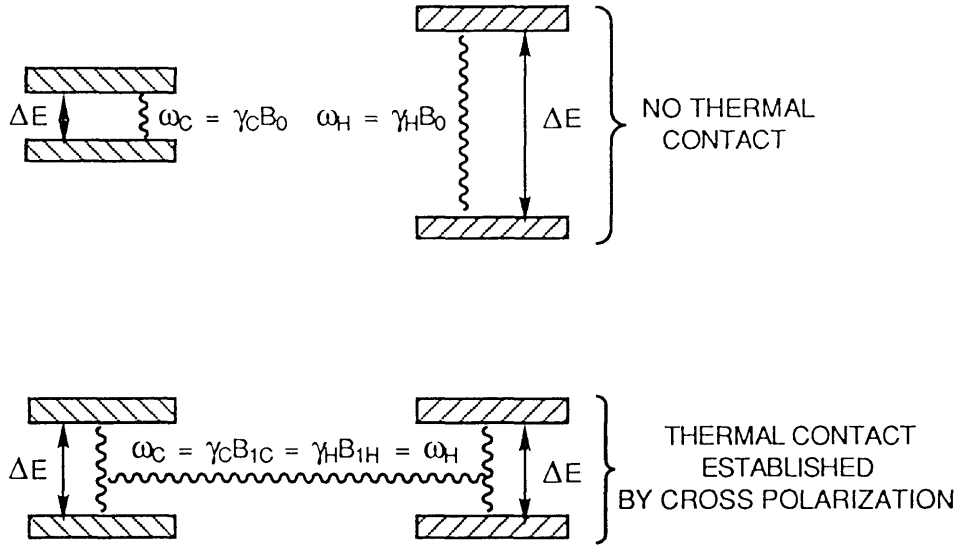

Figure 2.12. Thermal contact between carbon-13 and proton spin reservoirs achieved by cross polarization technique.

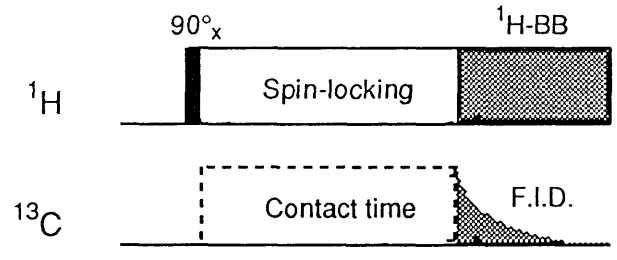

Figure 2.13. Cross polarization pulse sequence.

Firstly, the proton magnetization is rotated 90° to the y' axis and then is spin-locked by an on-resonance spin-locking pulse applied along y'. Proton spins are kept

locked along y' for the contact time t, during which carbon-13 are rotated along the y' direction, both sets of spins are locked, and by a correct choice of the magnitude of the spin-locking fields B_{1H} and B_{1C}, the net carbon magnetization may be enhanced by the proton reservoir. After the carbon magnetization has built up during the contact time, the locking field is switched off and the carbon F.I.D. recorded.

As the transfer of polarization between carbon-13 and protons occurs during the contact time, the intensity of the F.I.D. resulting from this experiment depends critically upon the length of the contact. When the intensity of the carbon-13 resonance signal is plotted against a variable contact time, the resulting curve consists in a sharp increase in intensity for very short times, where the exponentially increasing cross polarization T_{CH} is prevailing. After a maximum at the optimal contact time, the intensity will follow the exponential decay due to the proton spin-lattice relaxation $T_{1\rho}$, which prevails for long t. This is illustrated in figure 2.14., where small differences in optimal t for quaternary, aromatic and aliphatic carbons are showed.

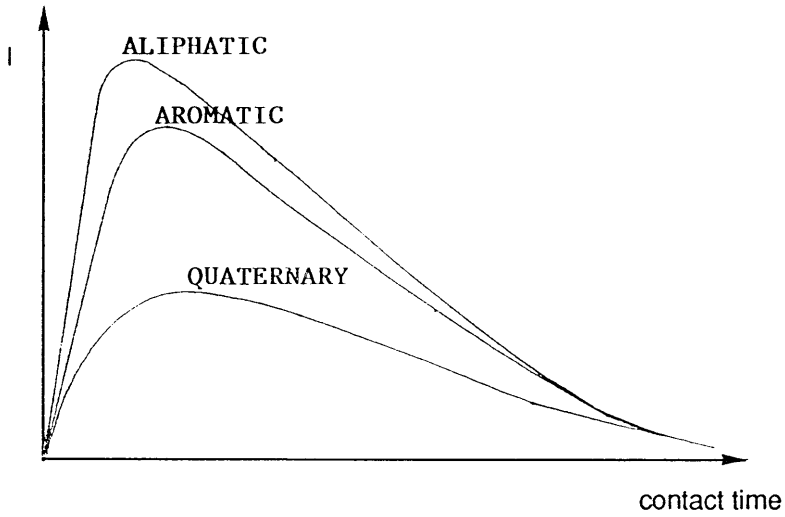

Figure 2.14. Carbon signal intensity (I) variations in function of the contact time.

These differences present some difficulties in the quantitative considerations based on CP/MAS spectra data.

The combination of high power decoupling, cross polarization and magic angle spinning (CP/MAS), yields to high resolution spectra of solids, and it has been applied in this research to the investigation of cell wall biodegradation by fungi.

2.4.4. Pulse Sequences in CP/MAS Experiments: Non-Quaternary Carbon Suppression (NQS) and Total Sidebands Suppression (TOSS)

The CP/MAS experiment is a multipulse technique itself, but a more complex extension of this simple sequence can allow us to extract more information from the spectra. Many pulse sequences have been developed for solid state studies, only those that have been applied in the experiments on cell wall degradation, the topic of this thesis, are here reported.

An important limitation of the CP/MAS technique in terms of structure elucidation, is that it is not readily possible to perform decoupling experiments, such as for example selective decoupling or off-resonance decoupling, which may be employed in the detection of carbon-13 N.M.R. spectra in solution. This is because the solid state interactions being removed by high power decoupling, are dipolar in nature and must be completely removed during acquisition: the use of coherent dipolar decoupling also eliminates the ^{1}H-^{13}C coupling, which carries structural information.

Some selection techniques have been devised to extract structural information by using the dipolar interaction itself. One of these is the non-protonated carbon selection, or non-quaternary carbon suppression (NQS) pulse sequence. This is based on the principle that the interaction between two spins depends on the internuclear distance ($1/r^3$), and therefore there will be a large difference in the dipolar broadening of carbon atoms with one or more hydrogen attached, compared to quaternary carbons. This pulse sequence differs from the CP experiment in the addition on a delay between the cross-polarization step and the acquisition, in which the proton field is turned off (figure 2.15.).

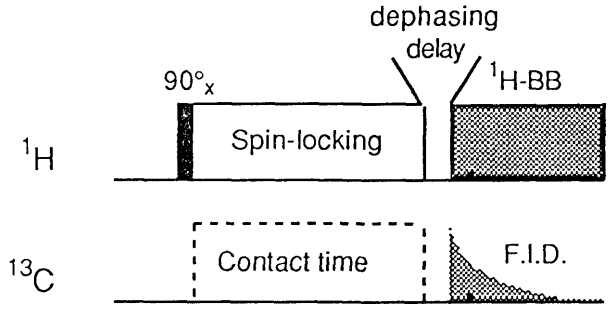

Figure 2.15. Non-protonated carbon selection pulse sequence (NQS).

During this delay, that is about 30-100 μs, the carbon spins will dephase under the influence of the proton dipolar field, but those with attached protons will dephase very quickly compared to those which do not. After this delay, the proton field is reapplied to decouple the dipolar interactions during the acquisition of the carbon-

13 F.I.D. The final spectrum will contain only the quaternary carbon signals, which were the only ones not completely dephased during the delay.

Another complication in the high resolution N.M.R. spectra, is the presence of peak spinning sidebands. Sidebands are rotational echoes that occur during refocussing of the magnetization due to magic angle spinning. These echoes are sometimes visible from the F.I.D., and their effect is to prolong the existence of the magnetization in the time domain, which results in a narrowing of the resonances in the frequency domain. The echoes are replicas of the initial decay, therefore the spinning sidebands are replicas of the isotropic line in the spectrum, separated by the spinning frequency. This may lead to complicated spectral features, where spinning sidebands overlap with other resonances.
Although at low magnetic field strengths the sidebands can be eliminated entirely by increasing the spinning speed, this is not possible at high fields, where spectra may be difficult to interpret. The total sidebands suppression (TOSS) pulse sequence has been developed to eliminate this effect. This method consists in generating Hahn spin echoes separated by time delays τ arranged such that the sidebands are inverted, but the isotropic peak is unaffected. The addition of spectra with normal and inverted sidebands intensities yields to a spectrum showing only the isotropic peaks. It must however be remembered, that spectra acquired by using the TOSS pulse sequence are quantitatively not reliable: this is because the sidebands contribute to the total signal intensity of a resonance peak, and their elimination leads to an underestimation of the resonance intensity.

Chapter 3

MATERIALS AND METHODS

3.1. Radical Intermediates in Veratryl Alcohol Oxidation by Ligninase

The production of radical intermediates during the oxidation of 3,4-dimethoxybenzyl alcohol (veratryl alcohol) and 1,4-dimethoxybenzene by purified ligninase was followed by ^{1}H-N.M.R. Veratryl alcohol and 1,4-dimethoxybenzene were supplied by Aldrich.

Ligninase was isolated from culture filtrates of the white-rot fungus *P. chrysosporium* as described by Harvey and coworkers (1989a). The activity of the enzyme was determined from the rate of oxidation of veratryl alcohol in the presence of hydrogen peroxide, followed spectrophotometrically at 310 nm, according to Tien and Kirk (1984). This wavelength correspond to the maximum of absorption of the product from veratryl alcohol oxidation, veratraldehyde.

All solutions were prepared in deuterated water (Aldrich) and buffered with 20 mM deuterated phosphate. Deuterium peroxide was prepared by adding sodium peroxide to deuterated water and deuterophosphoric acid likewise from phosphorus pentoxide (Aldrich). The pD of the solutions was calculated by subtracting 0.4 from the pH meter reading (Fersht, 1985).

3.1.1. Proton N.M.R. Experiments and Linewidth Measurements

All N.M.R. experiments were performed in nitrogen flushed 5 mm tubes with degassed solutions; the reaction volume was 0.5 ml and the enzyme turnover was initiated by addition of peroxide. Typical solutions were 2 mM veratryl alcohol or 1,4-dimethoxybenzene, 0.5 mM peroxide and 0.02 μM ligninase. The enzyme concentration was determined at 407.6 nm using a extinction coefficient of 133 mM^{-1} cm^{-1} (Gold et al., 1984). Various controls were carried out in the absence of the enzyme, or peroxide, or in the presence of enzyme that had been heated at 100°C.

^{1}H-N.M.R. spectra were obtained on a Bruker AC200 spectrometer operating at 200 MHz. A spectral window of 2000 Hz was used to sample 8192 data points; 8 transients were averaged for each spectrum with 2 initial dummy scans. A pulse to pulse time of 10.8 s was employed to ensure complete recovery of the

magnetization and the residual water was suppressed by a selective presaturation pulse.
The resonances' linewidths were calculated by measuring the width at half height of the methoxygroup signals.
All chemical shifts are reported relative to sodium 3-(trimethylsilyl)2,2,3,3-tetradeuteropropionate (TSP, Aldrich).

3.1.2. Inversion-recovery Experiment

The effect of the enzyme reaction on the spin lattice relaxation time was determined with an inversion recovery pulse sequence:

$$\pi - \tau - \pi/2 - \text{collect}$$

A fixed delay τ of 800 ms, corresponding to $[0.69 \cdot T_1]$ of the veratryl alcohol's methoxyl group was used. Under these conditions, the methoxyl signal is a null.
The signal intensity of the methoxygroups was monitored in the presence of ligninase, after addition of peroxide, in the same reaction conditions described paragraph 3.1.1.

3.2. One and Two-dimensional N.M.R. Experiments on Lignin

Organosolv lignin samples used for the N.M.R. experiments were prepared from spruce wood chips, by hydrolysis in 50% aqueous ethanol and 75% aqueous ethylenglycol mixtures at 135°C for 2 hours, according to the procedure described by Sarkanen and coworkers (1981). After the pulping reaction was stopped, the solvents were removed by evaporation under reduced pressure, leading to the precipitation of the organosolv lignin.
All the solutions used for the N.M.R. experiments described in the following paragraphs were filtered through 0.45 µm pore size polytetrafluoroethylene (PTFE) filters. Chemical shifts were referred to tetramethylsilane (TMS, Aldrich) or to sodium 3-(trimethylsilyl)2,2,3,3-tetradeuteropropionate (TSP, Aldrich), depending on the deuterated solvent used in the N.M.R. experiments.

3.2.1. Carbon-13 N.M.R. Experiments

Carbon-13 N.M.R. spectra of organosolv spruce lignin were recorded with a Bruker AM 300 N.M.R. spectrometer operating at 75.5 MHz for the carbon-13 nuclei frequency.
Lignin samples were dissolved in deuterated dimethylsulfoxide (200 mg/ml) in 10 mm N.M.R. tubes (Gold label, Aldrich). To decrease the solution's viscosity, the spectra were collected at 40°C. The broad band decoupling technique was used both to increase the sensitivity and to decouple the proton spins; 28000 transients were collected using a pulse angle of 53° corresponding to a 8 μs pulse width. The spectral width was 20000 Hz (220 ppm), with an acquisition time of 819 ms. A recycle delay of 3 s was used before each acquisition.
Distortionless Enhancement by Polarization Transfer (DEPT) pulse sequence was used to improve the sensitivity and the resolution of the carbon-13 N.M.R. spectra. The experiments were carried out on a Bruker AC200 spectrometer, operating at 50.3 MHz for the carbon-13 nuclei. The pulse sequence was:

Proton Excitation:	$\pi/2_x$ - Δ - π_x - Δ - θ_y - Δ -	decoupling		
Carbon Excitation:		$\pi/2_x$	π_x	collect

A fixed delay Δ of 3 ms corresponding to $(0.5 / J_{(CH)})$ was used, and the θ_y pulse was chosen to be 135 degree to give the CH and CH_3 signals positive, the CH_2 signals negative, and a null for quaternary carbons. The pulse lengths were calibrated so that the proton $\pi/2$ pulse on the decoupling channel was 19 μs for a decoupling power of 0H, and the carbon $\pi/2$ pulse was 10 μs. To allow complete phase cycling, 12000 transients were collected with an acquisition time of 369 ms and a spectral width of 11000 Hz (220 ppm). A recycle delay of 5 s was inserted between each scan.

3.2.2. Proton N.M.R. Experiments

All proton N.M.R. experiments were carried out on a Bruker AC200 N.M.R. spectrometer operating at 200 MHz for the hydrogen nuclei.
Lignin samples were prepared as described in section 3.2.; lignin model compounds 4-hydroxycinnamic acid, 4-hydroxy-3-methoxycinnamic acid and 3,5-dimethoxy-4-hydroxycinnamic acid were supplied by Aldrich.
The 1D spectra were collected in various deuterated solvents, such as dimethylsulfoxide, tetrahydrofuran, dioxane-water (5:1), with lignin concentration of 100 mg/ml in 5 mm N.M.R. tubes (Gold label, Aldrich). A spectral window of 2403

Hz was used to collect 4096 data points zero filled to 8192 data points, with an acquisition time of 852 ms. A $\pi/2$ pulse of 7.5 μs was used and 100 transients were averaged.

The 2D N.M.R. experiments were carried out on lignin and lignin model compounds in deuterated tetrahydrofuran (100 mg/ml). 2D spectra were recorded using the pulse sequence programs of the Bruker microprogram library.

COSY experiments were carried out using a spectral width of 2403 Hz in the F2 dimension with 1024 data points, and 1200 Hz in the F1 dimension with 256 data points. The 256 increments in the F1 dimension were zero-filled to 512 points before Fourier transformation. The acquisition time was 213 ms and a relaxation delay of 5 s was used. Each serial free induction decay was obtained averaging 16 transients to allow phase cycling and 4 dummy scans were introduced before averaging the transients. The $\pi/2$ pulse was calibrated at 7.5 μs. The spectra were non-phase sensitive (magnitude mode) and the 2D matrix was processed in both domains by using a shifted sinebell function with pure sine shape. The data matrix was symmetrized about the diagonal, and artefacts were identified.

The 2D J-resolved spectra of lignin were obtained at 70°C, using a spectral window of 2400 Hz in the F2 dimension, collecting 2048 data points with an acquisition time of 426 ms. Each free induction delay was obtained averaging 8 scans with 2 preliminary dummy scans; a recycle delay of 5 s was used before each scan. The spectral window in the F1 dimension was 19 Hz, with 64 increments zero-filled to 128 data points. The 2D data matrix was processed by using a shifted sinebell function with different degree of shift (pure sine and pure cosine).

3.2.3. Homonuclear Decoupling Experiment

Proton homonuclear decoupling experiments of lignin were carried out by using the inverse-gated pulse sequence. This technique allows the acquisition of decoupled spectra without NOE effect. This can be achieved by turning on the proton decoupler only during the signal acquisition, so as the coupling effects are immediately eliminated, and the NOE does not have time to build up (figure 3.1.).

Proton spectra were acquired by using the same acquisition parameters employed in other 1D N.M.R. experiments (paragraph 3.2.2.); 16 transients were averaged with 2 initial dummy scans. A delay of 1 s was inserted to allow the decoupling frequency to be set in the following positions: 6.50 ppm, 6.80 ppm, 6.90 ppm and 7.10 ppm. A control spectrum was obtained by setting the decoupler frequency at 8.69 ppm, a blank region in the lignin spectrum. Difference spectra were carried

out subtracting the decoupled spectra from the control spectrum, by using the software facilities of the Bruker DISR89 on the Aspect 3000 computer.

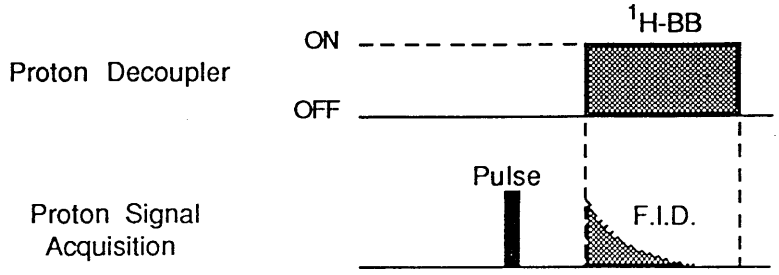

Figure 3.1. Pulse sequence for inverse-gated decoupling technique.

3.2.4. Hahn Spin-echo Experiment

Spin-echo experiments were carried out by using the Hahn pulse sequence:

$$\pi / 2 - \tau - \pi - \tau - \text{echo}$$

The acquisition parameters were the same as for other proton N.M.R. experiments on lignin (paragraph 3.2.2.). 16 transients were averaged and a recycle delay of 5 s was introduced before each acquisition; various τ delays were tested in the range between 1 and 500 ms.

3.2.5. Proton N.M.R. Spectra Simulation

The simulation experiments of proton N.M.R. spectra of lignin and lignin model compounds was carried out by using the Bruker software program "Parameter Adjustment in N.M.R. by Iteration Calculation" (PANIC) on a Bruker Aspect 3000 computer.

The spectral parameters defining the spin system of lignin model compounds, that is chemical shifts, scalar coupling constants and linewidths, were input in the PANIC program to calculate the theoretical spectrum. The model compounds considered in this experiments were the 4-hydroxycinnamic acid and the 4-hydroxy-3-methoxycinnamic acid. The linewidths in the aromatic region (from 6.00 ppm to 8.00 ppm) were then broadened to 10 Hz, 30 Hz, 50 Hz and 70 Hz, and the spectra obtained were compared to the experimental spectrum of organosolv spruce lignin.

3.3. Associative and Colloidal Behaviour of Lignin

The lignin sample used for the experiments reported in the following paragraphs was the same that was analysed by N.M.R. as described in section 3.2.

3.3.1. Molecular Weight Determination of Lignin by HPLC Gel-filtration

Molecular weight (MW) of organosolv spruce lignin was determined by gel-filtration on a Varian 5000 High Pressure Liquid Chromatograph (HPLC), with a Varian 2050 Variable Wavelength Detector, and a Spectra Physics SP 2050 Integrator.
A Zorbax HPLC column (Du Pont) with porous silica microspheres (PSM 60S) as stationary phase, and N,N'-dimethylformamide (DMF, Aldrich HPLC grade) as mobile phase were used.
Solutions in DMF of 10 mg / ml polystyrene molecular weight standards (Du Pont) with MW of 800, 2000, 4000, 9000, 17500 and 50000, were used to calibrate the HPLC system.
Organosolv spruce lignin was dissolved in DMF (0.25 mg / ml), filtered through a 0.45 μm pore size polytetrafluoroethylene (PTFE) filter, and 10 μl were injected into the HPLC apparatus with flow of 1 ml / min. Eluates were detected by measuring the absorbance at 280 nm, wavelength corresponding to the maximum absorbance of lignin.

3.3.2. Langmuir Blodgett Trough Experiments

Langmuir Blodgett trough experiments were performed to calculate the average cross-sectional area of organosolv spruce lignin molecules.
The instrument used was a home built Langmuir Blodgett trough, kindly made available by the Department of Chemical Engineering in Imperial College. The principle of the technique is illustrated in paragraph 6.2.
Lignin monolayer were obtained by deposition of 14 μl of a 1 mg / ml solution of lignin in chloroform-tetrahydrofuran (7:1) solvent mixture, on the water surface of the trough dish. After evaporation of the solvent mixture, the lignin monolayer was compressed by a movable barrier that reduces the area available to the molecules, while the surface pressure was measured by a movable float made by a filter paper soaked in chloroform and attached to a torsion wire.
The experiments were performed at constant temperature of 21.8°C.

3.3.3. Light Scattering Experiments

Light scattering experiments were carried out on organosolv lignin solutions in dioxane water (5:1), at concentrations ranging from 0.01 to 2.0 mg / ml, after filtering through a 0.45 μm pore size polytetrafluoroethylene (PTFE) filter.
The intensity of the scattered light was measured on a Perkin Elmer Luminescence Spectrometer LS50, at 625 nm a wavelength that was found to be unaffected by fluorescence effects of lignin, as shown in figure 3.2.
The intensity of the scattered light was read at a measurement angle of 90°, in a square 1 cm cuvette.

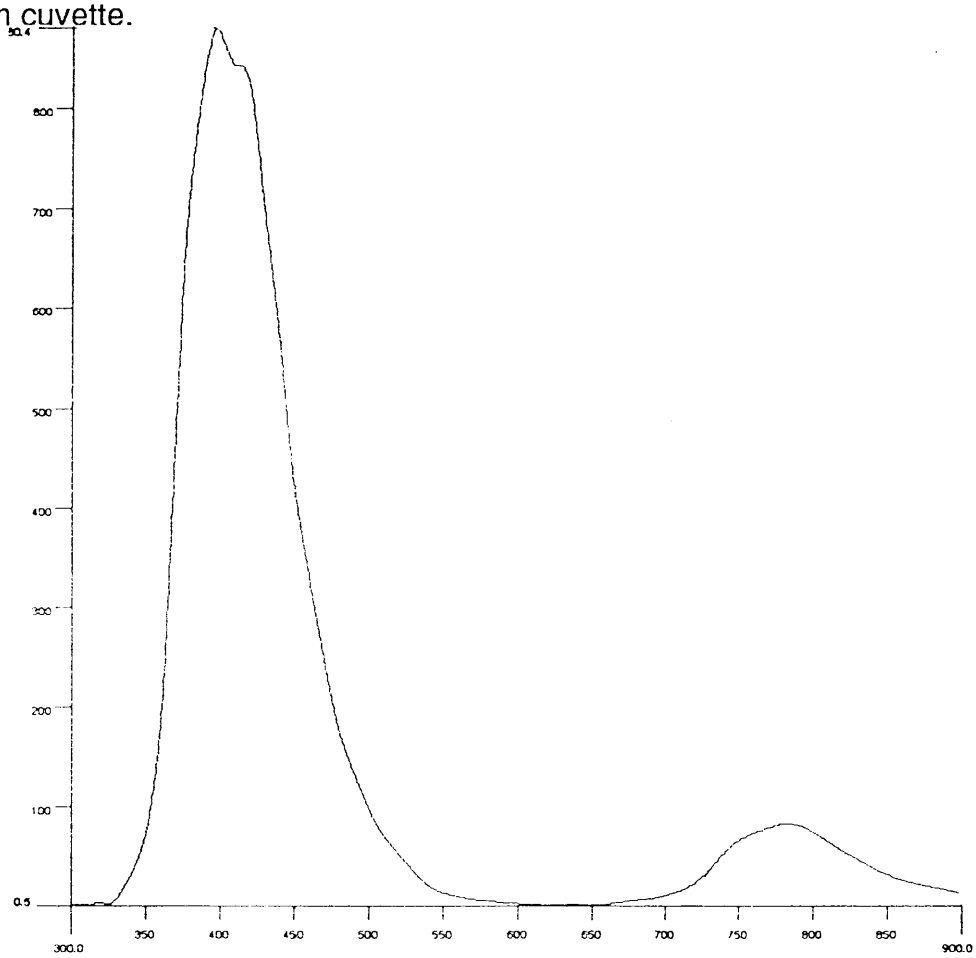

Figure 3.2. Fluorescence spectrum of organosolv spruce lignin [0.1 mg/ml in dioxane-water (5:1)], excitation at 312.8 nm.

In a dynamic light scattering experiment , a more complex apparatus is required. The light from a laser passes through a polarizer to define the polarization of the incident beam, and then impinges on the scattering medium. The scattered light then passes through an analyzer that selects a given polarization and finally enters a detector. The position of the detector defines the scattering angle θ. A diagram of the apparatus is shown in figure 3.3.

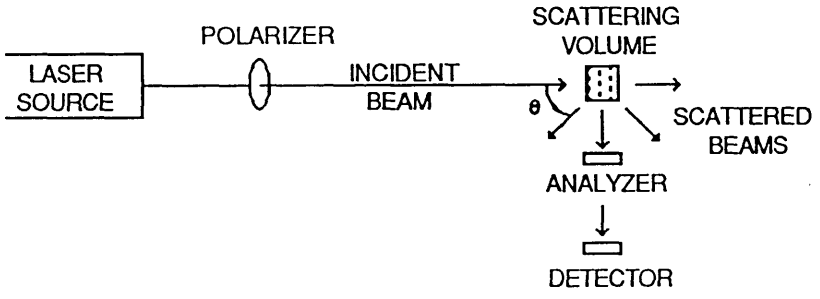

Figure 3.3. Schematic representation of a light scattering apparatus.

The quantity measured in dynamic light scattering experiments is the time-correlation function g(t) of the scattered intensity. The spectral features of the scattered light depend on the time scale characterizing the motions of the scatterers, that leads to information about the dimensions of the particles.
The dynamic light scattering experiments of lignin were performed in a Malven instrument on the same solutions that were used in the static experiments. A laser source at 632.8 nm was used, reading at a measurement angle of 90°. The samples were positioned in a toluene bath (refractive index of 1.50), in a square quartz cell (1 cm) at 25°C. The particle hydrodynamic radius was calculated with a Malven Correlator system, assuming a spherical shape and a sample viscosity of 1.167 cp.

3.3.4. Spin-lattice Proton N.M.R. Relaxation Times of Lignin

Spin-lattice proton N.M.R. relaxation times of lignin were measured in deuterated dioxane-water (5:1) solvent mixture (100 mg/ml). The inversion-recovery pulse sequence described in paragraph 2.2.1. was used by using the same acquisition parameters reported in paragraph 3.2.2.
A recovery delay of 10 s was used between each experiment, and 16 transients were averaged for each spectrum. A series of inter-pulses delays was used ranging from 0.1 ms to 10 s. The relaxation values were calculated using the Bruker DISR89 software facilities on an Aspect 3000 computer.

3.3.5. Effect of pH on Lignin Association: HPLC and SEM Experiments

Organosolv spruce lignin was solubilized in NaOH 0.1 M, at a concentration of 50 mg / ml aqueous solution, to give a pH 12. The solution was dived into aliquots,

whose pH was corrected by addition of HCl 0.1 M to reach pH 8, pH 6, pH 4 and pH 2. The final volume of each solution was adjusted by addition of distiled and deionized water to give a final lignin concentration of 1% wt / vol. The lignin solutions and suspensions so obtained, were divided into two pools: one was treated for HPLC gel-filtration molecular weight analysis, the other was analyzed to the scanning electron microscope (SEM).

HPLC gel-filtration. Lignin suspensions at different pHs were freeze-dried, and the powder resuspended in N,N'-dimethylformamide in the following concentrations: pH 12 1.0 mg / ml; pH 8, pH 6 and pH 4 0.40 mg / ml; pH 2 0.50 mg / ml and untreated control 0.25 mg / ml. The HPLC gel-filtration analysis was conducted under the same conditions described in paragraph 3.6.1.

SEM. Each lignin suspension was well shaken, and one drop was spotted on a glass slide (10 mm in diameter). The specimens were rapidly immersed in Acton 22 slush, cooled by liquid a nitrogen bath. After quick freezing step, the samples were transferred in a freeze-drier on a cold plate maintained at -30°C. The dry specimens were then coated with Gold and examined on a Philips 500 Scanning Electron Microscope.

3.4. Wide-line Solid State N.M.R. of Wood

Wide-line experiments were carried out on samples of beech (*Fagus sylvatica*), which is hardwood, and Scots pine (*Pinus sylvestris*), which is a softwood. Blocks of 50x3x3 mm size were cut from sapwood with the long axis parallel to the longitudinal tracheids. Each sample was fitted in a 5 mm N.M.R. tube and sealed with a tight fitting teflon cap. Spectra were acquired on a Bruker MSL200 wide bore instrument, and a broadband multinuclei probe with transverse coil was used.

3.4.1. Wide-line Proton N.M.R. Experiments

Proton spectra were acquired at 200.13 MHz; the 90° pulse length was 2.5 µs and the receiver dead time was 5 µs. Free induction decays were collected by averaging 128 transients, with phase alternation to reduce spurious signals; 2048 data points were acquired on 250 KHz spectral width. Pulse - to - pulse delays of 3 s were used to allow complete relaxation of the spins.

3.4.2. Wood Moisture Content Determination by Proton N.M.R.

Wood moisture content was estimated from the proton F.I.D. signal intensities, by using the equation reported by Hailey and coworkers (1985). This equation relates the moisture content with the proton density of wood and water, as follow:

$$\% mc = [M_0 / (S_0 - M_0)] \times [\rho_{H\,wood} / \rho_{H\,water}] \times 100$$

where: % mc is the percent moisture content
M_0 is the zero time intercept on the F.I.D. of the mobile signal component
S_0 is the zero time intercept on the F.I.D. of the total signal component
$\rho_{H\,water}$ is the proton density of water
$\rho_{H\,wood}$ is the proton density of wood

In the calculations a ratio of 0.5 was used for $\rho_{H\,wood} / \rho_{H\,water}$, according to Hailey and coworkers (1985). The moisture content was also determined by oven drying the wood samples until no further weight change occurred. By knowing the initial and final weight, the moisture was calculated as follow:

$$\% mc = [(\text{initial weight} - \text{final weight}) / \text{final weight}] \times 100$$

The correlation between data obtained on the same sample from both methods, was tested by linear regression analysis.

3.4.3. N.M.R. Relaxation Times Measurements

T_1 measurements were obtained using the inversion recovery pulse sequence. The 180° pulse length was 5.0 μs, and the 90° pulse was 2.5 μs. Series of 21 F.I.Ds. were collected using different delays τ, ranging from 10 μs to 7 s. A recycle delay of 7 s ($> 5xT_1$) was used to ensure complete recovery of the magnetization. All other acquisition parameters were the same as for the proton spectra previously described.
Series of F.I.Ds. were sampled at the third point from the zero time intercept, and experimental data were fitted to the function:

$$I = I_0 [1 - 2 \exp(-\tau / T_1)]$$

where: I is the intensity of the resonance at the delay τ
I_0 is the intensity of the fully relaxed resonance

This function was fitted for one and two components; all fitting procedures were carried out by using the SIMFIT software program on a Bruker ASPECT 3000 computer.

T_2^* was firstly estimated by linewidth analysis; the linewidth at half height of the peaks was calculated from the spectra, and their corresponding T_2^* values were calculated from equations:

$$T_2^* = 3.34 / 2\pi \Delta\nu_{1/2} \quad \text{for Gaussian lineshape}$$
$$T_2^* = 1 / \pi \Delta\nu_{1/2} \quad \text{for Lorentzian lineshape}$$

The fast decaying component was determined by solid echo experiments: the first part of the F.I.D. was selected, and the slow decaying contribution was subtracted from the overall signal intensity. The experimental data points so obtained were fitted to the Gaussian function:

$$I = I_0 \exp\left(-\sqrt{t / T_2}\right)$$

where: I is the intensity of the resonance at the time t, during signal intensity decay
I_0 is the intensity of the initial signal intensity

This function was fitted for one component, using the computer program above described.
A more precise and complete T_2 determination was made by using the CPMG pulse sequence. Acquisition parameters were the same as for inversion recovery experiments, but 22 series of spectra were collected applying different refocussing delays τ, ranging from 28 μs to 200 ms. Signal intensities data obtained by sampling series of F.I.Ds., were fitted to the equation:

$$I = I_0 \exp\left(-\tau / T_2\right)$$

where I and I_0 are described above. Fittings up to three components were performed with the same computer program.

3.4.4. Variable Moisture Content Experiments

N.M.R. spectra at different moisture contents were performed on the same beech wood sample. This was first soaked into distiled water for 12 hours, applying a vacuum for 15 minutes in order to remove air present in wood cell lumina and give access to water. It was then dried in step of 15 minutes at 70°C under vacuum, and

relative spectra and relaxation times determinations were made until water was completely removed.

3.4.5. Variable Temperature Experiments

The Bruker MSL 200 spectrometer used for these experiments was equipped with computer controlled variable temperature unit. All experiments were started at lowest temperature (1°C), ending at the highest temperature (90°C), to minimize the eventual water loss in the atmosphere of the N.M.R. tube. A delay of 20 minutes was introduced at every temperature change to allow the system to reach thermal equilibrium.

3.4.6. Wide-line Deuterium N.M.R.

Oven dried wood samples were left for 12 h soaking in deuterated water; a vacuum was also applied for 30 minutes to remove residual air from the cell lumen of wood to make more volume available to the deuterated water. Deuterium spectra were acquired at 30.72 MHz, by using the quadrupolar spin - echo pulse sequence with quadrature phase cycle:

$$\pi/2 - \tau - \pi/2 - \tau - \text{echo / collect}$$

The 90° pulse length was 3.4 μs and a delay τ of 15 μs was used between pulses to generate an echo in order to avoid signal distortions caused by the strong excitation. 128 transients were averaged collecting 4096 data point over a spectral width of 10 KHz. A recycle delay of 5 s was used.
Spectra were obtained at different deuterated water contents for the same wood samples. This was achieved by progressively oven drying a wet deuterated wood sample at 70°C under vacuum, and collecting spectra every 10 minutes. Before collecting the spectrum, the sample was left to cool at room temperature for 20 minutes.

3.4.7. Preparation of Samples for Degradation Experiments

Sample of decayed wood were kindly provided by the Timber Technology Group, Department of Biology, Imperial College. Blocks of 50x3x3 mm size of Beech (*Fagus sylvatica*) and Pine (*Pinus sylvestris*) woods were prepared from air dried

sapwood and then sterilized by irradiation using a ^{60}Co γ source at a level equivalent to 2.5 mrad. Four replicates of each sample were exposed for 6 weeks to the white-rot fungus *Coriolus versicolor* and to the brown-rot fungus *Coniophora puteana*. Sterile controls were also prepared and incubated for the same length of time on agar only. All fungi were grown on agar media containing 4% malt extract (Oxoid) and 2% agar (Oxoid Technical n. 3) in distiled water. All media were sterilized in an autoclave. Waterlogging during fungal growth was prevented by placing a sterile plastic mesh between the specimens and the mycelium. The decay process was stopped after 6 weeks by irradiation as described above.
The N.M.R. analysis was carried out on the samples fitted in 5 mm N.M.R. tubes, sealed with tight fitting caps. Proton N.M.R. relaxation times were measured as described above, averaging values determined on each replicate.
Statistical analysis of the results was applied, in order to test the significance of the variations between the values of the control and those of the decayed samples. The T-test was carried out on the means and the standard deviations obtained from four measurements; the null hypothesis was rejected when the probability that the observed difference occurred by chance was less than 1 in 100, that is with a significance level of 1%. Three degrees of freedom were applied, with a critical value for t of 5.84.

3.5. CP/MAS N.M.R. and FT/IR Spectroscopy on Sound and Decayed Wood Cell Walls

CP/MAS and FT/IR spectroscopy were applied to study Scots pine (*Pinus sylvestris*) and beech (*Fagus sylvatica*) wood cell walls, before and after degradation by brown-rot (*Coniophora puteana*) and white-rot (*Coriolus versicolor*) fungi.
To this purpose, the same samples analyzed by wide-line N.M.R. described in the previous paragraphs, were ground to 40 mesh prior high resolution spectroscopic analysis.
Spectra of powder organosolv spruce lignin and cellulose from Whatman n. 1 filter paper strips, were also obtained and compared with spectra of whole cell walls, in order to facilitate peaks assignments.

3.5.1. CP/MAS N.M.R. Spectroscopy Experiments

Carbon-13 CP/MAS N.M.R. spectra were obtained on Bruker MSL200 and AM300 instruments with solid state accessories and operating respectively at 50.32 and 75.47 MHz for carbon-13 frequency. A multinuclear MAS probe was used; the magic angle was adjusted at 54.7° by using the ^{79}Br spectrum of KBr, maximizing the number of spinning sidebands. Sample were packed in ceramic MAS rotors under vibration. Rotors were spun at 4500 Hz; the optimal contact time was determined by applying a variable delay τ ranging between 0.4-10 ms, to obtain the most favourable Hartmann-Hahn condition. The F.I.D. signal intensities were plotted as a function of the contact times. The cross-polarization time T_{CH}, and the proton spin lattice relaxation time in the rotating frame $T_{1\rho H}$, were determined by fitting the experimental data to the equation:

$$I = I_0 / (1 - T_{CH} / T_{1\rho H}) \times [\exp(-\tau / T_{1\rho H}) - \exp(-\tau / T_{CH})]$$

where: I is the intensity of the resonance at the time t, during signal intensity decay
I_0 is the intensity of the initial signal intensity
τ is the variable contact time

Fitting procedure was carried out by using SIMFIT software on a Bruker Aspect 3000 computer. Spectra were acquired with 2048 data points over a spectral width of 25 kHz; normally 40000 transients were averaged, inserting a pulse repetition delay of 3 seconds.
In order to simplify spectral features, total sidebands suppression (TOSS) and non-quaternary carbon suppression (NQS) pulse sequences were also applied. The TOSS experiment was carried out by using the same acquisition parameters described previously; delays were inserted between echoes whose length depended upon the exact rotor speed in the experiment. The calculation of these delays was done with the TOSSCALC Bruker software computer program. The same acquisition parameters were also used in the NQS experiments, where a defocussing delay of 30 μs was inserted before signal acquisition, in order to allow complete dephasing and signal loss of the protonated carbons.
The degree of cellulose crystallinity (X_c) was estimated from the area of the peaks at 84 and 89 ppm, according to the procedure described by Newman and Hemmingson (1990). X_c was calculated from the ratio of the area between 86.4-93.0 ppm and the area between 81.0-93.0 ppm.

3.5.2. FT/IR Spectroscopy Experiments

Infrared (IR) spectroscopy is an analytical technique concerned with the absorption of electromagnetic radiation in the region of 400-4000 cm^{-1}. The amount of energy associated with infrared light (4.73-47.3 kJ) corresponds to the quantity needed to increase bond vibrations of molecules. When the energy associated with a particular frequency matches the frequency of vibrations of a particular bond, an absorption band is observed in the spectrum.

FT/IR experiments were carried out on a Perkin Elmer FT/IR 1760X spectrometer, fitted with a diffuse reflection sample holder, that allowed the measurement of IR spectra on solid samples without KBr or paraffin pellet preparation. Spectra were acquired in transmittance mode, over a wavelength range of 800-4000 cm^{-1} averaging 100 transients: the spectrum of the sample holder was used as background blank for the sample spectra.

Chapter 4

RADICAL INTERMEDIATES IN VERATRYL ALCOHOL OXIDATION BY LIGNINASE

Lignin biodegradation is extensively carried out by white-rot fungi, in particular *Phanerochaete chrysosporium* is widely studied as one of the most efficient lignin degraders. This white-rot fungus during its growth on wood produces several extra-cellular enzymes, some of which have been implicated in the oxidative degradation of lignin. One of these, known as ligninase, is a glycoprotein of molecular weight 40 kD that has been shown to catalyse the hydrogen peroxide dependent oxidation of a wide variety of lignin model compounds and is thought to initiate the breakdown of lignin (Tien and Kirk, 1983; Glenn et al., 1983). The properties of this enzyme and the microbiology of white-rot fungi has been reported in details in paragraph 1.2. of this thesis. Stopped flow studies of this enzyme suggest that it reacts with hydrogen peroxide to give an intermediate, compound I as illustrated in figure 1.9. (Andrawis et al., 1988; Marquez et al., 1988). Reduction of Compound I in a single electron step will yield Compound II and a second one electron reduction will return the enzyme to the resting state (Harvey et al., 1989a). Electron paramagnetic resonance (E.P.R.) spectroscopy has identified substrate radicals as intermediates during the oxidation of a wide range of aromatic compounds by ligninase (paragraph 1.2.2.1.), and this is consistent with a catalytic cycle involving two one electron transfers from substrate to enzyme (Kersten et al., 1985 and 1987b).

Great interest in the research on lignin biodegradation has been shown in veratryl alcohol (3,4-dimethoxybenzyl alcohol). This is a secondary metabolite produced and secreted by the fungus at the same time as ligninase during its growth on wood. The occurrence of veratryl alcohol (VA) in ligninolytic cultures, its high affinity for ligninase (Tien et al., 1986), the induction effect exerted on ligninase biosynthesis (Faison et al., 1986), the protective role against inactivation of ligninase by hydrogen peroxide (Tonon and Odier, 1988) suggest a major involvement of this metabolite in lignin biodegradation. Furthermore, Leisola and coworkers (1988) measured the release of ^{14}C-enriched carbon dioxide from ^{14}C enriched lignin by the action of ligninase with and without the addition of VA. The degradation process was doubled when VA was added to ligninase.

Harvey and coworkers in 1986 proposed a mechanism whereby the veratryl alcohol is oxidized by ligninase *via* two one-electron steps, producing radical

cations that can act as mediators transferring oxidizing equivalents from the enzyme to the large, insoluble and hydrophobic lignin. Although radical intermediates were detected during the ligninase oxidation of a wide range of aromatic compounds, E.P.R. spectroscopy failed to detect VA radical generation (Tien et al., 1986). Tien and coworkers (1986) proposed that this substrate is oxidized *via* two-electrons pathway, without the formation of radicals. However, veratryl alcohol has been shown to enhance the oxidation rate of monomethoxylated aromatic compounds and these effects have been attributed to the known charge transfer properties of radical cations (Harvey et al., 1987). The same phenomenon was later observed by Valli and coworkers (1990); these authors explain their results by invoking a protective role of VA on enzymatic inactivation by hydrogen peroxide, making more enzyme available for the oxidation of recalcitrant substrates such as anisyl alcohol.
These results did not give an unambiguous interpretation of the phenomenon.
An alternative method to detect free radicals is offered by the N.M.R. spectroscopy. The presence of an unpaired electron on a molecule is expected to have noticeable effects on the N.M.R. spectra. This is because the magnetic moment associated with an electron is about 2000 times that of the proton; this yields a very efficient relaxation by dipolar coupling. As a consequence the detection of free radicals by N.M.R. relies on the shortening of the relaxation times of the N.M.R. signals, that is manifested as paramagnetic line-broadening. Furthermore, the linewidths of the N.M.R. resonances are also a valuable tool to detect the presence of dynamic processes, such as the exchange of the unpaired electron between paramagnetic and diamagnetic molecules. In this chapter are reported the results obtained on the oxidation of veratryl alcohol by purified ligninase studied by ^{1}H-N.M.R.

4.1. Dependence of Ligninase Activity on pH in Deuterated Medium

The ^{1}H-N.M.R. experiments were carried out in deuterated solutions, therefore the dependence of the activity of ligninase on pH in deuterated water was determined spectrophotometrically by measuring the absorbance at 310 nm, as described in section 3.1. The results obtained are reported in figure 4.1., where the activities measured in both deuterated and non deuterated media are plotted as function of pH.
The presence of deuterated buffer has an influence on the level of activity, which shows a lower value in deuterated media. However, the optimum pH value remains essentially unchanged at 2.75, and therefore all the N.M.R. experiments were carried out at the optimum pH value.

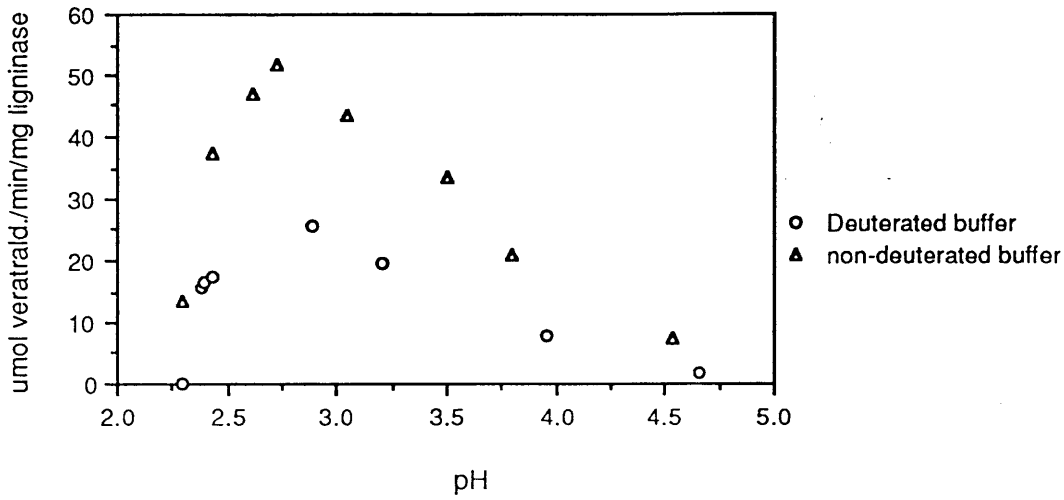

Figure 4.1. Ligninase activity as function of pH in deuterated and non deuterated phosphate buffer. The pD of the deuterated buffer was calculated by subtracting 0.4 from the pH meter reading.

4.2. ^{1}H-N.M.R. Spectra Following the Veratryl Alcohol Oxidation by Ligninase

The oxidation of veratryl alcohol (VA) by ligninase in presence of hydrogen peroxide was followed by ^{1}H-N.M.R. The reaction was carried out under anaerobic conditions in 5 mm N.M.R. tubes, and was started by the addition of hydrogen peroxide to the substrate-enzyme solution, as described in section 3.1.

4.2.1. Effects on the Resonance Linewidths of Veratryl Alcohol

The ^{1}H-N.M.R. spectra obtained during veratryl alcohol oxidation by ligninase in presence of hydrogen peroxide are shown in figure 4.2. The ^{1}H-N.M.R. spectrum of VA is shown at increasing times after initiating the catalytic activity of ligninase by addition of hydrogen peroxide. At the bottom of figure 4.2. is the control spectrum obtained before starting the reaction; the resonances corresponding to the methoxy (3.9 ppm), hydroxymethyl (4.6 ppm) groups and aromatic protons (6.9 - 7.0 ppm) can be identified.

It can be observed that all the resonances of the substrate are broadened by the effect of ligninase catalysis, whilst that of the acetone (2.2 ppm) is unaffected.

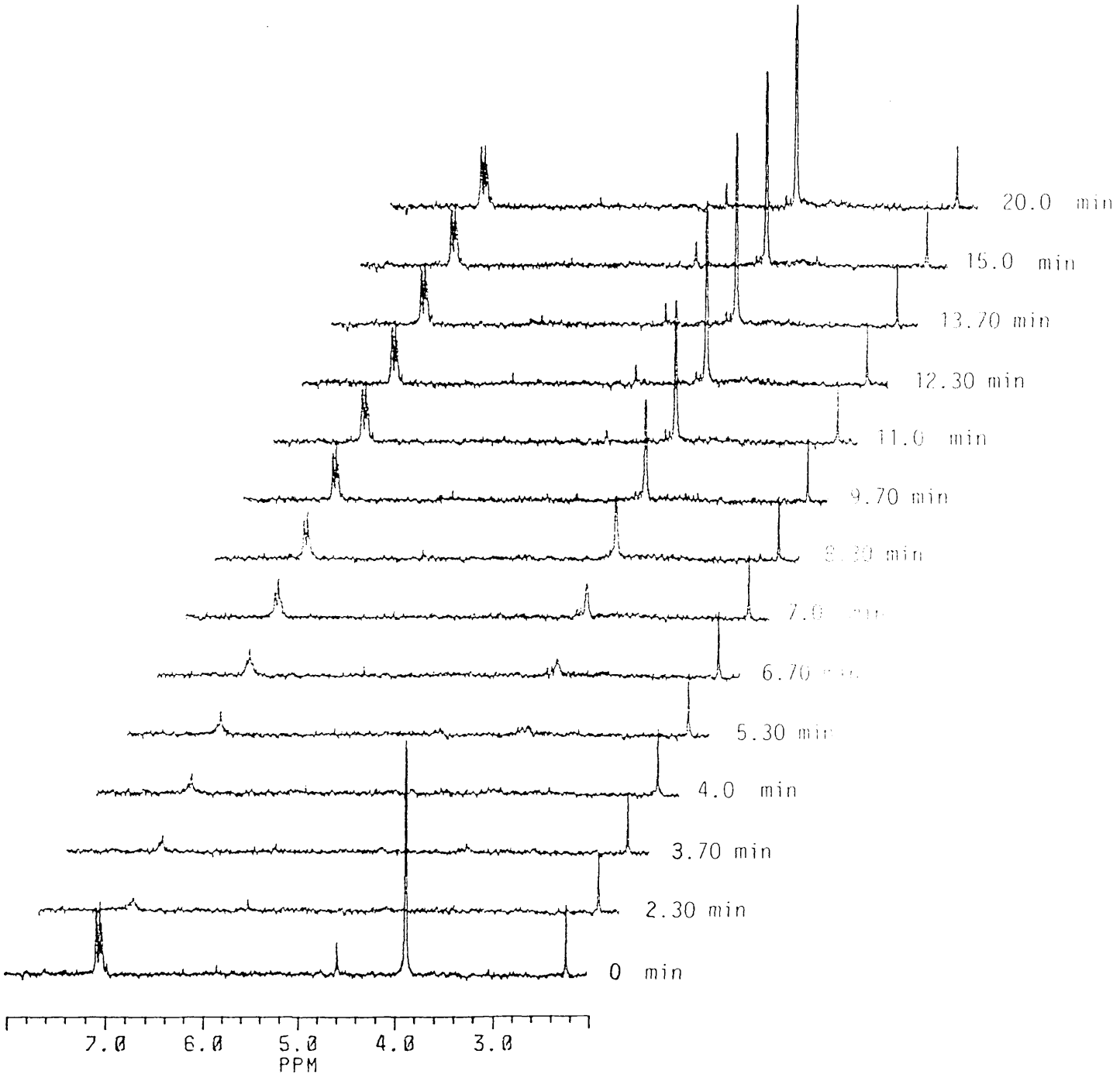

Figure 4.2. ^{1}H-N.M.R. spectra following the oxidation of veratryl alcohol by ligninase at pH 2.75. Reaction conditions: 0.09 μM ligninase in 20 mM deuterophosphate buffer and 2mM veratryl alcohol, to which 0.5 mM hydrogen peroxide was added to start the reaction. The first spectrum was acquired before adding hydrogen peroxide (0 min), and the subsequent spectra were acquired at the times indicated in the figure.

This broadening is specific and is consistent with the effect being due solely to the action of the enzyme on its substrate and does not arise from bulk susceptibility effects. When the reaction was quenched shortly after starting by addition of alkali to increase the pH to 10, then the original spectrum is restored, as shown in figure 4.3.

The reappearence of the original sharp resonances upon quenching the reaction suggests that the loss of intensity is not simply due to consumption of the substrate, but rather to some process associated with the enzyme turnover. When the concentration of hydrogen peroxide is decreased from that of the experiment illustrated in figure 4.2. to a value of 0.25 mM, the broadening and loss of intensity of the veratryl alcohol resonances occurs more slowly and to a lesser extent. Conversely, increasing the concentration of hydrogen peroxide to 0.77 mM still results in a loss of intensity but in this case resonances characteristics of veratraldehyde appear after about 4 minutes and the veratryl alcohol resonances are still broadened beyond detection. None of these changes is seen if the enzyme used has been heated to 100°C.

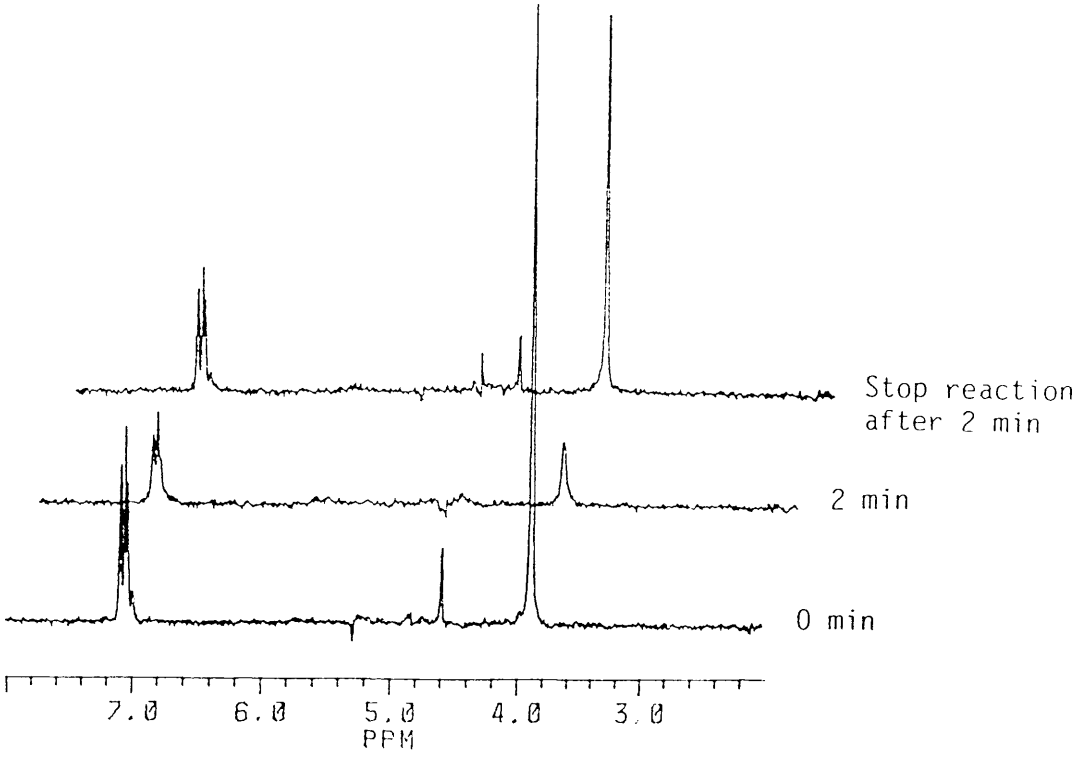

Figure 4.3. ^{1}H-N.M.R. spectra following the oxidation of veratryl alcohol (1mM) in the presence of ligninase and hydrogen peroxide (0.2 mM) in 20 mM deuterophosphate buffer (pH 2.75); the reaction is quenched after 2 min by addition of alkali (pH 10).

The loss of intensity of the substrate resonances is associated with an increase in their linewidth; the plot of the width at half height of the methoxyl resonances during reaction is shown in figure 4.4.

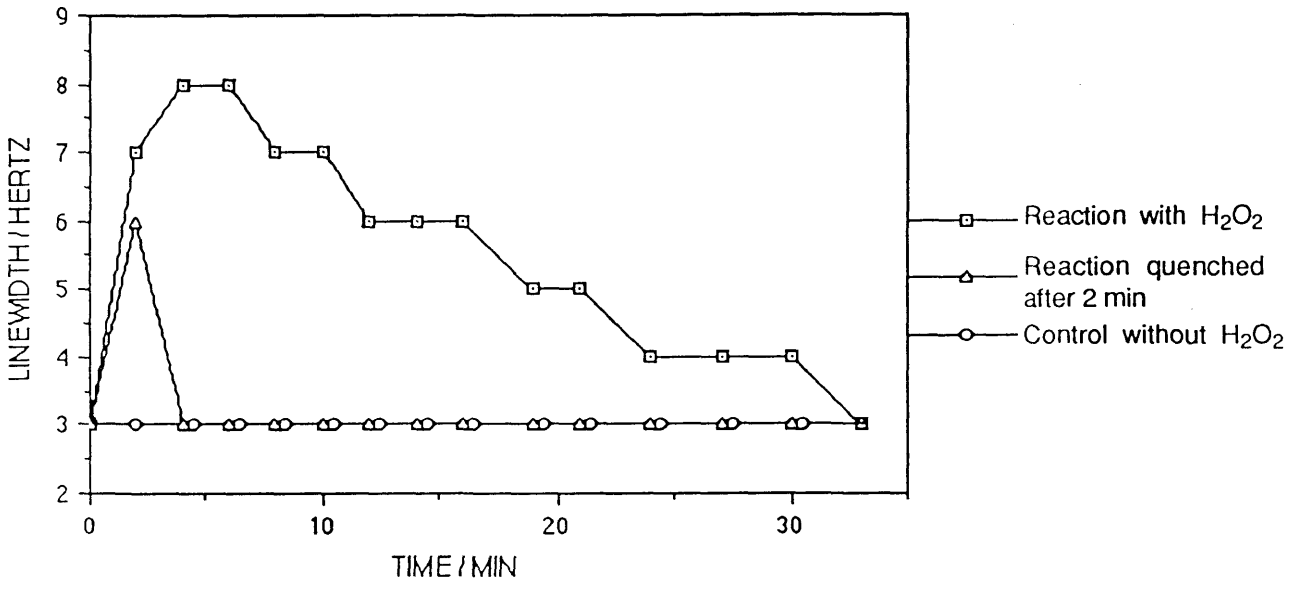

Figure 4.4. Width at half height of the veratryl alcohol methoxyl resonances. The reaction conditions are the same as in figure 4.2.

This broadening and loss of intensity of the resonances of veratryl alcohol is associated with a decrease in the proton transverse relaxation time T_2. This can be attributed to the generation of the veratryl alcohol radical cation during enzyme turnover. The presence of an unpaired electron will result in the rapid relaxation of nearby protons leading to a decrease in the transverse relaxation time (T_2) and hence to an increase in the linewidth. Previous E.P.R. measurements performed under similar conditions failed to detect any radicals. In the N.M.R. experiments reported here the broadening and complete loss of intensity of the resonances of veratryl alcohol (VA) can be explained if radicals ($VA^{+\bullet}$) are in redox exchange with much larger population of neutral molecules:

$$VA + VA^{+\bullet} \rightleftharpoons VA^{+\bullet} + VA$$

When the reaction was carried out at pH 4 no line broadening was observed, suggesting a much lower steady state radical concentration and consistent with the reduced enzyme activity at higher pH values. Line broadening at pH 4 could however be observed if the hydrogen peroxide and the enzyme were both increased 10 fold.

Providing that the exchange rate is rapid compared with the relaxation time of the neutral molecule then the observed relaxation time is given by the following equation (Kreilck, 1973):

$$1 / T_2 = \frac{f_p \, t_p \, A^2 / 4}{1 + (f_d \, t_p^2 \, A^2 / 4) + 2 t_p \, T_{1e}^{-1}}$$

where f_p and f_d are the fractions of paramagnetic and diamagnetic species respectively, t_p is the lifetime of the paramagnetic state, T_{1e} the electron longitudinal relaxation time and A the hyperfine coupling constant.
This shows that the few radicals that are present can influence the N.M.R. properties of the neutral form and can thus be detected through this indirect effect.

4.2.2. Effect on Longitudinal Relaxation Time of Veratryl Alcohol

As well as causing a decrease in T_2, the presence of a free radical in fast exchange with the neutral molecule would also be expected to decrease the longitudinal relaxation time, T_1. In order to observe this effect an inversion-recovery experiment was performed as described in paragraph 3.4., using the following pulse sequence:

$$\pi - \tau - \pi - \text{Collect}$$

When $\tau = 0.69 T_1$ then the N.M.R. resonance is a null, at times shorter than this the signal is inverted and at longer times it is positive. The inversion-recovery experiment reported in figure 4.5. was carried out at a τ value which yields a null for the methoxy groups in the absence of the catalytic action of ligninase.
When the reaction was started by addition of hydrogen peroxide, the methoxy group showed a positive intensity, indicating that the magnetization was recovering more rapidly than when there was no reaction. Similarly, the intensity of the aromatic resonances changed from negative towards positive intensity values, suggesting a shorter T_1 during the enzyme's turnover.
The decrease in T_1 of the veratryl alcohol resonances is associated with the ligninase activity, as shown by the observation that when the reaction stops or is quenched, then the substrate's methoxy groups resonance is again a null. It proved impossible to perform a complete inversion-recovery experiment with a range of τ values to gain information on the T_1 value of the intermediate, due to the limited time during which the enzyme reaction could be sustained.

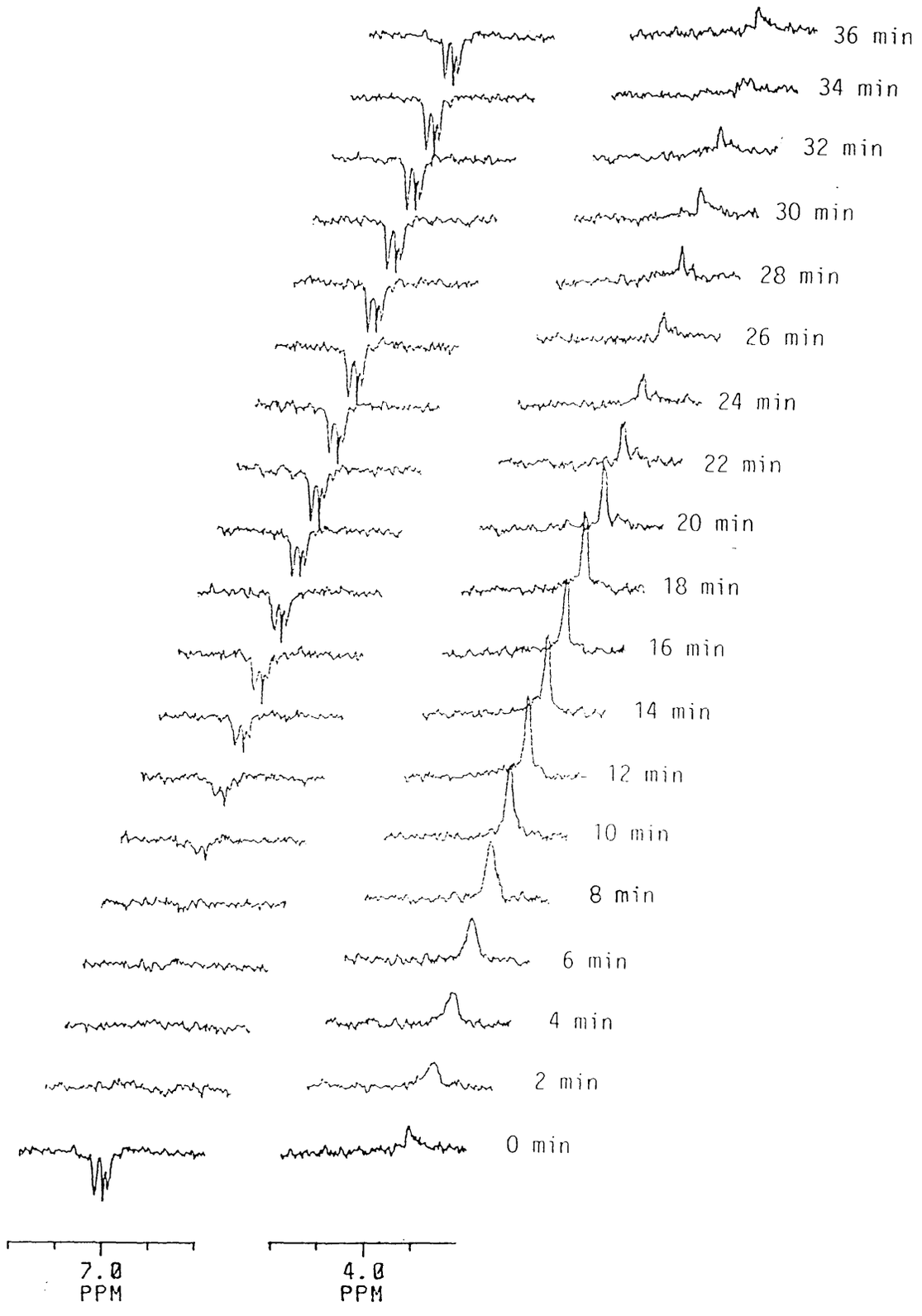

Figure 4.5. ^{1}H-N.M.R. spectra showing the decreasing longitudinal relaxation time T_1 of aromatic and methoxyl resonances of veratryl alcohol during oxidation by ligninase. A pulse sequence [π - τ - π - Collect] was used with $\tau = 0.69\ T_1$ to give a null for the methoxy resonances in the absence of enzyme turnover. The first spectrum was acquired before adding hydrogen peroxide (0 min), and subsequent spectra were acquired at the times indicated in the figure.

These data show that also T_1 relaxation time of veratryl alcohol are decreased by ligninase activity; this is consistent with the view that radical cation intermediates in fast exchange with neutral molecules are generated during ligninase turnover, in accordance with the observations on T_2 relaxation times.

4.3. Effect of the Presence of Radical Cation Intermediates on the ^{1}H-N.M.R. Spectrum of 1,4-dimethoxybenzene

1,4-dimethoxybenzene is another substrate for the ligninase, and when this compound is added to the enzyme with hydrogen peroxide, a free radical signal was detected by E.P.R. by Kersten and coworkers (1985).
An experiment was carried out by observing the effects of the presence of radical intermediates generated by ligninase activity, on the ^{1}H-N.M.R. spectrum of 1,4-dimethoxybenzene, under the same reaction conditions used for the experiments with veratryl alcohol.
The results are shown in figure 4.6.
It can be observed from figure 4.6. that the effect of the presence of radical intermediate generated by ligninase activity on 1,4-dimethoxybenzene are the same as those observed for veratryl alcohol: a considerable broadening and loss of intensity of the resonances.
The greater stability of the radical derived from 1,4-dimethoxybenzene at acid pH results in a much longer lived signal and the effect is still apparent even 40 minutes after starting the reaction.
These results are consistent with the interpretation that the extensive linebroadening associated with a decrease in transverse and longitudinal relaxation times are due to the generation of cation radical intermediates in fast exchange with the neutral molecules. This interpretation agrees with the E.P.R. data obtained by Kersten and coworkers (1985).

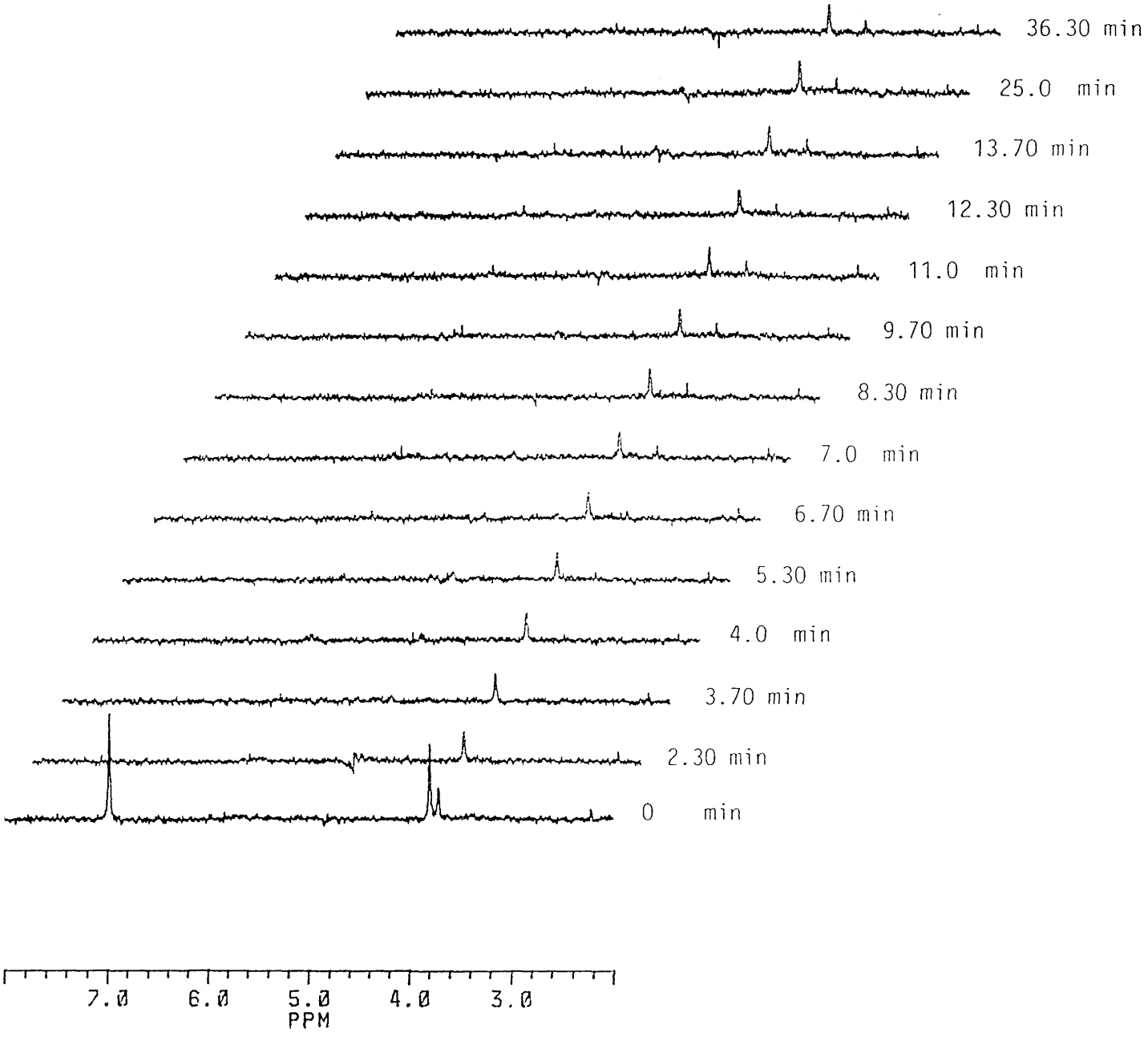

Figure 4.6. ^{1}H-N.M.R. spectra following the oxidation of 1,4-dimethoxybenzene by ligninase in presence of hydrogen peroxide. The reaction conditions are the same as in figure 4.2. The first spectrum was acquired before the addition of hydrogen peroxide (0 min), and the subsequent spectra were obtained at the times indicated in the figure.

In conclusion, oxidation of both veratryl alcohol and 1,4-dimethoxybenzene by purified ligninase and hydrogen peroxide results in substantial changes in the ^1H nmr spectra of the substrates. In both cases the effect on the spectrum is the same. Resonances broaden and then disappear. If the enzyme reaction is quenched, by the addition of alkali to increase the pH to 10, then the original spectrum is restored. Furthermore the broadening requires the presence of both hydrogen peroxide and the enzyme and the extent of broadening depends upon the concentration of the former.

These results suggest that the T_2 relaxation times of the substrate are shortened during ligninase's catalytic activity, and this is consistent with the generation of radical cation intermediates. The inversion-recovery experiment confirmed that also T_1 relaxation times are affected in the same mode by activity of the enzyme, and the observation is confirming the presence of radical cations intermediates as detected by E.P.R. for 1,4-dimethoxybenzene. Furthermore, the averaged linewidths observed suggest the presence of a rapid exchange process between the radicals and the neutral molecules; this phenomenon makes possible the detection of the radicals by the N.M.R. spectroscopy.

The detection of veratryl alcohol radicals supports the hypothesis that they are acting as mediators in the oxidation of lignin, as shown in figure 4.7.

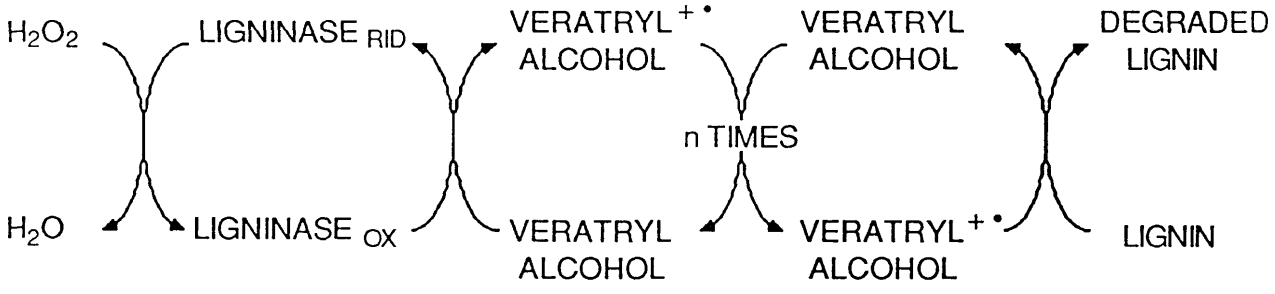

Figure 4.7. Hypothetical mechanism of lignin degradation with veratryl alcohol as mediator.

Furthermore, the process of fast charge transfer between radical and neutral molecules of veratryl alcohol is of considerable importance in the view of a mediation role of this fungal metabolite in lignin degradation. This may offer a model for the mechanism by which a complex biopolymer such as lignin, highly hydrophobic and with difficult access to the enzyme active site, can be degraded by the fungal enzyme ligninase.

Chapter 5

ONE AND TWO-DIMENSIONAL N.M.R. STUDIES OF LIGNIN

The elucidation of the structure of lignin is one of the most challenging problems in the chemistry of biomacromolecules; a general overview of our present knowledge on lignin has been presented in section 1.1.3. of this thesis. Despite the early identification of lignin in 1838 by Payen, who described lignin as "encrusting material embedding the cellulose in wood", and in spite of the multitude of scientific research devoted to its characterization, no definitive resolution to the problem of lignin structure has so far been achieved. This is due to several reasons: i) in part to the difficulties presented by the isolation of the polymer from the cell wall, ii) in part to the assumption that, although made on the basis of studies on altered lignin-derived products, lignin is a random network, iii) in part to objective analytical difficulties encountered when attacking the problem.

The application of N.M.R. spectroscopy has been one of the most rewarding methods to chemically characterize lignin. The non-destructive nature of this spectroscopic technique, combined with the detailed information obtainable at the chemical level and on the electronic environment, offers an excellent means to study a complex molecule such as lignin. Early N.M.R. studies were focussed on proton N.M.R. (^{1}H-N.M.R.); one of the earliest ^{1}H-N.M.R. studies on lignin appeared in 1964 by Ludwig and coworkers, who first compared lignin spectra with those of lignin model compounds. The approach to the problem remained virtually the same through the years in following studies (Lenz, 1968; Lundquist and Olsson, 1977; Lundquist 1979a and 1979b; Lundquist, 1980; Lundquist, 1981). The application of stronger static magnetic fields led to limited improvement in resolution, with only few more precise chemical shift assignments: the intrinsic linewidth of the signals restricted the potential of ^{1}H-N.M.R.

The advances of Fourier transform N.M.R. led to rapid application of carbon-13 N.M.R. (^{13}C-N.M.R.) to the problem. The wider chemical shift range (200 ppm) combined with the absence of ^{13}C-^{13}C spin-spin coupling complications, and the possibility of removal of ^{1}H-^{13}C spin-spin couplings by decoupling techniques, makes the ^{13}C nucleus is very interesting. This approach started a new era in the lignin studies, and the increased chemical shift signal dispersion of ^{13}C-N.M.R.

spectra resulted in advances in the knowledge of the carbon skeleton of lignin molecules (Chen and Robert, 1988).
More recently, the introduction of two-dimensional N.M.R. (2D N.M.R.) techniques in routine research opened new opportunities for the structural characterization of complex molecules. Very few applications of these techniques to the problem of lignin structure have been published. Lapierre and Monties (1987) applied 2D-N.M.R. INADEQUATE (Incredible Natural Abundance Double Quantum Transfer Experiments) on carbon-13 enriched lignin sample, to confirm and correct carbon-13 chemical shift assignments. Although attractive, the main limitation of 2D ^{13}C-N.M.R. on complex molecules such as lignin is the need to use carbon-13 enriched samples and still the extremely long time required for data collection (1 day and 13 hours for a single experiment of Lapierre and Monties).
An alternative is offered by other 2D ^{1}H-N.M.R. techniques. Only one paper has been published at present on this subject (Ede et al., 1990), and their data were presented at the same time as the results of this chapter at the Symposium on Modern Analysis of Wood held in Rayleigh (U.S.A.) in May 1989. The results obtained by Ede and coworkers (1990) are concerned with COSY and J-resolved ^{1}H-N.M.R. spectroscopy applied to derivatized (acetylated) spruce and synthetic lignins, and the authors limited the interpretation of their results to an attempt to assign the signals of the 2D spectra by comparison with model compounds. However, variations in resonances positions between lignin and the spectra of model compounds constitutes an obstacle to unambiguous assignments.

In this chapter are presented the results obtained from one and two-dimensional N.M.R. experiments on non-derivatized organosolv spruce lignin, a softwood lignin isolated through a fairly mild technique that involves simple solvent extraction (50% aqueous ethanol and 75% aqueous ethylenglycol mixtures) at 135° C. The results obtained are interpreted in terms of a potential structural content in the lignin analyzed.

5.1. Carbon-13 N.M.R. of Lignin

^{13}C-N.M.R. spectroscopy offer the advantage over ^{1}H-N.M.R. of a wider chemical shift range and the possibility of detecting ketones, esters and quaternary carbons, whose presence can only be inferred from ^{1}H-N.M.R. This leads to a comprehensive picture of the carbon skeleton of the molecule under investigation. Low sensitivity is a problem in recording these spectra, since a low natural abundance of the ^{13}C nuclei (1.1% of the total carbon present) is combined with a

small ^{13}C magnetogyric constant ($\gamma_C = \gamma_H / 4$). As consequence, for complex molecules such as lignin, a high quantity of sample is needed to achieve a good signal intensity, since there is a greater number of isotopomers that have ^{13}C nuclei at different positions in the molecule.

5.1.1. BB-Decoupled and DEPT Carbon-13 N.M.R. Experiments

The ^{13}C-N.M.R. spectra reported in this chapter were carried out using 200 mg/ml of organosolv lignin in dimethylsulfoxide; the spectra were recorded at 40°C to overcome broad lines arising from viscosity problems. Broad band (BB) decoupling was also applied to simultaneously decouple all protons from carbons, and improve the signal intensities; apart from the increase in the signal to noise ratio (S/N) due to the collapse of the multiple structure, proton decoupling give rise to an additional increase in the signal intensity due to the Nuclear Overhauser Enhancement (NOE).

Figure 5.1a. shows the BB decoupled ^{13}C-N.M.R. spectrum of organosolv spruce lignin.

The spectral features observed in spectrum 5.1a. are similar to those typically reported in literature for lignin samples, with broad ^{13}C signals. Chemical shift assignments are routinely made by comparison with the resonances positions of monomeric and dimeric lignin model compounds (Ludemann and Nimz, 1973; Kringstad and Morck, 1983).

To decrease the complexity of the ^{13}C-N.M.R. spectrum and to confirm the chemical shift assignments, the DEPT pulse sequence was also applied. This technique offers the possibility of editing ^{13}C subspectra, so that quaternary carbons, CH, CH_2 and CH_3 groups can be distinguished. The spectrum shown in figure 5.1b. was obtained with DEPT experimental conditions in which quaternary carbons were suppressed, CH_2 gave negative signals, CH_3 and CH gave positive signals.

The chemical shift assignments are reported in table 5.1., and were made on the basis of literature data (Ludemann and Nimz, 1973; Kringstad and Morck, 1983; Bardet et al., 1985; Robert and Chen, 1989; Fernandez et al., 1990).

Three main regions can be identified in the spectra of figure 5.1.

i) the 50-100 ppm region covers the range of the saturated aliphatic sp^3 carbon atoms of methoxy and side-chain groups, mainly involved in ether or alcoholic bonds. The assignments made to methylene carbons (from 28.5 to 63.6 ppm) are confirmed by the presence of negative signals in the DEPT spectrum.

ii) the 100-155 ppm region covers the frequency range where signals from aromatic and vinylic sp^2 carbons are usually found. The suppression of the signals

between 140 and 155 ppm in the DEPT spectrum confirm that those resonances are due to quaternary aromatic carbons.

iii) the region between 160 and 200 ppm comprehends signals 32 and 33 corresponding to carboxyl and carbonyl signals.

The results of table 5.1. show that the lignin sample under investigation is mainly composed of the four major lignin substructures reported in figure 5.2., namely the arylglycerol-β-aryl ether (β-O-4), pinoresinol (β-β), phenylcoumaran (β-5) and biphenyl (5-5').

The presence of these substructures is consistent with literature data on conifer lignin composition (Adler, 1977; Sakakibara, 1980).

Traces of hemicelluloses, mainly xylans were also found in the lignin preparation studied; resonance signals were assigned according to Lee and coworkers (1979) and Kovac and Hirsch (1980). The presence of xylans in lignin preparations is not surprising and can not be overcome, as lignin is known to be covalently bound to hemicelluloses, and its extraction inevitably carries traces of polysaccharides (Sarkanen and Ludwig, 1971).

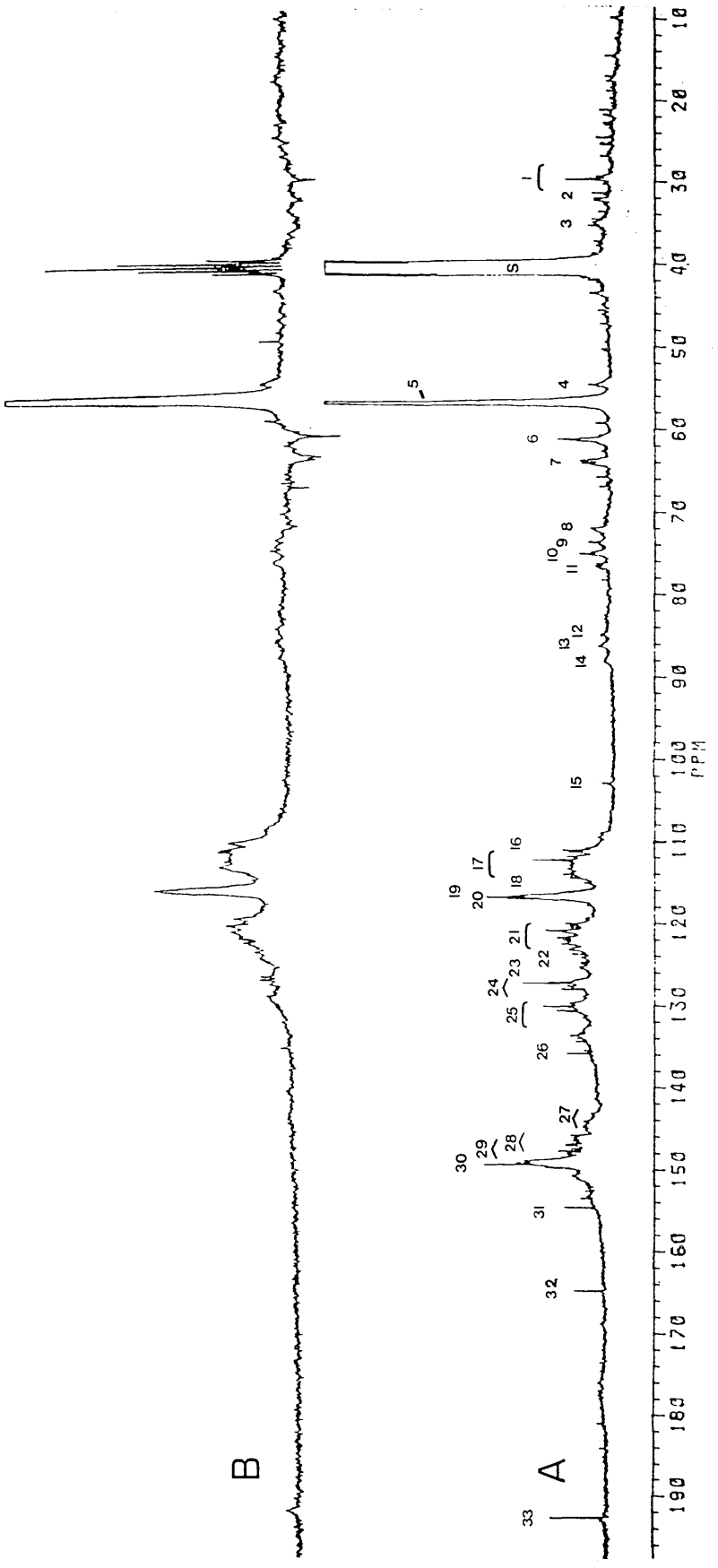

Figure 5.1. Carbon-13 N.M.R. spectra of organosolv spruce lignin in dimethylsulfoxide-d_6 at 200 MHz. (**A**) Broad-Band decoupled spectrum; (**B**) DEPT spectrum, showing negative CH_2 signals, positive CH and CH_3, null for quaternary carbons.

Table 5.1. Organosolv spruce lignin carbon-13 chemical shifts assignments. The signal numbers correspond to the peaks in spectra of figure 5.1.; the numbers indicated in squared brackets refer to the structures reported in figure 5.2.

Signal number	Chemical Shift ppm	Assignments
1	28.5 - 29.0	CH_2 in saturated alkyl groups
2	31.5	Cβ in G-CH_2-CH_2-CH_2OH structures [1]
3	34.3	Cα in G-CH_2-CH_2-CH_2OH structures [1]
4	53.9	Cβ in pinoresinol and phenylcoumaran structures [4,5]
5	55.7	methoxyl carbons in Ar-OCH_3
6	60.7	Cγ in G-CH_2-CH_2-CH_2OH structures [1] and in aryl ether structures [2a, 2b]
7	63.1 - 63.6	C5 in xylan, Cγ in phenylcoumaran structures [4], Cγ in G-CH=CH-CH_2OH structures [1]
8	71.0 - 72.5	Cα in aryl ether structures, threo and erythro forms [2a, 2b]
9	72.8	C2 in xylan
10	74.2	C3 in xylan
11	75.7	C4 in xylan
12	84.5	Cβ in aryl ether structures, erythroform [2a]
13	85.3	Cβ in aryl ether structures, threoform [2b]
14	87.2	Cα in pinoresinol and phenylcoumaran structures [4,5]
15	102.0	C1 in xylan
16	111.0	C2 in G-CH=CH-CH_2OH structures [1]
17	112.1 - 112.8 -113.8	C2 in various G units and aryl ether structures [2a, 2b]
18	115.3	C5 in various G units and aryl ether structures [2a, 2b]
19	118.9	C6 in various G units and pinoresinol and phenylcoumaran structures [4,5]
20	119.5	C5 in various aryl ether structures, G-CHOH-, G-CH=CH- structures [1, 2a, 2b]
21	120.3 - 121.2 -121.7	C6 in various G units
22	124.1	C5 in various G units substituted [1, 4]
23	125.8	C6 in G-CHO
24	125.9 - 126.3 -126.7	C1 and C5 in various substituted G units, C5 and C5' in biphenyl structures [3]
25	128.7 - 129.2 -132.3	C6 in aryl ethers and phenylcoumaran structures [2a, 2b,4] and Cα in various ArCH=CH
26	134.4	C1 in guaiacyl units and G-CH=CH- structures [1]
27	143.4 - 144.4	C4 in phenylcoumaran [4], C4 and C4' in biphenyl structures [3], Cβ in various ArCH=CH- structures
28	145.5 - 146.5	C4 in G-CH_2-, G-CH=CH-, G-CHOH- structures [1,2a, 2b]
29	147.3 - 148.2	C3 in guaiacyl units

	Cont.	Tab. 5.1.
30	149.5	C4 in guaiacyl units etherified [2a,2b]
31	153.1	C4 in G-CHO and G-CO-R structures
32	163.5	carbonyl carbon in G-CO-R, formyl carbon in G-CHO, carboxylic carbon in G-CH_2-COOH
33	190.8	formyl carbon in G-CHO and G-CH=CH-CHO, carbonyl carbon in G-CO-R

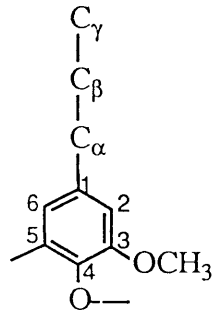

[1]
Guaiacyl unit
(G)

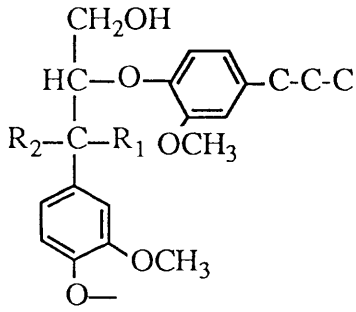

[2]
Arylglycerol-β-aryl ether structure
(β-O-4 type)
R_1 = OH, R_2 = H : erythro isomer [2a]
R_1 = H, R_2 = OH : threo isomer [2b]

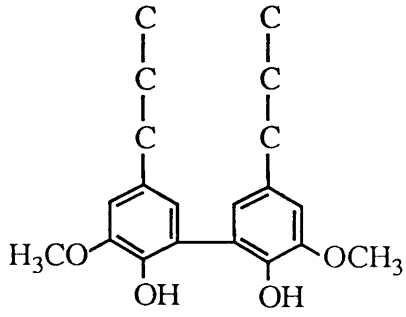

[3]
Biphenyl structure
(5-5' type)

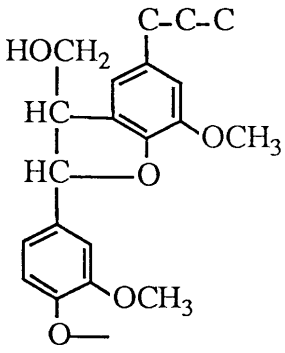

[4]
Phenylcoumaran structure
(β-5 type)

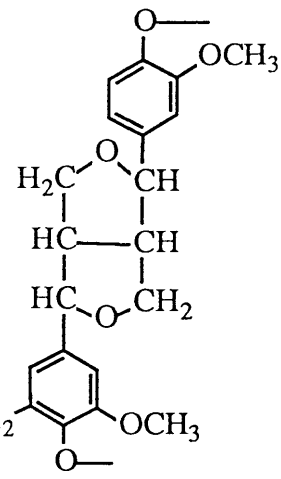

[5]
Pinoresinol structure
(β-β type)

Figure 5.2. Lignin substructures found by carbon-13 N.M.R.

5.1.2. FT/IR Experiments

FT-IR spectroscopy was also used to confirm the presence of chemical groups found by ^{13}C-N.M.R. Figure 5.3. shows the FT-IR spectrum obtained by diffuse reflectance of organosolv spruce lignin powder.
The IR absorption band assignments reported in table 5.2. were made according to literature data (Sarkanen and Ludwig, 1971).
The IR absorption bands assignments reported in table 5.2. confirm the ^{13}C-N.M.R. results. Although the FT-IR technique is more sensitive to low sample concentrations than N.M.R. and can be more speedily collected, the ^{13}C-N.M.R. technique has been shown to be more informative in terms of chemical structure allowing a more complete construction of the carbon backbone of the lignin molecule.

Table 5.2. Lignin IR absorption band assignments.

Band Position cm^{-1}	Assignment
815	Aromatic C-H out-of-plane deformations
855	same
915	same
970	=CH out-of-plane deformation (trans)
1035	Aromatic C-H in-plane deformation, and C-O deformation in primary alcohol
1085	C-O deformation, secondary alcohol and aliphatic ether
1140	Aromatic C-H in-plane deformation
1230	Aromatic ring with C-O stretching
1270	same
1370	C-H deformation (symmetric)
1430	Aromatic skeletal vibrations
1470	C-H deformation (asymmetric)
1510 - 1515	Aromatic skeletal vibrations
1605	same
1660 -1 715	Carbonyl stretching
2820	OH stretching in methyl and methylene groups
2850 - 2875	same
2920	same
3400 - 3425	OH stretching (hydrogen bonded)

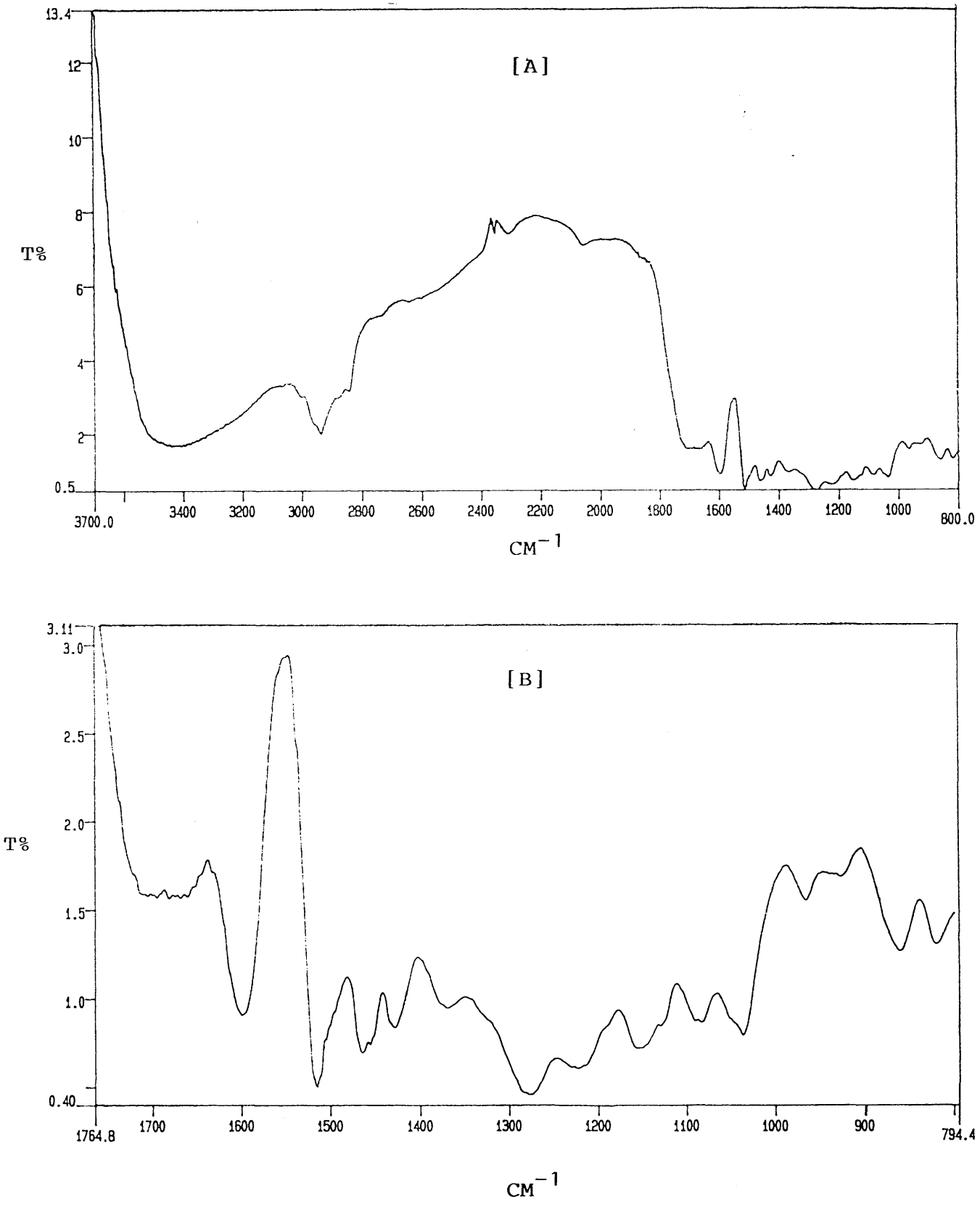

Figure 5.3. FT-IR spectra of organosolv spruce lignin. (**A**) 800-3700 cm^{-1} region; (**B**) finger print region (790-1760 cm^{-1} region).

5.2. Proton N.M.R. of Lignin

Most of the early N.M.R. work on lignin was focussed on proton N.M.R. spectroscopy (^{1}H-N.M.R.), (Lenz, 1968; Lundquist and Olsson, 1977; Lundquist, 1979a, 1979b, 1980, 1981). Despite the progress in the availability of high magnetic fields, the improvements in the resolution of ^{1}H-N.M.R. spectra of lignin remained limited, due to the intrinsic broad unresolved features of these spectra. Recently the possibility of application of two-dimensional (2D) techniques opened new potentials for the use of ^{1}H-N.M.R. in the determination of structures of relatively complex macromolecules.
2D-N.M.R. spectra report the information over an area rather than an axis as in conventional 1D spectra; this is an advantage as inevitably leads to a much improved resolution. Furthermore, by choosing the suitable pulse sequence, the 2D spectrum can reveal structural details not available from 1D ^{1}H-N.M.R. or ^{13}C-N.M.R.

5.2.1. One and Two-dimensional Proton N.M.R. Experiments

In this paragraph 1D and 2D ^{1}H-N.M.R. spectra of lignin model compounds and lignin are reported in order to gain more understanding on the nature of the lignin polymer.

Figure 5.4. shows the 1D spectrum of organosolv spruce lignin.
The features of the 1D spectrum of lignin are those that have been typically observed in many previous studies (Lundquist and Olsson, 1977; Lundquist, 1979a, 1979b, 1980, 1981); although the regions of the spectrum can be broadly assigned to aromatic (6.0 to 8.0 ppm), side-chain (2.0 to 5.0 ppm) and methoxy groups (3.8 ppm), the resolution is poor probably due to a combination of broad lines and a large number of spin systems leading to severe spectral overcrowding. The assignment of the signals depends entirely on the data obtained in literature for various lignin model compounds. Therefore chemical shift assignments were carried out according to published data (Lundquist 1981; Hauteville et al., 1986), and the outcome is reported in table 5.3.

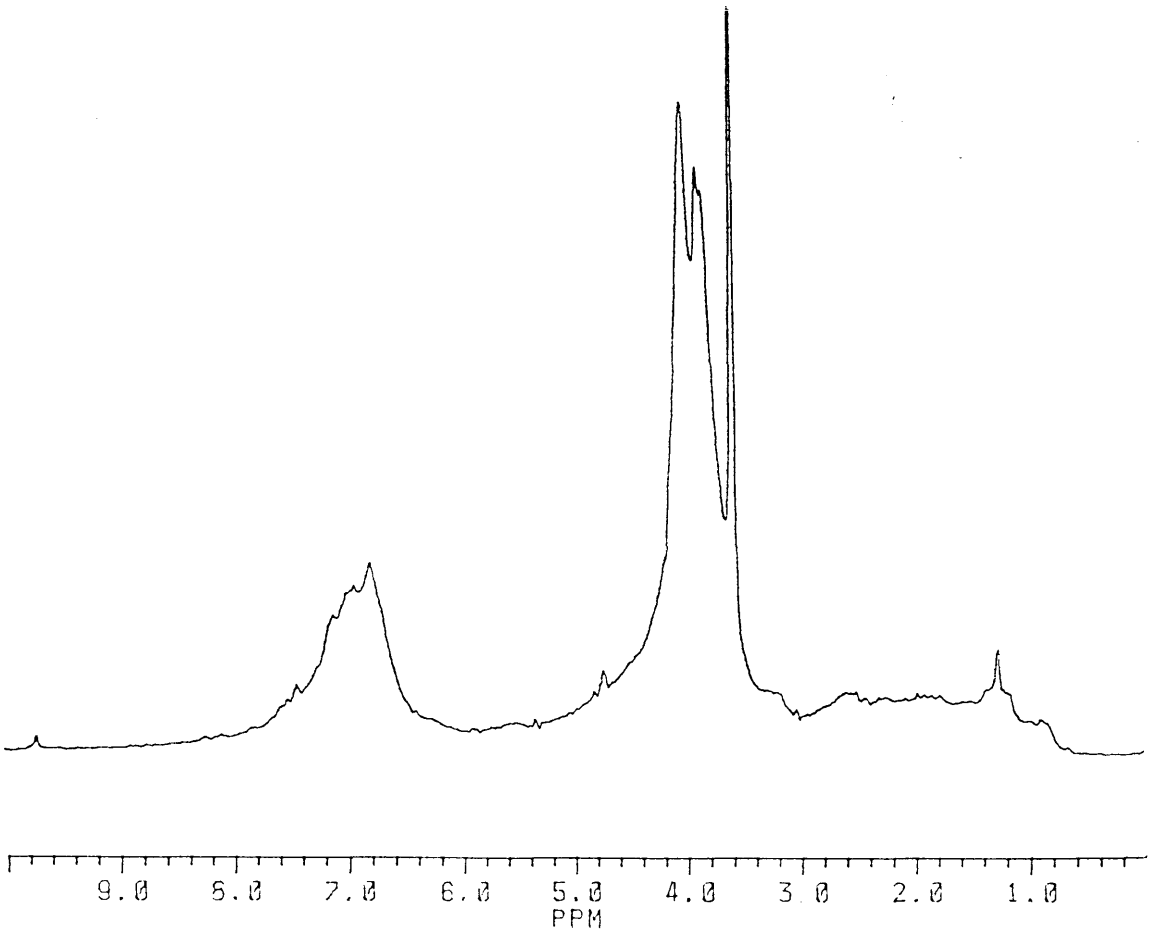

Figure 5.4. ^{1}H-N.M.R. spectrum of organosolv spruce lignin in deuterated dioxane/water (5:1).

An interesting observation on the ^{1}H-N.M.R. spectra of lignin is that despite the complexity and the highly aromatic nature of the lignin network, no up-field peaks have ever been detected. These peaks might be expected to occur as a consequence of random spatial distribution of molecular fragments, that may cause some molecular fragments to be in the shielding region of the aromatic rings (figure 2.2.).

Table 5.3. Chemical shift assignments of ^{1}H-N.M.R. signals of organosolv spruce lignin.

Spectral Region	Chemical Shift ppm	Assignments
1		
Aliphatic Region (0.75 - 3.55)	0.75 - 2.50	Aliphatic compounds (minor contaminants)
	2.50 - 3.55	Hydrogens on Cβ in β-1 and β-β structures
2		
Methoxyl Region (3.55 - 3.95)	3.55 - 3.95	Hydrogens on methoxyl groups (Ar-O-CH_3); hydrogens on Cβ in β-5 structures; hydrogens on Cγ in β-β structures
3		
Benzylic Region (4.50 - 6.25)	4.50 - 5.75	Hydrogens on Cγ in β-O-4, β-5, β-1 and β-β structures; hydrogens on Cα in β-β structures; hydrogens on Cγ in Ar-CH=CH-CH_2OR; hydrogens on Cβ in β-O-4 structures; hydrogens on Cα in β-5 structures
	5.75 - 6.25	Hydrogens on Cα in β-O-4 and β-1 structures; hydrogens on Cβ in Ar-CH=CH-CH_2OR;
4		
Aromatic Region (6.25 - 7.90)	6.25 - 7.23	Aromatic hydrogens in Ar-R; hydrogens on Cα and Cβ in Ar-CH=CH-CHO; hydrogens on Cα in Ar-CH=CH-CH_2OR
	7.23 - 7.90	Aromatic hydrogens in Ar-COR
5		
Strongly Deshielded Region (9.00 - 10.00)	9.58 - 9.86	Formyl hydrogens in Ar-CH=CH-CHO

In an attempt to extract more information from the ^{1}H-N.M.R. spectra, 2D technique were also applied.

The first of these techniques is J-resolved spectroscopy, which allows the separation of the hyperfine (spin-spin) couplings from the chemical shift components, as described in paragraph 2.3.1. of this thesis. During preliminary experiments, the J-resolved 2D matrix was processed by using a sine-bell window function non-shifted and $\pi/4$ shifted. The former gave 2D spectra with broad features, where the multiplet patterns could still be distinguished; the latter gave a considerable enhancement in resolution without loss of information, proving to be more advantageous.

The results obtained from the J-resolved spectra on organosolv spruce lignin are reported in figure 5.5.

The spectra of figure 5.5. reveals a considerable simplification of the proton envelope, allowing a precise determination of chemical shift positions, labelled by a number in the figure and reported in table 5.5.

Although the J-resolved spectrum shows a net resolution and reveals the multiplet feature of the peaks, no information can be gained on the resonances connectivities. The correlation resulting from scalar interaction between spin systems is revealed in the COSY ^{1}H-N.M.R. spectra.

Figure 5.6. shows the COSY spectrum of the same organosolv spruce lignin sample in deuterated dioxane/water mixture (5:1).

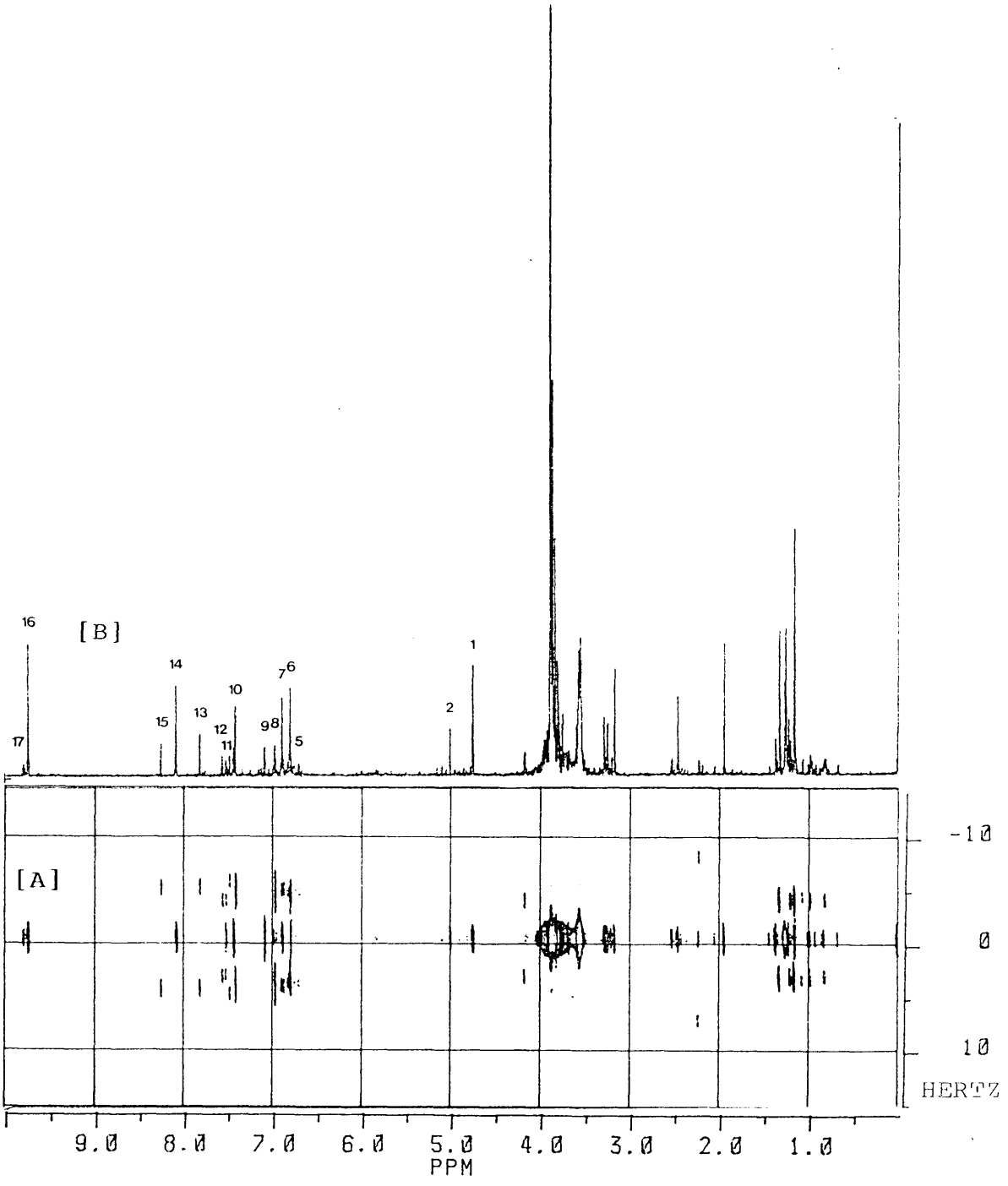

Figure 5.5. J-resolved ^{1}H-N.M.R. spectrum of the same lignin sample as in figure 5.4.; (**A**) the 2D spectrum; (**B**) the projection of the 2D spectrum onto the chemical shift axis.

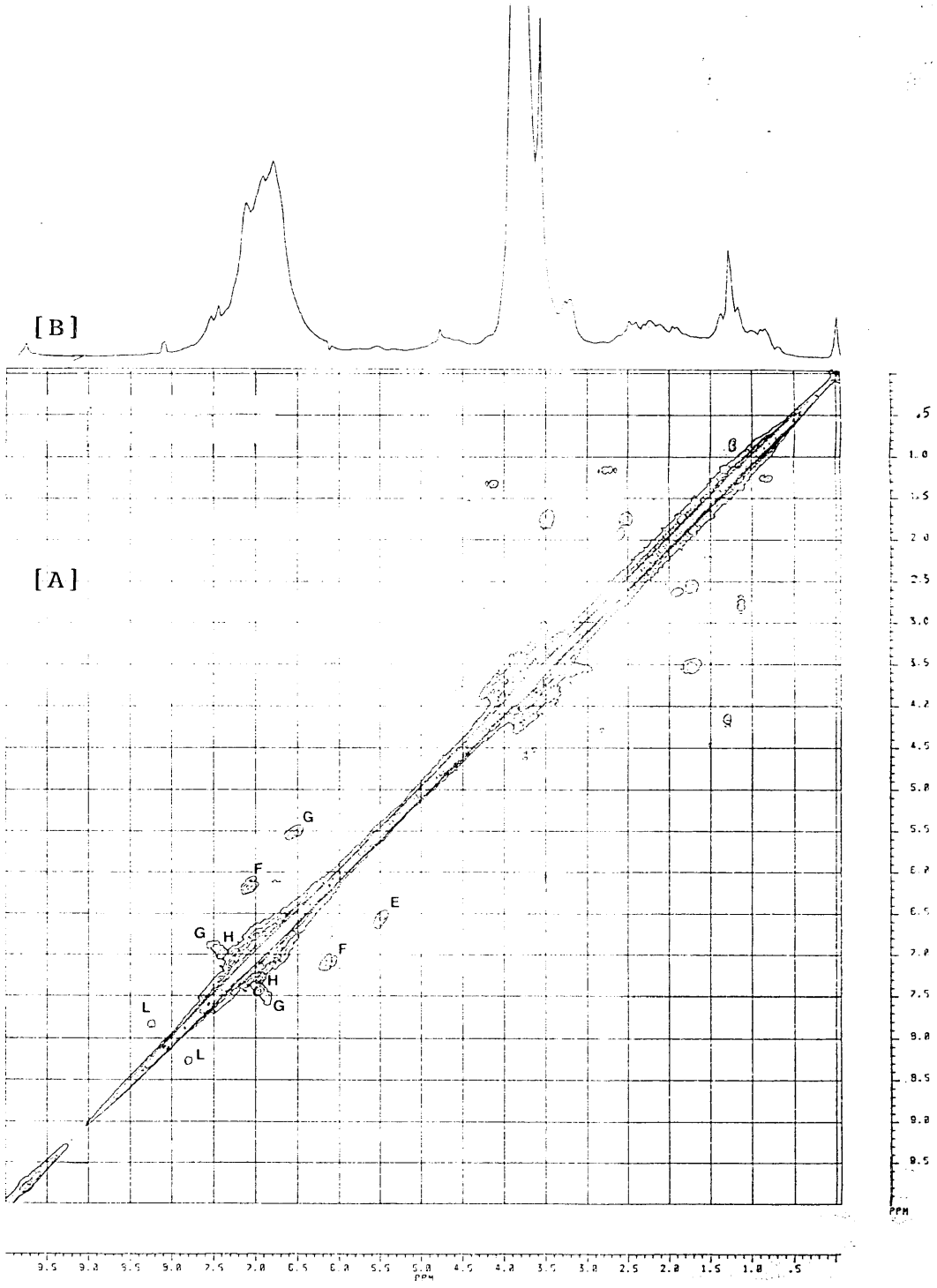

Figure 5.6. ^{1}H-N.M.R. COSY spectrum of the same lignin sample as in figure 5.4. and 5.5.; (**A**) the 2D spectrum; (**B**) the projection of the 2D spectrum onto the F2 axis.

In order to interpret the cross-peaks pattern, the lignin COSY spectra were compared to those obtained for three lignin model compounds (monomer units): 4-hydroxycinnamic acid, 4-hydroxy-3-methoxycinnamic acid and 3,5-dimethoxy-4-hydroxycinnamic acid. The aromatic regions of their COSY spectra are reported in comparison to the lignin aromatic region of COSY spectra (figure 5.7.).

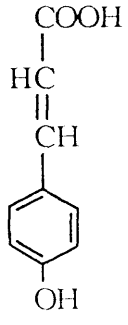

[HCA]

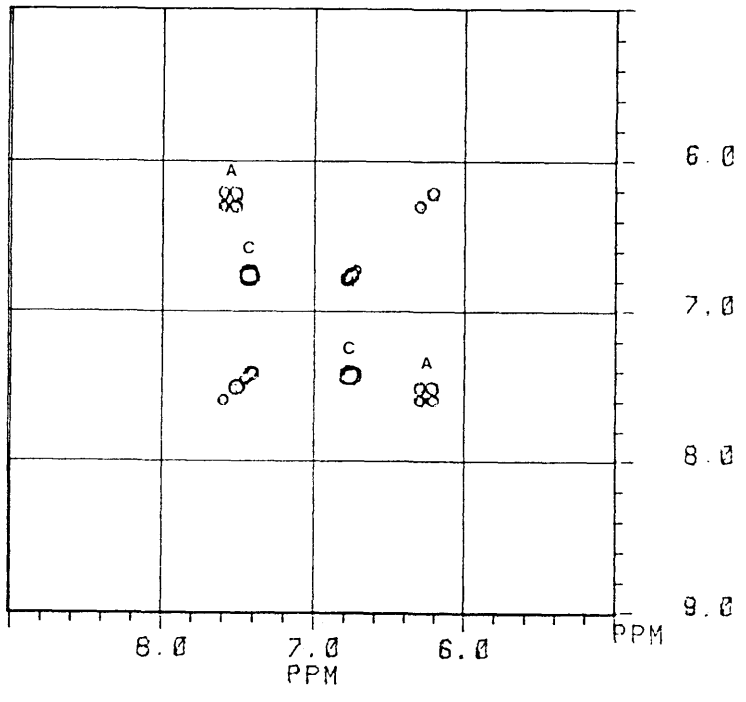

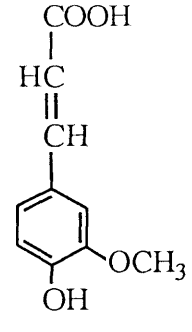

[MHCA]

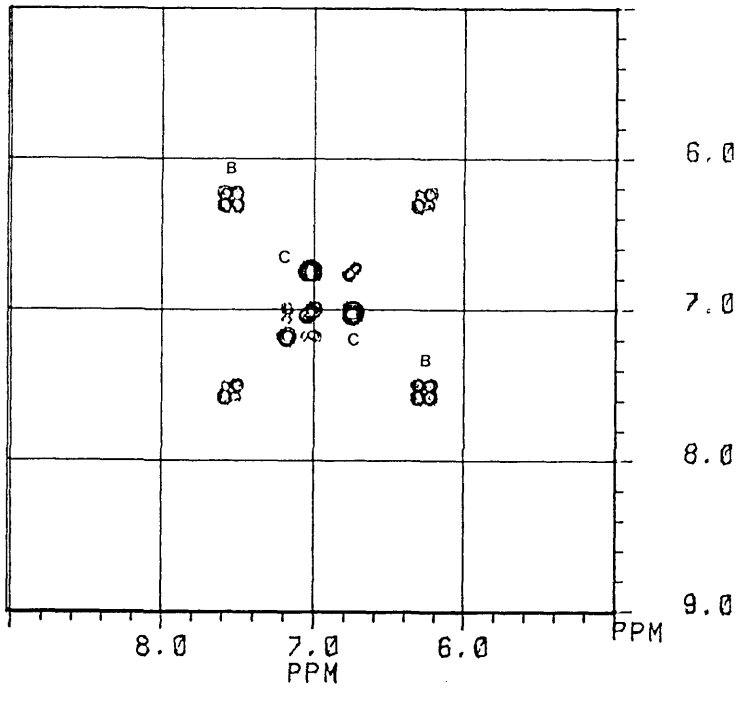

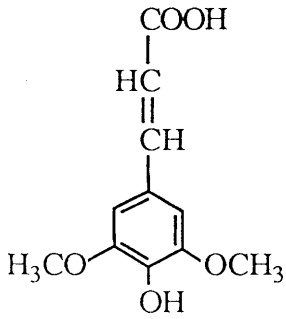

[DMHCA]

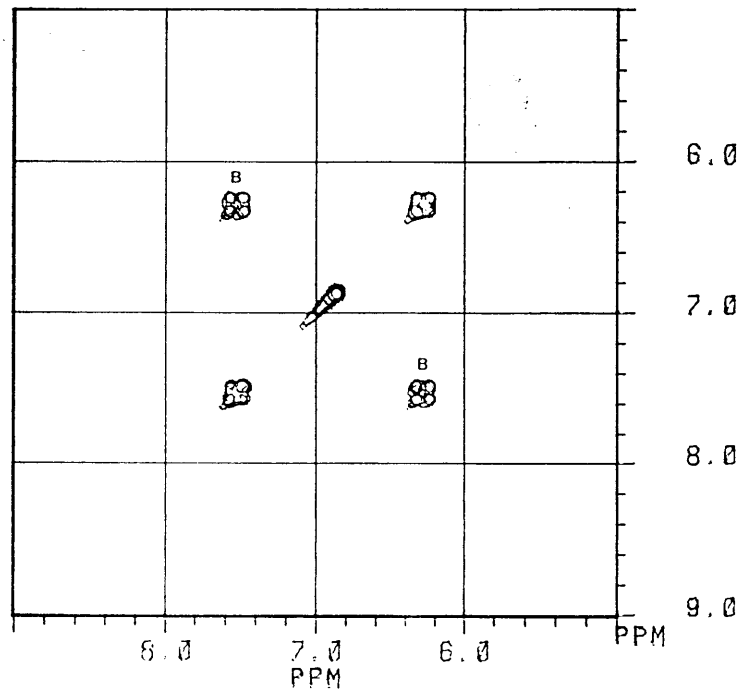

LIGNIN
see figure 1.7.

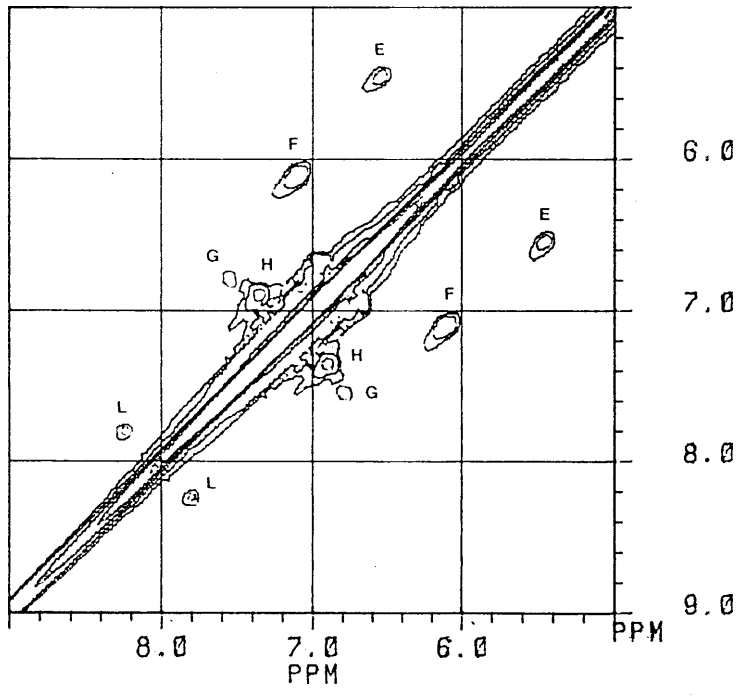

Figure 5.7. ^{1}H-N.M.R. COSY spectra of the aromatic region of 4-hydroxycinnamic acid [**HCA**], 4-hydroxy-3-methoxycinnamic acid [**MHCA**], 3,5-dimethoxy-4-hydroxycinnamic acid [**DMHCA**] and organosolv spruce lignin [**LIG**] in deuterated tetrahydrofuran.

From the spectra of figure 5.7. it can be noted that lignin model compounds and lignin do not present the same pattern of cross-peaks; most probably the lignin structure and interunit linkages have influence on the resonance positions, which is reflected onto the cross-peak coordinates. Table 5.4. reports the assignments for lignin monomer units and the results from the two-dimensional experiments on lignin are summarized in table 5.5.

Table 5.4. Chemical shift assignments of ^{1}H-N.M.R. signals of 4-hydroxycinnamic acid [HCA], 4-hydroxy-3-methoxycinnamic acid [MHCA] and 3,5-dimethoxy-4-hydroxycinnamic acid [DMHCA]; the letters labelling the cross-peaks refer to figure 5.7.

Chemical Shift ppm	Cross-peak ppm	Assignments
3.85	----	Hydrogens on methoxyl groups of [DMHCA]
3.89	----	Hydrogens on methoxyl groups of [MHCA]
6.21 - 6.29	7.51 - 7.59 (**A**)	Hydrogens on Cβ of [HCA]
6.24 - 6.32	7.50 - 7.58 (**B**)	Hydrogens on Cβ of [MHCA] and [DMHCA]
6.72 - 6.77	7.40 - 7.45 (**C**)	Hydrogens on C3 and C5 of [HCA]
		Hydrogens on C5 of [MHCA]
6.74 - 6.78	7.01 - 7.05 (**D**)	
6.88	----	Hydrogens on C2 and C6 of [DMHCA]
7.01 - 7.05	6.74 - 6.78 (**D**)	Hydrogens on C6 of [MHCA]
7.19	----	Hydrogens on C2 of [MHCA]
7.40 - 7.45	6.72 - 6.77 (**C**)	Hydrogens on C2 and C6 of [HCA]
7.50 - 7.58	6.24 - 6.32 (**B**)	Hydrogens on Cα of [MHCA] and [DMHCA]
7.51 - 7.59	6.21 - 6.29 (**A**)	Hydrogens on Cα of [HCA]

Table 5.5. Resonances chemical shifts from 2D ^{1}H-N.M.R. signals of organosolv spruce lignin; the peaks numbering refers to the resonances identified in the J-resolved spectrum of figure 5.5.; the letters labelling the cross-peaks refer to figure 5.7.

Peak Number	J - resolved Chemical shift	Multiplicity	COSY Cross-peaks
1	4.75	s	-----
2	5.00	s	-----
3	5.40	d	6.50 (**E**)
4	6.10	d	7.10 (**F**)
5	6.50	d	5.40 (**E**)
6	6.85	d	7.52 (**G**)
7	6.90	s	-----
8	6.95	d	7.40 (**H**)
9	7.10	s + d	6.10 (**F**)
10	7.40	d	6.95 (**H**)
11	7.50	s	-----
12	7.52	d	6.85 (**G**)
13	7.80	d	8.25 (**L**)
14	8.10	s	-----
15	8.25	d	7.80 (**L**)
16	9.56	s	-----
17	9.74	s	-----

Chemical shift assignments of lignin resonances are very difficult because the complexity of the macromolecule combined with shifts in lignin resonance positions with respect to model compounds leads to ambiguous results, as can be seen in the literature data (Lundquist, 1981; Robert, 1989; Ede et al., 1990). However, focussing on the aromatic region that is the most characteristic region for a highly aromatic polymer like lignin, some general considerations can be made.

Although the cross-peaks positions of lignin and lignin model compounds are not exactly the same, it may be expected that similar chemical structures cover the same chemical shift range. With this assumption, cross-peaks in the region

between 6.20 and 7.60 ppm can be attributed to the presence of coupled protons on unsaturated carbons on the side-chain (Ar-CH=CH-R); cross-peaks in the region 6.70 - 8.25 ppm can be attributed to coupled protons on aromatic C5 and C6 carbons. The analysis of the data reported in table 5.5. shows two sets of cross-peaks in the unsaturated side-chain region (cross-peaks E and F), and three sets in the aromatic region (G, H and L). The singlets at 6.90, 7.50 and 8.10 ppm can be attributed to proton attached to aromatic C2 that are not coupled to nearby protons. The analysis of the limited number of cross peaks of table 5.5, combined with the information gained from carbon-13 spectra of the same sample (paragraph 5.1.), suggests that few major substructures are present in the spruce lignin studied, as depicted in figure 5.8.

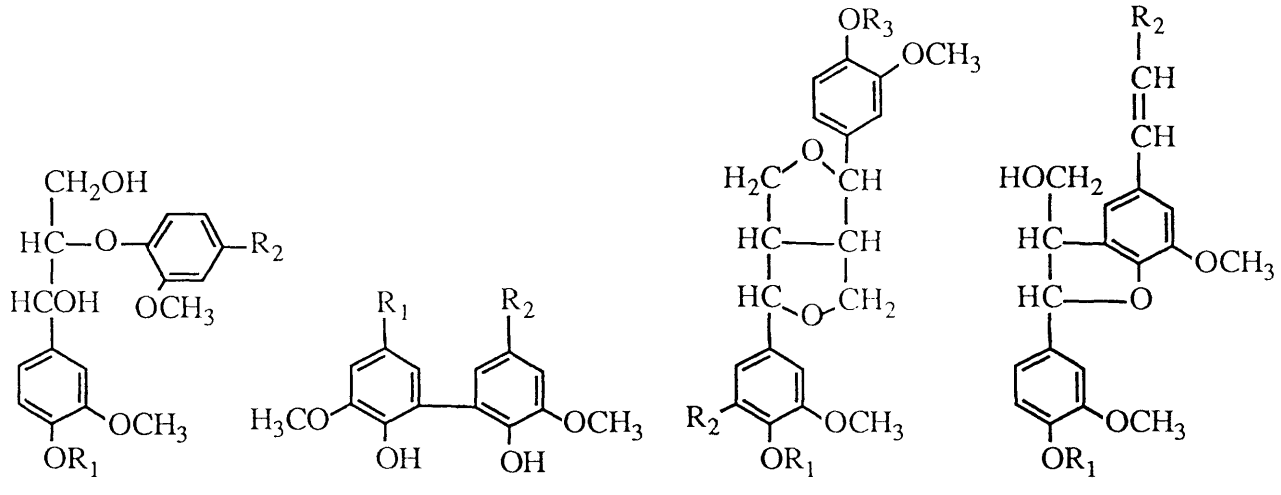

[1] β-O-4 structure

[2] 5-5' structure

[3] β-β structure

[4] β-5 structure

Figure 5.8. Spruce lignin substructures.

These results are consistent with literature data that indicate the presence of those substructures in gymnosperm lignin; the extent of the occurrence of the substructures is expected to be more than 50% for β-O-4, 25% for 5-5', about 13% for β-β and β-5 (Sakakibara, 1980).

Although the cross-peaks patterns can be attributed to the presence of the lignin substructures of figure 5.8., the most striking feature of the lignin COSY spectrum is the limited number of cross-peaks. In first analysis, the broad and unresolved features of the 1D spectra, still present in the diagonal region of the COSY spectra, are indicative of a large number of spin systems with large chemical shift distribution. Such a multitude of signals is expected to give a large number of sets

of cross-peaks: despite the intense unresolved diagonal peaks, the COSY spectra exhibit a relatively small number of cross-peaks.
This observation may be consistent with the presence of a limited number of spin systems, with relatively small chemical shift distribution and a short relaxation time giving rise to the broad features of the 1D spectra.

5.2.2. Homonuclear Decoupling Experiments

The homonuclear inverse-gated proton decoupling technique was applied to further study the hypothesis that a few broad resonances contribute to the lignin proton spectrum. This technique was used to select peaks from the broad features of the lignin aromatic region, without interference from the NOE. This was achieved by switching on the decoupler at specific frequencies only during signal acquisition, eliminating coupling effects but not allowing the NOE to build up. This led to the suppression of specific aromatic resonances (6.50 - 6.80 - 6.90 - 7.10 ppm), whose lineshape could be extracted from the difference spectra obtained in respect of a control spectrum where the decoupler was set in a blank region (8.69 ppm), as shown in figure 5.9.
The analysis of the linewidths at half height of the deconvoluted peaks, shows a considerable extent of resonance broadening. These results are consistent with the presence of broad resonances contributing to the lignin proton spectra.

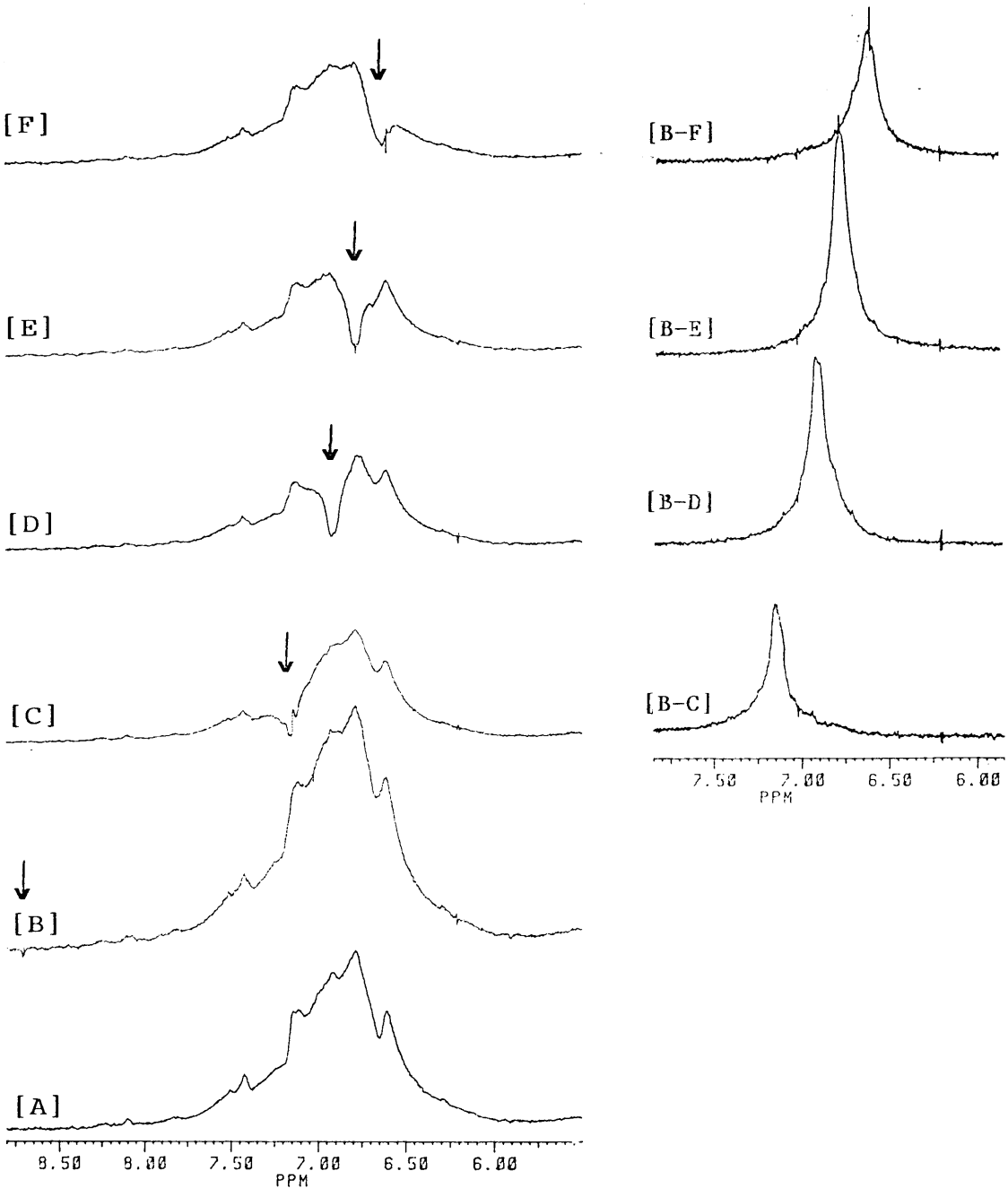

Figure 5.9. Proton homonuclear decoupling experiment on aromatic region of organosolv spruce lignin. On the left are shown the decoupled spectra, on the right are reported the corresponding difference spectra obtained by subtracting the irradiated spectrum from a control spectrum. (**A**) spectrum non decoupled; (**B**) control spectrum irradiated at 8.69; (**C**) spectrum irradiated at 7.10 ppm; (**D**) spectrum irradiated at 6.90 ppm; (**E**) spectrum irradiated at 6.80 ppm; (**F**) spectrum irradiated at 6.50 ppm.

5.2.3. Hahn Spin-Echo Experiment

The features of the ^{1}H-N.M.R. lignin spectrum have also been studied by the Hahn spin-echo technique. This pulse sequence allows us to distinguish between different peaks, selecting the resonances from even complex envelopes on the basis of their different T_2 relaxation time. The results obtained with the application of this technique using a delay, τ, of 45 ms are reported in figure 5.10.
It can be observed that the peaks' multiplicity reflects the identification made by 2D J-resolved techniques. Furthermore, the peaks' linewidths proved to be in the range of 20-30 Hz, values in the range measured by decoupling experiments, described in the preceding section.

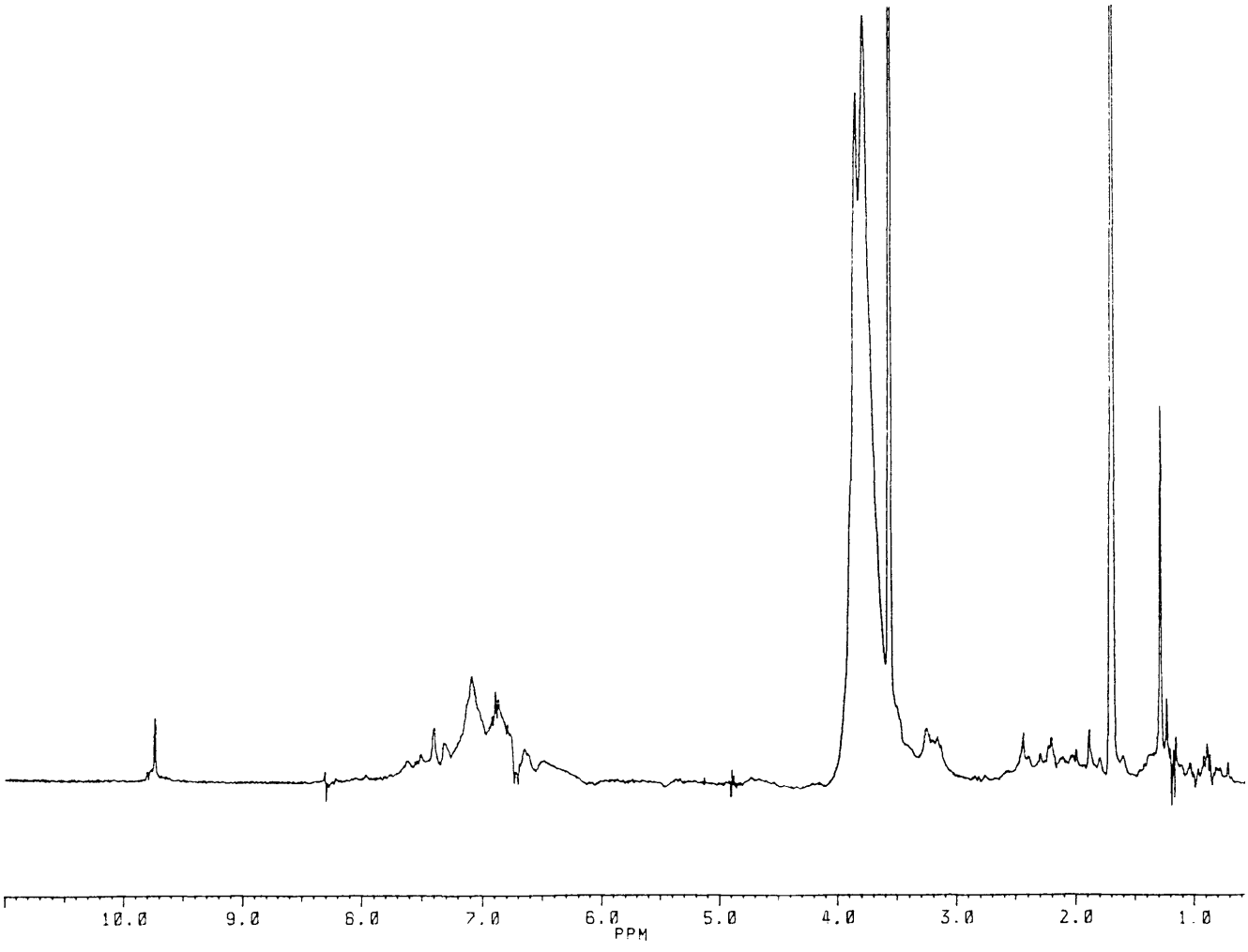

Figure 5.10. Hahn spin-echo ^{1}H-N.M.R. experiment on organosolv spruce lignin in deuterated dioxane-water (5:1). A delay τ of 45 ms was used.

5.2.4. Electron Spin Resonance Experiment

Electron Spin Resonance (E.S.R.) is a spectroscopic technique able to detect paramagnetic molecules that contain an unpaired electron in their structure. It follows that E.S.R. does not detect the bulk of an organic molecule, that generally has electrons paired in orbitals, but specifically detects paramagnetic centres. The results from the application of this technique on lignin are shown in figure 5.11.

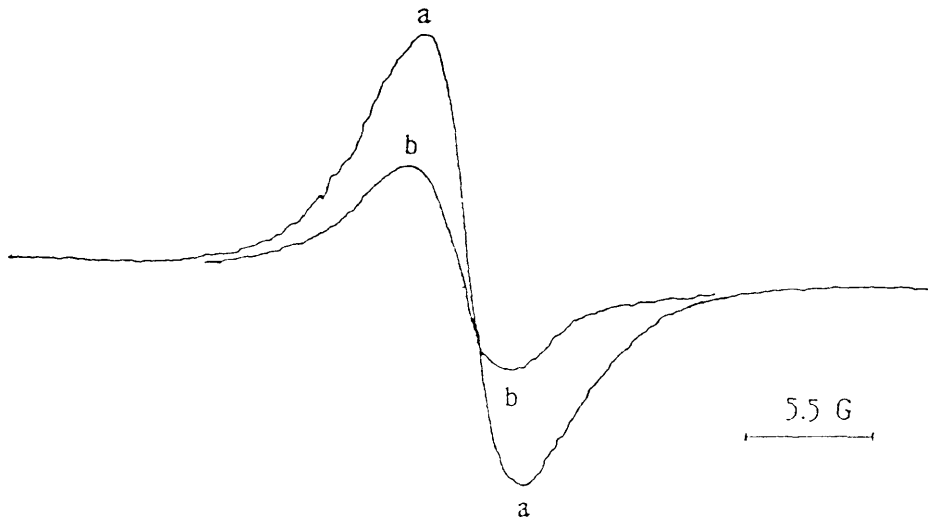

Figure 5.11. First derivative of the E.S.R. absorption spectrum of organosolv spruce lignin in tetrahydrofuran, before (a) and after addition of mercaptoethanol (b).

The E.S.R signal of figure 5.11. indicates the presence of a radical in the lignin network. The absence of hyperfine structure on the signal suggest the presence of an unpaired electron delocalized on the polymer. An attempt to quench the radical signal was made by addition of a reducing agent, mercaptoethanol; although about 60% of the signal could be quenched (figure 5.11b.), further addition of reducing agent did not yield to additional decrease in the signal. This suggests the presence of both transient and permanent radicals, in accordance with literature data on lignin-related compounds, i.e. humic acids and fulvic acids (in Schitzer and Khan, 1978). Dirkx et al. (1987) also found that the exposure of lignin samples increases the radical signal, probably due to the formation of phenoxy free radicals.
The presence of unpaired electrons in the lignin structure is certainly expected to have an impact on the N.M.R. spectral features: the presence of the radical will decrease the N.M.R. spin-spin relaxation time T_2 causing linebroadening.

This observation may provide an explanation of the broad N.M.R. lines observed in the decoupling experiments, whose presence was also inferred from the 2D N.M.R. results.

5.2.5 Lignin ^{1}H-N.M.R. Spectra Simulation

Computer simulation of N.M.R. spectra are a useful mean to confirm chemical shift assignments or general spectra interpretation. In this study this technique was used to simulate ^{1}H-N.M.R. spectra of lignin model compounds and to investigate the effect of the linewidth on the final spectra in comparison to lignin experimental spectra.
Figure 5.12. reports the computer simulated spectra of lignin model compounds in comparison to their relative experimental spectra. It can be observed that a complete correspondence between experimental and simulated spectra was achieved.
By further computer simulations on the aromatic region (6.50 - 7.50 ppm), it was possible to obtain a simulated spectrum of both the model compounds together, with different levels of linebroadening (figure 5.13.). The similarity between the experimental spectrum of lignin and the broadened simulated model compounds spectra is considerable. The closest similarity is shown for a line-broadening value of 70 Hz, but lignin spectral deconvolution obtained from decoupling experiments showed a peak linewidth of 25 - 32 Hz, confirmed by the Hahn spin-echo experiment and the linewidths at the basis of the COSY cross-peaks (40 Hz). This suggests that the actual experimental ^{1}H-N.M.R. spectrum of lignin is composed of few more peaks than those considered in the simulation experiment; this is reasonable taking into account the lignin substructures of figure 5.8. found for this sample. However, the simulation experiment shows that is actually possible to obtain the lignin spectral feature by simply taking into account the broadening of a limited number of resonances.

These data support the view that the N.M.R. spectra of lignin may actually consist of few broad resonances, rather than many overlapping signals. The extensive linebroadening may be due to the presence of a radical delocalized within the lignin network and responsible for a decrease in the N.M.R. spin-spin relaxation.
Although the orthodox view considers lignin as a random heterogeneous and highly cross-linked network with many substructures, these results suggest that the lignin sample analyzed has a much less complex structure than expected. In this interpretation, the relatively simple features of the lignin N.M.R. spectra may reflect a

degree of structural organization within the molecule, as described in the following paragraph.

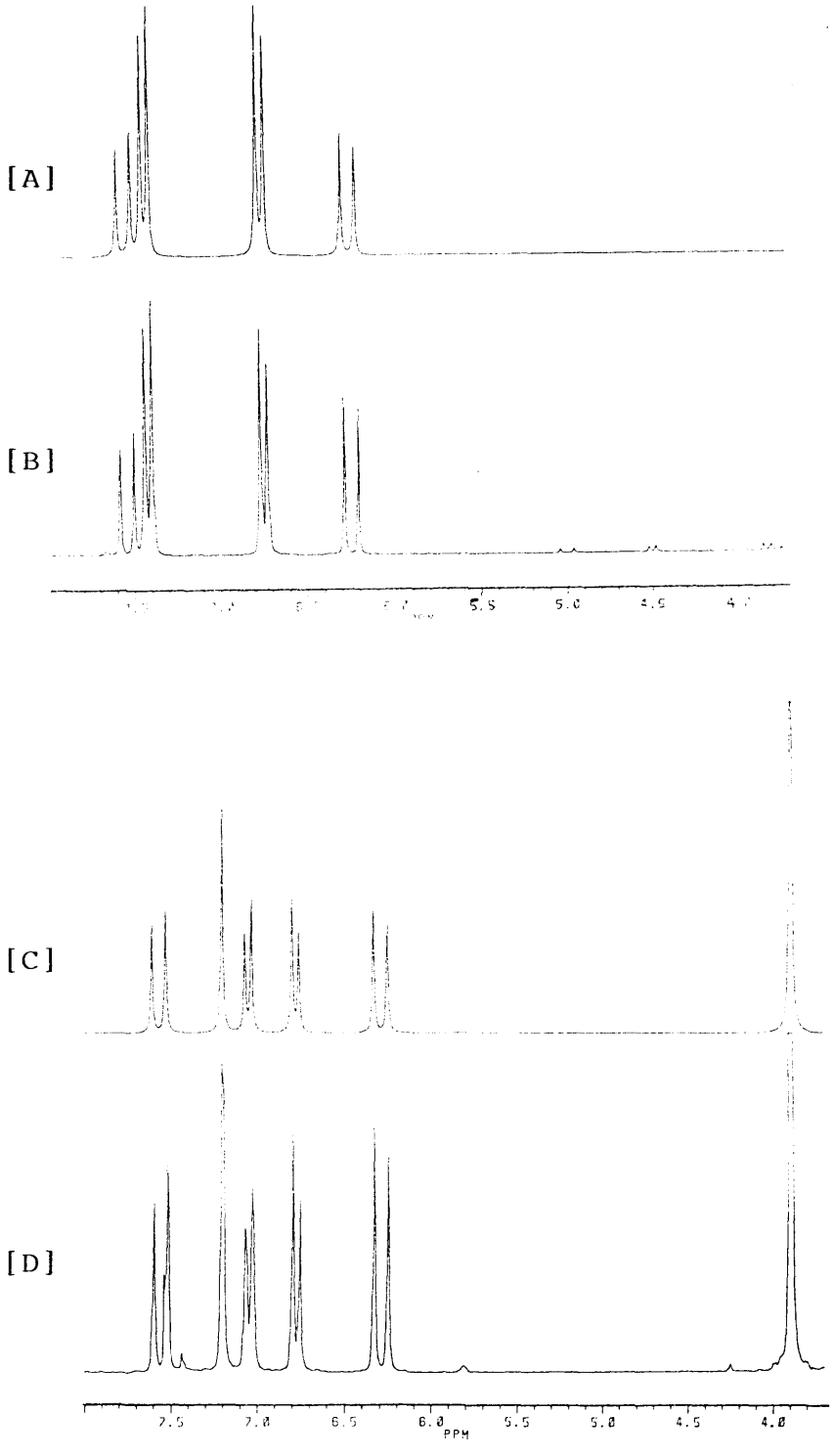

Figure 5.12. Computer simulated and experimental ^{1}H-N.M.R. spectra of lignin model compounds: simulated (**A**) and experimental (**B**) spectra of p-hydroxycinnamic acid; simulated (**C**) and experimental (**D**) spectra of p-hydroxy-3-methoxycinnamic acid.

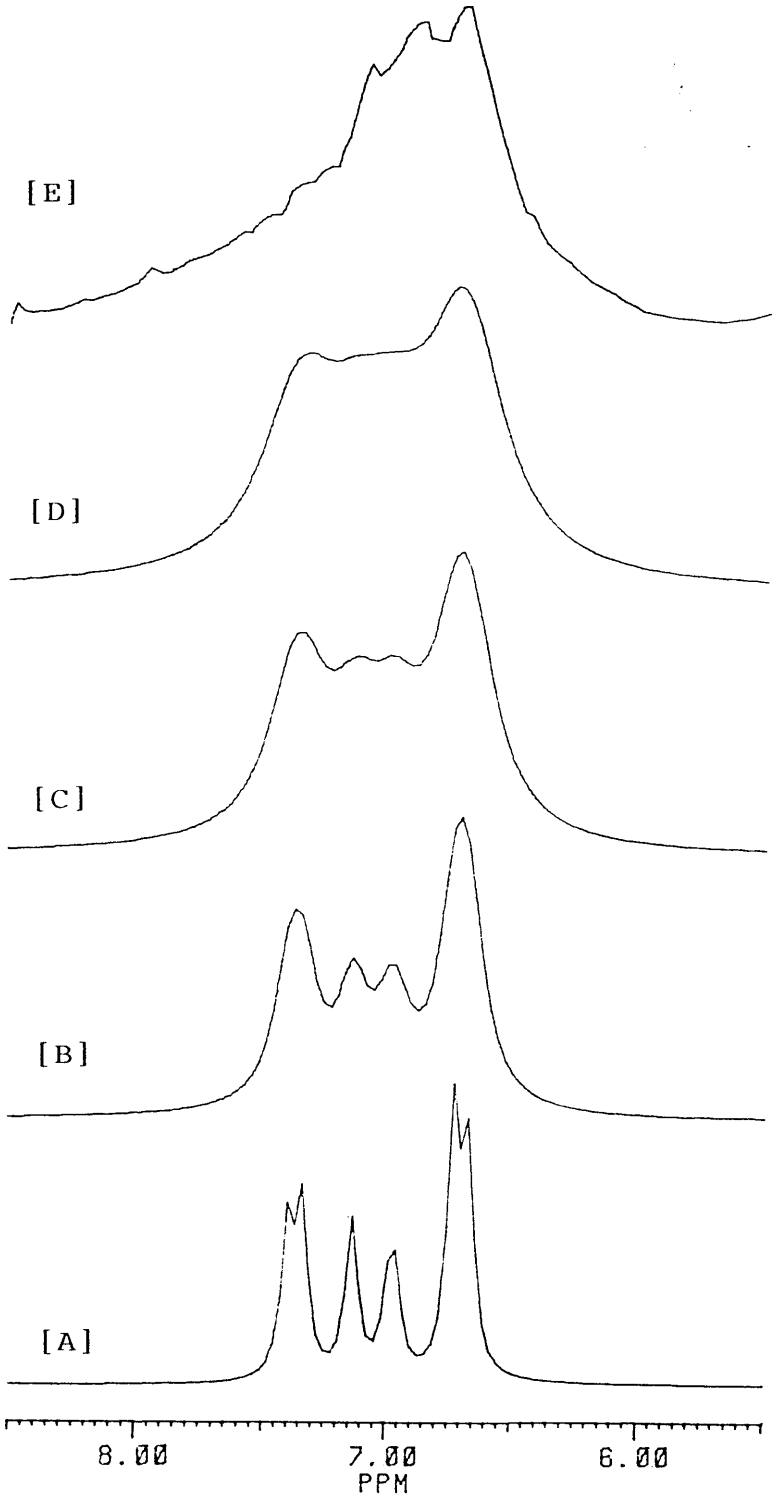

Figure 5.13. Computer simulated ^{1}H-N.M.R. spectra of p-hydroxycinnamic and p-hydroxy-3-methoxycinnamic acids lignin model compound units, at increasing linewidths and compared to the experimental spectrum of lignin: line-broadening of 10 Hz (**A**), 30 Hz (**B**), 50 Hz (**C**), 70 Hz (**D**), and experimental spectrum of lignin (**E**).

5.3. Lignin: Potential Structural Content

The ^{1}H-N.M.R. data presented in the previous paragraphs lead to an interesting consideration about a potential structural content in the sample analysed.
The J-resolved 2D spectra showed well-resolved definite peaks at precise chemical shifts values. These data suggested that the proton spectra of lignin consist of a few broad resonances. Although the nature of a 2D J-resolved spectrum may select resonances with long spin-spin relaxation times (sharp lines), experiments conducted processing data without any window function showed that even when the projection on the chemical shift axis is as broad as in the conventional 1D spectra, the peak pattern across the plane of the 2D spectra still carries the same information.
The quite different COSY experiment showed correlated resonances sharing scalar interactions through a limited number of cross-peaks, which reflected chemical shift and multiplicity in agreement with the J-resolved spectra. Although the cross-peaks are intense and well defined, and in spite of an intense and broad diagonal peaks feature, the paucity of cross-peaks is consistent with a small number of spin systems with a relatively small chemical shift distribution. This is rather unexpected for a complex random molecule such as lignin, in which chemical shift anisotropy due to different environments of chemically equivalent groups could have been expected to generate large sets of cross-peaks, as depicted in figure 5.14.
The linewidth at the base of the peaks of figure 5.14. was set at 50 Hz, a value found from the proton decoupling experiments and in agreement with the actual linewidth of COSY spectra of figure 5.6. and 5.7.; the coupling between protons was set at 10 Hz, as found in J-resolved spectra and confirmed in COSY spectra. The two resonances at 6.10 ppm (peak n. 4) and 7.10 ppm (peak n. 9) and their cross-peak "F" were offset at higher and lower fields to mimic the broadening observed in the F2 projection reflecting chemical shift anisotropy. The result is a spread set of cross-peaks F, Fa, Fb, Fc, and Fd.
Homonuclear decoupled, Hahn spin-echo and spectral simulation experiments shows that the broad poorly resolved lignin ^{1}H-N.M.R. spectra can be obtained with few broad lines. The presence of a strong E.S.R. signal due to the presence of unpaired electrons in the lignin network offers an explanation for such extensive N.M.R. line-broadening.
Furthermore, the absence of up-field proton signals due to aromatic ring current effects on side-chain groups is also consistent with the lack of NOE cross-peaks between aromatic and side-chain groups in NOESY experiments.

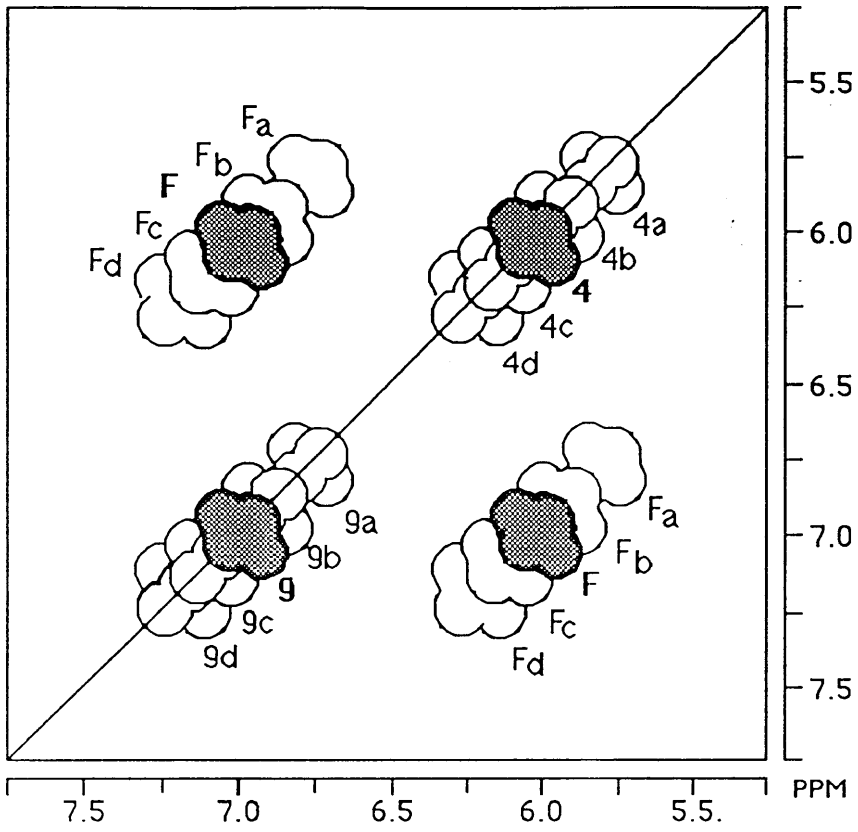

Figure 5.14. Picture showing as chemically equivalent doublets in different environments would give rise to sets of COSY 2D ^{1}H-N.M.R. cross peaks. The shadowed peaks correspond to the experimental cross-peak labelled as F (6.10 x 7.10 ppm) in table 5.5. The peaks labelled with letters a, b, c and d represent the same peak in bold, but shifted by anisotropic effects.

In an attempt to explain these results, it may be suggested the lignin network presents repeating domains of aromatic rings separated from side-chain aliphatic moieties; in particular, if supposedly the aromatic rings are stacking one on top of the other, no ring current effects would be observed on aliphatic resonances, and uniform chemical environments would be presented. To test the feasibility of this hypothesis, molecular modelling was carried out on a lignin fragment. N.M.R. data suggested the presence of β-O-4 structures in the sample studied, and this is consistent with literature data (Adler, 1977; Sakakibara, 1980) that showed these structures are predominant (>50%) in the majority of lignins. Therefore the molecular modelling was carried out on a lignin fragment of three guaiacyl units linked by β-O-4 type of bonds (figure 5.15.).

The lignin fragment was modelled to a "folded structure" with aromatic rings on parallel planes and lying on stacks, and to a "open structure" with the aromatic ring on a planar extended conformation. The atoms' coordinates were energy minimized in terms of bond angles and length, and the resulting structures are reported in figure 5.16. It is intended that these structures are purely indicative that

such conformation may be compatible with the lignin fragment considered. A more quantitative approach would be to determine which structure is energetically favoured: this is difficult as strictly it would depend also on intramolecular, intermolecular and solvent interactions that could not be easily determined.

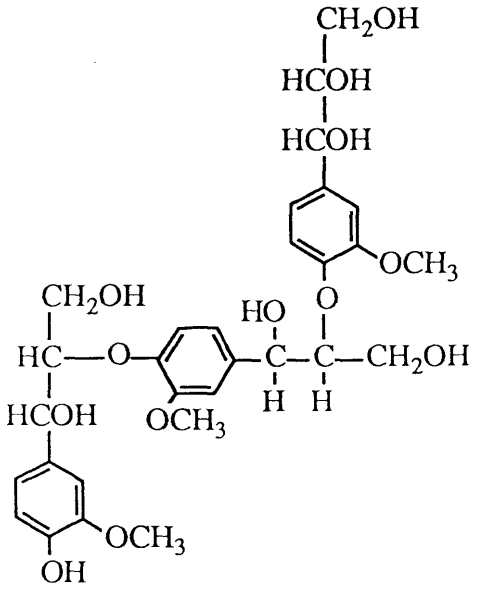

Figure 5.15. Structural formula of the lignin fragment considered for molecular modelling (three monomeric units linked by β-O-4 bonds).

It is relevant that literature data on theoretical molecular modelling of two phenylpropane units bound by β-O-4 linkages, reported a global energy minimum for a folded structure in which the aromatic ring are on parallel planes (Gravitis and Erins, 1983). This study was carried out on non-methoxylated aromatic units. Elder and coworkers (1988) also reported molecular orbital calculation studies on mono-methoxylated β-O-4 linked aromatic compounds (figure 5.17a.) very similar to those considered in this study. These authors also found an energy minimum for a folded arrangement with aromatic rings on parallel planes (figure 5.17b.); furthermore these authors showed as the erythro structure is slightly more stable than the threo, with steric energies of 23.25 Kcal/mole and 23.45 Kcal/mole respectively. This result is supported by other research that showed that in natural lignin the erythro isomer is 1.5 times more abundant than threo (Taneda et al., 1989).

These theoretical data are consistent with the model presented in figure 5.16c.

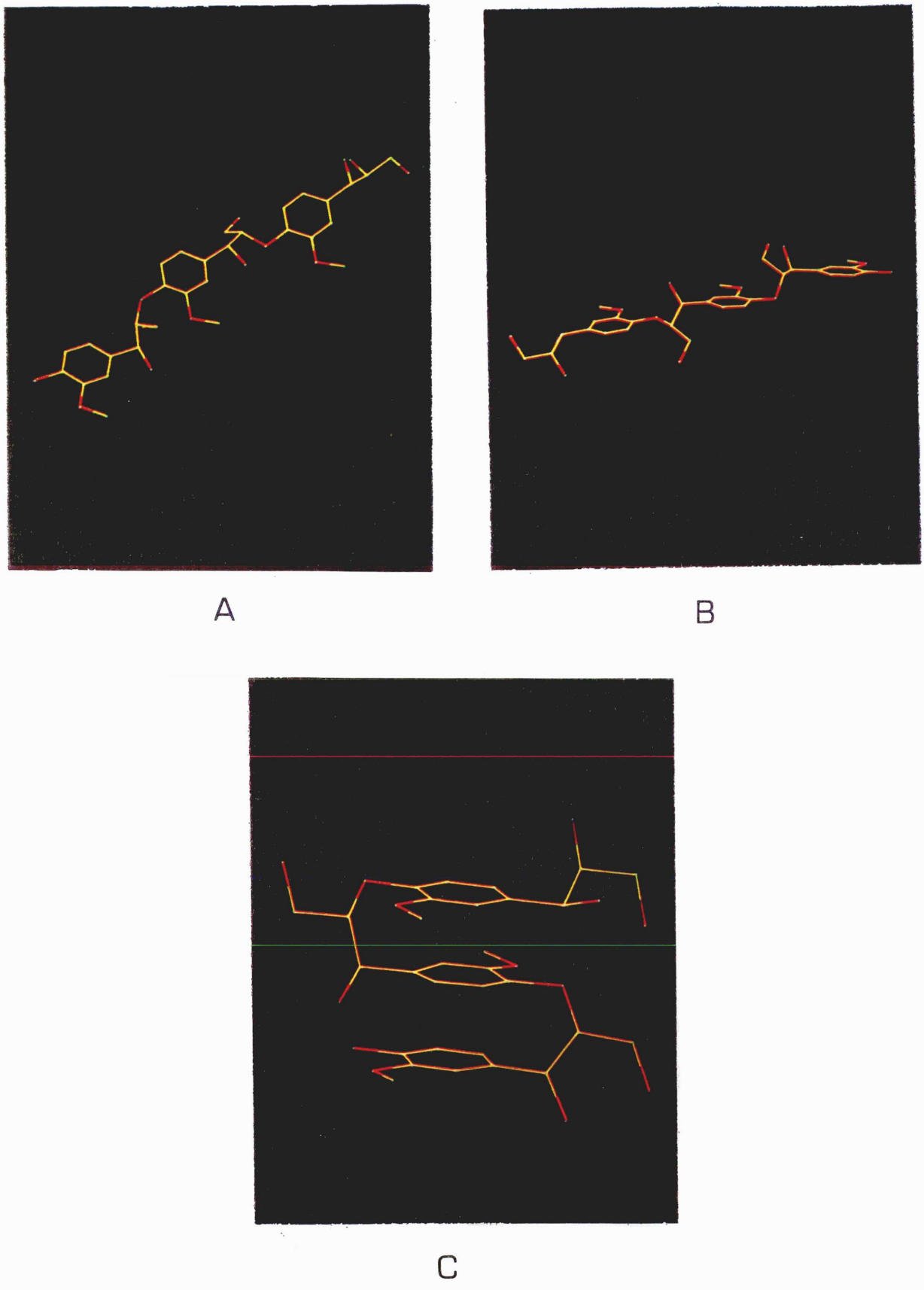

Figure 5.16. Open (**A, B**) and folded (**C**) structure of β-O-4 lignin fragment.

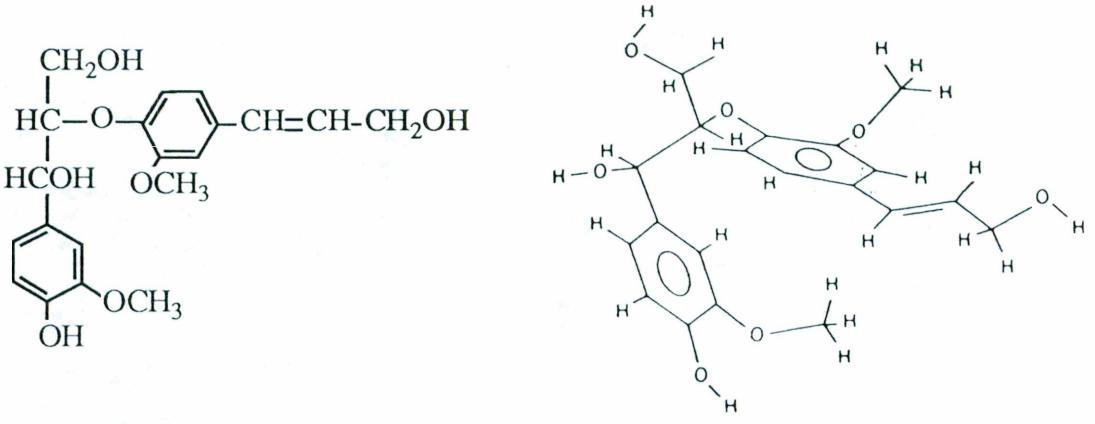

[a] [b]

Figure 5.17. Structural formula (a) and geometrically optimized structure (b) of lignin model compound (modified from Elder et al. 1988).

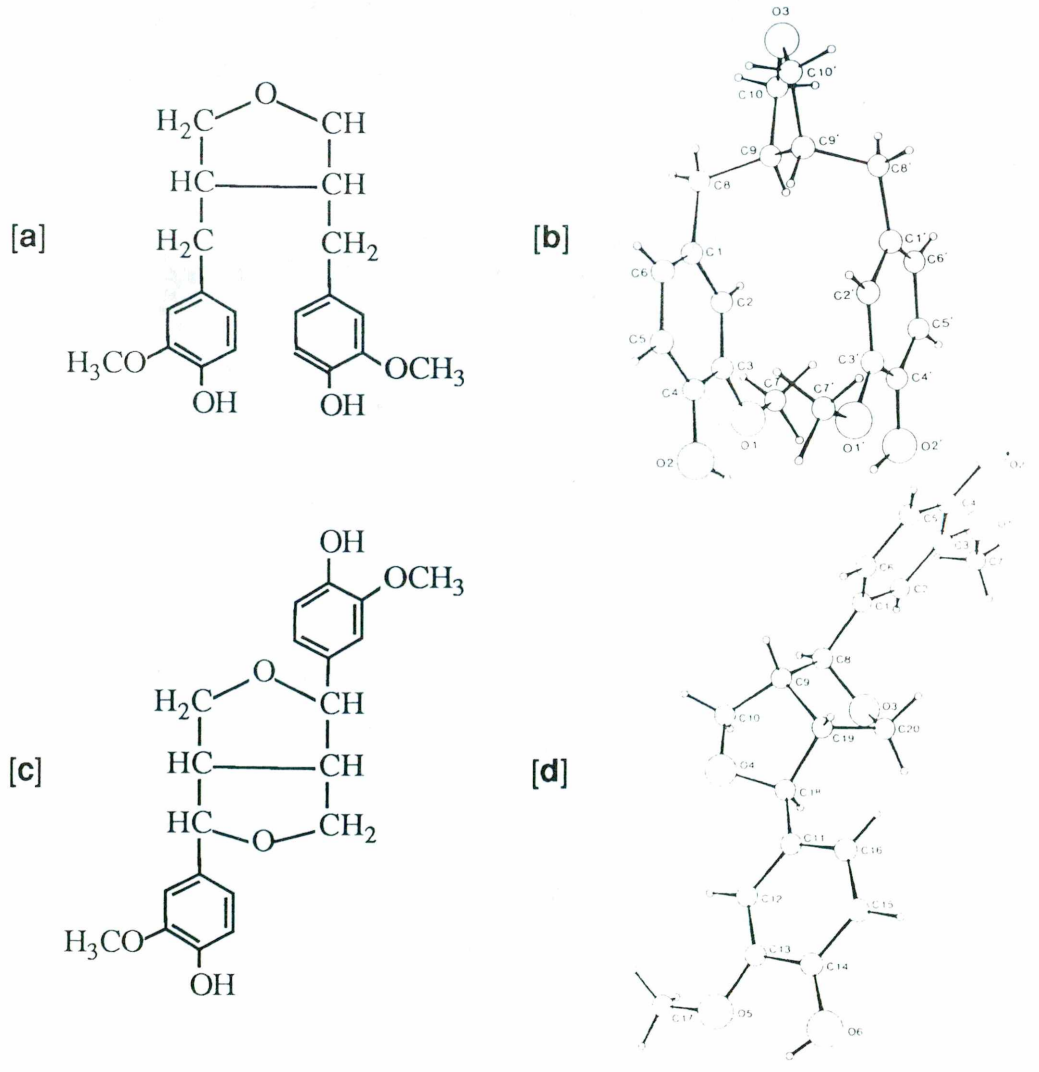

Figure 5.18. Structural formula of 3.4-divanillyltetrahydrofuran and pinoresinol (a,c) and their relative crystal structures (b, d), (modified from Lundquist and Stomberg, 1988).

Moreover, the crystal structure of lignin models containing β-β linkages have been reported by Lundquist and Stomberg (1988). These authors determined that the 3.4-divanillyltetrahydrofuran (figure 5.18a.) crystal structure exhibits aromatic ring stacking (figure 5.18b.); the pinoresinol (figure 5.18c.), instead, showed a planar conformation (figure 5.18d.). The crystals of both compounds consist of monomeric molecules held together by Van der Waals forces and weak hydrogen bonds; there are also intramolecular hydrogen bonds between adjacent hydroxy and methoxy groups.

The overall picture emerging from these data shows that the major lignin subunits, β-O-4 (>50%), β-β (~15%) have precise conformations involving either a planar arrangement or stacking of aromatic rings. This may well play an important role in lignin, where the close association with hemicelluloses could introduce definite structural constraints: stacking between carbohydrate and aromatic residues has been demonstrated and clearly defined by Quiocho and coworkers (Vyas et al., 1988) for the complexes between arabinose-binding and galactose-binding proteins and their respective ligands, and also interactions between non-polar surface ("hydrophobic patches") of carbohydrates and aromatic amino acids have been reported (Derewenda, 1989; Weiss, 1988). Interestingly the hydrophobic patches claimed by these studies on C3-C4-C5 of arabinose units are very similar to the structure exhibited by C3-C4-C5 of xylose β(1-4) linked to form hemicellulose, whose presence was detected in this study by ^{13}C-N.M.R.
Fry (1987) claimed a template-like effect of polysaccharides during the peroxidase-catalyzed polymerization of lignin. Also, the concentration of hemicelluloses is higher in the middle lamella and in the inner regions of the secondary walls where lignin is present (Blanchette and Abad, 1988); the link between the two macromolecules is also proved by solution and solid state N.M.R. studies (Kolodziejski et al., 1982; Gerasimowicz et al., 1984), which not only showed that the two polymers can never be completely separated due to covalent ether bonds (see figure 1.7., chapter 1), but also more significantly that the two polymers exhibit a common $T_{1\rho}$ (Newman and Hemmingson, 1990).
This led the authors to conclude that lignin and hemicelluloses are so intimately associated that spin diffusion is present and results in the observation of a single averaged value of $T_{1\rho}$. It may be worth remembering that the spin diffusion effect consists of the spin energy propagation between neighbouring nuclei by energy-conserving spin transitions, and it occurs over distances less than 0.1-0.3 nm (McBrierty and Douglass, 1981).
Interestingly Atalla and Agarwall (1985) reported "Raman microprobe evidences for lignin orientation in the cell walls of native wood", showing that in most instances,

the aromatic rings of the lignin units are oriented parallel to the plane of the cell wall surface. These data indicate that a preferential arrangement is actually present in native cell walls. Earlier observations (Sarkanen and Ludwig, 1971) also reported that although the matrix components of the cell wall (lignin and hemicelluloses) appear to be amorphous at the X-ray analysis, UV-dichroism studies showed that the lignin component is to a certain extent oriented.
The ensemble of these results leads to interesting questions about the structure of lignin. Although it is difficult to relate the information obtained on isolated fragments to the "unaltered" state of lignin in the cell wall, it may be reasonable to expect that a certain structural content is retained in isolated lignin fragments, provided that they were extracted by mild procedures.

The N.M.R. data reported in this chapter suggest the presence of repeating domains of aromatic rings in lignin, separated by side-chain aliphatic moieties. This is consistent with the Raman results obtained by Atalla and Agarwall (1985) that were interpreted as a preferential parallel arrangement of lignin's aromatic rings in the native cell wall. Moreover, polysaccharides have been shown to have a template-like effect on lignin during its polymerization (Fry, 1987), and this intimate relationship is maintained in the assembled cell wall (Newman and Hemmingson, 1990).

The main conclusion to be drawn from all these observations is that the cell wall assembly may have a precise structural arrangement that is also extended to the lignin component. Such structural content could potentially persist in isolated lignin fragments when the extraction procedures have not been too severe. The intimate interaction between lignin and hemicelluloses originates during the biosynthesis of lignin. The potential structure deriving from the hemicellulose's template-like effect on lignin, may impose precise structural constraints. For example, it may be possible to envisage the matching of linear fragments of lignin as in figure 5.16a. over the hydrophobic patches of a hemicellulose's chain. A stable structure can potentially be obtained by stacking lignin's aromatic rings over the original template. A precise structural arrangement between the cell wall components could be the origin of the rigidity imparted by lignin to the flexible polysaccharidic fibres. In addition to the mechanic properties, the lignin's precise arrangement has a protective effect on the polysaccharides against microbial degradation.

Chapter 6

ASSOCIATIVE AND COLLOIDAL BEHAVIOUR OF LIGNIN

Early work suggested a view of lignin as a complex three dimensional polymer network. Its structure in wood was visualized as branched with linear chains cross-linked by a variety of interchain covalent bonds (Adler, 1977). The strongest argument in favour of this "network theory" is that native lignin is insoluble in all neutral solvents, and this, according to the theory, is due to strong covalent lignin-lignin bonds present in wood. The solubilization of this complex inevitably involves breaking bonds, yielding molecular fragments, and leading to the polydispersity in molecular weight of soluble lignin derivatives.

Recently, some work has shed a new light on the behaviour of lignin in solution, in respect of its molecular weight; Dutta and Sarkanen (1990) reported size-exclusion chromatography data consistent with an associative process amongst lignin molecules. These and previous results from the same group (Garver et al., 1989; Sarkanen et al., 1984; Sarkanen et al., 1982) showed an increase in molecular weight of kraft lignin solutions over time. The authors suggested the presence of "non-covalent" interactions between individual lignin molecular components.

In an early work, Lindstrom (1979) showed an association process taking place between kraft lignin molecules, and speculated on a colloidal behaviour of kraft lignin. This author also reported the presence of stable lignin sols in aqueous solution, whose extent of aggregation was followed by gel permeation chromatography and viscometric measurements; however, no light scattering measurements were made. More recently, the colloidal dispersion of lignin in water has received further attention in view of biodegradation studies. Kurek et al. (1990a) reported the preparation of colloidal dispersions of milled wood and enzymatically liberated lignin in water from dimethylformamide, with no major molecular alterations as shown by UV and IR spectra. The same authors claimed a higher ligninase activity based on H_2O_2 consumption, towards the colloidal lignin compared with the ordinarily precipitated lignin (Kurek et al. 1990b). This finding raises interesting questions on the role of the physical state of lignin and its accessibility to enzymatic biodegradation, stressing the importance for further studies on the lignin polymer structure.

In this chapter are reported studies conducted on the associative and colloidal behaviour of organosolv spruce lignin. This sample offers the advantage of being

exposed to fairly mild solubilization conditions, and therefore is structurally much closer to the native lignin than the kaft preparations studied so far. The molecular weight characterization is followed by molecular dimensions determination and studies of light scattering properties of the lignin colloidal solutions. The associative behaviour is studied as function of pH rather than time as for previous works (Dutta and Sarkanen, 1990).

6.1. Lignin Molecular Weight Determination

The molecular weight (MW) of organosolv spruce lignin was determined by HPLC gel-filtration, with porous silica gel microspheres (Zorbax PSM 60S, Du Pont) as stationary phase, and N,N'-dimethylformamide (DMF) as mobile phase, as described in paragraph 3.3.1.

The HPLC column was calibrated with polystyrene standards; the results are reported in table 6.1., and the relative calibration curve obtained by plotting the log MW against the HPLC retention time (RT), is reported in figure 6.1.

The MW calibration curve of figure 6.1. shows a good correlation between log MW and the retention time, with a correlation coefficient of 0.999: this indicates that the system was well calibrated in a range of MW between 800 and 17500 daltons.

Table 6.1. HPLC gel-filtration of polystyrene MW standards in DMF (Zorbax PSM 60S column, flow 1 ml/min).

Standards MW	log MW	Retention time / min
800	2.90	5.03
2000	3.30	4.45
4000	3.60	4.10
9000	3.95	3.62
17500	4.24	3.21
50000	4.70	2.93

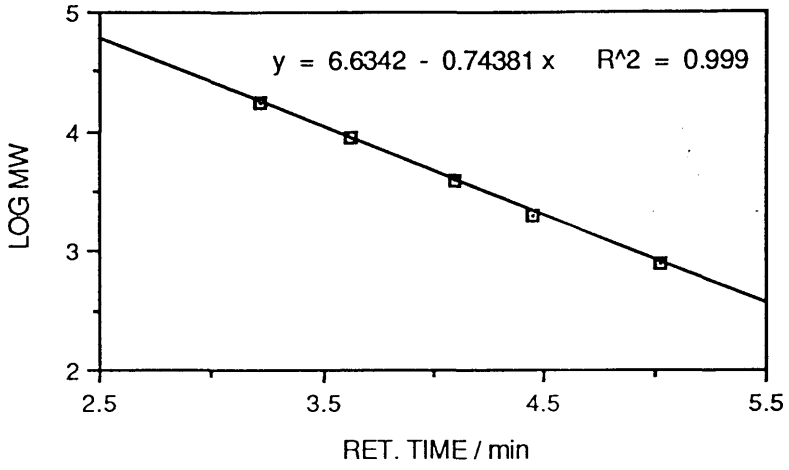

Figure 6.1. MW calibration curve of Zorbax PSM 60S HPLC column with Polystyrene standards in DMF, flow 1 ml/min.

Figure 6.2. shows the elution profile of an organosolv spruce lignin sample. From figure 6.2. three major fractions can be identified, labelled as (a), (b) and (c); their MW was determined by using the relation logMW-RT found from figure 6.1.:

$$\log MW = 6.63 - 0.74\ RT$$

The results obtained are reported in table 6.2.

Fraction (a) and (c) show MW values that are not strictly in the range in which the column was found to respond linearly to the standards. However, as a polystyrene standard of MW 50000 showed a RT of 2.93, a purely indicative estimate of molecular weight for lignin fraction (a) is about 70000.

These data are consistent with the presence of a highly polymerized lignin component (MW > 20000), that is probably the most representative of the native lignin.

The feature of the peaks with RT 2.59 of figure 6.2. is indicative of a relatively low polydispersity in the sample; however the process of solubilization inevitably breaks the polymer network into soluble fragments of lower molecular weight, yielding polydispersity in the low MW fraction of figure 6.2. This may explain the presence of fragments of relatively low MW (837 and < 800), probably hydrolyzed moieties during the sample preparation.

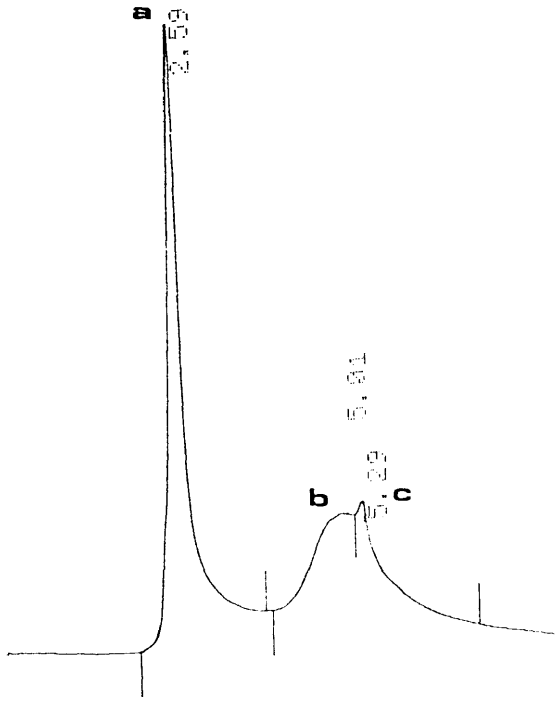

Figure 6.2. HPLC gel-filtration elution profile of organosolv spruce lignin in DMF (Zorbax PSM 60S column, flow 1 ml/min). The retention times are indicated.

Table 6.2. Organosolv spruce lignin HPLC gel-filtration fractions.

Fraction	RT / min	Peak area / %	MW
(a)	2.59	58	> than 20000
(b)	5.01	22	837
(c)	5.29	20	< than 800

The majority of the lignin sample here analyzed appears to be highly polymeric (58 %), and given an average conifer lignin formula weight of 183 g/mole (Adler, 1977), the sample results to consist of about 380 C-9 monomer units.

6.2. Langmuir-Blodgett Trough Experiment: Determination of the Lignin Average Molecular Area

The Langmuir-Blodgett trough is a relatively simple instrument designed to measure the surface pressure π of a molecular monolayer floating on a non-miscible solvent, whilst varying the area available to the monolayer itself.
The apparatus consists in a rectangular dish containing a solvent (liquid phase) that is not miscible with the molecules of interest. These are distributed in a known number as a monomolecular layer on the air-water interface. The surface area is varied by a non-wettable movable barrier that reduces the interface area available to the monolayer, causing an increase in the surface pressure measured by a movable float. The plot of π against the area available to the molecule is an isotherm that shows the behaviour of π with the variation of the physical state of the monolayer. When the area available is large compared to the monolayer extension, the π is extremely low (0.1-0.5 mN m^{-1}), due to the high dilution of the molecules; under these conditions the molecules exhibit a gas-like behaviour. As the area is decreased, the distances between molecules are reduced and the monolayer shows a liquid expanded behaviour, that through intermediate steps tends to the liquid condensed state and finally to a solid-like character, where the area occupied per molecule approaches the actual molecular size. This step is accompanied by a significant increase in the surface pressure. In the very last step, the area available to each molecule is smaller than the molecular size, and the molecules will overlap one on the other, destroying the monomolecular layer and causing a drop in the surface pressure.
In a typical isotherm, the region of steep variation of π with the area corresponds to the liquid condensed stage, where the molecules occupy an area equal to their molecular size. By extrapolating the slope of π to intersect the x-axis ($\pi = 0$), the area value on this point is the "limiting area", that can be considered very close to the cross-sectional area of the molecules (Gaines, 1966; Mohwald, 1990).
Therefore this technique can be useful to estimate molecular dimensions: by this method the x-axis can be calibrated to the molecular system under investigation. By knowing the number of molecules deposited and the initial and final interface area, the area available to each molecule is:

$$A_m = A_t / (N_A \cdot n)$$

where A_m is the area available to each molecule, A_t is the area available to the all monolayer, N_A is the Avogadro number ($6.023 \cdot 10^{23}$) and n is the number of moles deposited.
This technique was applied in this research to organosolv lignin to calculate the average cross-sectional area of this molecule. The experiment was performed

according to the procedure described in paragraph 3.3.2., and the isotherm obtained is shown in figure 6.3.

The isotherm of figure 6.3. shows the typical pattern of a monolayer of molecular species in function of decreasing area available. The first part of the curve (G) exhibit surface pressure values less than 0.35 mN m^{-1}, which is indicative of high area available associated with a high dilution of the molecules with gas-like behaviour. This is followed by a step (LE) in which π increases to 6.3-8.0 mN m^{-1}, and is indicative of liquid like character of the monolayer, due to a decrease in the area available for each molecule. The liquid-expanded state (LE) is followed by an intermediate state (I) in which the area occupied per molecule approaches the molecular size. When this point is reached, a steep increase in the slope is observed (LC), and the system appears to be in a liquid condensed state, with surface pressure up to 45.5 mN m^{-1}. A further decrease in area causes destruction of the monolayer, with drop in surface pressure values as observed in (S).

The calibration of the area available for each molecule critically depends upon the molecular weight of the sample under investigation. Although lignin is a complex polymer whose molecular weight determination is not straightforward, an average estimation of 70000 may be extracted from HPLC gel-filtration data, as reported in paragraph 6.1.

Figure 6.3. shows that the steep increase in surface pressure corresponding to the liquid condensed state of the lignin monolayer, occurs for an area per molecule of 19 x 10^3 $Å^2$. As this is the stage at which each molecule occupies its molecular area, 19 x 10^3 $Å^2$ can be taken as an average value for the cross-sectional area of the lignin molecules analyzed.

Given the complex structure of lignin, it is difficult to predict the molecular arrangement at the water-air interface; however, in the light of molecular area and molecular weight it is possible to make some suggestions. It is reasonable to assume that the lignin monolayer is spread on the water surface such that hydrophilic moieties, generally represented by polar groups of the side chains, that are in close contact with the water interface, whereas apolar aromatic moieties may be exposed to the air phase. This is schematically represented in figure 6.4a; a similar model has been reported in literature for tri-p-cresyl phosphate molecules (figure 6.4b.), showing a cross-sectional molecular area of 95.0 $Å^2$ (Gaines, 1966).

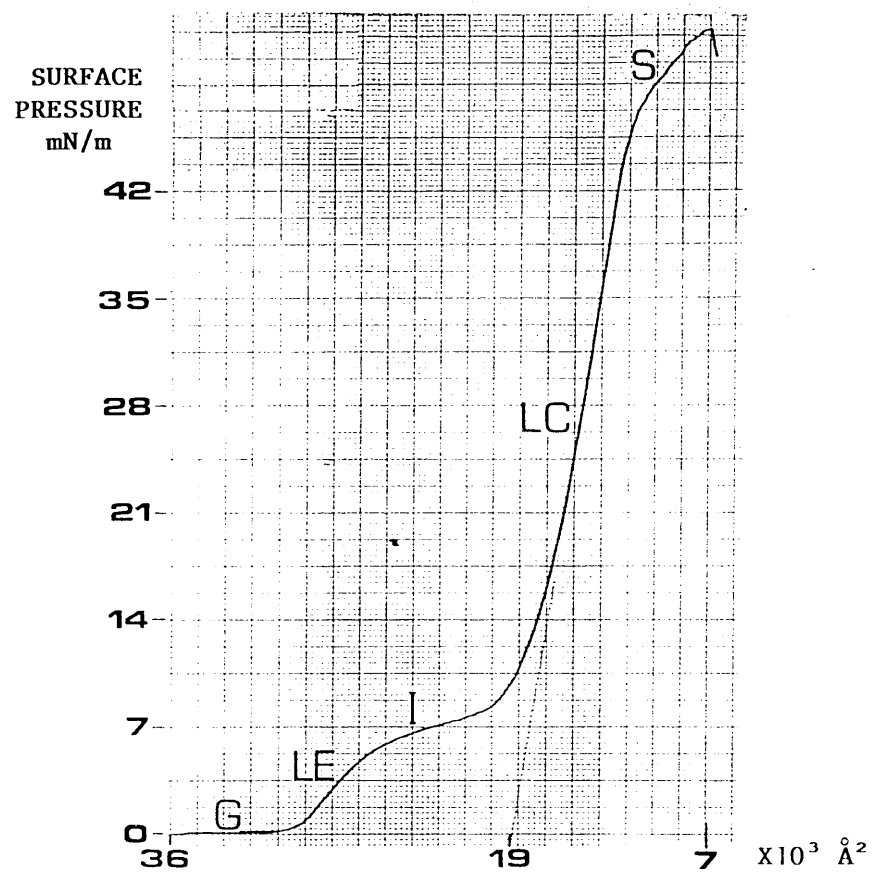

Figure 6.3. Surface pressure versus area per molecule isotherm obtained on the Langmuir-Blodgett trough for a organosolv spruce lignin monolayer on water surface.

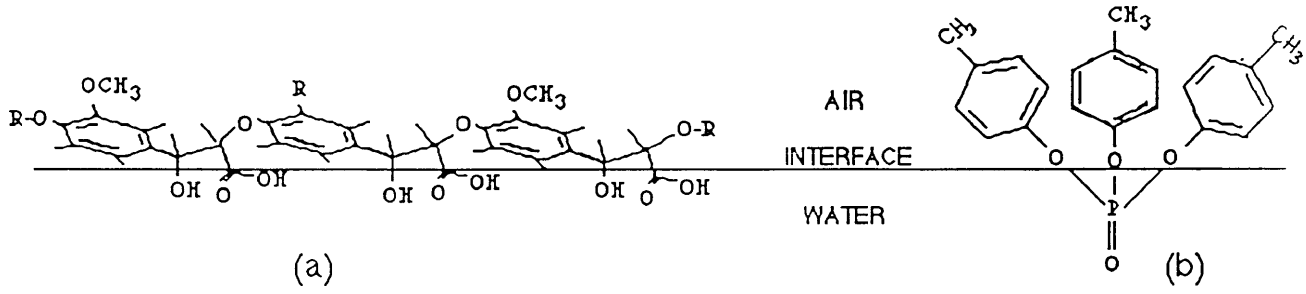

Figure 6.4. Schematic arrangement on water-air interface of a molecular monolayer of a lignin fragment (a) and of tri-p-cresyl phosphate (b). The picture is purely indicative.

It has been discussed in paragraph 6.1. as a lignin molecule of average MW 70000 it may contain 380 C-9 aromatic units of average MW 183 g/mole. According to the values reported in literature for the molecule of figure 6.4b., a lignin bearing 380 aromatic units could be expected to form a monolayer of an indicative area of 12 x 10^3 Å^2. The higher value of 19 x 10^3 Å^2 experimentally obtained suggest that

indeed lignin forms a monolayer on the water surface, and the higher value is accounted for by the C-3 side-chains and methoxyl groups attached to aromatic units, that contribute to a more expanded structure than that of figure 6.4b.

6.3. Light Scattering Experiments of Lignin Solutions

Light scattering spectroscopy is concerned with the light scattered from translational and rotational degrees of freedom of particles. In fact, when light impinges on matter, the electric field of the light induces an oscillating polarization of the electrons in the molecules. These behave as as secondary sources of light, and subsequently radiate or "scatter" light, a phenomenon commonly called Rayleigh scattering. Frequency shifts due to loss of energy by photons, the angular distribution, the polarization and the intensity of the scattered light are determined by the size, shape and molecular interactions in the scattering materials.
As the intensity of the scattered light is often weak, the light sources commonly used are very intense, such as lasers. Laser light scattering experiments have been applied to study the structure and dynamics of diverse systems, such as solids, liquid crystals, gels, solutions of biological macromolecules, dispersion of microorganisms, dispersions of viruses and membrane vesicles (Berne and Pecora, 1975).
The equipment necessary to carry out light scattering experiments is described in paragraph 3.3.3. The quantities measured in these experiments are the time-correlation function g(t) of the scattered intensity. It has been shown that for macromolecular solutions with spherical particles, the g(t) is an exponential decaying function of time, with time constant τ (in Berne and Pecora, 1975). This can be written as:

$$g(t) = \exp(-t/\tau)$$

The measurement of the exponential decay of the time-correlation function by dynamic light scattering can be used to measure the hydrodynamic radius of spherical particles in solution. In fact, it can be shown that :

$$\tau = 1/(D K^2)$$

and

$$K = (4\pi/\lambda)\, n \sin(\theta/2)$$

where: D is the self-diffusion coefficient
K is the constant defined above

λ is the laser wavelength
n is the solution refractive index
θ is the scattered beam angle

According to the Einstein relation, the self-diffusion coefficient is defined as:

$$D = k_B T / \zeta$$

where: k_B is the Boltzmann constant
T is the temperature
ζ is the friction constant

For spherical particles, the friction constant ζ can be approximated (Stokes approximation) as:

$$\zeta = 6 \pi \eta R_H$$

where η is the viscosity and R_H is the average hydrodynamic radius of the particles. By combining these formulae, it can be written that:

$$R_H = k_B T / 6 \pi \eta D$$

This relation allows an estimate of the hydrodynamic radius of spherical particles by dynamic light scattering experiments.

In this research, organosolv spruce lignin samples were studied by conventional and dynamic light scattering techniques to investigate a potential aggregation phenomenon of lignin in solution.

As preliminary experiment, the intensity of the light scattered by series of solution of lignin at different concentration in dioxane-water (5:1), was measured according to the procedure described in paragraph 3.3.3. The results obtained from this experiment are reported in figure 6.5.
From figure 6.5. it can be observed that a dramatic increase in scattered light intensity is found between 0.5 and 0.8 mg/ml lignin concentration.

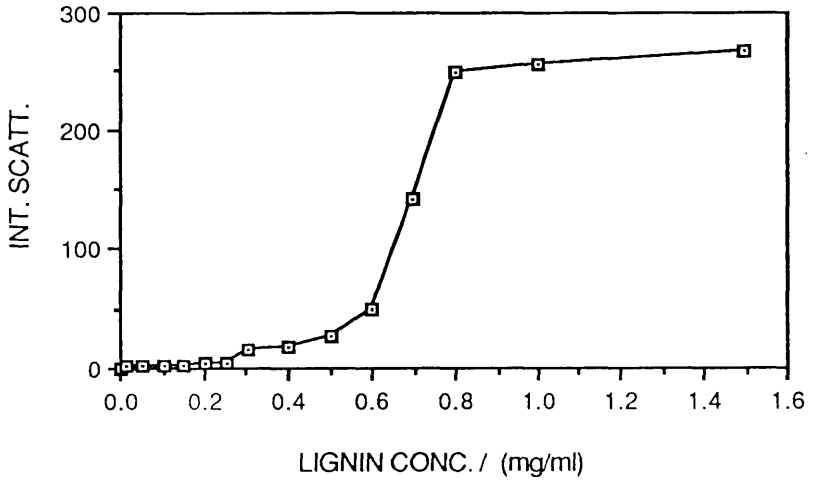

Figure 6.5. Intensity of light scattered by organosolv spruce lignin solutions at 625 nm, as a function of lignin concentration.

Because lignin solution exhibits strong absorption in the UV region with a tail in the visible region, it was not possible to extend light scattering measurements to concentrations above 1.5 mg/ml, due to intense absorption interference.
The step of increment in scattered light intensity above 0.5 mg/ml suggests that an aggregation process occurs. As the increment tends to a plateau above 0.8 mg/ml, there may be indication of formation of discrete particles, whose assembly requires more than one molecule of lignin.
The self- assembling reversible behaviour occurs at concentration above 0.5 mg/ml, which would correspond to the so-called critical micellar concentration in detergent or other amphylite solutions.

To further investigate this phenomena, the same lignin solutions were examined in a dynamic light scattering apparatus, as described in paragraph 3.3.3. The results are reported in figure 6.6.
The exponential decay pattern of the scattered light shown in figure 6.6. is consistent with the presence of aggregates in the solution analyzed.
Assuming a spherical shape and introducing a sample viscosity of 1.17 cp, these aggregates are found to have an hydrodynamic radius of 619 Å, with no significant variations between 0.8 mg/ml and 2.0 mg/ml lignin concentration.

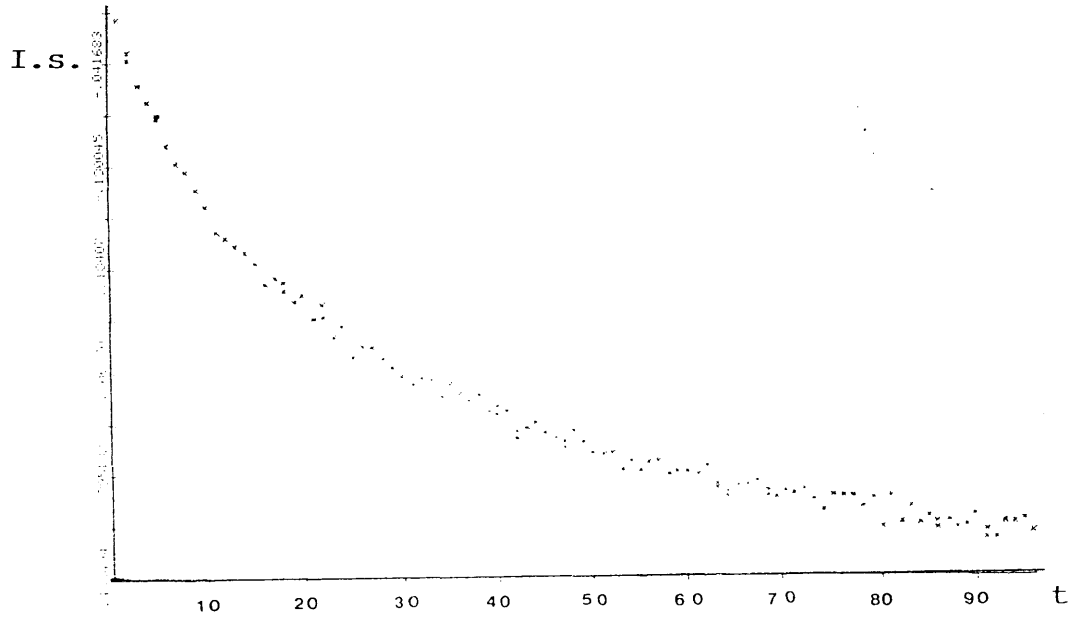

Figure 6.6. Exponential decay pattern of the time-correlated function in a dynamic light scattering experiment on a organosolv lignin sample (0.8 mg/ml) in dioxane water (5:1) solvent system.

Table 6.3. Viscosity values of soluble lignins, xylan and cellulose of MW 50000 (modified from Sarkanen and Ludwig, 1971).

Macromolecule	Solvent	Viscosity / (dl g^{-1})
Organosolv lignin	Pyridine	0.08
Kraft Lignin	Dioxane	0.06
Lignosulfonate	0.1 M NaCl	0.05
Xylan	Cupriethylenediamine	2.16
Cellulose	Cupriethylenediamine	1.81

Experiments carried out on more dilute samples did not show defined decay pattern, and more concentrated samples presented absorption interference. The assumption of a spherical shape for the aggregates is supported by early viscosity measurements (in Sarkanen and Ludwig, 1971) that reported lignin solution viscosity values much lower than those measured for linear (cellulose) and branched (xylan) cell wall polymers of equal molecular weight (table 6.3.).

From the average hydrodynamic radius value, it can be calculated that the average surface of the spherical particles is 480 x 10^4 Å^2. Given the molecular average cross-sectional area value of 19 x 10^3 Å^2 calculated with the Langmuir-Blodgett technique (paragraph 6.2.), each particle results to be an assembly of an average of 256 lignin molecules.

It may be interesting at this point to consider two examples of well studied colloidal systems: latex particles and soap micelles. The former are heavily cross-linked polymer particles, which behaves as rigid balls; the latter are formed by amphiphilic molecules such as long chain fatty acids or phospholipids, that in water tend to gather into spherical aggregates (micelles), in which the polar heads face outwards to the polar water molecules, and the hydrophobic chains lie buried in the aggregate's core (Prost and Rondelez, 1991). Given the absence of obvious polar and apolar heads in lignin moieties, it seems difficult to reason the aggregation process in terms of micelles. Considered the complex structure of lignin molecules, it is difficult to predict their arrangement in the aggregates, but it may be however possible to identify apolar patches formed by aromatic rings, and polar sites along the side-chains: these patches are likely to combine at intra and intermolecular level leading to the aggregates. This suggests that lignin aggregates are closer to the latex particle than to the soap micelle model for colloidal systems. Figure 6.7 is a speculative suggestion of the interactions between two lignin molecular fragments.

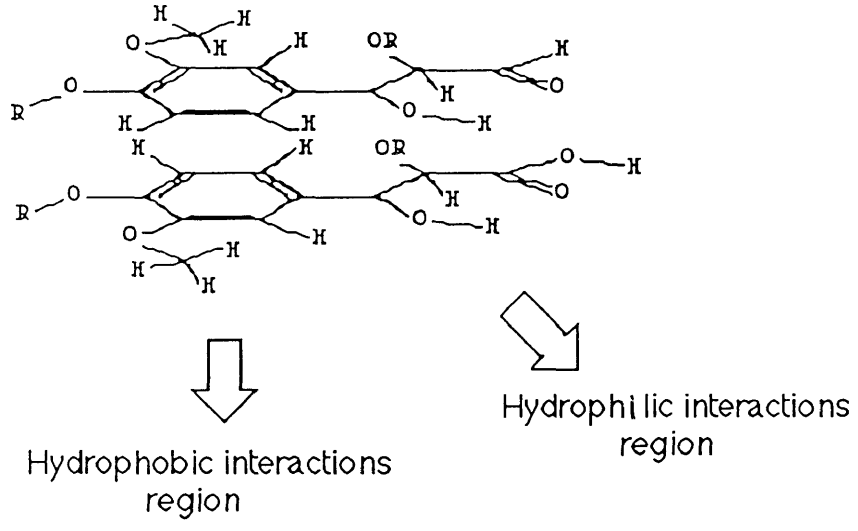

Figure 6.7. Schematic representation of possible interactions between two lignin molecular fragments in a lignin aggregate.

6.4. Influence of Lignin on Proton N.M.R. Relaxation Times of the Solvent

The effect of the presence of lignin aggregates on the solvent molecules was studied by measuring the spin-lattice proton N.M.R. relaxation times (T_1) of the solvent resonances. This parameter is sensitive to molecular motions, and its variation can be diagnostic of increased or restricted molecular mobility.
Table 6.4. shows the T_1 variations of the solvent resonances, dioxane-water (5:1), without and with the addition of lignin, and at different temperatures with lignin.

Table 6.4. T_1 relaxation times of dioxane-water 5:1 with and without lignin and at different temperatures. Data are reported in seconds, and the standard deviations are indicated in the brackets.

Chemical Shift ppm	T_1 / sec			
	200 MHz 25° C		300 MHz with lignin	
	without lignin	with lignin	25° C	70° C
4.02 (at 25°C) 3.51 (at 70°C) Water	6.57 (0.011)	1.75 (0.023)	2.10 (0.017)	3.23 (0.032)
3.58 Dioxane	4.94 (0.018)	3.32 (0.020)	5.29 (0.007)	> 10

From these data it can be observed as the addition of lignin in the solvent system causes a dramatic decrease in the water relaxation time (73%), while a considerably smaller effect is observed on the dioxane T_1 values (33%). Furthermore, increasing the temperature causes a marked increase in the dioxane relaxation times (>100% variation), but just a limited effect is observed on the water peak (35% variation); the water resonance also shifts to higher fields, from 4.02 to 3.51 ppm.
These data suggest a restriction in water mobility due to the presence of lignin; this may be indicative of the presence of hydrogen bonds between the water molecules and the polar side-chain groups of the polymer. This may be interpreted with a "trapping" of the water molecules in the lignin aggregates.

6.5. Effect of pH on Lignin Molecular Weight: HPLC Gel-filtration and Scanning Electron Microscopy Experiments

The experiments reported in this paragraph are concerned with the study of the influence of pH on the lignin aggregation process. While the HPLC gel-filtration molecular weight determinations were carried out on lignin sample that were re-suspended in N.N'-dimethylformamide (DMF) after pH treatment, the scanning electron microscopy experiments were carried out on freeze dried specimens obtained from a drop of lignin suspension at a certain pH, as described in paragraph 3.3.5. In both situations the final observations are believed to reflect the modifications induced on the molecules while in solution, during the pH variation.
The HPLC gel-filtration MW determinations were carried out according to the procedure described in paragraph 3.3.4., on organosolv spruce lignin samples that were exposed to different pHs ranging from 10 to 2, freeze dried and re-solubilized in N,N'-dimethylformamide (DMF). The resulting elution profile of the samples is shown in figure 6.8., and the molecular weight (MW) analysis is reported in the graph of figure 6.9.

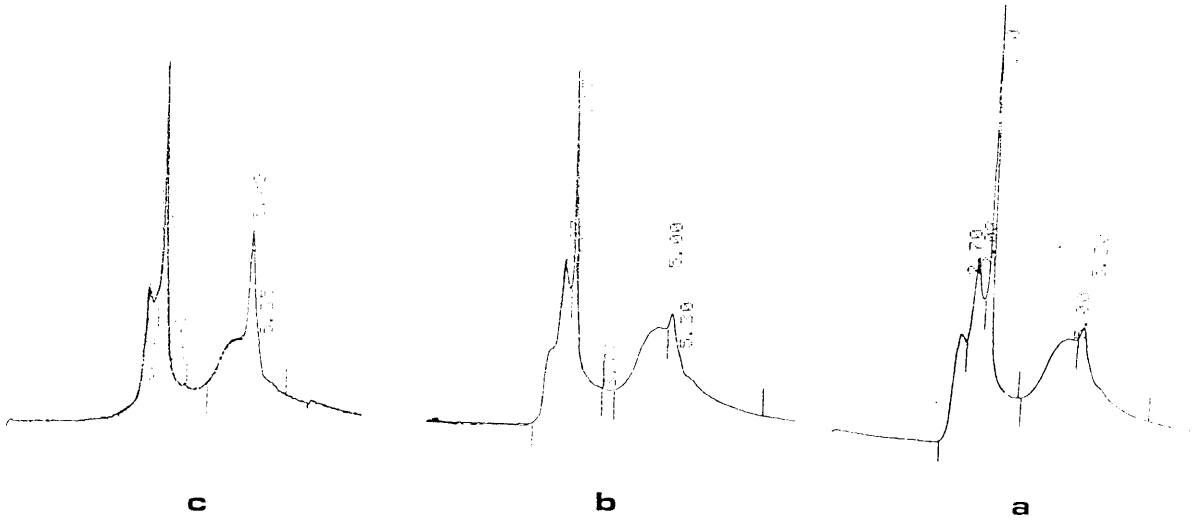

Figure 6.8. HPLC gel-filtration elution profiles of organosolv spruce lignin in DMF. Sample were freeze dried from aqueous solution at pH 2 (profile a), pH 8 (profile b) and pH 12 (profile c). [Zorbax PSM 60S column, flow 1 ml/min, as described in 3.3.1.].

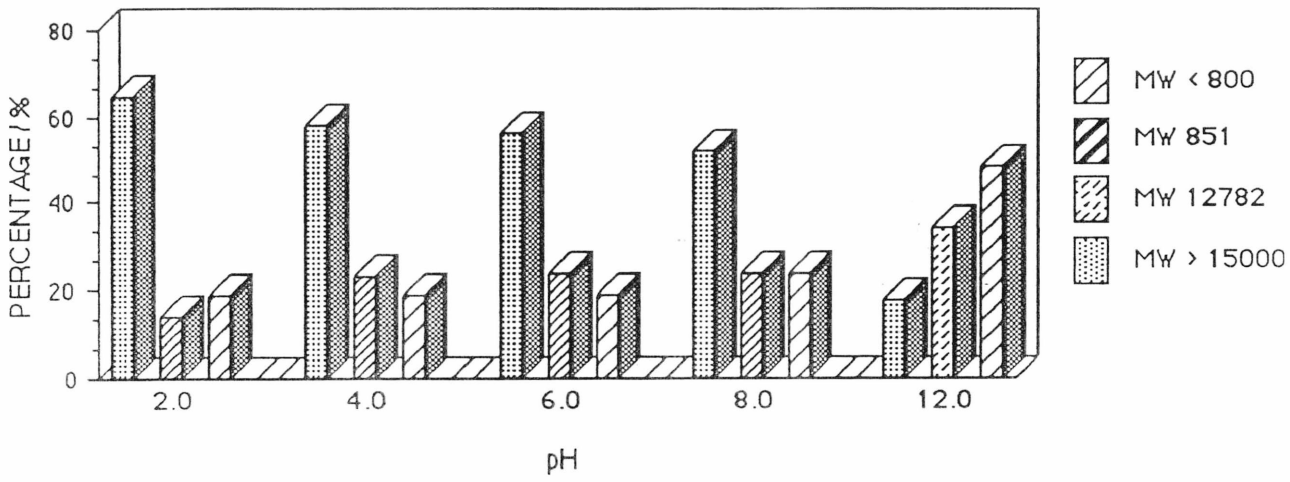

Figure 6.9. Results from molecular weight analysis of organosolv lignin exposed at different pHs (values are indicated in the graph).

The molecular weight analysis shows a significant decrease in the low MW components from 48% at pH 12 to 19% at pH 2, accompanied by an increase in high MW components from 18% at pH 12 to 65% at pH 2.
Interestingly from the chromatograms of figure 6.8. it can be noted that the variations on the peak features, induced by the sample pre-treatment at various pHs, are not continuous but discrete: the decrease in the area of certain peaks is not due by a general broadening caused by more polydispersity, but an increase in the area of defined peaks is observed.
These data suggest that a pH dependent aggregation process occurs; moieties at low molecular weight seem to assemble into high molecular weight aggregates. The pH dependence of the MW variations may indicate that polar interactions between lignin ionizable groups, such as carboxylic, phenolic and hydroxyl are involved, and although DMF can well solubilize these aggregates, it has no influence on these interactions, maybe due to the lack of ionizable groups in DMF molecules.

The same lignin samples were freeze dried after pH exposure on a microscope slide, and observed at the Scanning Electron Microscope (SEM), according to the procedure illustrate in paragraph 3.6.4.
The effect of pH on lignin is shown in figure 6.10. at two levels of magnification for each sample.

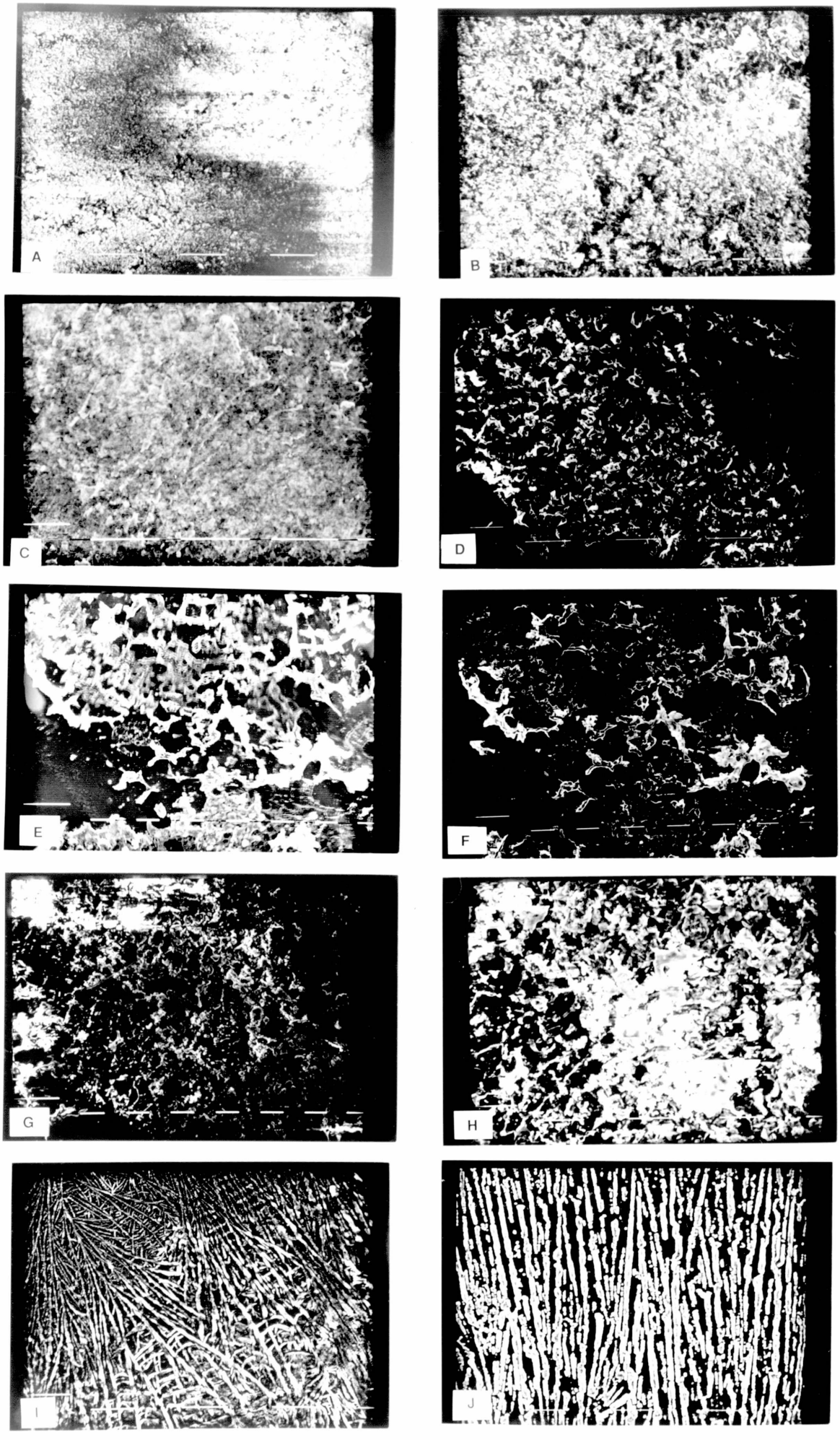
A
B
C
D
E
F
G
H
I
J

Figure 6.10. SEM micrographs of organosolv spruce lignin exposed to various pHs: A, B at pH 12 (X640 and X2560); C, D at pH 8 (X640); E, F at pH 6 (X320); G, F at pH 4 (X320 and X640); I,J at pH 2 (X640).

The SEM micrographs of figure 6.10. show that the pH in effect has an influence on the arrangement and shape of lignin. The pictures show a gradual transition from a very fine layer of grain particles at pH 12, to a sponge-like arrangement at intermediate pHs, and a more fibrous organization at low pH. The SEM observations have a parallel in the literature, where humic and fulvic acids have also been reported to behave in similar manner under the same conditions (Chen and Schnitzer, 1976). These molecules have a polyaromatic structure, that very closely resemble the chemical composition of lignin.

This suggests an aggregation between lignin units that becomes evident when the pH is lowered to the acidic region, as lignin pass from a soluble to a colloidal aggregate form.

According to the classical description of molecule aggregates, there are two principal forces involved in such process: the electrostatic and the van der Waals forces (Prost and Rondelez, 1991). The van der Waals interaction is always present, and it is due to the difference in polarizability between the molecules and the solvent. When the molecules bear ionizable groups, there is also an electrostatic repulsion, which is screened by the counter-ions present in solution. As lignin contains such groups, the combination of these forces may be sufficient to describe its colloidal behaviour and tendency to aggregate. It may be inferred that at high pH the lignin particles contain carboxyl, phenolic and hydroxyl groups dissociated and therefore are negatively charged. Under these circumstances, the electrostatic repulsion between molecules is large enough to stabilize the solution against aggregation. As the pH is lowered, the electrostatic repulsion becomes weaker, the van der Waals and the hydrogen bond interaction become dominant, and a progressive aggregation is possible.

This phenomenon may not be due to the simple precipitation rate of lignin in function of pH, as the shape and feature of the polymer changes significantly, and the MW determination by HPLC gel-filtration has shown as this situation persists when lignin is completely re-solubilized in organic solvents. Moreover, MW variations have found to be discrete rather than continuous MW variations. Although the aggregation process is reversible in water, organic solvents lacking ionizable groups such as DMF have no effect, probably due to an inability in changing electrostatic interactions between lignin aggregates.

The main conclusion to be drawn from the results obtained from different techniques reported in this chapter, is that indeed the lignin sample studied form aggregates under the conditions analyzed.

This phenomenon may be relevant as it can affect the molecular weight characterization and may also play an important role in biodegradation studies carried out *in vitro* with purified enzymes. The physical state of lignin in solution could have a substantial influence on its accessibility to the enzymatic attack. This may offer an explanation to the early lack of success reported on degradation studies carried out *in vitro* with purified ligninase (Haemmerli et al., 1986b), whilst recent studies by Kurek and coworkers (1990b) and Hammel and Moen (1991) have found lignin degradation by carrying the experiments in solutions containing 10-20% of organic solvent (DMF).

Chapter 7

WIDE-LINE SOLID STATE N.M.R. OF SOUND AND DECAYED WOOD

This part of the research focussed on the solid state proton N.M.R. of wood. The objective was to interpret proton spectra and related relaxation times of wood as a potential non-destructive method to test its extent of degradation after fungal attack.

The major contribution to the proton N.M.R. of biological systems comes from water and it is known that the physical properties of water in biological systems are significantly altered from the pure liquid state due to severe constraints in mobility, especially at macromolecular interfaces (Packer, 1977). Differences in mobility are reflected in N.M.R. relaxation rates and this offers the basis for one application of this technique, namely Magnetic Resonance Imaging (M.R.I.), where the differences in relaxation rates provide the contrast between structures, producing magnetic resonance pictures. An example of a useful application of these studies is to water bound to cellular components, in the detection of malignant tumours: N.M.R. T_1 and T_2 relaxation times of water protons in malignant neoplasms are longer than those in benign neoplasm and normal tissues (McBrierty and Douglass, 1981).

Wood normally contains water as an integral part; this can reach levels such that it dominates the proton N.M.R. signal. The role of water in wood is of commercial importance for timber technology: several characteristics of wood such as strength, thermal and electrical conductivity, resistance to deterioration and dimensional changes, are all strongly dependent upon the water content in the cell walls. Also, the affinity of water for wood is of physiological importance for the plants: water covers uniformly the cell wall surface, in a layer where molecules are bound by cohesion forces. These allow water to climb from the roots to the leaves, where it can take part in the photosynthetic reactions with carbon dioxide, to primarily give carbohydrates.

Early N.M.R. studies conducted on water in wood (Hsi et al., 1977; Riggin et al., 1979) and in cellulosic gels (Carles and Scallan, 1973; Froix and Goedde, 1976) reported a multiexponential behaviour of relaxation times. It had been concluded that this behaviour was due to part of the water being intimately associated to the cell wall components, while another was present in the cell lumen and free to diffuse. Some authors measured relaxation times of wood in relation to its anatomical structures (Hailey et al., 1985; Menon et al., 1987) and produced M.R.

images (Menon et al., 1989). However, literature data are often different and contradicting, as experiments were conducted on different types of wood, at different moisture contents and temperatures.
None of these studies were conducted on wood samples subjected to fungal attack. In this chapter the relaxation times of water in softwood and hardwood samples are analysed as function of moisture content and temperature, using both protonated and deuterated water. This provides the background for the study of relaxation rate variations between sound and degraded woods.

7.1. Wide-line Proton N.M.R. of Wood

7.1.1. Moisture Content Determination

The proton N.M.R. spectrum of solid samples of wood consists in a broad peak with a superimposed sharp peak. Drying the sample under vacuum at 80°C for 90 minutes removes the sharp peak, leaving the broad component only. This is shown for a beech sample in figure 7.1.

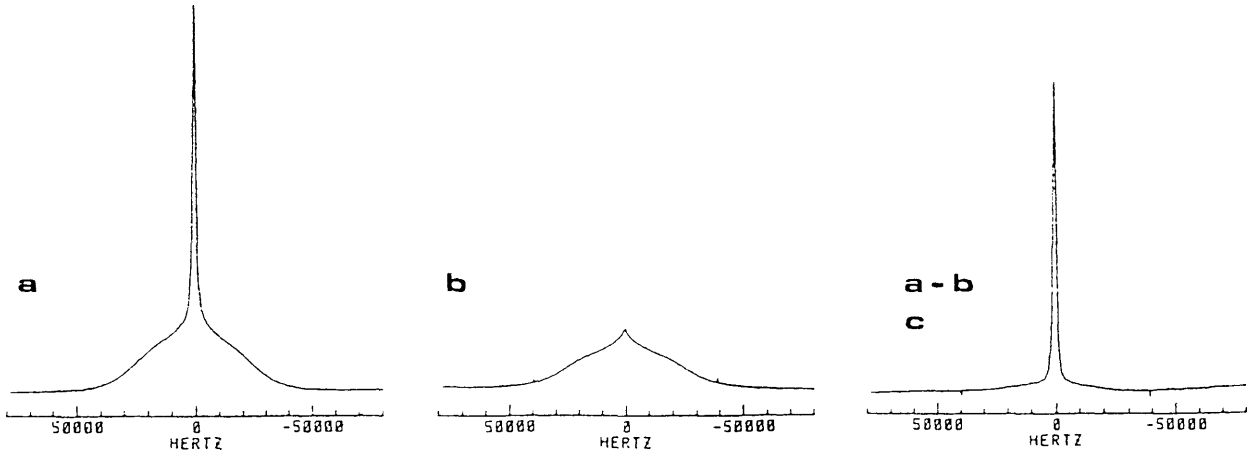

Figure 7.1. Wide-line proton N.M.R. spectra of a beech sample before (a) and after (b) drying under vacuum at 80°C for 90 min. Spectrum (c) was obtained by subtraction of (b) from (a).

The peak width at half height is 43.5 kHz for the broad and 488 Hz for the sharp components respectively. This considerable difference can be explained by a significantly different mobility of the molecules that give rise to the two peaks.

Proton spectra of solid samples consist of broad absorption lines due to the effect of a dominant dipolar interaction, characteristic of species with restricted mobility. Polycrystalline solid materials exhibit the so-called Pake doublet pattern shown in figure 2.8.; however such a pattern is not resolved in the spectra of wood shown in figure 7.1., probably due to a strong dipolar interaction that causes substantial broadening and to the small superimposed peak at the isotropic chemical shift, present even after an extended drying procedure.
The situation is different for the sharp line. The linewidth is very sensitive to the occurrence of molecular motions: these have the effect of averaging the dipolar contributions by random fluctuations in the angular and distance terms which contributes to the dipolar interactions. When the motion is fast, the dipolar effect tends to be averaged to zero, and is possible to observe smaller interactions, such as chemical shifts. This phenomenon is responsible for the narrower linewidth presented by the sharp peak, that tends to occupy its isotropic chemical shift position, set arbitrarily to 0 Hz in the spectra of figure 7.1.

These considerations suggest that the broad peak can be assigned to wood and probably water tightly bound to it, and the sharp peak can be assigned to water. The fact that drying procedure removes the sharp peak, supports the view that this spectral component is due to the water which occupies wood cell lumina.
The linewidth value of this free water (488 Hz) is however larger to that of pure water: this could be due to residual constraints in mobility, magnetic field inhomogeneity and possibly presence of paramagnetic impurities present in the biological sample. The superimposed small peak present even after complete drying procedure, is probably due to more mobile fragments of the cell wall macromolecules, or to tightly bound water which could not be removed.

The two spectral components discussed above, obviously have a correspondence in the free induction decay (F.I.D.) signal: the broad peak is responsible of a fast decaying signal present in the first part of the F.I.D., while the sharp peak is related to a slowly decaying component. When the sample is dry, the slowly decaying component is no longer present (figure 7.2.).
Assuming that the slowly decaying contribution to the F.I.D. is due to the free water present in the sample, a method for evaluation of wood moisture content based on the F.I.D. signal intensities has been developed by Menon et al (1987). This method has been further developed in this research, where the moisture content was calculated by both weight determination and N.M.R. signal intensity measurements, as described in paragraph 3.4.2. of this thesis. The data obtained on the same samples by these two methods are reported in figure 7.3.

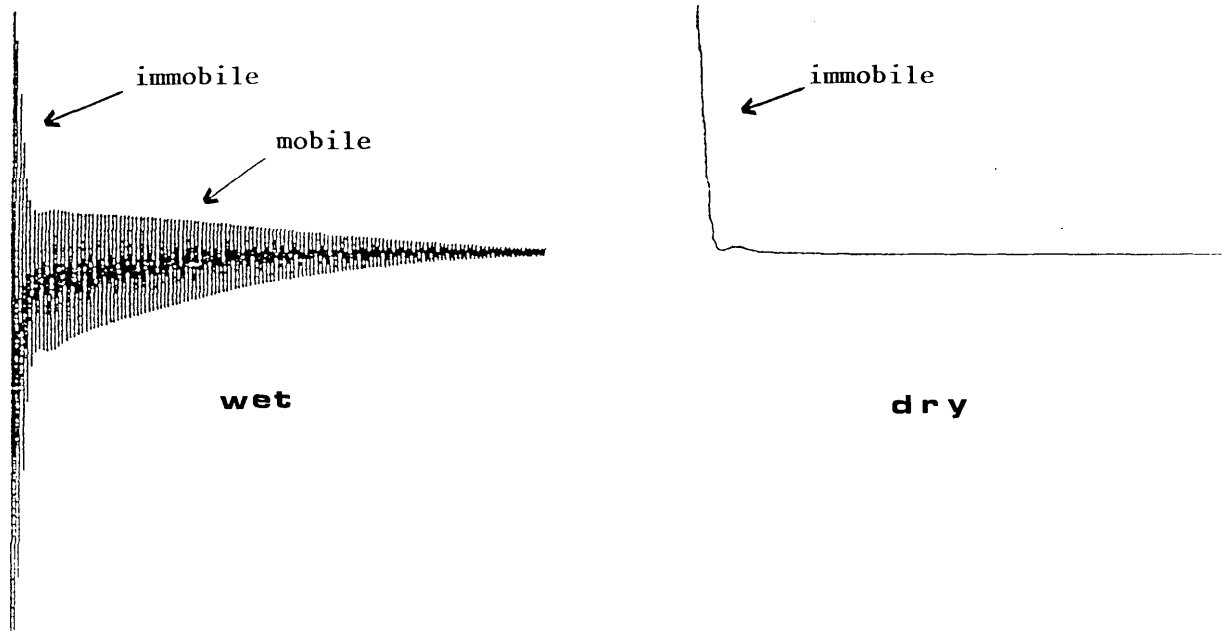

Figure 7.2. Free Induction Decay (F.I.D.) of proton N.M.R. signal of a beech sample. Signals of mobile and immobile proton are indicated.

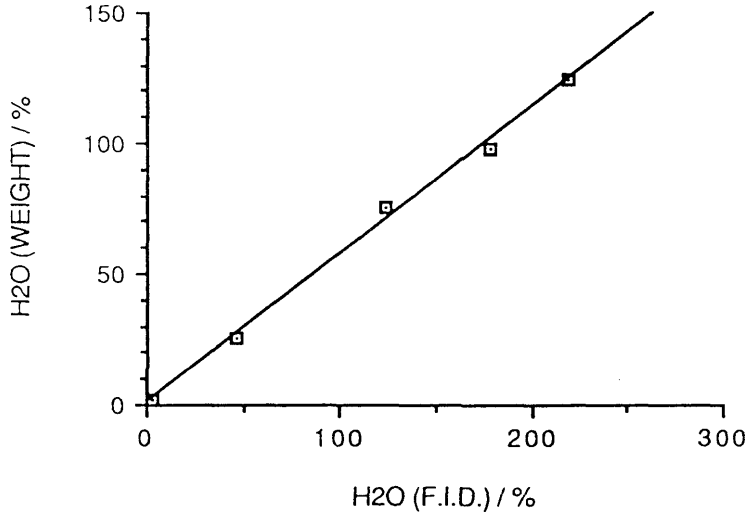

Figure 7.3. Plot of moisture content values determined by oven dry weight method, against water content values determined from F.I.D. intensities. The straight line is the result from linear regression analysis of the data points.

The linear regression analysis obtained by fitting the data of figure 7.3. to a straight line, led to the equation:

$$y = 1.035 + 0.563\,x \qquad R^2 = 0.997$$

where y is the moisture content determined by the oven dry weight method, and x is the moisture content obtained from the F.I.D. signal intensity data. The correlation coefficient confirms a good agreement between the two sets of data.
The presence of the intercept value and the deviation of the slope from 1 are indicative of a systematic error present in the method that leads to a systematic underestimation of the moisture content by the N.M.R. analysis. The values obtained from N.M.R. analysis should be corrected according to the above equation, in order to obtain the value of water content in terms of weight. Thus N.M.R. may provide a simple, fast and non-destructive procedure for measuring water content.

7.1.2. Proton N.M.R. Relaxation Time Measurements

Relaxation times depend on the existance of molecular motions to generate randomly varying magnetic fields: it follows that valuable information about these motions can be extracted from relaxation rate data. In particular, in cases such as wide-line solid state N.M.R. spectra of wood, where no chemical shift information is available, relaxation time analysis become a very important element in the characterization of this material.

7.1.2.1. T_1 measurements

The intensities of F.I.D. signals from an inversion recovery experiment carried out on a beech wood sample, are reported in figure 7.4.
The full line was obtained by fitting the exponential recovery to a single component, as described in paragraph 3.4.3. Although data could also be fitted to two T_1 components, only one of these was found to be reliably reproducible.
Results from this fitting procedure for pine and beech woods are reported in table 7.1.
The fact that only one T_1 value could be found, in a system that from spectral features contains at least two sets of spins with different mobilities, can be explained by the spin diffusion phenomenon. This involves the diffusion of magnetization amongst the spins: the strong proton dipole-dipole coupling maintains communication between all the spins, resulting in all nuclei having a single common relaxation time. Spin diffusion is analogous to thermal conductivity within the spin system, and it has been calculated to occur over a distance of 10 nm (McBrierty and Douglass, 1981). Usually this phenomenon occurs when there are centres for efficient relaxation such as paramagnetic centres, lattice imperfections or mobile molecular end groups; it is difficult to determine which of these causes is

effective in wood samples, but is reasonable to expect a combination of these factors. Wood certainly contains paramagnetic centres, it is also probable that there are lattice imperfections and more mobile end groups in cell wall biopolymer domains.

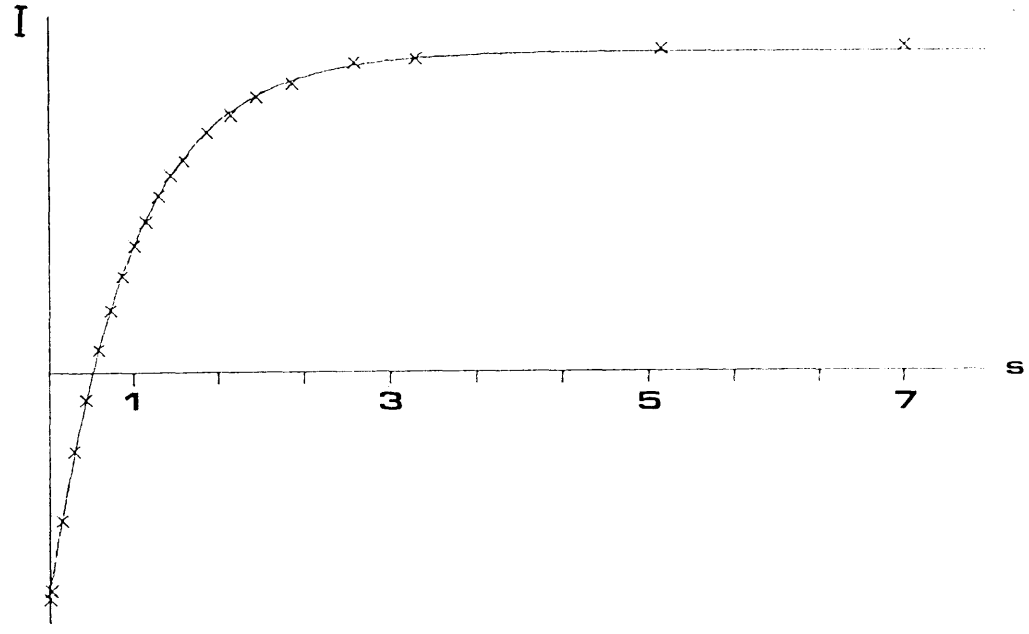

Figure 7.4. Plot of T_1 data from an inversion recovery experiment on a beech sample. The full line was obtained after fitting data to the exponential function described paragraph 3.4.3. The (x) are the experimental data points.

Table 7.1. T_1 values of wood samples. The standard deviation (std) and moisture content percent (m.c.%) are reported.

Sample	m.c. / %	T_1 / ms	std
Scots Pine (*Pinus sylvestris*)	10	98	0.03
Beech (*Fagus sylvatica*)	17	452	0.01

From table 7.1. it can also be noted that the T_1 value obtained for pine is 4.6 times longer than that obtained for beech. This may be due to the intrinsic differences between the two types of wood, both at microscopic and molecular levels.
At the microscopic level, the difference between the two woods lies in the cell lumen dimensions and structures. Conifer wood is formed largely by tracheids with a

diameter less than 50 µm, and the cell lumen is completely enclosed by a cell wall: the diffusion of water must involve passage through pit membrane. Beech wood consists mainly of vessels, fibres as well as some tracheids. Vessels are usually formed by open-ended elements, with cell lumina 10 fold bigger than tracheids, and the water is free to diffuse along the structure without necessarily passing through either a cell wall or a pit membrane.

Given that a considerable contribution to the T_1 value is due to the free water present in the cell walls and this is sensitive to diffusion processes, as speculated by Brownstein (1980), then the restrictions of a smaller volume for molecular diffusion may be reflected in the shorter relaxation times showed by pine samples.

Furthermore, on a molecular scale, pine is a softwood and as such is more homogeneous: for example its lignin is mainly formed by guaiacyl units, containing only one methoxyl group in position 3 of the aromatic rings. Beech, on the other hand is a hardwood, and is more heterogeneous; its lignin for example is formed by a mixture of guaiacyl as well as sinapyl units, presenting an higher methoxyl content. Other differences in molecular arrangements in the cell wall, lead beech wood to contain more mobile molecular moieties that may contribute to lengthen the overall spin-lattice relaxation times, possibly through a spin-rotation mechanism.

7.1.2.2. T_2 measurements

A preliminary estimate of spin-spin relaxation times was made by analysis of spectral linewidth, for both sharp and broad wood components. The results obtained by using this method (described in paragraph 3.4.3.) are reported in table 7.2.

The T_2^* values for the broad and sharp peaks are considerably different for both wood samples; T_2^* values are however only indicative, being strongly affected by magnetic field inhomogeneity that, especially in the case of solid samples, are not negligible.

These problems were resolved by using the solid echo technique, that causes the spins to refocus producing an echo signal unaffected by field inhomogeneity. The analysis of the first part of the echo signal shows a Gaussian function typical for solid materials, reported in figure 7.5. The fitting of this Gaussian function, led to the full line of figure 7.5., and the relative values are reported in table 7.2.

As predictable, the T_2 values obtained with the echo technique are longer than those obtained from linewidth analysis, and can be attributed to the bulk wood polymers.

Table 7.2. T_2 relaxation times calculated by analysis of the peak linewidths (T_2^*), and by Gaussian fitting on F.I.D. echo intensities (T_2). The standard deviation (std) is also reported.

Sample	T_2^* / ms Broad Peak Gaussian Lineshape	T_2^* / ms Sharp Peak Lorentzian Lineshape	T_2 / ms Gaussian Lineshape (std)
Scots Pine (*Pinus sylvestris*)	0.011	0.489	0.017 (1.60)
Beech (*Fagus sylvatica*)	0.012	0.652	0.018 (1.08)

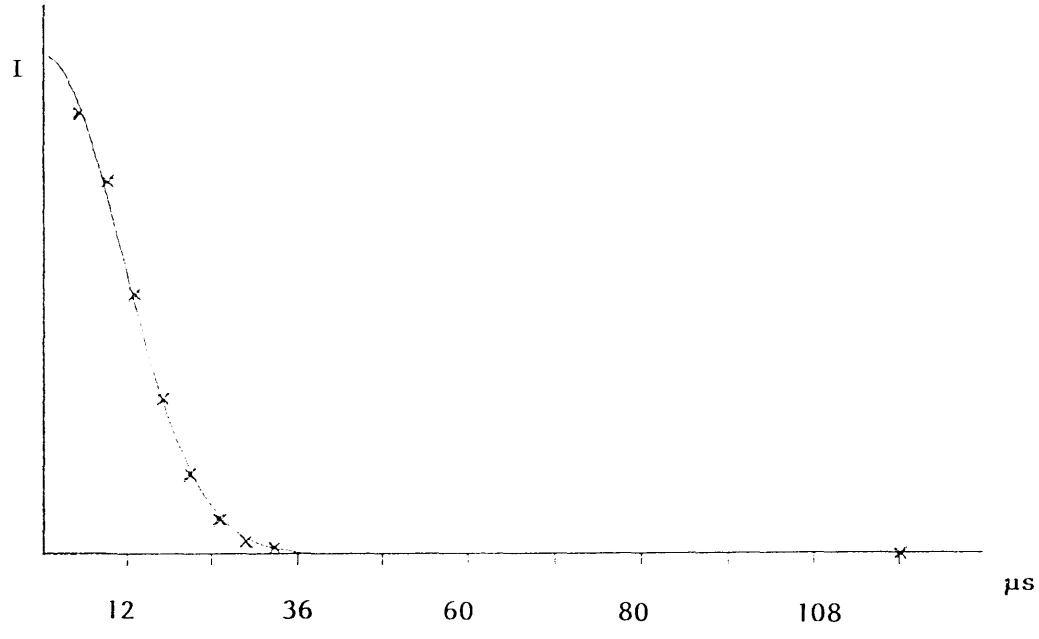

Figure 7.5. T_2 plot of beech sample obtained sampling the first part of the F.I.D. from a spin-echo experiment. The full line was obtained after fitting the data to a Gaussian function; the (x) are the experimental data points.

More complete and detailed information was gained from CPMG experiments. The data points obtained from these experiments showed a multiexponential decay (figure 7.6.), and were therefore fitted to deconvolute more than one T_2 component, whose results are reported in table 7.3.

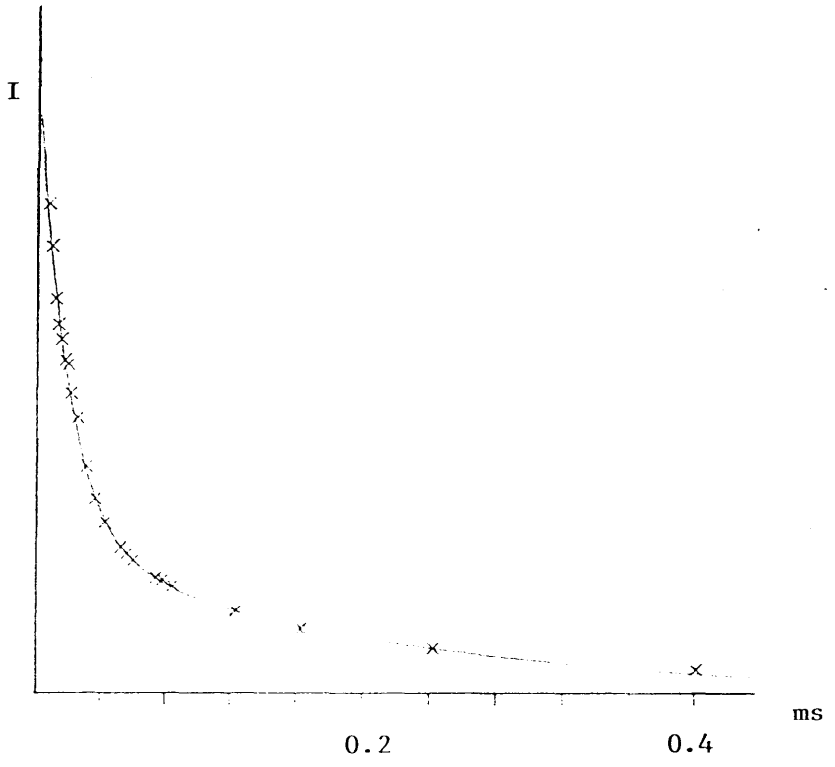

Figure 7.6. Plot of T_2 obtained from a CPMG experiment on a beech sample. The full line represents the fitting of the data to the exponential function as described in paragraph 3.4.3.; (x) are the experimental data points.

Table 7.3. T_2 relaxation time values obtained from CPMG experiments. Slow (T_{2m}), fast (T_{2f}) decaying T_2 components, moisture contents (m.c.) and standard deviations (std) are reported.

Sample	m.c. / %	T_{2m} / ms	T_{2f} / ms	std
Scots Pine (*Pinus sylvestris*)	10	0.204	0.030	0.04
Beech (*Fagus sylvatica*)	17	0.553	0.048	0.07

Fitting was carried out with two and three components, but only two components were found in the range of moisture content of 10-17% presented by the samples analysed: a faster and a slower decaying component, that have been arbitrarily labelled as T_{2f} and T_{2m}. Literature reports suggest a wood fibre saturation point of 38% (Hsi et al., 1977). As the samples in this analysis present a moisture content below this value, it is then reasonable to expect the absence of free water, and this suggests that the components contributing to the relaxation times are wood and absorbed water. Therefore T_{2f} can be attributed to immobile components, such as

wood and molecules tightly bound to it, whilst T_{2m} is likely to belong to water that covers the cell wall surfaces. The differences between T_2 and T_1 values is usual for solid state samples.
These values are longer than those estimated from the linewidth because the magnetic field inhomogeneities are eliminated with the CPMG technique.
T_2 and T_1 show a similar pattern to published data, albeit a direct comparison is not straightforward as experiments were conducted on different woods and at different magnetic field strengths.
The identification of two components shows that spin diffusion is not effective on T_2 ; in fact, spin diffusion occurs on the T_1 timescale, which is too long to affect spin-spin relaxation.

7.1.3. Moisture Content Effects on N.M.R. Relaxation Times of Wood

Both spin-lattice and spin-spin relaxation time measurements were found to vary with the wood water content: for example beech samples showed a T_1 of 452 ms with water content of 17%, and 906 ms when the moisture was 124%. For this reason the behaviour of the spin-lattice relaxation time was studied as a function of wood moisture contents, according to the procedure described in paragraph 3.4.4.; the data obtained are shown in figure 7.7.

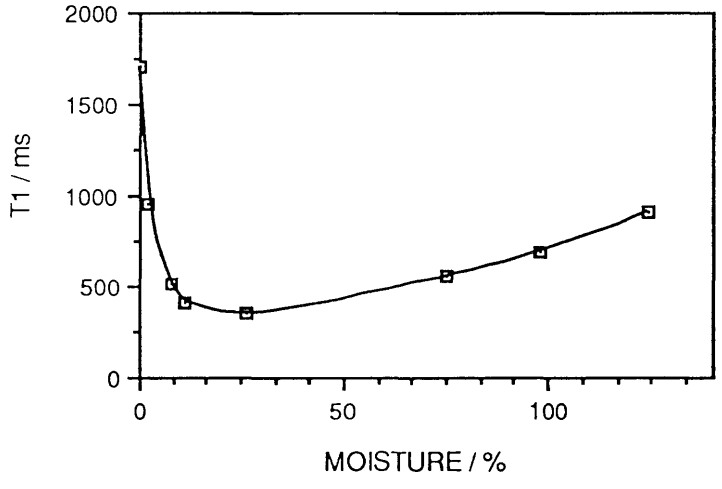

Figure 7.7. T_1 values in function of different moisture contents of a beech sample. The full line was obtained by interpolation between the data points.

The shape of the curve observed in figure 7.7. can be explained by the prevalence of different physical states of the water in the sample. A minimum T_1 value of 350 ms is present at 26% m.c.: this is the region of the fibre saturation point of wood

(Hsi et al., 1977). Above m.c. of 26%, the major contribution to T_1 comes from water which is free in the cell wall lumen, that is behaving as a true liquid, it increases the overall average T_1. Below a moisture content of 26%, the contribution of the solid components prevails: cell wall and its tightly bound hydration water are responsible of the increase of T_1, as spin-lattice relaxation of solids is relatively long.
Deconvolution of T_1 into its components was attempted, but a poor reproducibility of the results was obtained. This is attributed to spin diffusion in the range of moisture contents examined.
Spin-spin relaxation times were also found to vary with the water content in beech samples. The plot of average T_2 values at different moisture contents is shown in figure 7.8.: however spin-spin relaxation times data could reliably be deconvoluted into three contributions: a slow (T_{2s}), a medium (T_{2m}) and a fast (T_{2f}) decaying component (table 7.4.).

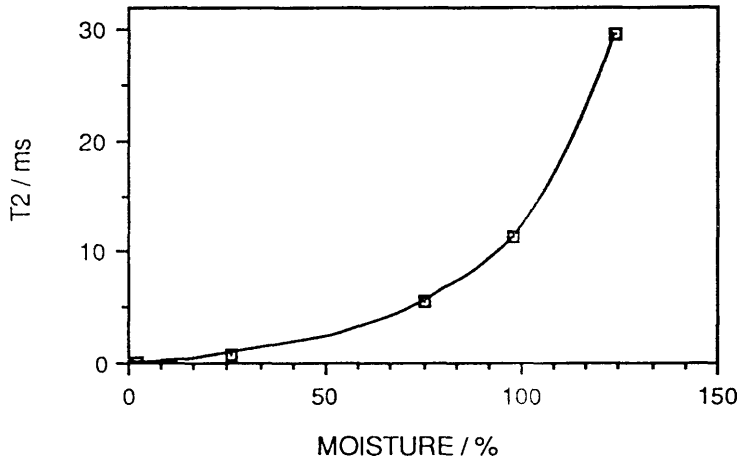

Figure 7.8. T_2 values in function of different moisture contents of a beech sample. The full line was obtained by interpolation between the data points.

Data of table 7.4. show how a progressive decrease in water content leads firstly to the disappearance of the slow component T_{2s} below 75% moisture contents, then of the medium component T_{2m} below 26% m.c., leaving the fast component T_{2s} only, typical of a dried sample. Considering that the wood fibre saturation point is around 38% water, these results may be explained by the progressive removal of water shells from the cell wall. In this view, T_{2s} can be attributed to the free water, that is no longer present at 26% m.c., because this is below the fibre saturation point, and the water is expected to be absorbed on the cell wall. In this range of moisture only the fraction of water (T_{2m}) which is probably the water in closer contact with the cell wall remains. This water is reversibly bound to cell wall structures, as it can be removed by drying. When this also is removed below m.c. 2%, only the fast decaying component remains (T_{2f}), which can be attributed to the cell wall and its structural water.

Table 7.4. T_2 relaxation times from a beech sample at different moisture contents (m.c.); T_{2s} = slow decaying component; T_{2m} = medium decaying component; T_{2f} = fast decaying component; std = standard deviation.

m.c. / %	T_{2s} / ms	T_{2m} / ms	T_{2f} / ms	std
124	51.628	1.705	0.026	0.01
98	19.652	1.719	0.038	0.01
75	19.929	1.653	0.035	0.03
26	----	1.875	0.045	0.03
2	----	0.525	0.045	0.03
0	----	----	0.033	0.04

A decrease in the T_{2s} values occurs as the water content diminishes. This seems to be significant for T_{2s} values, showing variations in the range of 34-62%. Variations in T_{2m} and T_{2f} are not significant, being around 10%, which is the range of error of the method.

The decrease in T_{2s} indicates that a model comprising only free and bound water is too simplistic. A more accurate description would involve an ordered structure close to the cell wall surface with increasingly mobile components in successive layers, as depicted in figure 7.9.

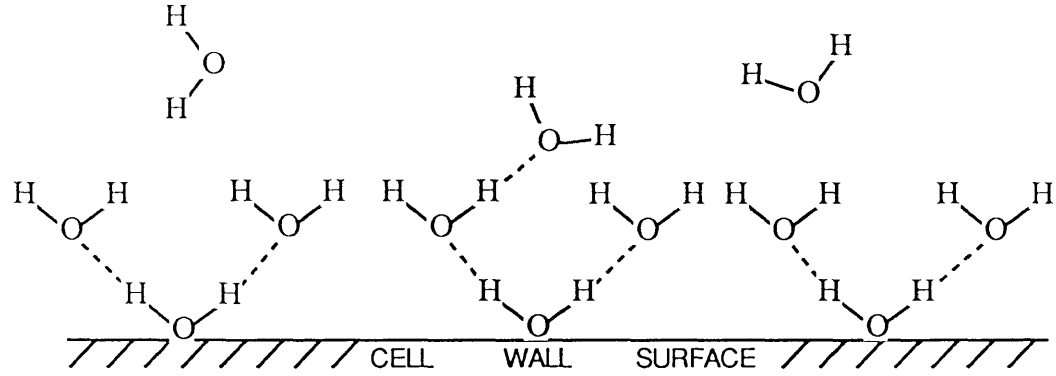

Figure 7.9. Multilayer model of water in wood.

The water in the first few layers could be "ice-like" whilst those in the further layers would be "water-like". As the moisture content decreases, the "water-like" molecules are lost first.

The moisture content was found not only to affect the T_2 values, but also the relative intensities of the T_2 components (figure 7.10.).

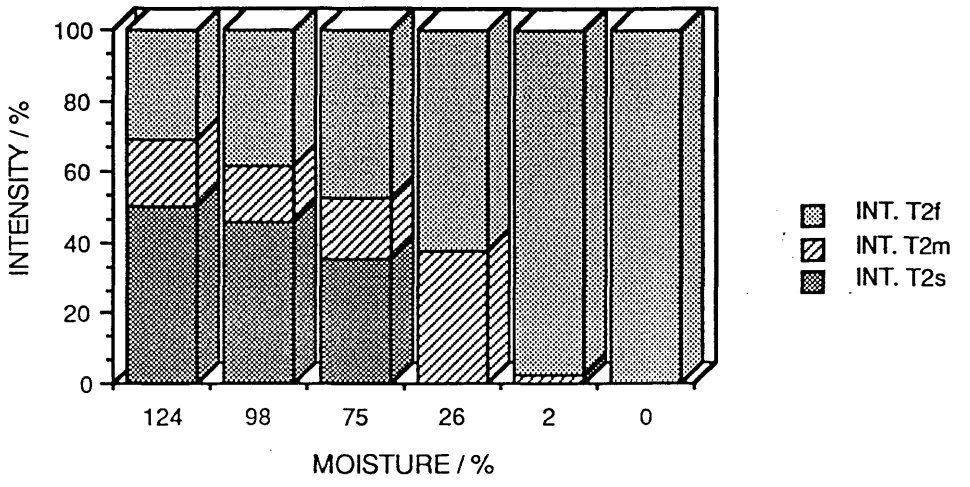

Figure 7.10. Intensities of T_2 components in function of different moisture contents. Data were normalised to 100% within each set of T_2.

Data reported in figure 7.10. may be explained by the progressive removal of water layers from the cell wall, leaving in the end the cell wall components only (100% intensity). Assuming a model where the water content is above the fibre saturation point of 38%, the additional water adds to the slowly relaxing population, it may be possible to calculate the fraction of the total protons which relax slowly (P_{slow}) from the equation:

$$P_{slow} = \frac{w - 0.38}{w}$$

where w is the total water content expressed in grams of water per gram of dry wood, and 0.38 is the fibre saturation point.

Figure 7.11. reports the plot of data calculated by using the above equation in comparison with experimental intensity data: a good agreement between experimental and theoretical data is shown.

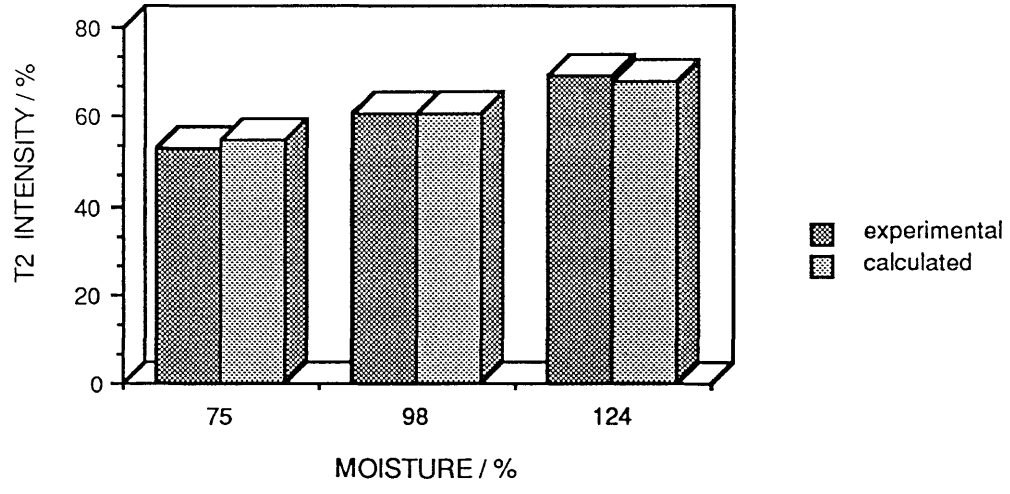

Figure 7.11. Theoretical and experimental T_2 intensities of free water components at different moisture contents.

As the intensity of the medium component is part of the P_{slow} value, the T_{2m} component can be considered as belonging to water loosely bound to the cell wall, that is the interface layer between tightly bound water (T_{2f}) and the free water (T_{2s}). This supports the model of a shell distribution of water around the cell wall, involving a tightly bound layer, a "liquid-like" layer and an "ice-like" layer between them.

7.2. Wide-line Deuterium N.M.R. of Deuterated Water in Wood: Temperature and Moisture Effects on the Linewidth

Deuterium N.M.R. spectra were obtained on beech wood samples soaked in deuterated water, as described in paragraph 3.4.6. Deuterium and proton spectra were collected in parallel, at regular intervals during the drying procedure, with the advantage that deuterium is selective for water components only, and a direct comparison with the proton spectra of the whole spin populations, may facilitate the assignment of proton signals. Figure 7.12. shows the results.

Deuterium spectra of water in wood consist of a broad doublet, with a sharper singlet superimposed. This nucleus has a spin of 1, and therefore possesses a quadrupolar moment, which means that in the presence of a non-symmetrical electric field quadrupolar relaxation dominates.

The broad doublet of figure 7.12. is consistent with a nuclear population experiencing this kind of interaction; this is characteristic for a species with restricted mobility, such as water present as hydration layer on the cell wall. When rapid molecular motion is present, the quadrupolar shift tends to be averaged to zero, and a single peak in the isotropic chemical shift position is observed. This is the case of the sharper peak present in the wood spectrum, which can therefore be attributed to free water.

As drying progresses, the first peak that is removed is the singlet assigned to the free water, which after 70 minutes of drying at 80°C leaves the doublet only. When the sample is completely dry, no residual deuterium signal is observed, suggesting a very slow exchange of deuterium with protons of the cell wall polymers, in accordance with literature data (Carles and Scallan, 1973).

Another interesting observation is the linewidth variation of both deuterium peaks: during water removal, both sharp and broad resonances become broader, as shown in figure 7.13.

This behaviour may be explained using the water layer model proposed in the previous paragraph: the drying procedure removes layers of water with higher levels of freedom, whose contribution to the averaged linewidth is reduced, leading to an increase of the overall linewidth. A sudden increase in the linewidth of the

broad component is observed after 60 minutes: this may be explained by a complete removal of more mobile components, leaving the rapidly relaxing populations only. In fact after 60 minutes all the free water has been removed, as shown by the sharp linewidth variations of figure 7.13b.
This is also reflected in the variation in quadrupole constant C, that can be calculated from the formula:

$$C = 4/3\ \Delta\nu_{1/2}$$

This is found to increase during drying, as shown in table 7.5., indicating a selection of new spin populations revealed at each drying step, with a sudden increase at 60 minutes.

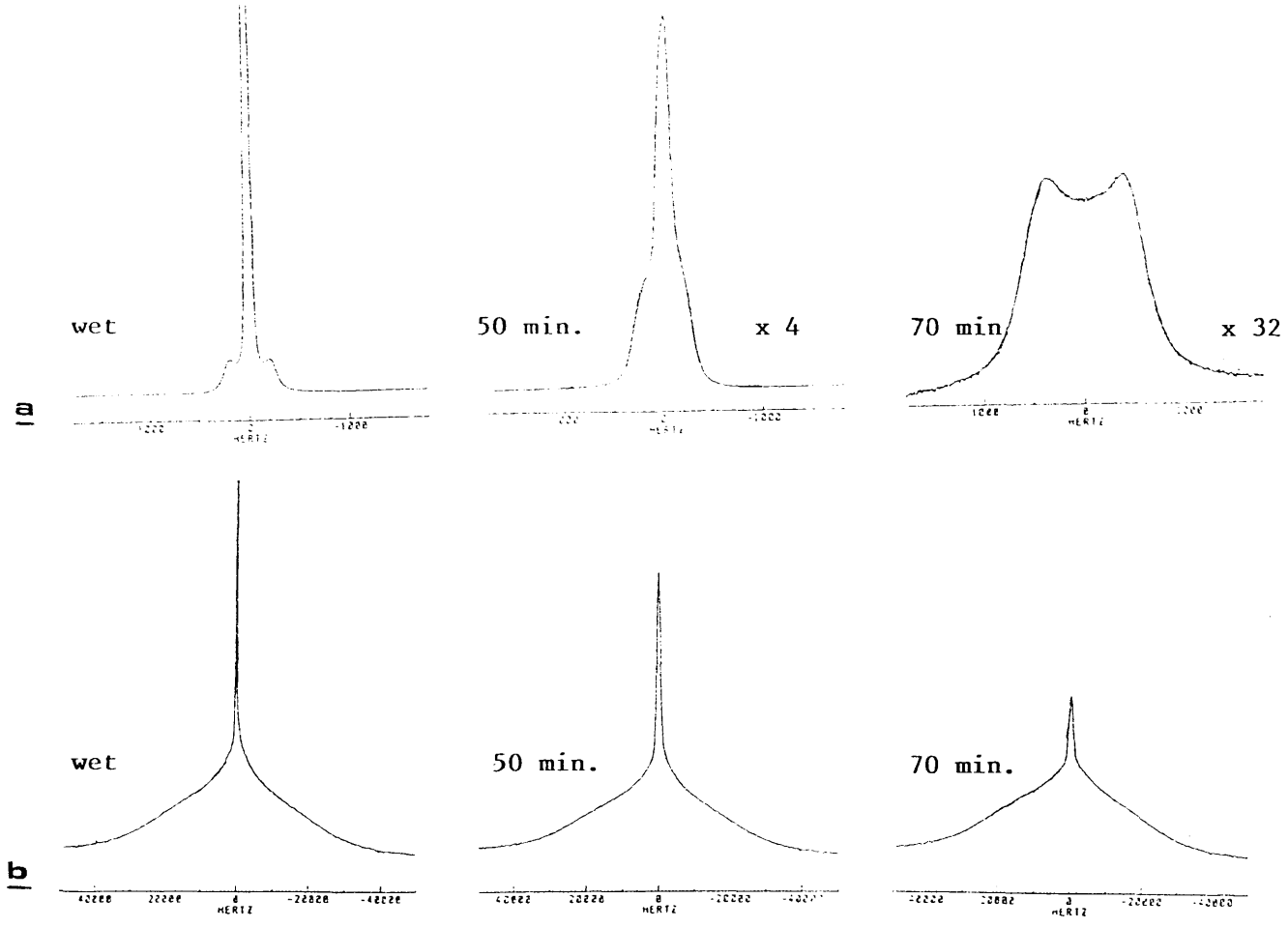

Figure 7.12. Wide-line deuterium (a) and proton (b) N.M.R. spectra of a beech sample, acquired in parallel during drying under vacuum at 70°C at the indicated times.

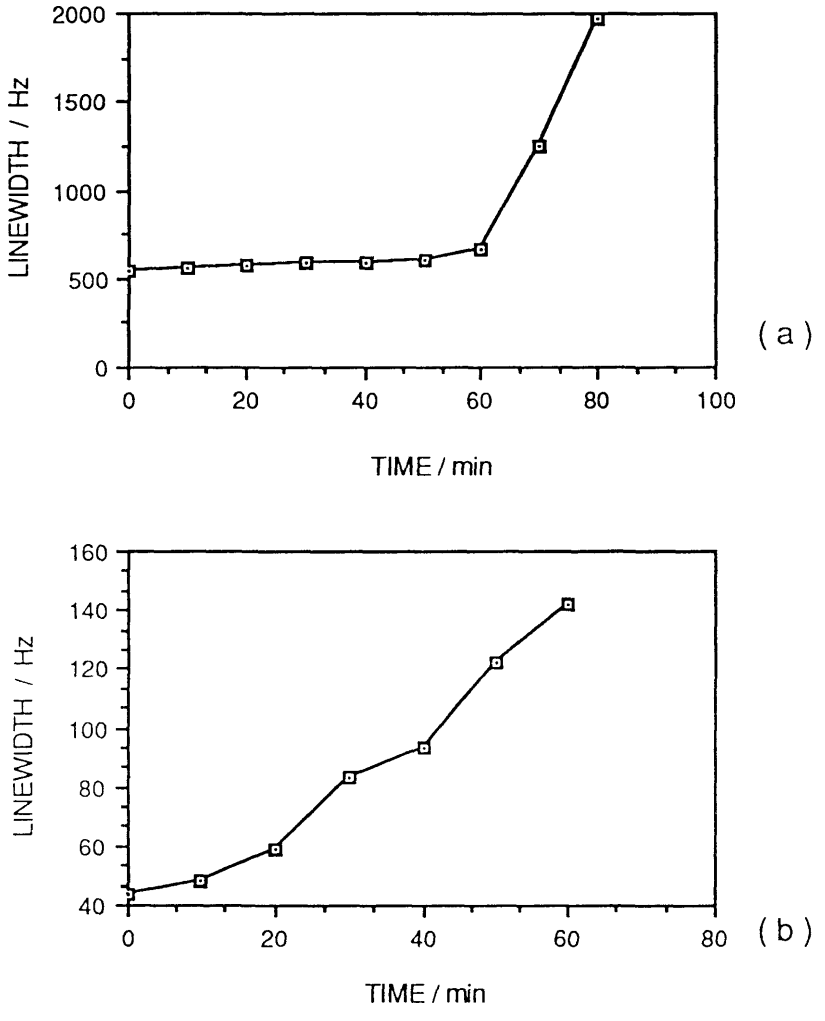

Figure 7.13. Linewidth at half height variations of broad (a) and sharp (b) deuterium peaks during drying time intervals.

Table 7.5. Variation of quadrupole constant C of deuterium at different deuterated water contents in a beech sample during drying time intervals.

Time / min	Quadrupole constant / Hz
0	460
10	488
30	508
70	1021

Another experiment on wet wood samples was carried out by varying the temperature, according to the procedure described in paragraph 3.4.5. The linewidths of the two peaks were measured and the results are shown in figure 7.14.

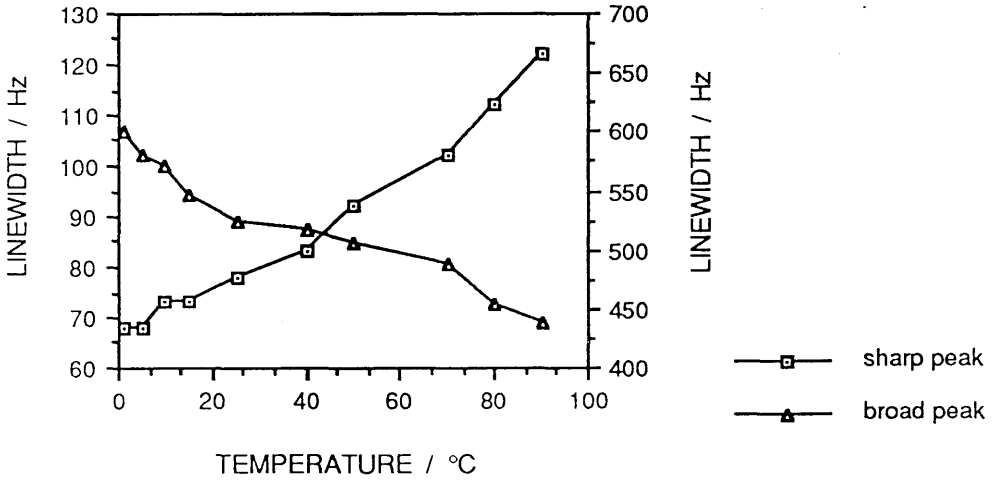

Figure 7.14. Linewidth at half height variations of sharp and broad peaks of deuterium as function of temperature.

An increase in temperature led to a broadening of the sharp component, and correspondingly a sharpening of the broad doublet. This can be explained by an exchange process occurring between the two kind of water, whose linewidths tend to an average value as the temperature increases the rate of exchange. The coalescence point, at which the two peaks would merge into one, is not reached in the range of temperature studied.

These data support the model suggested on the basis of the proton relaxation time results and illustrated in figure 7.9. This consists on a multilayer arrangement of water molecules around the cell wall biopolymers. Water molecules exhibit different degree of mobility depending on the layer that they occupy, and the associated degrees of mobility is reflected in the relaxation time values. The removal of molecules by drying or the enhancement in the exchange of molecules between different layers caused by an increase in temperature are reflected by variations of relaxation times, and consequently in the resonances' linewidths.

The understanding of the behaviour relaxation times in wood provides a sound background for performing similar experiments in biodegraded samples of wood, where a correlation between extent of biodegradation and variation in relaxation times may be found.

7.3. Proton Relaxation Times Measurements on Decayed Wood

The objective of these studies was to study the correlation of the extent of wood degradation after fungal attack, with a variation in the N.M.R. relaxation times. The assumption in this approach was that the degradation process on wood would be reflected by an increase in its relaxation times, due to an increased mobility of the water associated with the cell wall, and possibly also of parts of cell wall macromolecules. Relaxation times are in fact known to carry information about molecular dynamics, covering different ranges of motional frequencies depending on the parameters analysed (T_1 or T_2).

In this view, and on the basis of data illustrated through the previous paragraphs, samples of decayed woods at a constant moisture content (7-8%) and temperature (25°C) were subjected to inversion-recovery and CPMG experiments, to measure both T_1 and T_2 relaxation times.

However, due to variation inherent with both the biological processes and the N.M.R. method of measurement, a statistical analysis of the data was also necessary. The significance of the variations were determined with the T-test.

The experiments and the data analysis were performed as described in paragraph 3.4.7., and the results of these investigations are reported in table 7.6.

Table 7.6. Relaxation time values of wood samples before and after fungal decay. (x) is the mean of 4 measurements ; (s) is the standard deviation and (t) is the result of the T-test. Data were analysed in a confidence interval of 99% with a critical value t to 5.84 (3 degrees of freedom). The values underlined are those for which the null hypothesis is rejected (i.e. the variation is significant).

Sample		T_1 / ms m.c. 7-8%	T_1 / ms dried	T_{2s} / ms m.c. 7-8%	T_{2f} / ms m.c. 7-8%	T_{2f} / ms dried
Scots Pine (*Pinus sylvestris*)						
Control	x	87	563	0.150	0.012	0.027
	s	7.28	6.96	0.15	0.01	0.01
Brown-rot decay	x	<u>130</u>	<u>712</u>	<u>0.248</u>	0.022	0.031
(*Coniophora puteana*)	s	6.71	7.84	0.03	0.01	0.01
	t	8.68	28.42	6.43	3.12	0.51
White-rot decay	x	<u>763</u>	<u>1218</u>	<u>0.312</u>	0.040	<u>0.245</u>
(*Coriolus versicolor*)	s	51.58	32.61	0.01	0.01	0.02
	t	25.95	39.28	17.89	4.78	17.01
Beech (*Fagus sylvatica*)						
Control	x	431	920	0.206	0.026	0.028
	s	15.56	15.00	0.02	0.01	0.01
Brown-rot decay	x	<u>589</u>	<u>1060</u>	<u>0.326</u>	0.032	0.042
(*Coniophora puteana*)	s	30.97	24.64	0.03	0.01	0.01
	t	9.11	9.71	6.54	0.15	2.19
White-rot decay	x	<u>877</u>	<u>1200</u>	<u>0.373</u>	0.037	0.047
(*Coriolus versicolor*)	s	35.35	79.47	0.02	0.02	0.07
	t	23.09	6.92	12.01	1.36	3.33

Table 7.6. shows that an increase in relaxation times of decayed wood is effectively observed when compared with the control values.

T_1 relaxation measurements show in all cases an increase. In particular, white-rot decay on Scots pine shows the highest increase (8.8 fold at 7% m.c.), followed by white-rot decay on beech samples (2.0 fold).

Brown-rot decay also is noticeable, yielding a 1.49 fold increase in Scots pine and a 1.4 fold increase in beech.

T_1 values estimated on completely dried samples exhibits the same pattern; the absolute values are however higher than in the moist samples, as explained previously this is due to the removal of "liquid-like" water components and leaving the solid contributions only.

All these increases are statistically significant, showing a 99% limit of confidence.

Figure 7.15. depicts in a histogram the increase in T_1 values.

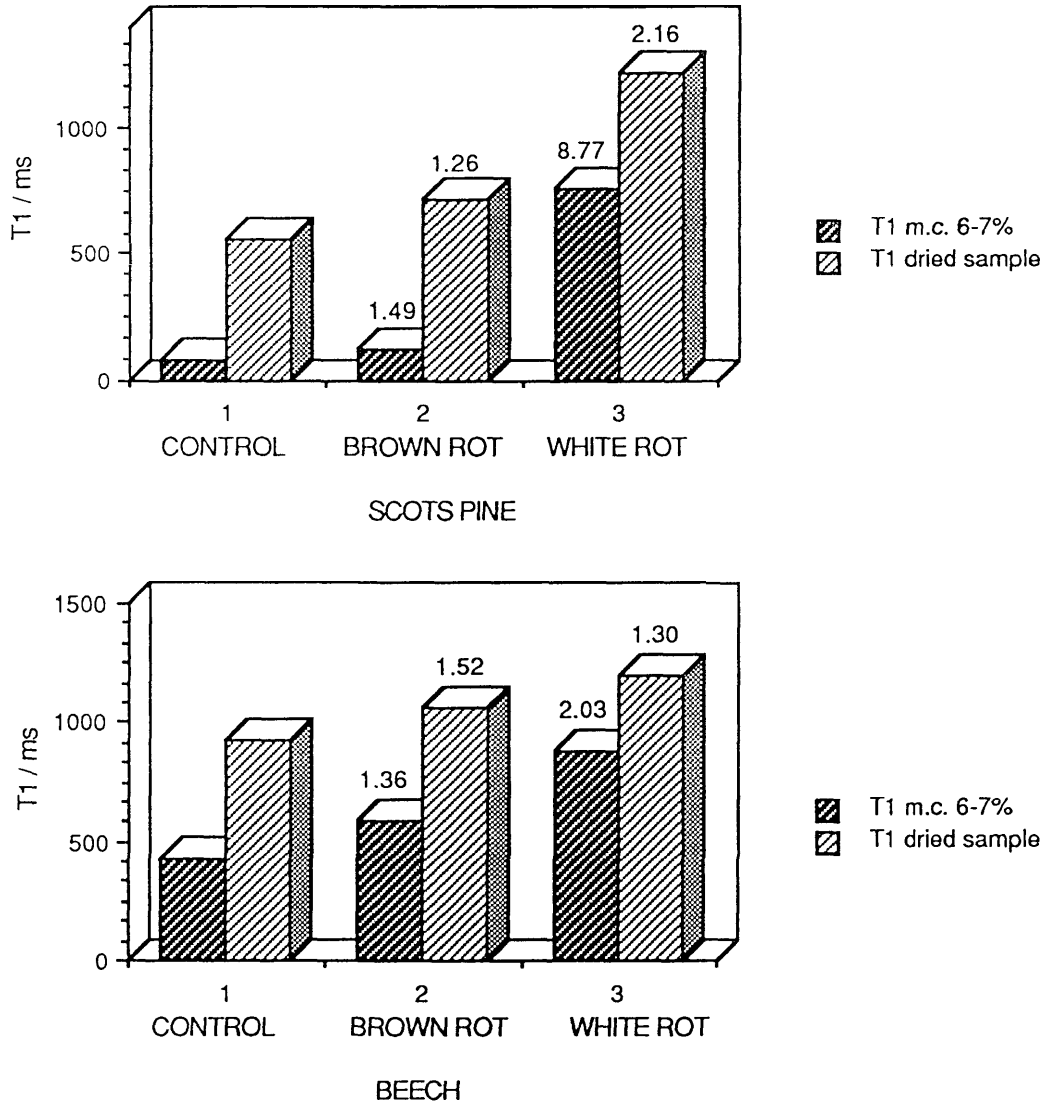

Figure 7.15. T_1 increase as function of biodegradation for Scots pine and beech woods. The number on each column is the increase factor in respect to the controls.

T_2 relaxation time values were deconvoluted into two components for m.c. of 7-8%, and one component only for dry samples.

Measurements conducted on the moist samples, show that the slowly decaying component exhibits the same pattern as the T_1 data. The highest increase in T_{2s} is shown by the Scots pine white-rot decayed samples (increase of 3.3 fold), followed by white-rot decay on beech samples (increase of 1.8 fold), and comparable increases for brown-rot decay on both types of wood (1.7 fold for pine and 1.6 for beech). The fast decaying component T_{2f} in both moist and dry samples also show the maximum increase for white-rot decay of pine (3.3 fold); minor differences appear for the other samples. Statistical tests show that the differences in the slowly relaxing component T_{2s} are significant with a confidence limit of 99%, whereas the fast relaxing components T_{2f} present much higher margin of error, for both moist and dried samples. Although some differences in T_{2f} are in margin of confidence of 90-98%, the reliability of these variations is poor. Figure 7.16. illustrates the increase in T_{2s} for pine and beech samples.

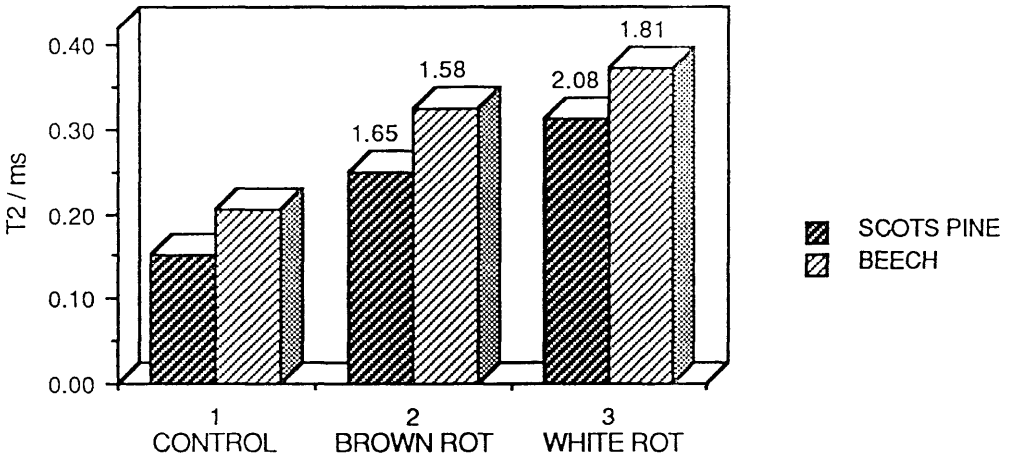

Figure 7.16. T_{2s} component increase as function of decay by fungi on pine and beech moist samples. The number on each column is the increase factor in respect to the controls.

From these observations, it emerges that T_1 and T_{2s} variations are carrying information about the biodegradation which occurred in the cell wall.

Both these relaxation times are associated with the water absorbed on the cell wall; this is therefore providing indirect information on the breakdown of the cell wall macromolecules. This is consistent with observations made on other systems, such as tumour cells, where diagnostic tests are based on the detection of mobility variations of water by magnetic resonance methods. Extending this approach to biodegradation studies, magnetic relaxation measurements of water bound to wood

can provide a non-destructive method for determining the extent of the process; these may also offer the basis for magnetic resonance imaging studies (Foster and Hutchison, 1987).
Furthermore, brown-rot and white-rot fungi have also shown a different degree of degradation towards the two types of wood. As reported in the introduction to this thesis, it is known that these fungi attack the cell wall by different mechanism and to a different extent. White-rot fungi present a complex enzymatic set, and are capable of complete breakdown of all the cell wall components (Crawford, 1981). Brown-rot fungi are known to preferably attack polysaccharides, leaving a polymeric, chemically modified lignin network. The data presented in this chapter reflect these diverse situations; although a detailed analysis of the separate cell wall components was not possible, this study shows that in fact the white-rot fungi have degraded the cell wall assembly to a larger extent than the brown-rot fungi.
Also, white-rot fungi have been more effective on Scots pine, as supported by other analytical techniques carried out on the same wood samples (chapter 8).

The main conclusion to be drawn from the data presented in this chapter, is that wide-line solid state N.M.R. offers a useful analytical tool for studies on biodegradation of wood.
It has been shown that this technique is able to give an estimate of the moisture content of wood samples, in alternative to weight loss measurements during drying procedure. The advantage of the N.M.R. method is that the sample is not modified. Moreover, relaxation time measurements under different moisture and temperature conditions allow the assignment of different relaxing components to "water-like" and "ice-like" layers of water molecules in the cell wall.
Fungal attack on cell wall structures has been found to cause significant variations in the relaxation times (T_1 and T_{2s}) of free water. Both these parameters have been found to increase during fungal attack, reflecting a higher degree of mobility of the water in a destructured environment.
This finding offers a non-destructive test to determine the extent of degradation of wood samples.

Chapter 8

CP/MAS SOLID STATE N.M.R. AND FT/IR SPECTROSCOPY OF WOOD CELL WALL BIODEGRADATION

8.1. CP/MAS Carbon-13 N.M.R. Spectroscopy

Several studies have been reported in literature on the application of carbon-13 cross-polarization / magic angle spinning (CP/MAS) N.M.R. spectroscopy to structural studies of the cell wall and its isolated components.

Great attention has been focussed on the cellulose. It is known that cellulose is present in the cell wall partly in a crystalline and partly in an amorphous form. These two components can be distinguished in CP/MAS spectra of isolated cellulose (Atalla et al., 1980). More detailed studies carried out by VanderHart and Atalla (1984), showed that not only the native (cellulose I) and the alkali treated cellulose (cellulose II) can be detected by the CP/MAS technique, but also two native cellulose I crystalline modifications, cellulose I_α and I_β. Furthermore, cellulose II and cellulose I_β would represent different chain conformations, and have inequivalent successive glucosidic linkages along the chain. In a separate study carried out by Cael and coworkers (1985), it was suggested that CP/MAS spectra of native cellulose are linear combinations of two spectra that correspond to the presence of a two-chain and eight-chain unit cells.

These investigations proved that high resolution solid state N.M.R. can provide valuable information complementary to the electron diffraction and X-ray techniques.

More complex spectral features are observed when whole cell walls are analyzed: these are due to hemicelluloses and lignin that also contribute to the spectra. Kolodziejski and coworkers in 1982 showed by CP/MAS that the carbohydrate and lignin fractions can not be completely separated during extraction procedures: lignin is always removed with cellulose during holocellulose preparation, addressing the question of the existence of a lignin-carbohydrate complex. Gerasimowicz and coworkers in 1984 strengthend this view by showing relaxation profiles that suggest an intimate association between lignin and carbohydrates. Cell wall components were found to exhibit a single T_1 value, indicating that spin diffusion is occurring between lignin and carbohydrate nuclei in close aggregates. More recently, Newman and Hemmingson (1990) found that lignin and hemicelluloses show a common $T_{1\rho H}$ (5.9 ms for hardwoods), leading to the

conclusion that these two components are intimately in contact so that nuclear spin diffusion results in the observation of a single average $T_{1\rho H}$.
CP/MAS technique has also proved to be quantitatively reliable: Himmelsbach and coworkers (1983) determined the ratio of carbohydrate and lignin between grass species from single spectra of whole plant material. Other authors (Haw et al., 1984; Hatfield et al., 1987) also reported methods to gain quantitative information from lignin and other cell wall components. Relatively little research has been focussed on the application of CP/MAS N.M.R. to the topic of cell wall biodegradation. Schaefer and coworkers (1981) reported CP/MAS spectra on the catabolic transformation of isolated lignin in fungal cultures; Hemmingson and coworkers (Hemmingson and Wong, 1989; Hemmingson and Morgan, 1989) reported a CP/MAS N.M.R. study on the photochemical degradation of lignocellulosic materials.

On the basis of this background, the use of high resolution solid state carbon-13 N.M.R. was extended in this research to characterize and study the molecular modifications of cell wall from hardwood (*Fagus sylvatica*) and softwood (*Pinus sylvestris*), after the biodegradation by brown-rot (*Coniophora puteana*) and white-rot (*Coriolus versicolor*) Basidiomycetes. The samples analyzed were the same studied by wide-line N.M.R., whose results are reported in chapter 7.

8.1.1. Optimal Contact Time Determination

The optimal contact time for wood samples was determined in order to obtain the best cross-polarization during the CP/MAS experiments. Figure 8.1. shows the results of an experiment carried out on pine wood, where N.M.R. signal intensities are reported as a function of contact times.
From the fitting procedure, a value of 0.24 ms (std 0.02) and 5.23 ms (std 0.01) were found respectively for T_{CH} and $T_{1\rho H}$. Since these values were calculated from data measured on F.I.D.s intensities, they reflect an average relaxation time estimation for all the different peaks in the CP/MAS spectra.
It is known that different spectral components exhibit slightly different T_{CH} and $T_{1\rho H}$, depending on the amount of hydrogens that are attached to different carbons (see figure 2.14.). An optimal contact time is much longer than T_{CH} and much shorter than $T_{1\rho H}$ for all components, and theoretically corresponds to the maximum of the fitted curve shown in figure 8.1. Although the maximum of this curve proved to be around 0.9 ms, the CP/MAS experiments were carried out using a contact time of 1.5 ms. This was to prevent eventual intensity errors for spectral components with

higher optimal contact times, for example aromatic ring carbon nuclei, preventing intensity errors greater than 10%. This value is in good agreement with literature data, in which quantitative experiments have been carried out with contact times between 1 and 2 ms (Haw et al., 1984; Hatfield et al., 1987).

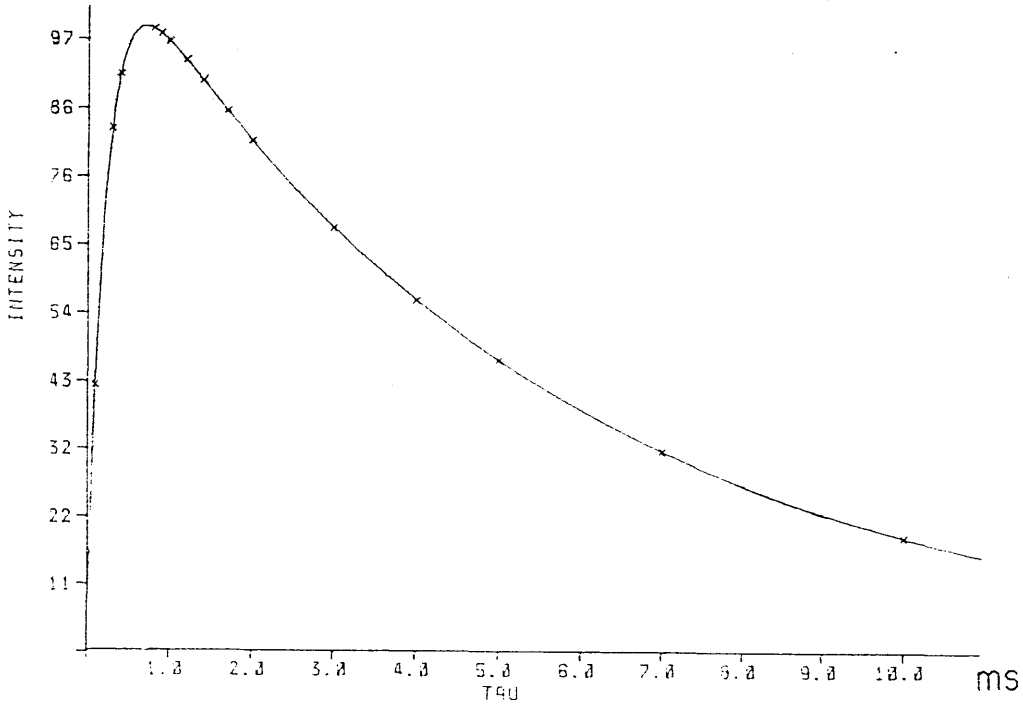

Figure 8.1. Plot of free induction decay (F.I.D.) intensities versus variable contact times. The full curve was obtained fitting the experimental data points (x) to the equation: $I = I_0 / (1 - T_{CH} / T_{1\rho H}) \cdot [\exp(-\tau / T_{1\rho H}) - \exp(-\tau / T_{CH})]$

8.1.2. CP/MAS N.M.R. Spectra of Cellulose, Lignin and Whole Cell Wall

Carbon-13 CP/MAS N.M.R. spectra of isolated cellulose and lignin were obtained to facilitate the interpretation of whole cell wall spectra (figure 8.2.).

Figure 8.2a. shows the spectrum obtained for cellulose: the spectral features are consistent with previous literature data (Atalla et al.; 1980; Earl and VanderHart, 1980). Chemical shift assignments have been carried out according to Atalla and coworkers (1980). The peak at 66 ppm and the shoulder at 63 ppm are assigned to the C-6 carbon, the overlapping peaks at 70-80 ppm are due to C-2, C-3 and C-5 carbons. The sharp signal at 89 ppm and the broad shoulder at 84 ppm are both due to the C-4 carbon; the peaks at 105 ppm are assigned to the C-1 carbon.

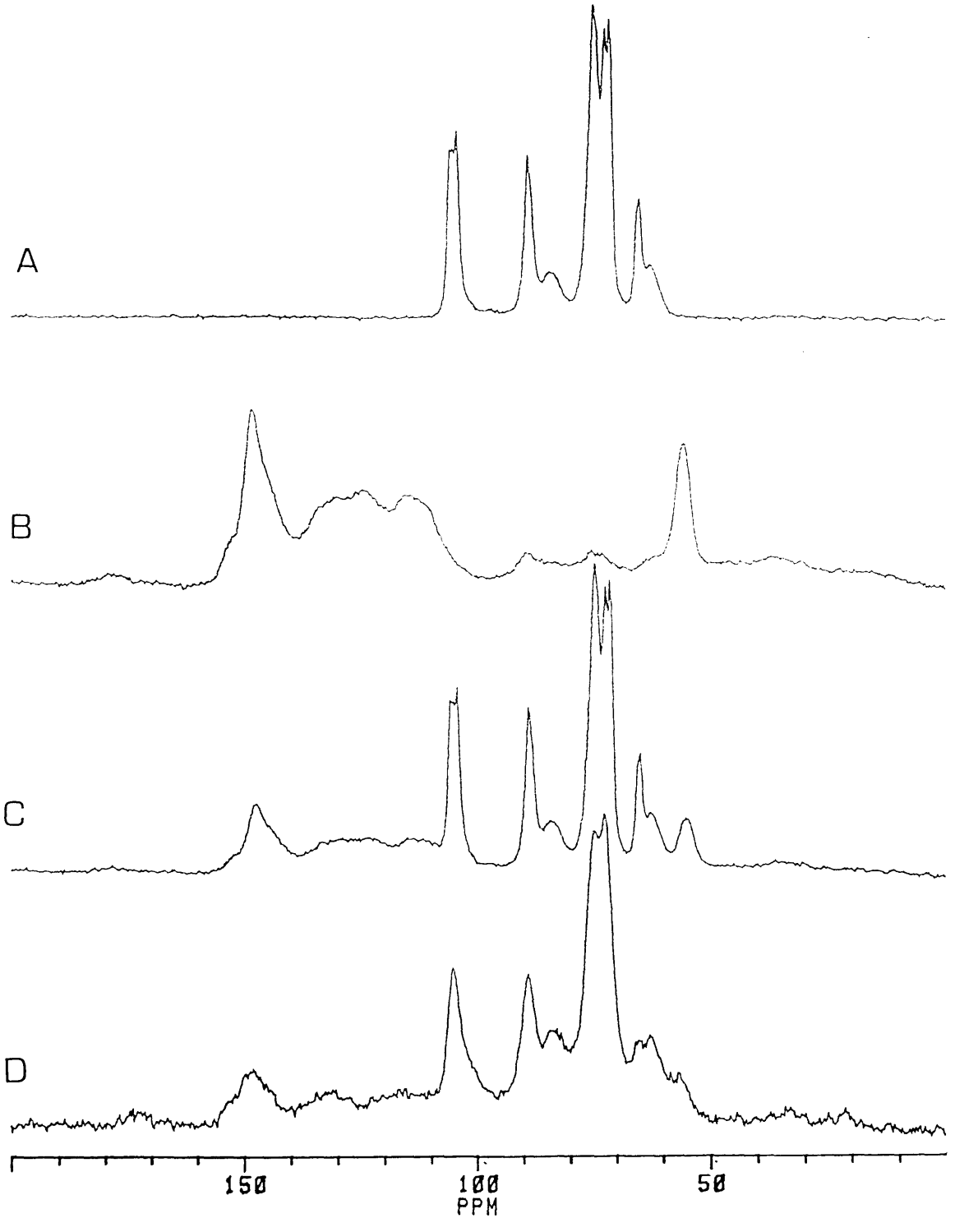

Figure 8.2. CP/MAS carbon-13 spectra of (a) cellulose, (b) spruce lignin, (c) addition of (a+b), and (d) whole cell walls from pine wood.

Generally it can be noted that some of the carbon nuclei generate both a sharp and a broad peak. According to Earl and VanderHart (1980), the sharp resonances are representative of anhydroglucose carbons in crystalline environments, whereas the broad resonances are due to carbons in amorphous regions or areas on the surface of the cellulose elementary fibrils, lacking a high degree of lateral organization. Peaks at 89 and 84 ppm are diagnostic for the degree of crystallinity of cellulose. This was calculated from the ratio of the areas of these peaks, and it was found to be 0.65. This value is in good agreement with literature data (Newman and Hemmingson, 1990), who reported values between 0.68 and 0.65.
The splitting of the peak at 105 ppm is revealing the presence of cellulose type I and cellulose type II. The former is the native cellulose, while the latter is the conversion product obtained by a mercerization or regeneration process. As the sample analyzed was cellulose from Whatman filter paper No 1, it is reasonable to expect that cellulose type II is the result of alkali treatment during its preparation.
Figure 8.2b. reports the CP/MAS spectrum of isolated softwood lignin. The spectrum exhibits the broad features typical of lignin, extending primarily in the aromatic region. The only intense contribution in the aliphatic region is the sharp peak at 56 ppm, assigned to the methoxy groups. The broad background present between 60 and 100 ppm is assigned to side chains sp^3 carbons, with contributions at 75 and 89 ppm from traces of hemicellulose components, deriving from the lignin-carbohydrate complex. The region between 100 and 140 ppm is assigned to C-2, C-5 and C-6 aromatic ring and side chain sp^2 carbons, with particular reference to C-1 aromatic carbon at 135 ppm. The peak at 148 ppm corresponds to the oxygen substituted C-4 aromatic ring carbon, and the peak at 154 ppm is due to the C-3 (and C-5 for syringyl units) aromatic carbons with methoxy groups attached.
Figure 8.2c. is the result of the addition of cellulose and lignin spectra: when this spectrum is compared to the one of whole pine cell wall of figure 8.2d., a close similarity can be observed. However, the presence of a broad background can be noted in the aliphatic region of the wood spectrum: this is due to the hemicellulose components that are not present in the addition spectrum. Hemicelluloses exhibits many spectral features similar to those of cellulose, but their signals tend to be broader, reflecting the heteropolymeric nature of these carbohydrates. The presence of hemicelluloses is visible from the characteristic peak at 103 ppm, that appears as a shoulder on the side of the 105 ppm peak of cellulose: this is due to C-1 hemicelluloses carbons.
Another characteristic of the whole cell wall spectrum is the presence of a single cellulose C-1 carbon peak at 105 ppm. This is consistent with the presence of only the natural cellulose type I.

An attempt to simplify the relatively complex spectra of wood, was made applying the total sidebands suppression pulse sequence (TOSS). Figure 8.3. reports the spectrum obtained for pine wood.

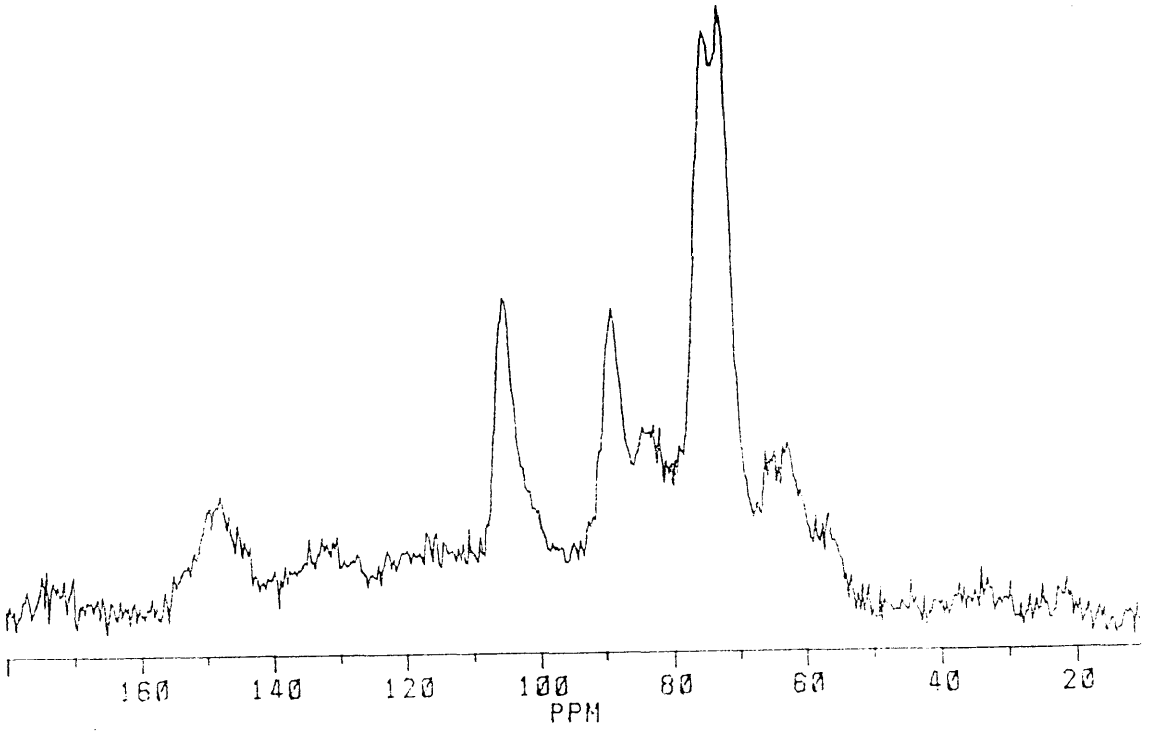

Figure 8.3. CP/MAS-TOSS carbon-13 spectrum of pine wood.

As can be noted, no appreciable spectral improvement was obtained. This suggested that the crowded cell wall spectrum is in fact due to broad chemical shifts, without significant contribution from spinning sidebands. Therefore, the simple CP/MAS technique was found to be suitable for our investigations.

8.1.3. CP/MAS Spectra of Pine and Beech Woods

Figure 8.4. shows the CP/MAS spectra of pine and beech woods.

Assignments of carbon-13 resonances were made on the basis of literature data (Atalla et al., 1980; Maciel et al., 1981; Kolodziejski et al., 1982) and on the basis of the considerations reported in the previous paragraph. Data are reported in table 8.1.

To confirm some spectral assignments, the non-quaternary carbon suppression pulse sequence (NQS) was applied, yielding to the spectrum shown in figure 8.5.

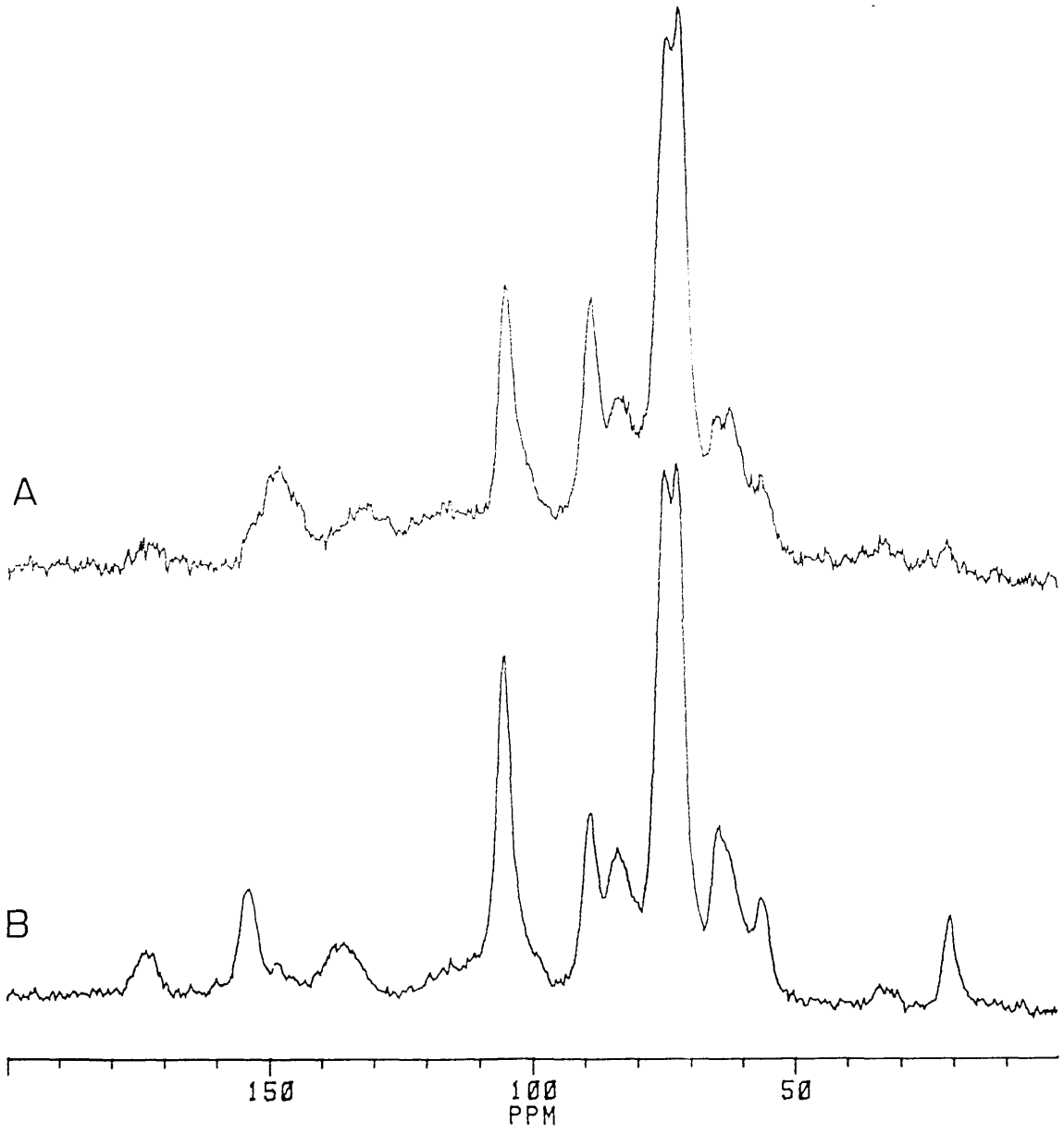

Figure 8.4. CP/MAS carbon-13 spectra of (a) pine and (b) beech woods.

Table 8.1. Assignments of carbon-13 chemical shifts of CP/MAS N.M.R. spectra of wood.

Chemical Shifts (ppm)	Assignments
21.5	Acetate groups in hemicelluloses
56	Aryl methoxyl carbons of lignin
63	C-6 carbon of amorphous cellulose or C-6 on the surface of fibers
66	C-6 carbon of crystalline cellulose
63 - 66	Background of C-6 carbon of hemicelluloses
70 - 80	Overlapped signals of C-2, C-3 and C-5 in cellulose; broad background of C-2, C-3 and C-5 carbons of hemicelluloses
84	C-4 carbon of amorphous cellulose or C-4 on the surface of fibers
89	C-4 carbon of crystalline cellulose
84 - 98	Background of C-4 carbon of hemicelluloses
103	Shoulder of C-1 carbon of hemicelluloses
105	C-1 carbon of cellulose
110 - 140	C-2, C-5 and C-6 carbon of aromatic rings and side-chains sp^2 carbons of lignin
135	C-1 carbon of aromatic ring carbons of lignin
148	C-4 carbon of lignin aromatic ring containing free phenolic groups attached
154	C-5 carbon of lignin aromatic ring containing methoxy groups
150 - 160	Oxygen substitute aromatic ring carbons (C-3 and C-4)
174	Carbonyl groups of lignin and carboxyl groups of hemicelluloses

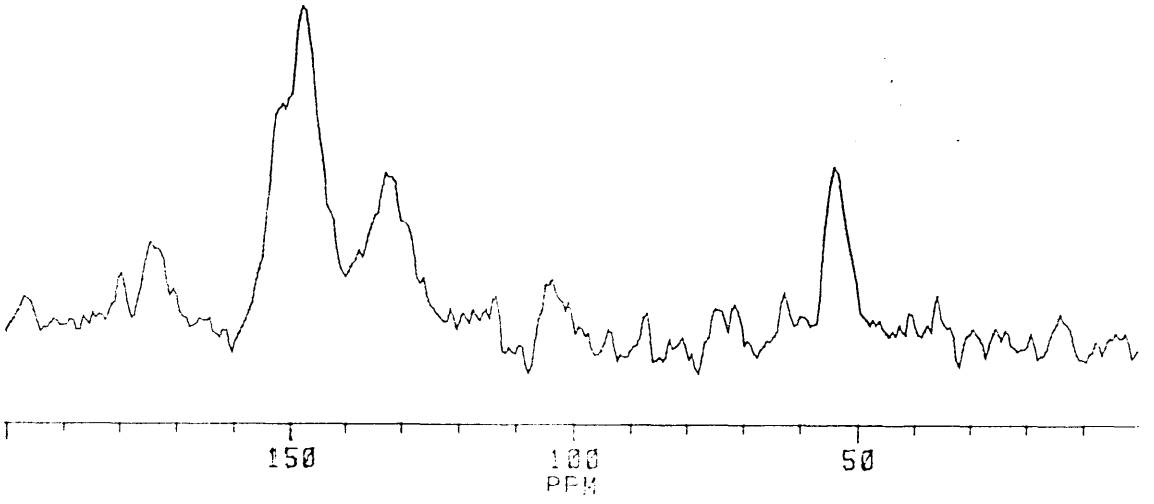

Figure 8.5. CP/MAS TOSS-NQS carbon-13 spectrum of pine wood. Quaternary carbons only are selected.

The NQS technique eliminates all protonated carbon signals, leaving quaternary carbons only and possibly residual signals from very mobile molecular fragments. Spectrum of figure 8.5a. shows the quaternary carbonyl and carboxyl groups of lignin and hemicelluloses at 174 and 182 ppm, the aromatic C-4 carbons of lignin at 148 ppm, with a shoulder at 154 ppm due to C-5 aromatic carbons bearing methoxy groups. Another peak that was not readily identified in the whole spectrum, is resolved at 135 ppm and it belongs to quaternary C-1 carbons of lignin aromatic rings. The peak at 56 ppm is the residual signal of the mobile lignin methoxy groups. These results fit the assignments given in table 8.1. and are consistent with literature data (Hatfield et al., 1987).

Comparing the spectra of pine and beech wood, it appears that the major differences are in the lignin and hemicelluloses components. Cellulose is present as type I in both wood samples, as shown by the single peak at 105 ppm. Intensities of the peaks at 84 and 89 ppm show that pine wood appears to contain cellulose with a higher degree of crystallinity than that of beech sample. This is consistent with previous quantitative estimation by Newman and Hemmingson (1990), who in general reported higher cellulose crystallinity for softwoods than for hardwoods.

Pine lignin shows a more pronounced peak at 148 ppm, beech lignin at 154 ppm. This feature is accompanied by a more intense methoxy peak at 56 ppm in beech wood. Since the 148 ppm peak is diagnostic of phenolic carbon, with methoxy groups attached, pine wood appears to be richer in non-methoxylated phenolics,

while beech appears richer in methoxylated phenolics. These results are consistent with the nature of the two woods, pine lignin being from softwood is mainly formed by mono-methoxylated guaiacyl units, and beech lignin being from hardwood, is formed also by di-methoxylated syringyl units.
Beech wood also shows more intense peaks at 22 ppm and 174 ppm, due to the acetate groups present in the hemicelluloses; some of the intensity at 174 ppm could also be due to carboxyl groups of hemicelluloses uronic acids. Differences in the hemicellulose contents between these two kinds of wood have also been shown in literature (Sterk et al., 1987). Table 8.2. shows that indeed the content of acetyl groups and xylans (the main monomer of hemicelluloses) is higher in beech woods than in pine woods.

Table 8.2. Percentage composition of pine and beech woods (Sterk et al., 1987).

Components	Beech (*Fagus sylvatica*)	Pine (*Pinus nigra*)
Glucan	50.4	47.1
Xylan	23.7	3.2
Mannan	----	9.1
Acetyl	5.3	----
Lignin	26.4	28.3
Extractives	6.9	6.7
Ash	1.1	0.3

8.1.4. CP/MAS Spectra of Degraded Cell Walls

Pine and beech wood samples were studied by CP/MAS technique after fungal attack; the samples were the same as those previously analyzed by wide-line N.M.R. The resulting spectra are reported in figure 8.6. for pine, and 8.7. for beech wood.

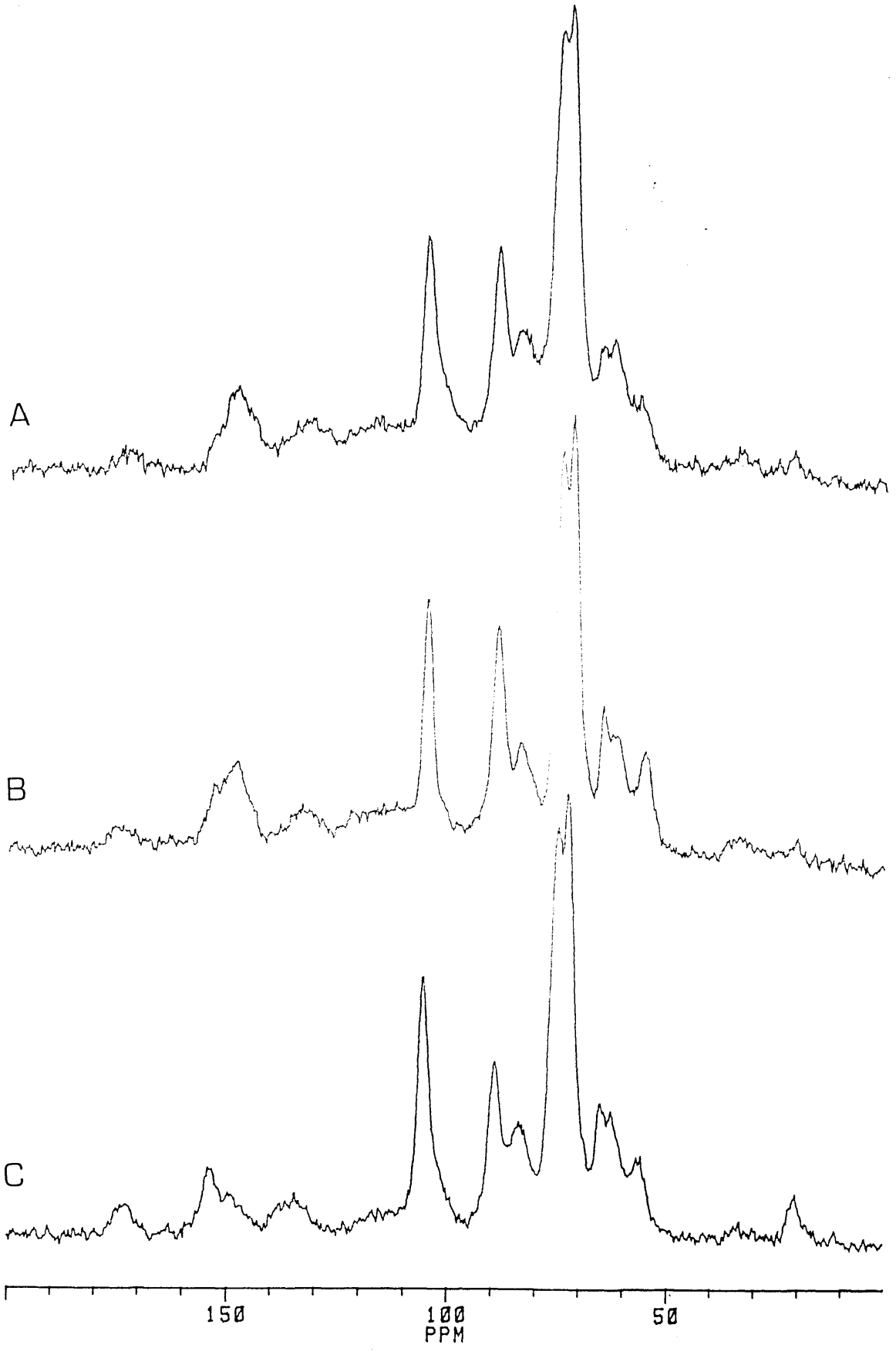

Figure 8.6. CP/MAS carbon-13 N.M.R. spectra of pine woods: (a) sound control, (b) subjected to brown-rot decay by *Coniophora puteana*, (c) subjected to white-rot decay by *Coriolus versicolor*.

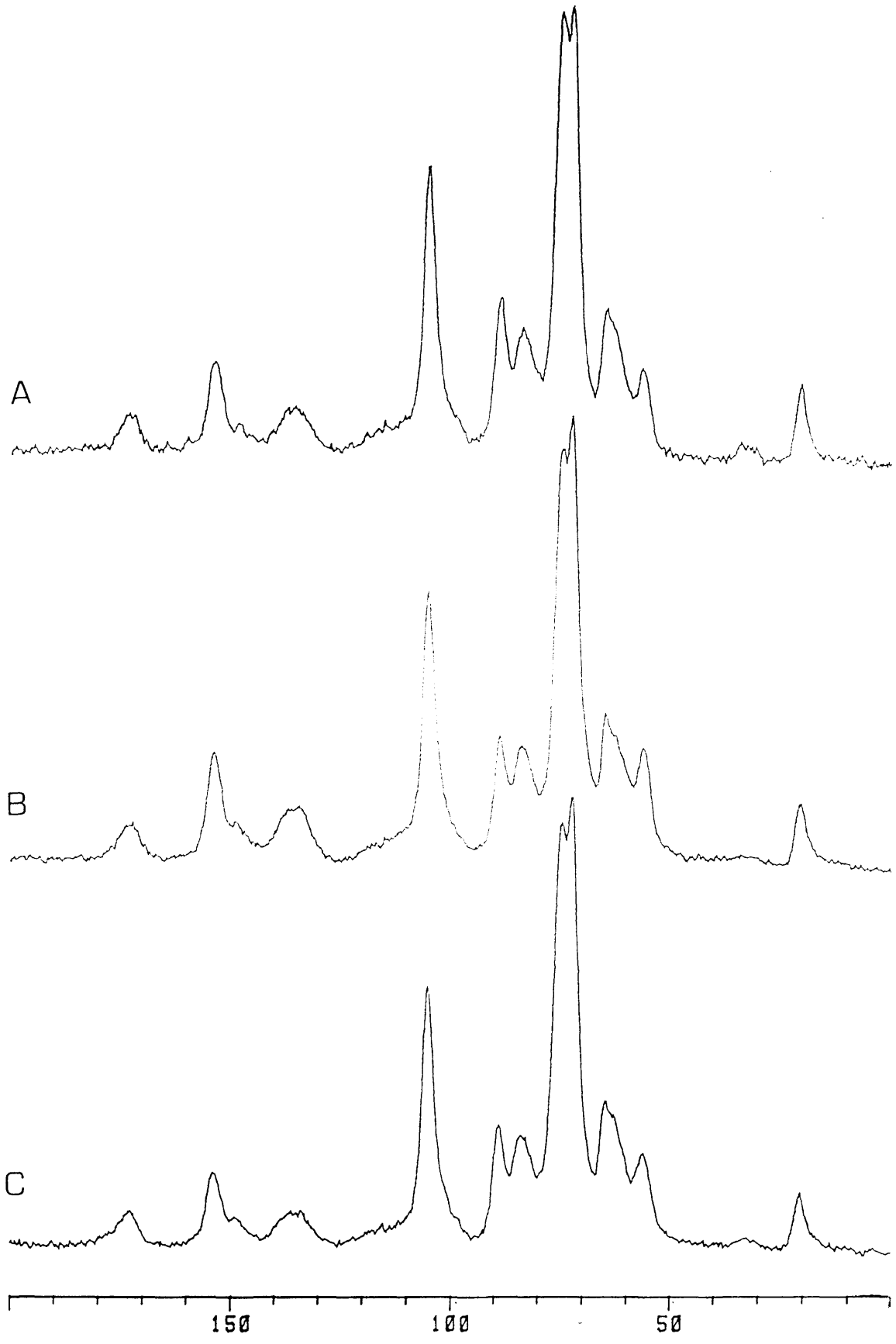

Figure 8.7. CP/MAS carbon-13 N.M.R. spectra of beech woods: (a) sound control, (b) subjected to brown-rot decay by *Coniophora puteana*, (c) subjected to white-rot decay by *Coriolus versicolor*.

Differences in peak intensities can be observed as the biodegradation process takes place. In particular, in the aliphatic region of spectra 8.6. the ratio between the intensities of the peaks at 110 and 89 ppm corresponding to cellulose resonances, are altered by the biodegradation. Overlapping signals makes it difficult to determine whether the cellulose or the hemicellulose components are more affected. However, by observing the shoulder at 103 ppm assigned to C-1 carbons of hemicelluloses, it can be noted that its intensity is reduced, especially by white-rot attack on pine wood (figure 8.6c.) The biodegradation of hemicelluloses reduces the broad background contribution to the aliphatic part of the spectrum, and it may be responsible for the apparent sharpening of some peaks in this region. The pine sample subjected to white-rot shows a decrease in both carbohydrate and lignin components, the latter detected as a substantial decrease in the intensity around 150 ppm. Such intensity variations are shown in the difference spectrum of figure 8.8a.

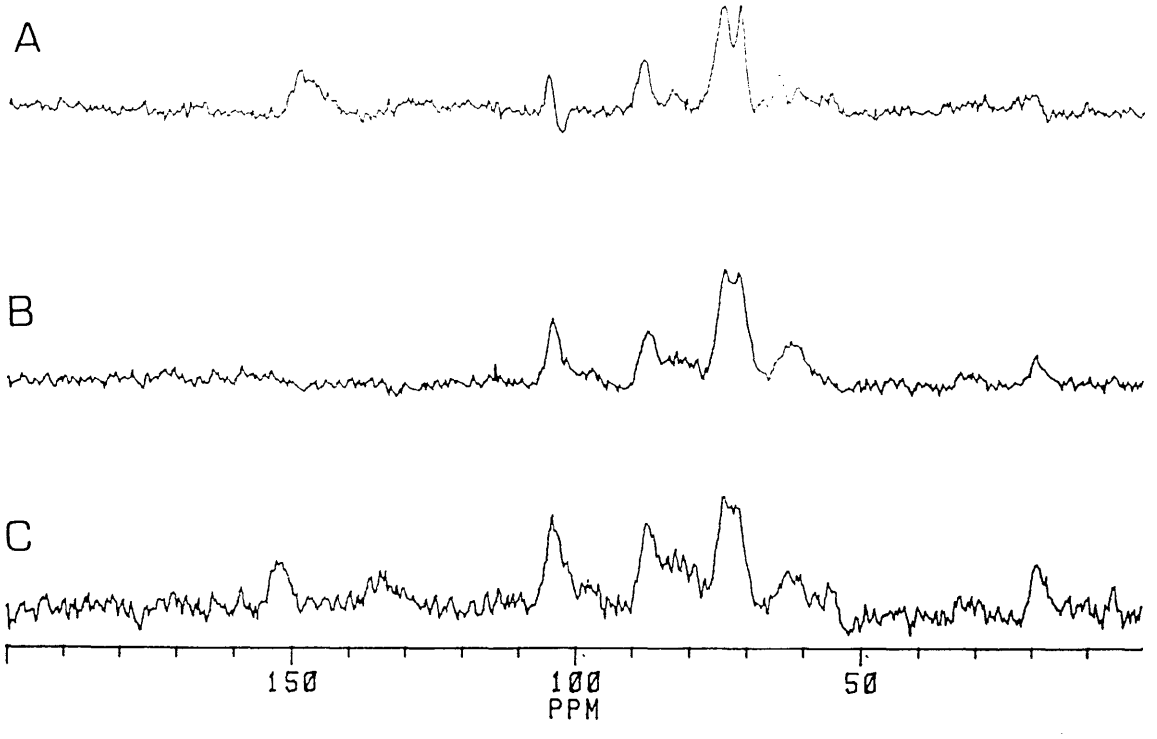

Figure 8.8. CP/MAS carbon-13 difference spectra: (a) pine sample subjected to white-rot decay (spectrum 8.6a. - spectrum 8.6b.); (b) beech sample subjected to brown-rot (spectrum 8.7a. - spectrum 8.7b.); (c) beech sample subjected to white-rot (spectrum 8.7a. - spectrum 8.7c.).

Figure 8.8b. shows that the degradation of aromatic rings is accompanied by an increase in the peak at 174 and 22 ppm, corresponding to carbonyl and carboxyl groups and their attached methyl groups. These groups are known to be the

oxidation products of cell wall structures (Buswell and Odier, 1987). Beech samples also show a similar pattern; brown-rot fungi appear to attack preferentially the carbohydrates (figure 8.8b.), while white-rot fungi attack the lignin component as well (figure 8.8c.) However, a sharpening in the aromatic and methoxy resonances manifested by the samples treated with brown-rot, may indicate a higher degree of mobility gained by a modified but still polymeric lignin. This could correspond to the enzymatically liberated lignin known to be produced by these fungi (Kirk and Shimada, 1985).

Since the conditions generally accepted for the acquisition of quantitative CP/MAS spectra were satisfied, quantitative analysis of these spectra has been made. Previous quantitative determinations on wood samples by CP/MAS have been reported in literature (Haw et al., 1984; Hatfield et al., 1987), and have been shown to fit with results obtained by standard chemical standard methods. In this research, the quantitative calculations have been made by modifying and adapting the considerations of Haw and coworkers (1984).

Although carbon-13 spectra of wood may appear at first complex and difficult to deconvolute, some general considerations can substantially simplify the system. To a first approximation, the spectra can be divided into the aromatic region containing lignin resonances, and in the aliphatic region, containing mainly cellulose and hemicellulose resonances. As the cellulose and hemicellulose signals are impossible to separate, it follow that in these calculations they will be both encompassed by the term carbohydrates.

A relative measure of the lignin aromatic carbon content can be obtained integrating the signals between 160 and 109 ppm, and this area will be referred as A_{low}. The integration of the region between 109 and 50 ppm contains a relative measure of the carbohydrate carbons and of the alkyl side-chain (C-α, C-β, C-γ) and methoxyl (OCH_3) carbons of lignin (A_{high}).

The carbohydrate component can be described by the empirical formula $C_6H_{10}O_5$, with a formula weight 162 g/mol (Haw et al., 1987); this formula is completely correct for cellulose, and describes very closely hemicelluloses, whose contribution to the spectrum is much lower. Conifer lignin can be described by an average formula $C_9H_{7.12}O_2(H_2O)_{0.40}(OCH_3)_{0.92}$ with formula weight 183 g/mol (Adler, 1977). Considering that the average lignin repeat unit has 9.9 carbons, 6 of which account for the total intensity measured by A_{low}, it follows that the lignin intensity (A_{lig}) is:

$$A_{lig} = (9.9/6)\, A_{low}$$

Lignin carbon contributions C-α, C-β, C-γ and OCH_3 have to be deducted from the total intensity A_{high}, to calculate the relative carbohydrate contribution A_{carb}:

$$A_{carb} = A_{high} - (3.92/6)\, A_{low}$$

where $(3.9/6)\, A_{low}$ is the lignin contribution to the aliphatic region. These quantities can be normalized to a total integrated signal intensity of one:

$$A'_{lig} = A_{lig} / A_{lig} + A_{carb} \qquad \text{and} \qquad A'_{CARB} = A_{CARB} / A_{lig} + A_{carb}$$

A dry-weight percent lignin content can be calculated for pine samples by:

$$wt\%_{pine\ lig} = (183/9.9)A'_{lig} / [(183/9.9)A'_{lig} + (162/6)A'_{carb}]$$

Similar evaluations can be made on hardwood beech lignin, taking into account that this contains a higher methoxyl content, with an average empirical formula of $C_9H_{6.43}O_2(H_2O)_{0.53}(OCH_3)_{1.39}$ and formula weight 199 g/mol (Adler, 1977). It follows:

$$A_{lig} = (10.4/6)\, A_{low}$$

$$A_{carb} = A_{high} - (4.4/6)\, A_{low}$$

$$wt\%_{beech\ lig} = (199/10.4)A'_{lig} / [(199/10.4)A'_{lig} + (162/6)A'_{carb}]$$

The results obtained from these calculations are reported in figure 8.9.

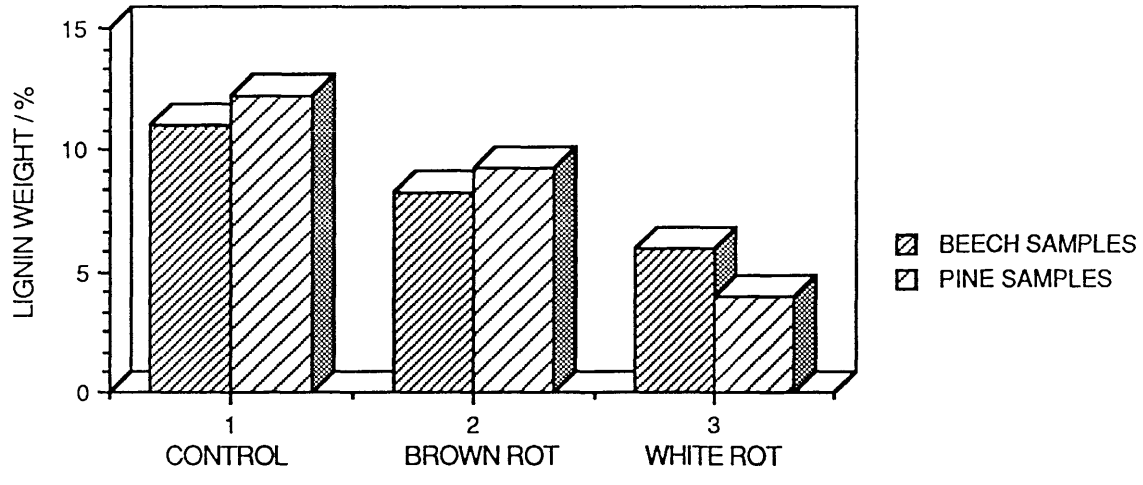

Figure 8.9. Dry-weight percent lignin content evaluated from integration of CP/MAS carbon-13 spectra of pine and beech samples before and after brown-rot or white-rot attack.

Comparing these results obtained from the two fungi studied, it appears that a major proportion of the lignin has been degraded by the white-rot *Coriolus versicolor*. These data are consistent with the earlier wide-line results obtained on the same samples that showed a higher extent of degradation on pine samples after white-rot attack (chapter 7).

In general these results are consistent with the oxidative biodegradation of cell wall components, involving lignin aromatic ring cleavage, lignin side-chain and carbohydrates oxidation leading to an overall increase in carbonyl and carboxyl content. Brown-rot fungi appear to degrade preferentially polysaccharides, leaving a modified lignin polymeric network, whilst white-rot fungi appear to degrade both polysaccharide and lignin, in agreement with literature data (Kirk and Shimada, 1985; Enoki et al., 1988; Blanchette and Abad, 1988). Therefore CP/MAS N.M.R. proved to be a suitable non-destructive technique able to produce information at the molecular level and of quantitative nature on the biodegradation of whole cell walls.

8.2. FT/IR Spectroscopy on Cell Wall Degradation

Infrared (IR) spectroscopy has been applied by several authors to a study of cell wall molecular components. Early investigations using this technique are described by Sarkanen and Ludwig (1971), who reported comprehensive absorption band assignments for synthetic and isolated lignins. More recently IR spectroscopy has been applied to the study of rumen degradation of cereal straw cell walls (Russell et al.,1989), and to the *in sacco* digestion of grass (Himmelsbach, 1989). Although IR spectra of cell wall components showed considerable complexity, these studies revealed that this technique can provide overall information on molecular changes during biodegradation. One of the major advantages of IR is that it is relatively quick and, as with CP/MAS N.M.R. can be applied on intact solid samples, without extraction and solubilization steps.

In this research FT/IR spectroscopy by diffuse reflectance was applied to the same samples previously analyzed by wide-line and CP/MAS solid state N.M.R., to obtain parallel information on wood cell wall degradation by *Basidiomycetes* .
Figure 8.10. shows the spectra obtained for sound samples of pine and beech woods; signal assignments were made by using literature data (Sarkanen and Ludwig, 1971; Hemmingson and Wong, 1989) and are reported in table 8.3.

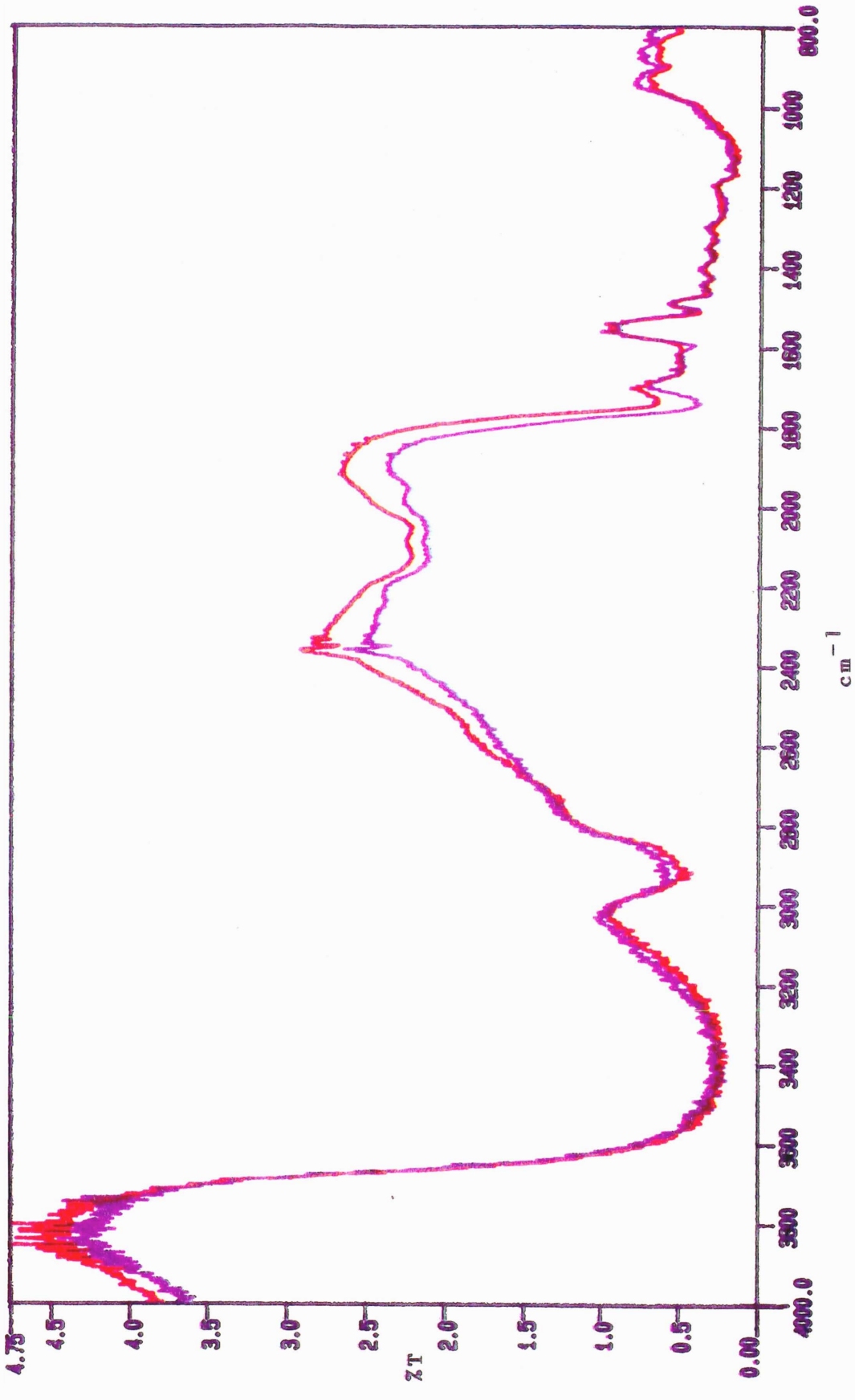

Figure 8.10. FT/IR diffuse reflection spectra of pine (red trace) and beech (violet trace) woods.

Table 8.3. Assignments of FT/IR bands of wood spectra.

Band Position cm^{-1}	Functional group
3600 -3200	O-H Alcohols
2960 - 2850	O-H Methyl and methylene groups
1780 - 1670	C=O Carbonyls
1670 - 1650	C=C Alkenes
1600 - 1500	C=C Aromatic
1265 - 1235	O-H Phenolic
1200 - 800	O-H Alcohols (primary and secondary) and alyphatic ethers
910	C=C Alkenes

Given the complex structure of the cell wall assembly, it is not surprising to observe that the spectra of figure 8.10. show a considerable overlap of absorption bands. In general, the fingerprint region of the two spectra (1500-800 cm^{-1}) is very similar. The only major difference appears at 1780 cm^{-1}; this band is assigned to the carbonyl groups, and therefore the higher intensity manifested by the beech spectrum suggests a higher carbonyl content in the beech sample. This observation is paralleled by CP/MAS N.M.R. data, that also showed higher carbonyl content for beech than for pine woods, probably due to differences in lignin and hemicelluloses between the two kinds of wood (see table 8.2.).

Figure 8.11. and figure 8.12. show the spectra of pine and beech samples respectively, before and after fungal degradation.

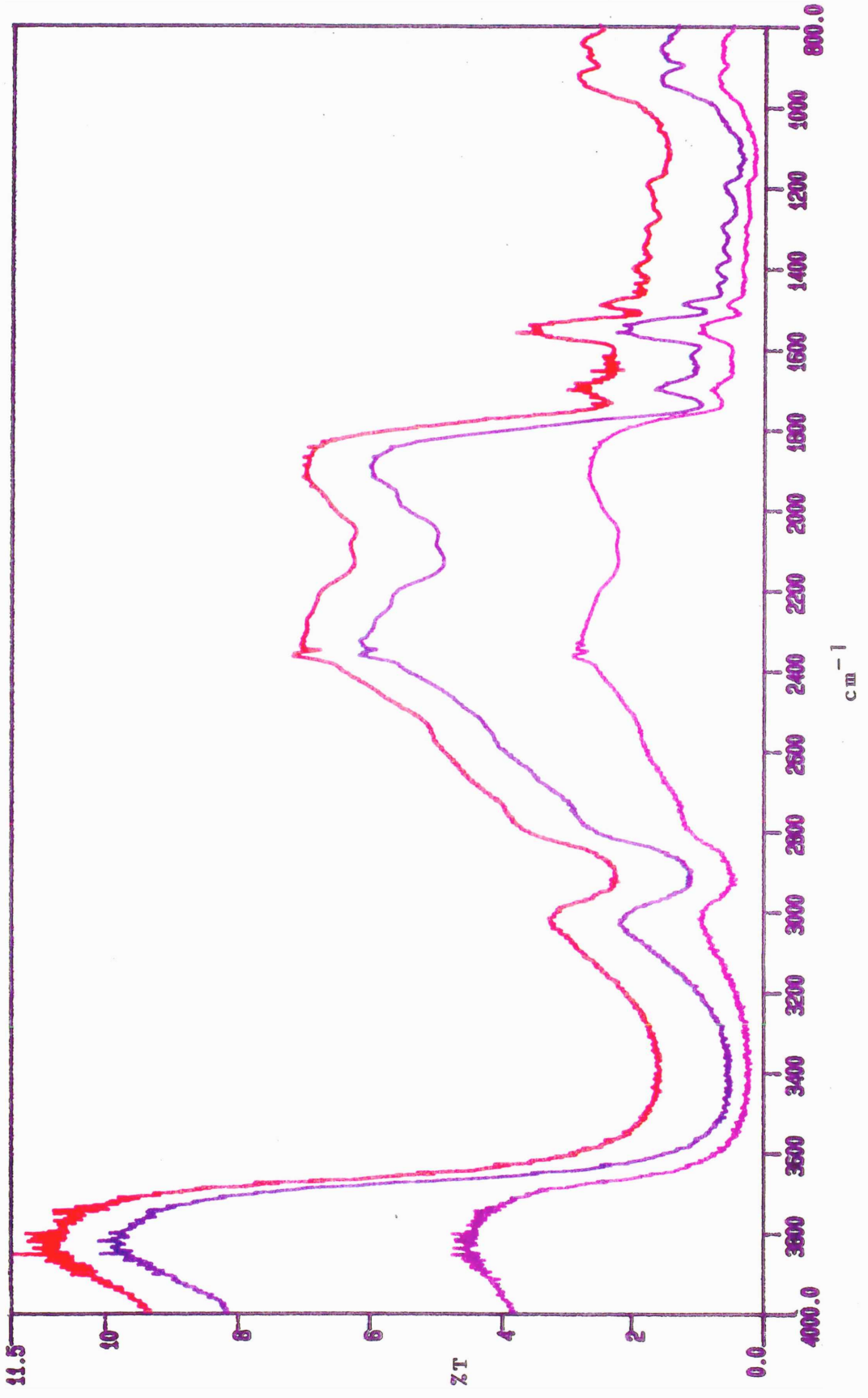

Figure 8.11. FT/IR diffuse reflection spectra of pine woods: sound control (violet trace); after brown-rot attack (red trace); after white-rot attack (blue trace).

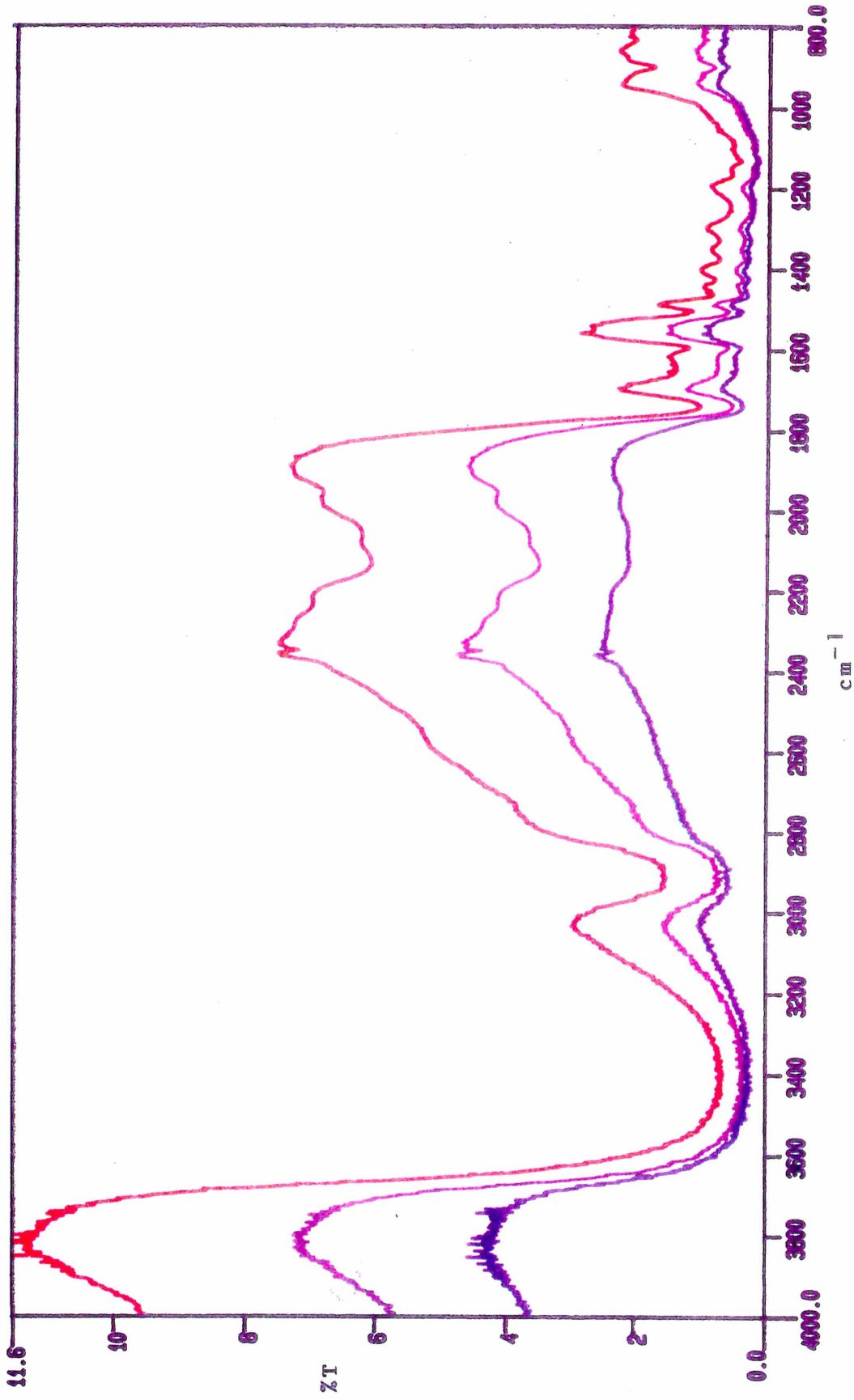

Figure 8.12. FT/IR diffuse reflection spectra of beech woods: sound control (blue trace); after brown-rot attack (violet trace); after white-rot attack (red trace).

As the degradation process took place, variations on cell wall components are detected in the IR spectra. Increases in the absorption band intensities corresponding to alkenes RCH=CHR (910 cm^{-1}), phenolic O-H (1235-1265 cm^{-1}), carbonyl C=O (1670-1780 cm^{-1}), alcoholic O-H and methyl and methylene groups (2850-2960 cm^{-1}) are observed for both wood samples, with higher intensities for sample subjected to white-rot decay.
The increase of these molecular functional groups is consistent with the known biodegradation patterns. The oxidation of aromatic structures of lignin leads to an increase in phenolic O-H, and their cleavage may be responsible for the formation of carbonyl and carboxyl C=O groups and alkenes RCH=CHR structures. Carbonyl, carboxyl and alcoholic groups are also formed during carbohydrate and lignin side-chain biodegradation. These data are consistent with the results obtained by CP/MAS N.M.R. analysis.

In conclusion, CP/MAS N.M.R. and FT/IR spectroscopy provide detailed information on the degradation of wood cell walls by fungi, with the advantage of their non-destructive nature.
CP/MAS N.M.R. spectra allow a distinction between carbohydrate and lignin components, making possible the detection of different attack patterns by different fungi. Brown-rot fungi have been shown to attack preferentially the carbohydrates, whilst white-rot extensively degrade the lignin component as well.
Spectral features, such as peak linewidths, give information about modification in mobility of molecular fragments. In this view, the sharpening of lignin resonances after brown-rot attack may indicate a higher mobility of fragments that probably correspond to the so-called "enzymatically liberated lignin" (Kirk and Shimada, 1985). Combining the results obtained from CP/MAS spectra with those from FT/IR spectra, the overall information is consistent with a degradation process involving aromatic ring cleavage, increasing in carbonyl and carboxyl groups, increasing in phenolic groups deriving from cleavage of lignin subunits.
Furthermore, the CP/MAS N.M.R. technique offers the possibility of quantitative determinations of the lignin content before and after fungal attack.

Although these studies were performed with fungi, the same changes in spectral characteristics should also be observed during enzymatic degradation. In the light of the difficulties reported by numerous workers in studying the degradation of lignin *in vitro*, CP/MAS N.M.R. and FT/IR spectroscopies may offer a more unambiguous approach.

General Conclusions and Future Perspectives

The results reported in this thesis have shown that nuclear magnetic resonance (N.M.R.) spectroscopy can provide useful information on lignin biodegradation, both in solution and in the solid state.

Solution N.M.R. studies have shed new light on the mechanism of lignin degradation by ligninase.
Proton N.M.R. studies conducted on the oxidation of veratryl alcohol (VA) by ligninase have shown that VA radical intermediates are generated during enzyme turnover. Furthermore, the effect on the linewidths of VA resonances indicates that a rapid exchange of the unpaired electron is occurring between the paramagnetic and diamagnetic molecules.
These data support the model proposed by Harvey and coworkers in 1986, that involves a mechanism of mediation of VA radical cations in lignin degradation. The N.M.R. data presented in this thesis provide evidence that indeed VA radical cations are generated during ligninase turnover, and that a charge exchange process is occurring between the substrate molecules.
Mediation role by small molecules that can freely diffuse transferring oxidizing equivalent from the enzyme active site to the bulk lignin is increasingly being accepted; a similar hypothesis has been proposed for manganese ions that act as mediator for the manganese dependent peroxidase (Cui and Dolphin, 1990).
At the present the crystal structure of ligninase is being solved by Poulos and coworkers; preliminary results were presented at the International Congress of Inorganic Biochemistry held in August 1991 (Oxford). These results showed that ligninase has a buried active site that is unlikely to be accessible to a complex polymer such as lignin. A mediation role of veratryl alcohol could explain how a hydrophobic and insoluble polymer such as lignin can be degraded by ligninase.
One and two-dimensional N.M.R. studies conducted on organosolv spruce lignin suggest that the lignin sample analyzed may possess an organized three dimensional structure. Recently the "network theory" that proposes a random organization of lignin is being questioned (Sarkanen and Dutta, 1990; Lewis and Yamamoto, 1990). New experimental evidence seems to support the view of an organized lignin network. Atalla and Agarwall (1985) reported the presence of oriented aromatic rings of lignin in native cell wall, consistent with earlier studies

(Sarkanen and Ludwig, 1971) that reported UV-dichroism data showing that lignin is to a certain extent oriented.

The N.M.R. data, supported by molecular modelling of lignin fragments and published crystal structure of lignin model dimers (Elder et al. 1988; Lundquist and Stomberg, 1988), show that the β-O-4 and β-β subunits have precise conformations, involving either a planar arrangement or a stacking of aromatic rings. These results refer to the major lignin subunits: β-O-4 and β-β structures account for more than 70% of the interunits linkages in lignin. The presence of other minor substructures and the previous failure to detect structural regularity may be caused by objective analytical difficulties combined with modifications that occur during lignin extraction. Most of the published work on lignin organization relied on lignins extracted under strong acidic conditions, such as 70% sulphuric acid. Yasuda and Ota (1987) reported the presence of several condensation reactions during the treatment of lignin with dilute and concentrated sulphuric acid, in the same conditions as in ordinary lignin extraction. These reactions yielded products similar to the minor lignin subunits.

The results presented in this thesis were obtained on isolated lignin fragments subjected to mild solvent extraction procedures, that are more likely to maintain the characteristics of the native lignin.

These observations may open new speculations on the real, un-altered, structure of lignin, on the role that this may play in its biodegradation, and on the reciprocal arrangements of the cell wall components. For example lignin has been found to be closely associated with the hemicelluloses, and their degradation seems to proceed in parallel: chemical analysis of wood degraded by white-rot fungi indicates that hemicelluloses are preferentially removed when lignin is degraded (Blanchette and Abad, 1988). The relationship between these two polymers consists not only in a covalent linkage (Gerasimowicz et al., 1984), but also in a close contact in space (Newman and Hemmingson, 1990).

Such association might originate in the biosynthesis step during cell wall growth: a "template-like" effect of the polysaccharides during lignin biosynthesis has been proposed by Fry (1987). This phenomenon might introduce definite structural constraints to the lignin orientation. For example, Quiocho and coworkers (Vyas et al., 1988) have shown that hydrophobic patches on carbohydrate chains in glycoprotein cause stacking of aromatic aminoacids. Given i) the similarity between the hydrophobic patches seen in these studies and those presented by hemicelluloses; ii) the bound and close physical association of lignin and hemicelluloses; iii) the finding that suggest aromatic ring stacking between lignin units, it might be interesting to further explore the lignin-hemicellulose interactions.

It may be possible to envisage the building of a stable cell wall assembly involving stacking of aromatic rings of lignin over a hemicellulose template. The evolution in space of the hemicellulose chains might create definite domains of stacking of aromatic rings of lignin, achieving a short range order. The lack of the long range order, essential for diffraction, precludes obtaining further structural information from this technique. It this respect, N.M.R. techniques may provide complementary information on lignin structure. Further N.M.R. research on lignin model compounds and hemicellulose chains might be able to provide information in their reciprocal arrangement by using the nuclear Overhauser effect .

An interesting point in lignin biodegradation studies is that although many findings indicate the key role played by ligninase and veratryl alcohol in fungal cultures (Leisola et al., 1988), great difficulties have been encountered in the depolymerization of lignin *in vitro* by isolated enzyme systems. On the contrary, the polymerization of lignin after ligninase catalysis has been reported by Haemmerli and coworkers (Haemmerli et al., 1986b).

To explain this phenomenon it has been speculated that the fungus has a mechanism for regulating the biodegradation of lignin that involves the immobilization of lignin by the fungal polysaccharides. Leisola and Garcia proposed in 1989 that the fungus achieve the biodegradation of lignin by removing the degradation products through the cell membrane. These authors showed that when lignin is degraded by fungal mycelia, it appears to be bound to the polysaccharide slime layer of the fungus. Leisola and Garcia proposed that covalent bonds are formed between the lignin particles added to the culture and the hypha polysaccharides; these bonds would resemble to those that lignin has with hemicelluloses in the native wood. The immobilization of lignin to the fungal mycelium might prevent the spontaneous repolymerization reaction.

These studies stress the importance of the interplay in roles between cell wall components.

Furthermore, the presence of "organized arrays" of aromatic rings of lignin suggested by the N.M.R. studies presented in this thesis, may be expected to assume some importance in the lignin breakdown process. The radical cation mediators of veratryl alcohol generated by ligninase catalysis may be able to transfer the charge to the lignin network, and the charge transfer may continue through the lignin structure, up to the point at which the balance between charge transfer and breakdown of the radical cation changes in favour of breakdown. An hypothetical picture illustrating this model is presented in figure 9.1.

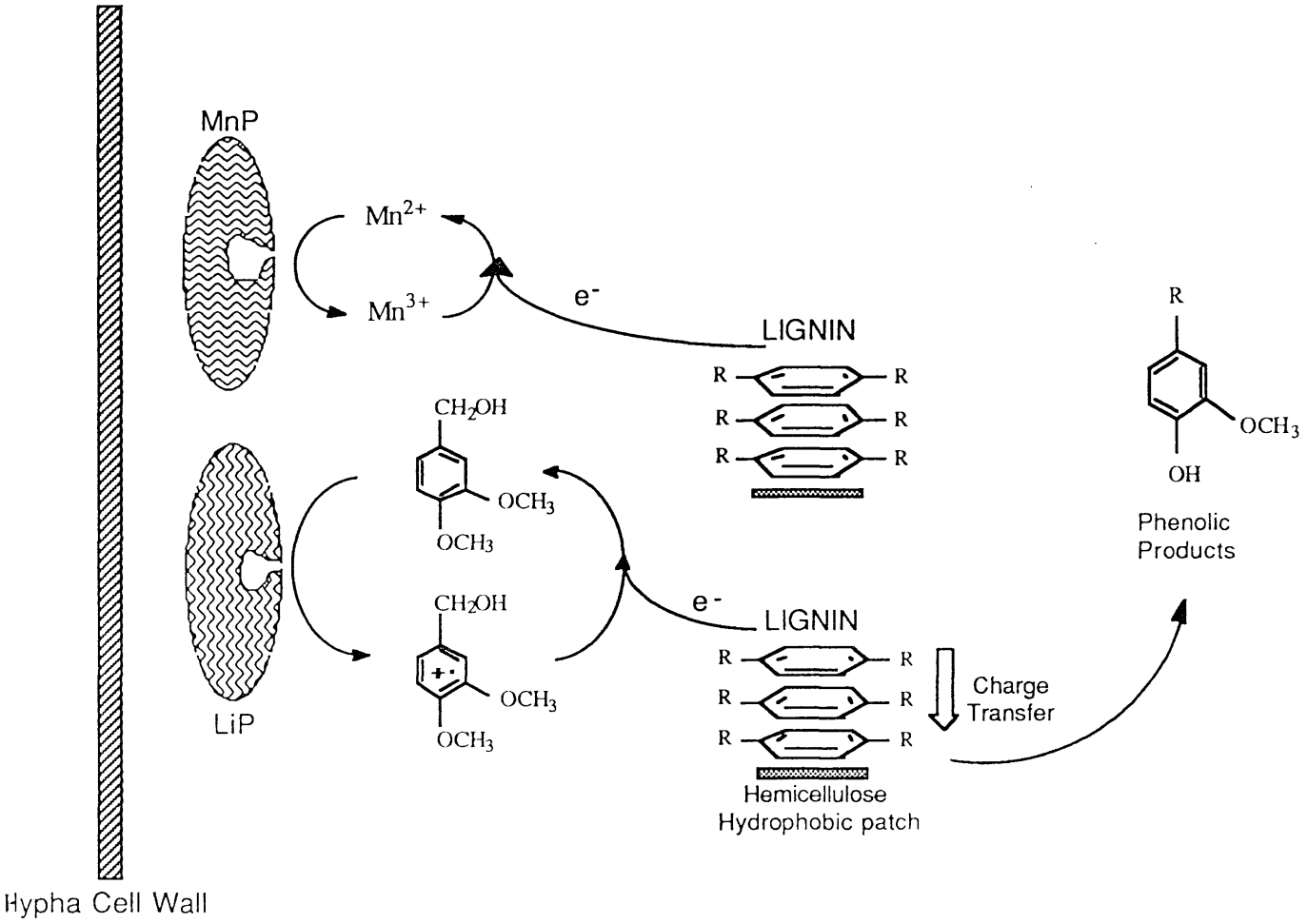

Figure 9.1. Schematic model for mechanism of lignin degradation. The process may occur near the outer mucillaginous sheath of the fungal hypha; LiP = Ligninase; MnP = Mn Peroxidase.

The results obtained from the application of several spectroscopic techniques to lignin samples in solution, indicated that the lignin sample analyzed forms aggregates. These results have a certain importance as they reveal a particular physical state of lignin in solution, that may have to take into account when considering its availability to the enzymatic activity. The physical state of lignin in solution may be expected to play a role in biodegradation studies conducted *in vitro* with purified enzymes.

In support of this view, recently Kurek and coworkers (1990b) reported an higher ligninase activity when a "colloidal lignin preparation" was used in the experiments *in vitro*. Furthermore, Hammel and Moen (1991) found that the degradation of lignin by ligninase occurs when the experiments were carried out in solution containing 10-20% of organic solvent (N,N'-dimethylformamide). These authors,

however, did not investigate the influence that these conditions can have on the physical state of the lignin used in the experiments.
These findings raise interesting questions on the role that lignin itself has in its biodegradation: failure to detect degradation in simple *in vitro* experiments indicate that there are factors to be taken into account other than simply the enzymes and their catalytic condition. Aromatic ring stacking in lignin, hydrophilic/hydrophobic forces that cause its aggregation, interaction of lignin with hemicellulose components, are all factors that may have to be considered in the design of biodegradation experiments.

Solid state N.M.R. also proved to be a useful mean of investigation the cell wall degradation by white-rot and brown-rot fungi.
Wide-line proton relaxation time measurements carried out on wood samples, showed that different relaxing components could be distinguished, and could be attributed to the bulk cell wall, "ice-like" and "liquid-like" layers of water molecules.
The relaxation time values of the free ("liquid-like") water showed an increase in wood samples that were attacked by fungi. These variations were found to be significant, and could be caused by an increase in mobility of water in a destructured environment.
This finding offers a non-destructive test that can be used to determine the extent of degradation in wood samples. An example of the application of such test could be the quantitative estimation of the efficacy of a wood preservative against fungal attack.
High resolution carbon-13 cross polarization / magic angle spinning (CP/MAS) N.M.R. also provided useful information on the biodegradation by white-rot and brown-rot fungi, at a molecular level. This technique allow the distinction between the polysaccharide and the lignin components. Different mechanism of attack were found for different fungi: white-rot were shown to extensively degrade both polysaccharides and lignin, whilst brown-rot were shown to attack preferentially the carbohydrates.
Both kinds of fungi carried out an oxidative degradation on the cell wall components, causing an increase in phenolic, carbonyl and carboxyl groups.
Quantitative determinations on the extent of degradation on lignin were also possible, showing a 23% by weight of degradation on spruce wood decayed by brown-rot, and 61% by white-rot.
Although these studies were performed with fungi, the same changes in spectral characteristics should also be observed during enzymatic degradation. In the light of the difficulties reported by numerous workers in studying the degradation of

lignin *in vitro*, CP/MAS N.M.R. spectroscopy may offer a more unambiguous approach, as extraction procedures on lignin are not necessary.

Bibliography

E. Adler, (1977) *Wood Sci. Technol.*, **11**,169

L. A. Andersson, V. Renganathan, T. M. Loehr and M. H. Gold, (1987) *Biochem.*, **26**, 2258

A. Andrawis, K. A. Johnson and M. Tien, (1988) *J. Biol. Chem.*, **263**, 1195

R. H. Atalla and U. P. Agarwall, (1985) *Science*, **227**, 636

R. H. Atalla, J. C. Gast, D. W. Sindorf, V. J. Bartuska and G. E. Maciel, (1980) *J. Am. Chem. Soc.*, **102**(9), 3249

A. R. Ayers, S. B. Ayers and K. E. Eriksson, (1978) *Eur. J. Biochem.*, **90**, 171

M. Bardet, M. F. Foray and D. Robert, (1985) *Makromol. Chem.*, **186**, 1495

B. J. Berne and R. Pecora, (1975) "Dynamic Light Scattering: Applications to Chemistry, Biology and Physics"; John Wiley & Sons Inc., New York

R. A. Blanchette and A. R. Abad, (1988) *Holzforschung*, **42**(6), 393

J. J. Bono, P. Goulas, N. Portet and J. L. Seris, (1987) In : "Lignin Enzymic and Microbial Degradation", E. Odier (ed.); INRA, Publ., Paris, 87

K. R. Brownstein, (1980) *J. Magn. Res.*, **40**, 505

J. A. Buswell and E. Odier, (1987) *CRC Critical Rev. Biotechnol.*, **6** (1), 1

J. J. Cael, L. W. Kwoh, S. S. Bhattacharjee and S. L. Patt, (1985) *Macromol.*, **18**, 819

D. M. Camaioni and J. A. Franz, (1984) *J. Org. Chem.*, **49**, 1607

J. E. Carles and A. M. Scallan, (1973) *J. Appl. Polym. Sci.*, **17**, 1855

H. Chanzy and B. Henrissad, (1985) *FEBS Lett.*, **184**, 285

C. L. Chen, (1989) *Meth. in Enz.*, **161**, 110

C. L. Chen and H. Chang, (1985) In : "Biosynthesis and Biodegradation of Wood Components", T. Higuchi (ed.); Academic Press Inc., New York, 535

C. L. Chen and D. Robert, (1988) *Methods in Enz.*, **161**, 137

Y. Chen and M. Schnitzer, (1976) *Soil Sci. Soc. Am. J.*, **40**, 682

D. L. Crawford and R. L. Crawford, (1980) *Enzyme Microb. Technol.*, **2**, 11

R. L. Crawford, (1981) "Lignin Biodegradation and Trasformation"; Wiley-Interscience, New York

R. L. Crawford and D. L. Crawford, (1984) *Enzyme Microb. Technol.*, **6**, 434

F. Cui and D. Dolphin, (1990) *Holzforschung*, **44**, 279

Z. Derewenda, J. Yariv, J. R. Helliwell, A. J. Kalb, E. J. Dodson, M. Z. Papiz, T. Wan and J. Campbell, (1989) *EMBO J.*, **8**(8), 2189

A. E. Derome, (1987) "Modern N.M.R. Techniques for Chemical Research"; Pergammon Press, Oxford

O. G. Dirckx, D. M. Masson and X. M. Deglise, (1987) In : "Proceedings of the Fourth Int. Symp. on Wood and Pulping Chemistry"; Paris, 441

P. J. Dodson, C. S. Evans, P. J. Harvey and J. M. Palmer, (1987) *FEMS Microbiol. Lett.*, **42**, 17

S. Dutta and S. Sarkanen, (1990) In : "Proceeding of the Material Research Society", J. D. Passaretti and D. F. Caufield (eds.); Pittsburgh,

W. L. Earl and D. L. VanderHart, (1980) *J. Am. Chem. Soc.*, **102**(9), 3251

R. M. Ede, G. Brunow, L. K. Simola and J. Lemmetyinen, (1990) *Holzforschung*, **44**(1), 95

T. J. Elder, M. L. McKee and S. D. Worley, (1988) *Holzforschung*, **42**(4), 233

A. Enoki, H. Tanaka and G. Fuse, (1988) *Holzforschung*, **42**(2), 85

K. E. Eriksson, (1989) In : "Enzyme Systems for Lignocellulose Degradation", M. P. Coughlan (ed.); Elsevier Applied Science, London and New York, 101

D. E. Eveleigh, (1987) *Phil. Trans. R. Soc. Lond. A*, **321**, 435

B. D. Faison and T. K. Kirk, (1985) *Appl. Environ. Microbiol.*, **49**(2), 299

B. D. Faison, T. K. Kirk and R. L. Farrell, (1986) *Appl. Environ. Microbiol.*, **52**(2), 251

R. Farrell, (1987) *Phil. Trans. R. Soc. Lons.*, **A 321**, 549

N. Fernandez, R. Morck, S. C. Johnsrud and K. P. Kringstad, (1990) *Holzforschung*, **44**(1), 35

A. Fersht, (1985) "Enzyme Structure and Mechanism"; W.H. Freeman and Company, New York

M. A. Foster and J. M. S. Hutchison, (1987) "NMR Imaging"; IRL Press, Oxford-Washington DC

M. F. Froix and A. O. Goedde, (1976) *Macromol.*, **9**(3), 428

S. C. Fry, (1987) *J. Exp. Botany*, **38**(190), 863

C. A. Fyfe, (1983) "Solid State N.M.R. for Chemists"; C.F.C. Press, Ontario, Canada

G. L. Gaines (1966) "Insoluble Monolayers at Liquid-Gas Interfaces"; Wiley-Interscience, New York

T. M. Garver, M. L. Iwen and S. Sarkanen, (1989) In : "International Symposium on Wood and Pulping Chemistry"; *TAPPI*, Raleigh, N.C. U.S.A., 113

W. V. Gerasimowicz, K. B. Hicks and P. E. Pfeffer, (1984) *Macromol.*, **17**(12), 2597

G. Gilardi, P. J. Harvey, A. E. G. Cass and J. M. Palmer, (1990) *Biochim. Biophys. Acta*, **1041**, 129

J. K. Glenn and M. H. Gold, (1985) *Arch. Biochem. Biophys.*, **242**, 329

J. K. Glenn, M. A. Morgan, M. B. Mayfield, M. Kuwahara and M. H. Gold, (1983) *Biochem. Biophys. Res. Comm.*, **114**, 1077

M. H. Gold, L. Akileswaran, H. Wariishi, Y. Mino and T. M. Loehr, (1987) In : "Lignin Enzymic and Microbial Degradation", E. Odier (ed.); INRA Publ., Paris, 113

M. H. Gold, M. Kuwahara, A. A. Chiu and J. K. Glenn, (1984) *Arch. Biochem. Biophys.*, **234**(2), 353

M. H. Gold, H. Wariishi, K. Valli, M. B. Mayfield, V. J. Nipper, J. A. Brown and D. Pribnow, (1990) In : "Biotechnology in Pulp and Paper Manufacture", T. K. Kirk and H. Chang (eds.); Butterworth-Heinemann, Bostom, 447

J. Gravitis and P. Erins, (1983) *J. Appl. Polymer Sci. Appl. Polymer Symp.*, **37**, 421

S. D. Haemmerli, M. S. A. Leisola and A. Fiechter, (1986b) *FEMS Lett.*, **35**, 33

S. D. Haemmerli, M. S. A. Leisola, D. Sanglard and A. Fiechter, (1986a) *J. Biol. Chem.*, **261**(15), 6900

J. R. T. Hailey, R. S. Menon, A. Mackay, A. E. Burgess and J. S. Swanson, (1985) In : "Proceedings of the Fifth Symposium on Non-desctructive Testing of Wood"; Pullman, Washington, U.S.A., 175

K. E. Hammel, B. Kalyanaraman and T. K. Kirk, (1986) *J. Biol. Chem.*, **261**(36), 16948

K. E. Hammel, M. Tien, B. Kalyanaraman and T. K. Kirk, (1985) *J. Biol. Chem.*, **260**(14), 8348

K. H. Hammel and M. A. Moen, (1991) *Enzyme Microb. Technol.*, **13**(13), 15

P. J. Harvey, G. Gilardi and J. M. Palmer, (1989b) In : "Enzyme System for Lignocellulose Degradation", M. P. Coughlan (ed.); Elsevier Applied Science, London and New York, 111

P. J. Harvey and J. M. Palmer, (1990) *J. Biotechnol.*, **13**, 169

P. J. Harvey, J. M. Palmer, H. E. Schoemaker, H. L. Dekker and R. Wever, (1989a) *Biochim. Biophys. Acta*, **994**, 59

P. J. Harvey, H. E. Schoemaher and J. M. Palmer, (1987) In : "Lignin Enzymic and Microbial Degradation", E. Odier (ed.); INRA, Publ., Paris, 145

P. J. Harvey, H. E. Schoemaker, R. M. Bowen and J. M. Palmer, (1985) *FEBS Lett.*, **183**, 13

P. J. Harvey, H. E. Schoemaker and J. M. Palmer, (1986) *FEBS Lett.*, **195**, 242

G. R. Hatfield, G. E. Maciel, O. Erbatur and G. Erbatur, (1987) *Anal. Chem.*, **59**, 172

M. Hauteville, K. Lundquist and S. von Unge, (1986) *Acta Chem. Scand.*, **B 40**, 31

J. F. Haw, G. E. Maciel and H. A. Schroeder, (1984) *Anal. Chem.*, **56**(8), 1323

J. A. Hemmingson and K. R. Morgan, (1990) *Holzforschung*, **44**(2), 127

J. A. Hemmingson and H. Wong, (1989) *Holzforschung*, **43**(2), 141

T. Higuchi, (1985) In : "Biosynthesis and Biodegradation of Wood Components", T. Higuchi (ed.); Academic Press Inc., New York, 557

T. Higuchi, Shimada.F., F. Nakatsubo and M. Tanahashi, (1977) *Wood Sci. Technol.*, **11**, 153

D. S. Himmelsbach, F. E. Barton and W. R. Windham, (1983) *J. Agric. Food Chem.*, **31**(2), 401

D. S. Himmelsbach, (1989) In : "Physico-Chemical Characterization of Plant Residues for Industrial and Feed Use", A. Chesson and E. R. Orskov (eds.); Elsevier Applied Science, London and New York, 3

F. Horii, A. Hirai and R. Kitamaru, (1987) *Macromol.*, **20**, 2117

E. Hsi, R. Hossfeld and R. G. Bryant, (1977) *J. Coll. Interf. Sci.*, **62**, 369

A. Huttermann, C. Herche and A. Haars, (1980) *Holzforschung*, **34**, 64

M. E. Jonsson, E. Petterson and B. Reinhammar, (1986) *Acta Chem. Scand.*, **22**, 2135

P. J. Kersten, B. Kalyanaraman, K. E. Hammel and T. K. Kirk, (1987b) In : "Lignin Enzymic and Microbial Degradation", E. Odier (ed.); INRA, Publ., Paris, 75

P. J. Kersten and T. K. Kirk, (1987a) In : "Lignin Enzymic and Microbial Degradation", E. Odier (ed.); INRA, Publ., Paris, 107

P. J. Kersten, S. K. Stephens and T. K. Kirk, (1990) In : "Biotechnology in the Pulp and Paper Manufacture", T. K. Kirk and H. Chang (eds.); Butterworth-Heinemann, Boston,

P. J. Kersten, M. Tien, B. Kalyanaraman and T. K. Kirk, (1985) *J. Biol. Chem.*, **260**, 2609

H. Kessler, M. Gehrke and C. Griesinger, (1988) *Angew. Chem. Int. Ed. Engl.*, **27**, 490

T. K. Kirk, (1971) *Ann. Rev. Phytopathol.*, **9**, 185

T. K. Kirk, (1975a) *Holzforschung*, **29**, 99

T. K. Kirk, (1987b) *Phil. Trans. R. Soc. Lon.*, **A 321**, 461

T. K. Kirk and E. Adler, (1970) *Acta Chem. Scand.*, **24**, 3379

T. K. Kirk, W. J. Connors, R. D. Bleam, W. F. Hackett and J. K. Zeikus, (1975b) *Proc. Natl. Acad. Sci. USA*, **72**, 2515

T. K. Kirk and R. L. Farrell, (1987a) *Ann. Rev. Microbiol.*, **41**, 465

T. K. Kirk and M. Shimada, (1985) In : "Biosynthesis and Biodegradation of Wood Components", T. Higuchi (ed.); Academic Press Inc., New York, 579

T. K. Kirk, M. Tien, P. J. Kersten, M. D. Mozuch and B. Kalyanaraman, (1986) *Biochem. J.*, **236**, 279

W. Kolodziejski, J. S. Frye and G. E. Maciel, (1982) *Anal. Chem.*, **54**(8), 1419

P. Kovac and J. Hirsch, (1980) *Carbohydr. Res.*, **85**, 177

R. W. Kreilck, (1973) In : "N.M.R. of Paramagnetic Molecules", G. N. LaMar, W. J. Horrocks and L. H. Holm (eds.); Academic Press Inc., New York,

K. P. Kringstad and R. Morck, (1983) *Holzforschung*, **37**, 237

D. Kuila, M. Tien, J. A. Fee and M. R. Ondrias, (1985) *Biochem.*, **24**, 3394

B. Kurek, B. Monties and E. Odier, (1990a) *Holzforschung*, **44**(6), 407

B. Kurek, B. Monties and E. Odier, (1990b) *Enzyme Microb. Technol.*, **12**(10), 771

M. Kuwahara, J. K. Glenn, M. A. Morgan and M. H. Gold, (1984) *FEBS Lett.*, **169**, 247

C. Lapierre and B. Monties, (1987) *Holzforschung*, **41**(1), 51

J. Y. Lee, A. Ishizu, S. Hosoya and J. Nakano, (1979) *Wood Cellul. Chem. Technol.*, **13**, 739

M. Leisola, C. Brown, M. Laurila, D. Ulmer and A. Fiechter, (1982) *Eur. J. Appl. Microbiol. Bitechnol.*, **15**, 180

M. S. A. Leisola and S. Garcia, (1989) In : "Enzyme Systems for Lignocellulose Degradation", M. P. Coughlan (ed.); Elsevier Applied Science, London and New York, 89

M. S. A. Leisola, S. D. Haemmerli, R. Waldner, H. E. Schoemaker, H. W. H. Schmidt and A. Fiechter, (1988) *Cell. Chem. Technol.*, **22**, 267

M. S. A. Leisola, B. Schmidt, U. Thanei-Wyss and A. Fiechter, (1985) *FEBS Lett.*, **189**(2), 267

M. S. A. Leisola, D. C. Ulmer, A. Waldner and A. Fiechter, (1984) *J. Biotechnol.*, **1**, 331

B. L. Lenz, (1968) *TAPPI*, **51**(11), 511

N. G. Lewis and E. Yamamoto, (1990) *Annu. Rev. Plant Physiol. Plant Mol. Biol.*, **41**, 455

T. Lindstrom, (1979) *Colloid and Polym. Sci.*, **257**, 277

L. G. Ljungdahl, (1989) In : "Enzyme System for Lignocellulose Degradation", M. P. Coughlan (ed.); Elsevier Applied Science, London, New York, 5

H. D. Ludemann and H. Nimz, (1973) *Biochem. Biophys. Res. Comm.*, **52**(4), 1162

C. H. Ludwig, B. J. Nist and J. L. McCarthy, (1964) *J. Am. Chem. Soc.*, **86**, 1196

K. Lundquist, (1979a) *Acta Chem. Scand.*, **B 33**(1), 27

K. Lundquist, (1979b) *Acta Chem. Scand.*, **B 33**(6), 418

K. Lundquist, (1980) *Acta Chem. Scand.*, **B 34**(1), 21

K. Lundquist, (1981) *Acta Chem. Scand.*, **B 33**, 497

K. Lundquist and T. Olsson, (1977) *Acta Chem. Scand.*, **B 31**(9), 788

K. Lundquist and R. Stomberg, (1988) *Holzforschung*, **42**(6), 375

G. E. Maciel, D. J. O'Donnell, J. J. H. Ackerman, B. H. Hawkins and V. J. Bartuska, (1981) *Makromol. Chem.*, **182**, 2297

L. Marquez, H. Wariishi, H. B. Dunford and M. H. Gold, (1988) *J. Biol. Chem.*, **263**(22), 10549

C. K. Mathews and K. E. VanHolde, (1990) "Biochemistry"; The Benjamin/Cummings Publishing Company, Redwood City, CA U.S.A.

V. J. McBrierty and D. C. Douglass, (1981) *J. Polym. Sci.: Macrom. Rev.*, **16**, 295

R. S. Menon, A. L. Mackay, S. Flibotte and J. R. T. Hailey, (1989) *J. Magn. Res.*, **82**, 205

R. S. Menon, A. L. Mackay, J. R. T. Hailey, M. Bloom, A. E. Burgess and J. S. Swanson, (1987) *J. Appl. Polym. Sci.*, **33**, 1141

K. Miki, R. Kondo, V. Renganathan, M. B. Mayfield and M. H. Gold, (1988) *Biochemistry*, **27**, 4787

Y. Mino, H. Wariishi, N. J. Blackburn, T. M. Loehr and G. M.H., (1988) *J. Biol. Chem.*, **263**, 7029

H. A. Mohwald, (1990) *A. Rev. Phys. Chem.*, **41**, 441

F. F. Morpeth, (1985) *Biochem. J.*, **228**, 557

R. H. Newman and J. A. Hemmingson, (1990) *Holzforschung*, **44**, 351

M. L. Niku-Paavola, (1987) In : "Lignin Enzymic and Microbial Degradation", E. Odier (ed.); INRA, Publ., Paris, 119

K. J. Packer, (1977) *Phil. Trans. R. Soc. Lond.*, **B 278**, 58

J. M. Palmer, P. J. Harvey and H. E. Schoemaker, (1987) *Phil. Trans. R. Soc. Lond.*, **A 321**, 495

F. Parisi and M. A. Parisi, (1989) In : "Enzyme Systems for Lignocellulose Degradation", M. P. Coughlan (ed.); Elsevier Applied Science Ltd, London, 243

A. Pasczcynski, V. B. Huynh and R. L. Crawford, (1985) *FEMS Microbiol. Lett.*, **29**, 37

A. Pasczcynski, V. B. Huynh and R. L. Crawford, (1986) *Arch. Biochem. Biophys.*, **244**, 750

J. Prost and F. Rondelez, (1991) *Nature*, **350**(Suppl.), 11

J. Puls and K. Poutanen, (1989) In : "Enzyme Systems for Lignocellulose Degradation", M. P. Coughlan (ed.); Elsevier Applied Science, London and New York, 151

V. Renganathan and M. H. Gold, (1986) *Biochemistry*, **25**, 1626

V. Renganathan, K. Miki and M. H. Gold, (1985) *Arch. Biochem. Biophys.*, **241**, 304

M. T. Riggin, A. R. Sharp, R. Kaiser and M. H. Schneider, (1979) *J. Appl. Polym. Sci.*, **23**, 3147

D. Robert and C. L. Chen, (1989) *Holzforschung*, **43**(5), 323

J. D. Russell, I. Murray and A. R. Fraser, (1989) In : "Physico-Chemical Characterization of Plant Residues for Industrial and Feed Use", C. a. Orskov (eds.); Elsevier Applied Science, London and New York, 13

A. Sakakibara, (1980) *Wood Sci. Technol.*, **14**, 89

K. V. Sarkanen and C. H. Ludwig, (1971) "Lignins: Occurrence, Formation, Structure and Reactions"; Wiley-Interscience, New York

S. Sarkanen, D. C. Teller, E. Abramowski and J. L. McCarthy, (1982) *Macromol.*, **15**(4), 1098

S. Sarkanen, D. C. Teller, J. Hall and J. L. McCarthy, (1981) *Macromol.*, **14**, 426

S. Sarkanen, D. C. Teller, C. R. Stevens and J. L. McCarthy, (1984) *Macromol.*, **17**(12), 2588

J. S. Schaefer, M. D. Sefcik, E. O. Stejskal, R. A. McKay and P. L. Hall, (1981) *Macromol.*, **14**(3), 557

M. Schnitzer and S. U. Khan, (1978) "Soil Organic Matter"; Elsevier Sci. Publ. Co., Amsterdam

H. E. Schoemaker, P. J. Harvey, R. M. Bowen and J. M. Palmer, (1985) *FEBS Lett.*, **183**(1), 7

M. Shimada, T. Hattori, T. Umezawa, T. Higuchi and T. Okamoto, (1987) In : "Lignin Enzymic and Microbial Degradation", E. Odier (ed.); INRA Publications, Paris, 151

H. Sterk, W. Sattler and H. Esterbauer, (1987) *Carbohydrate Res.*, **164**, 85

H. Taneda, N. Habu and J. Nakano, (1989) *Holzforschung*, **43**(3), 187

M. Tien and T. K. Kirk, (1983) *Science*, **221**, 661

M. Tien and T. K. Kirk, (1984) *Proc. Natl. Acad. Sci. USA*, **81**, 2280

M. Tien, T. K. Kirk, C. Bull and J. A. Fee, (1986) *J. Biol. Chem.*, **261**(4), 1687

F. Tonon and E. Odier, (1988) *Appl. Environ. Microbiol.*, **54**(2), 466

J. Trojanowski, K. Haider and V. Sundman, (1977) *Arch. Microbiol.*, **114**, 149

U. M. Tuor, S. D. Haemmerli, H. E. Schoemaker, H. W. H. Schmidt and M. S. A. Leisola, (1990) In : "Biotechnology in Pulp and Paper Manufacture", T. K. Kirk and H.-M. Chang (eds.); Butterworth-Heinemann, Boston, 389

D. C. Ulmer, M. S. A. Leisola and A. Fiechter, (1984) *J. Biotechnol.*, **1**, 13

K. Valli, H. Wariishi and M. H. Gold, (1990) *Biochemistry*, **29**, 8535

D. L. VanderHart and R. H. Atalla, (1984) *Macromol.*, **17**, 1465

R. Voelkel, (1988) *Angew. Chem. Int. Ed. Engl.*, **27**, 1468

N. K. Vyas, M. N. Vyas and F. A. Quiocho, (1988) *Science*, **242**, 1290

H. Wariishi, L. Akileswaran and M. H. Gold, (1988) *Biochem.*, **27**, 5365

H. Wariishi and M. H. Gold, (1989) *FEBS Lett.*, **243**(2), 165

M. Wayman and S. R. Parekh, (1990) "Biotechnoly of Biomass Conversion"; Open University Press, Milton Keynes, U.K.

W. Weiss, J. H. Brown, S. Cusack, J. C. Paulson, J. J. Skehel and D. C. Wiley, (1988) *Nature*, **333**, 426

U. Westermark and K. E. Eriksson, (1974a) *Acta Chem. Scand.*, **B 28**, 209

U. Westermark and K. E. Eriksson, (1974b) *Acta Chem. Scand.*, **B 28**, 204

J. M. Willis and F. G. Herring, (1987) *Macromol.*, **20**, 1154

T. M. Wood, (1985) *Biochem. Soc. Trans.*, **13**, 407

T. M. Wood, (1989) In : "Enzyme System for Lignocellulose Degradation", M. P. Coughlan (ed.); Elsevier Applied Science, London and New York, 17

T. M. Wood and S. I. McCrae, (1979) *Developments in Food Science*, **2**, 257

S. Yasuda and K. Ota, (1987) *Holzforschung*, **41**(1), 59

W. Zimmermann, (1989) In : "Enzyme Systems for Lignocellulose Degradation", M. P. Coughlan (ed.); Elsevier Applied Science, London and New York, 167